Variability studies of a sample of IntraDay Variable sources

Dissertation

zur

Erlangung des Doktorgrades (Dr. rer. nat)

der

Mathematisch-Naturwissenschaftlichen Fakultät

der

Rheinischen Friedrich-Wilhelms-Universität Bonn

vorgelegt von

Nicola Marchili

aus

Perugia, Italien

Bonn (March 2009)

Angefertigt mit Genehmigung der Mathematisch-Naturwissenschaftlichen Fakultät
der Rheinischen Friedrich-Wilhelms-Universität Bonn

1. Gutachter **Prof. Ulrich Klein**

2. Gutachter **Priv.-Doz. Dr. Walter K. Huchtmeier**

Tag der Promotion: 25. Juni 2009

A papà

“ Qualche volta la polvere da sparo
non prende fuoco per umidità,
altre volte s’accende senza il fiammifero
o l’acciarino.
Basterebbe il tascabile briquet
se ci fosse una goccia di benzina.
E infine non occorre fuoco affatto,
anzi un buon sottozero tiene a freno
la tediosa bisava, l’Ispirazione.
Non era troppo arzilla giorni fa
ma incerottava bene le sue rughe.
Ora pare nascosta tra le pieghe
della tenda e ha vergogna di se stessa.
Troppe volte ha mentito, ora può scendere
sulla pagina il buio il vuoto il niente.
Di questo puoi fidarti amico scriba.
Puoi credere nel buio quando la luce mente.”

Eugenio Montale

Contents

Abbreviations

AGN:	Active Galactic Nuclei
ALAT:	sub-scans (or flux-densities) in scanning direction Elevation
ALON:	sub-scans (or flux-densities) in scanning direction Azimuth
CCF:	Cross-Correlation Function
$DACF$:	Discrete Auto-Correlation Function
DoY:	Day of the Year
FSRQ:	Flat-Spectrum Radio Quasar
FWHP:	Full Width at Half Power
IDV:	IntraDay Variability
ISM:	InterStellar Medium
ISS:	InterStellar Scintillation
LSR:	Local Standard of Rest
MASIV:	Micro-Arcsecond-Scintillation-Induced Variability survey
MJD:	Modified Julian Date
m_i:	modulation index
SF:	Structure Function
SR:	Sinusoidal Regression
TEC:	Total Electron Content
VLA:	Very Large Array
VLBI:	Very Long Baseline Interferometer

Chapter 1

Intraday variability

Among the characteristics of Active Galactic Nuclei (AGNs), one of the most remarkable is the strong time variability they show on time scales from minutes to dozens of years, both in total flux-density and polarization, over the whole observable electromagnetic spectrum. The study of the diverse aspects of such variability is one of the main tools we have for the investigation of the AGN physics. Causality arguments allow to deduce information about the size of the emitting regions by estimating the variability time scales; the amplitude of the variations, their frequency dependence, the changes in polarization degree and angle – just to mention some essential aspects – provide strong constraints for any model which aims to explain the nature of AGN.

In the present chapter we give a short review on IntraDay Variability (IDV), i.e. the variability in the radio cm-bands characterized by time scales faster than two days. We focus on the radio frequencies, introducing the history, the main findings, the models proposed for explaining the phenomenon and the open questions which this thesis – as well as future IDV studies – have still to face. A deeper discussion of the topics can be found in Fuhrmann (2004) and Wagner and Witzel (1995).

1.1 An IDV overview

Radio variability on time scales of from days to weeks was observed in AGNs as early as 1971 (see e.g. Kinman and Conklin (1971), Wills (1971), Andrew et al. (1971)). Soon, propagation-induced effects were associated to the detected fluctuations (see, e.g., Shapirovskaya (1978), Rickett et al. (1984)), triggering the research for flickering by refractive scattering effects (Heeschen, 1984). One of these projects, carried out with the Effelsberg 100 m telescope, led to the discovery of significant variability on time scales shorter than one day (see Witzel et al. (1986), Heeschen et al. (1987)). These experiments mark the beginning of intraday variability. Initially, the results were received with skepticism (Beall et al., 1989), but the accuracy of the calibration methods and the repeatability of IDV experiments at different telescopes demonstrated that the variability was real. In May 1989 simultaneous observations of the quasar S4 0917+624 with the Effelsberg Telescope and the VLA gave perfectly consistent results (Witzel (1990), Qian et al. (2001)). Even more remarkably, in January 1990 a multi-frequency campaign for the observation of S5 0716+714 led to the discovery of a correlation between the variability observed in radio and optical light curves, implying that its origin is intrinsic to the source (Quirrenbach et al., 1991). This experiment is the starting point of a debate about the

physical origin of IDV which is still ongoing. The hypothesis that strong variability on such short time scales could be intrinsic to the sources opened immediately the issue of the extreme brightness temperatures – far in excess of inverse Compton limit (10^{12} K; see Kellermann and Pauliny-Toth (1969)) – which IDV would imply. Propagation effects, such as InterStellar Scintillation (ISS), were suggested as a likely alternative scenario, but none of the models proposed so far could fit all the IDV characteristics inferred from more than 20 years of observations.

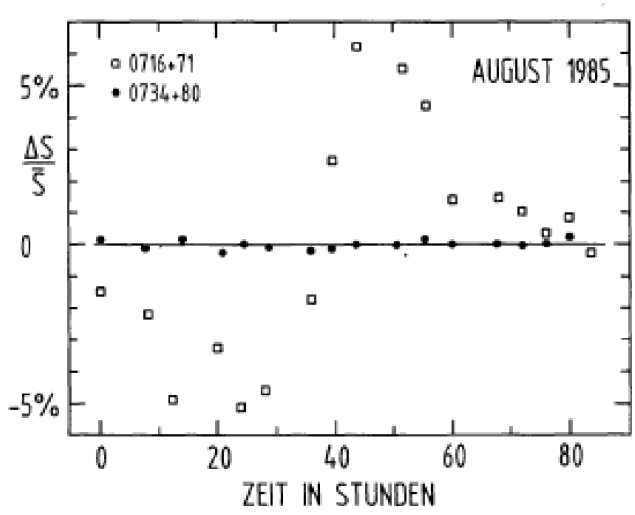

Figure 1.1: The variability curve of 0716+714: one of the first IDV detections, from Witzel et al. (1986).

The variability time scales provide an obvious criterion for the classification of IDV sources. Heeschen et al. (1987) proposed to subdivide the sources as follows (see also Quirrenbach et al. (1992)):

- The objects showing some variability, but only on time scales considerably longer than 2 days, were defined as **type-I** IDV sources. This category includes both classical flickering sources and intraday variable objects.
- The sources characterized by time scales shorter than 2 days were defined as **type-II**.

The two-day borderline between the categories is somehow arbitrary, but it becomes significant when we consider the issue of the IDV origin. Since the time scale plays the main role in the estimation of the brightness temperature, this classification may be used for a rough separation between the sources whose variability could be explained in terms of intrinsic processes, without encountering a too serious obstacle in the inverse Compton limit, and the ones for which an intrinsic explanation would only be possible given a new theoretical approach.

From the first IDV experiments, it was immediately clear that the phenomenon has to do with the compactness of the sources. Steep-spectrum objects – for which the most of the radiation comes from optically thin regions – show no IDV activity, while Flat-Spectrum Radio Quasars (FSRQs) are often affected. In 1992, Quirrenbach et al. (1992) investigated variability in two complete samples of FSRQs, finding type-II IDV in $\approx 25\%$

of the sources. Recently, the results of the MASIV survey (which searched for IDV in a sample of more than 400 sources; see Lovell et al. (2003a) and Lovell et al. (2003b)) seem to indicate that the phenomenon is more common than previously thought, finding that more than 20-30% of the observed flat-spectrum radio sources exhibit 2-10% rms variations on time scales over 2 days (Lovell et al., 2008).

The discovery of sources showing variations of the order of 100% of the average flux-density on time scales of less than 1 hour is a breakthrough in the history of IDV. Examples of these extreme objects are PKS 0405-385, J 1819+384 and PKS 1257-326 (see, respectively, Kedziora-Chudczer et al. (1997), Dennett-Thorpe and de Bruyn (2000), Bignall et al. (2003)). The high degree of variability and the discovery of seasonal cycles in the variability time scales strongly points towards a source-extrinsic effect; the detection of a difference in the arrival times of the flux-density variations at two different telescopes for J 1819+384 and PKS 1257-326 demonstrated that the variability, in these two cases, is due to InterStellar Scintillation (ISS). These extreme sources are defining a new class of IDV objects: the **fast scintillators**.

Despite the observational evidence summarized above, the nature of IDV in the fast scintillators is still matter of debate. Among the open issues, the fact that the explanation of the variability in terms of diffractive scattering in J 1819+384 leads to brightness temperatures of the order of 10^{15} K (Macquart and de Bruyn, 2006), far in excess of the inverse-Compton limit (see section 1.2). The situation is even more complicated, if we take into account the classical IDV categories. For type-I sources, it is likely that a major contribution to the variability comes from source-intrinsic effects. For type-II, instead, the key-problems are still unresolved. The main arguments used for demonstrating the extrinsic nature of the fast scintillators' variability do not apply to type-II sources. In the case of S4 0917+624, however, a seasonal cycle in the time scales has been claimed (Rickett et al., 2001). The sudden fall of the source in a quiescent state did not allow further investigations. The discovery of fast IDV sources with characteristics in between type-II and fast scintillators, such as J 1128+592 and 1156+295 (see Gabányi et al. (2007), Savolainen and Kovalev (2008)), could represent an important step towards the comprehension of IDV, since it may reveal the similarities and the differences between the two classes. For J 1128+592, clear evidence of a seasonal cycle has been found.

It is likely that the variability detected in type-II IDV sources is affected by both source-intrinsic and source-extrinsic effects, which would justify the difficulties so far encountered in exhaustively explaining the variability characteristics they show. In this sense, the study of type-II IDV may provide the missing key for successfully disentangling intrinsic and extrinsic variability, and hence separating the information concerning the sources from the one concerning the InterStellar Medium (ISM).

1.2 Source-intrinsic models

The causality argument

Let us consider the case that intraday variability is intrinsic to the sources. Causality arguments would immediately allow an estimation of an upper limit to the size of the emitting region:

$$d \leq c\,\tau \tag{1.1}$$

where d: the linear size of the emitting region
c: the speed of light
τ: the time scale of the variability

Once we convert d into an apparent angle using the luminosity distance, Eq. 1.1 can be used for calculating the maximum angular size of the emitting region (see Pen (1999), Fuhrmann (2004)). Given the time scale τ:

$$\theta[\mathrm{mas}] = 0.173\left(\frac{(1+z)^2\tau[\mathrm{d}]}{D_l[\mathrm{Mpc}]}\right) \tag{1.2}$$

where θ: the angular size of the emitting region
z: the redshift of the source
D_l: the luminosity distance of the source

For values of z, D_l and τ typical of type-II IDV sources, θ can easily be of the order of tenths of μas, or even smaller. If intraday variability is intrinsic to sources, the resolution it allows to achieve is much higher than by space- and mm-VLBI, which shows how important can be IDV for the study of AGNs[1].

The brightness temperature

The angular size of the emitting region has a direct relation with its brightness temperature T_b (see, e.g., Kraus (1997)). If we consider an emitting component with Gaussian brightness distribution:

$$T_b[\mathrm{K}] = 1.22\cdot 10^{12}\frac{S[\mathrm{Jy}]}{\left(\theta[\mathrm{mas}]\,\nu[\mathrm{GHz}]\right)^2} \tag{1.3}$$

where S: the flux-density
ν: the frequency of the radiation

which, together with Eq. 1.2, leads to

$$T_b[\mathrm{K}] = 4.5\cdot 10^{10} S[\mathrm{Jy}]\left(\frac{\lambda[\mathrm{cm}]D_l[\mathrm{Mpc}]}{\tau[\mathrm{d}](1+z)^2}\right)^2 \tag{1.4}$$

where λ: the wavelength

The region where the variability originates has to emit a flux-density at least as high as the the maximum flux variation ΔS. Therefore we can find a lower limit to T_b by substituting S with ΔS in Eq. 1.3. This way, the IDV characteristics of a source allow an estimation of the brightness temperature in the emitting region.

The Doppler factor

If the radiation comes from a bulk of plasma in relativistic motion along the line of sight to the source (Marscher and Scott, 1980) (a quite realistic hypothesis, as the apparently superluminal motions often detected in FSRQ seem to demonstrate, see e.g. Schalinski

[1]The statement is still valid for ISS-induced variability, although in this case the spatial resolution that IDV allows to investigate is about a factor ten lower (Rickett, 1998).

et al. (1987)), Eq. 1.4 has to be changed in order to take into account the effect of the relativistic aberration with the Doppler factor D:

$$\mathcal{D} = \frac{1}{\gamma\,(1 - \beta\, cos\phi)} \tag{1.5}$$

where γ: the bulk Lorentz factor
β: the bulk velocity in units of c
ϕ: the angle between the direction of motion and the line of sight

The Doppler factor $\mathcal{D}$ has an influence on different quantities:

- the measured flux-density
- the observed wavelength
- the time scale of the variability.

For an *isotropically emitting bulk of plasma moving along the jet*, the emitted flux-density S is lower than the measured one S_{obs}, because of Doppler boosting:

$$S = \left(\frac{1+z}{\mathcal{D}}\right)^{3-\alpha} S_{obs} \tag{1.6}$$

where α is the spectral index ($S \sim \nu^{-\alpha}$). The emitted wavelength λ appears Doppler shifted relative to the observed one λ_{obs}:

$$\lambda = \left(\frac{\mathcal{D}}{1+z}\right)\lambda_{obs} \tag{1.7}$$

Finally, the boosting causes the observed variability time scale τ_{obs} to appear shorter than it really is:

$$\tau = \left(\frac{\mathcal{D}}{1+z}\right)\tau_{obs} \tag{1.8}$$

We can include all the variations induced on Eq. 1.4 by the change from the comoving to the observer frame in the correction factor $\mathcal{F}$:

$$T_b = \mathcal{F}\left[4.5 \cdot 10^{10} S_{obs}\left(\frac{\lambda_{obs} D_l}{\tau_{obs}(1+z)^2}\right)^2\right] \tag{1.9}$$

The estimation of $\mathcal{F}$ requires some assumptions on the origin of the radiation; in case of an isotropically emitting blob (see, e.g. Rees (1978)) Eq. 1.6, 1.7 and 1.8 lead to

$$\mathcal{F} = \left(\frac{1+z}{\mathcal{D}}\right)^{3-\alpha} \tag{1.10}$$

which, for a flat-spectrum source ($\alpha \approx 0$), becomes

$$\mathcal{F} = \left(\frac{1+z}{\mathcal{D}}\right)^{3} \tag{1.11}$$

For a continuous jet, it can be demonstrated (see (Begelman et al., 1984), Urry and

Padovani (1995)) that

$$\mathcal{F} = \left(\frac{1+z}{\mathcal{D}}\right)^2 \tag{1.12}$$

Violation of the inverse-Compton limit

If we take into consideration the amplitudes and the time scales of the variations observed in some IDV experiments at GHz frequencies, it is not uncommon, using Eq. 1.9, to find brightness temperatures of the order of $10^{17} - 10^{19}$ K. These values largely exceed the inverse-Compton limit $T_{IC} \approx 10^{12}$ K (see Kellermann and Pauliny-Toth (1969)). When $T_B > T_{IC}$, the relativistic electrons in the emitting region scatter the synchrotron radiation up to X-rays. This leads to a catastrophic cooling, which should bring the brightness temperature to values lower than T_{IC} in a very short time (of the order of few hours). The violation of the inverse-Compton limit is therefore a major problem for explaining IDV in terms of effects which are intrinsic to the sources.

The most simple way to overcome the problem would be to assume a value of $\mathcal{F}$ high enough to bring T_B down to the order of T_{IC}. Essentially, this could be achieved by hypothesizing large Doppler factors or a special geometry of the emitting region. In the latter case, the exponent in Eq. 1.11 could take values also significantly higher than 3 (Qian et al., 2006). Both the solutions present downsides: several IDV sources would require values of $\mathcal{D}$ of more than 100 for avoiding the violation of the inverse-Compton limit (Qian et al., 1991), in apparent contradiction with the results of VLBI superluminal motions observations. The conditions required in order to increase the exponent in Eq. 1.11 appear peculiar; no strong evidence in their favour have been found so far.

There are other possible solutions to the problem of the inverse-Compton catastrophe. For example, the flux-density variations may be due to changes in the Doppler factor because of fast fluctuations in the angle between the flux beam and the line of sight. Small swings of the jet could account for significant variability, without any implication on the brightness temperature of the emitting region. It can not be ruled out, moreover, that under non-stationary conditions a short phase of violation of the inverse-Compton limit could cause flux variations on time scales which are comparable with the IDV ones. According to Kellermann (2002), however, such phases should not last for more than few hours. Coherent, or partially coherent, emission processes – which are expected to take place in jets, particularly for processes involving magneto-hydro-dynamics – and a more homogeneous ordering of the magnetic field in the jet Qian et al. (2006) have been also hypothesized as possible explanations.

In conclusion, an intrinsic origin of IDV can not be ruled out, under hypotheses which do not appear too unrealistic. The main difficulty for the proposed models is to find independent evidence for confirming the correctness of the assumptions, and hence demonstrate that the apparently peculiar conditions they seem to require are instead not peculiar at all.

1.3 Source-extrinsic models

Source-extrinsic explanations of IDV are essentially limited to two possible effects: microlensing from fine-scale structures within galaxies (i.e. individual stars close to the line

of sight to the sources) and interstellar scintillation. Given the small size scale of the emitting regions in IDV sources, it is likely that both these propagation effects do often contribute to the observed variability. However, the importance of such contributions is still unclear.

1.3.1 Microlensing

Several arguments seem to contradict the idea of IDV being generally induced by microlensing. Among them:

- Multi-frequency IDV experiments frequently show a strong wavelength dependence of the variability, a fact which can not be explained in terms of microlensing, which is an achromatic effect.
- The short IDV time scales require very fast changes between the relative position of the emitting region and the lens. When translated into velocity, these changes do often imply apparently superluminal motion, which of course can not occur but in the source plane. This consideration reduces the role of microlensing just to an amplification factor of intrinsic events. Large part of the problems which arise when we try to explain IDV in terms of intrinsic effects still exists if we hypothesize microlensing as the origin of the variability.
- Lensing foreground galaxies should frequently be seen to exist along the line of sight of IDV sources, but this is not observed.

We will no further discuss the microlensing scenario; a detailed description can be found in Wagner and Witzel (1995). We just borrow the conclusions of the authors: while none of the indications is conclusive alone, all together they argue against microlensing playing a major role in IDV.

1.3.2 Interstellar scintillation

The idea that the interstellar medium can induce variability on the measured flux density of compact sources is not only reasonable, but almost unavoidable. In the beginning of the chapter we mentioned that propagation effects were suggested as origin of fast radio variability almost as soon as such variability was discovered. Scattering phenomena at MHz wavelengths due to the Earth's atmosphere are known almost since the beginning of radio astronomy, while the role played by ISS on pulsar variability had to wait the end of the '60s to be understood Scheuer (1968). Consequently, the explanation of IDV at GHz frequencies in terms of scintillation effects came as a natural extension of common experience. The success of the ISS models in explaining the variability observed in the fast scintillators gave further support to the arguments of those who explain IDV as a purely source-extrinsic effect. This conclusion, though, has to be taken very carefully, since many pieces still do not fit into the puzzle.

In order to show the strength and the weakness of the ISS model, it is necessary to introduce its fundamental aspects in some detail. A detailed description of scattering processes in different regimes (weak+strong, refractive, and diffractive scattering) can be found in Narayan (1992), which we closely follow.

The Fresnell-Kirchhoff integral

Let us assume a radio source at infinity and a scattering screen at distance D from the observer. If the wavefront from the source has unit amplitude, and if $\phi(x, y)$ is the phase change introduced by the screen at transverse position (x, y), the complex wave amplitude after crossing the screen is $exp[i\phi(x, y)]$, and the amplitude $\psi(X, Y)$ received at position (X, Y) on the observer plane is:

$$\psi(X,Y) = \frac{e^{-i\pi/2}}{2\pi {r_f}^2} \int\int exp\left[i\phi(x,y) + i\frac{(x-X)^2 + (y-Y)^2}{2{r_f}^2} \right] dx\, dy \tag{1.13}$$

where λ: the wavelength of the radiation
$r_f = \sqrt{(\lambda D/2\pi)}$: the Fresnel scale

The integral in Eq. 1.13 is known as the Fresnel-Kirchhoff integral. In the limit of small-angle scattering ($\mid x - X \mid, \mid y - Y \mid \ll D$), the second term inside the exponential represents the contribution to the phase due to the additional path length from (x, y) to (X, Y).

Once that the phase change introduced by the screen is known, the effect of the scattering can be accurately established. When $\phi(x, y) = 0$, the amplitude of the radiation received at any point after the screen is equal to 1, which means no scattering is observed. Most of the collected radiation comes from a region within a radius $\sqrt{2} \cdot r_f$ – the 'first Fresnel zone'. Consequently we can think to r_f as the length scale over which the radiation stays coherent in phase when the scattering is negligible. When the radiation passes through a turbulent medium, instead, random phase fluctuations are introduced into the wavefront. The problem can be confronted using a statistical approach.

Let us define the diffractive length scale r_{diff} as the transverse separation $\sqrt{x^2 + y^2}$ for which the root mean square phase difference $\left(\phi(x' + x, y' + y) - \phi(x', y')\right)^2$ is equal to 1 rad. We can interpret r_{diff} as the length scale over which the phase shift introduced by the medium is coherent. The two length scales r_f and r_{diff} are basically everything we need for discussing the main aspects of ISS. According to the ratio between them, we can define different scattering regimes: weak scintillation for $r_f/r_{diff} \ll 1$, strong scintillation for $r_f/r_{diff} \gg 1$

For the following discussion we will assume that the turbulence in the ISM can be described by means of a Kolmogorov spectrum. This assumption, combined with the cold plasma dispersion relation, allows to describe r_{diff} for ionospheric, interplanetary and interstellar scattering as follows:

$$r_{diff} \sim \lambda^{-\frac{6}{5}} {D_s}^{-\frac{3}{5}} \tag{1.14}$$

where D_S: the pathlength through the turbulent medium

If we assume the medium to extend till the observer, $D_S = D$, and using the definition of r_f we can write

$$\frac{r_f}{r_{diff}} \sim \lambda^{\frac{17}{10}} D^{\frac{11}{10}} \tag{1.15}$$

If we assume instead that the screen is thin and localized at distance $D \gg D_S$ from the observer, then

$$\frac{r_f}{r_{diff}} \sim \lambda^{\frac{17}{10}} D^{\frac{1}{2}} \tag{1.16}$$

Equations 1.15 and 1.16 are very important. They help us to discriminate between different scattering regimes. They also reveal us that the strength of the scattering increases with wavelength and distance.

Weak scattering

The condition $r_f/r_{diff} \ll 1$, which characterizes weak scattering, implies that the random phase fluctuations introduced by the screen within the first Fresnel zone are small. The most of the radiation collected after the scattering, therefore, will still come from a region of size comparable to r_f. The mild perturbation due to scattering will create focusing/defocusing regions in which the measured radiation will be higher/lower than in the case of no scintillation. We call these regions 'scintles'.

Since the flux variations are strongest at the Fresnel scale (see Narayan (1992), Matheson and Little (1971)), the time scale of the variability expected for weak scattering is

$$\tau_w = \frac{r_f}{v} \tag{1.17}$$

where v: the transverse velocity between the scattering medium and the observer-source line of sight

It can also be demonstrated that the modulation index of the variability (which is a measure of its strength, see chapter 3 for more details) is

$$m_w \sim \left(\frac{r_f}{r_{diff}}\right)^{\frac{5}{6}} \tag{1.18}$$

and that the intensity variations are correlated over a bandwidth $\Delta\nu$ which is of the order of the radiation frequency ν

$$\Delta\nu_w \sim \nu \tag{1.19}$$

Equations 1.17, 1.18 and 1.19, combined with Eq. 1.14 allow a basic description of the manifestations of weak scattering in terms of just two unknown parameters, which are D and v. Any change in the variability time scale would be reflected into the modulation index; the frequency dependence of the variability strength is known. Multi-frequency IDV experiments looking for the variability parameters described above should provide a solid test for the weak scattering model of IDV.

It is worth to mention that, in case of extended sources, the equations describing the time scale and the modulation index of the variability change, according to the equations below:

$$\tau_e \sim \tau_w \frac{\theta_s}{\theta_f} \tag{1.20}$$

where θ_s: the angular size of the source
θ_f: the Fresnel angle, r_f/D

$$m_e \sim m_w \left(\frac{\theta_f}{\theta_s}\right)^{\frac{7}{6}} \tag{1.21}$$

Strong scattering

It can be demonstrated that when $r_f \gg r_{diff}$, i.e. in regime of strong scattering, the variability amplitude is characterized by two peaks at widely separated length scales.

- Given the fact that the phase fluctuations in the screen stay coherent just within a circle of radius r_{diff}, it is intuitive that the strongest variability should occur on this length scale. This phenomenon is called diffractive scintillation.
- Relative weak variability also occurs on the so-called refractive scale $r_{ref} = \frac{{r_f}^2}{r_{diff}}$, which is much larger than r_f.

Diffractive scintillation

In case of diffractive scintillation, the region which contributes to the measured flux-density is characterized by a length scale $D \cdot \theta_{scatt} \sim \frac{D \cdot \lambda}{r_{diff}} \sim r_{ref}$. The patches of coherent radiation, on the other hand, have size of the order of $r_{diff} \ll r_{ref}$. This means that each point of the observer plane receives radiation from a large number of regions of the scattering screen which essentially have no phase correlation between each other. It is evident, consequently, that the variability induced by diffractive scintillation is extremely strong.

The size of the diffractive scale leads immediately to the estimation of the variability time scale:

$$\tau_{diff} = \frac{r_{diff}}{v} \tag{1.22}$$

where, once again, v is the transverse velocity between the scattering medium and the observer-source line of sight. The modulation index is

$$m_{diff} \approx 1 \tag{1.23}$$

Diffractive scintillation is a narrow band phenomenon:

$$\Delta\nu_{diff} \sim \left(\frac{r_{diff}}{r_f}\right)^2 \tag{1.24}$$

The equations above are a very powerful tool for testing if diffractive scintillation is responsible for intraday variability or not. This extreme kind of scattering plays a major role when dealing with sources characterized by very small sizes (of the order of μas), like pulsars. It is usually thought that it does not affect extragalactic sources; the only detection up to now regards the fast scintillator J 1819+3845 (Macquart and de Bruyn, 2006).

Refractive scintillation

The last manifestation of scattering we discuss here is refractive scintillation. This occurs as a consequence of large-scale inhomogeneities in the scattering screen on length scales of

the order of r_{ref}: when the phase fluctuations act on the diffractive-scale patches in such a way as they focus the radiation towards the observer, the measured flux-density will be higher, while in case of defocusing it will be smaller. We present below the quantities which characterize this type of scintillation.

The variability time scale for refractive scintillation can be estimated, as usual, by means of the length scale:

$$\tau_{ref} = \frac{r_{ref}}{v} \tag{1.25}$$

while the modulation index depends on the amplitude of the phase fluctuations on r_{ref} scale. It can be demonstrated that

$$m_{ref} \approx \left(\frac{r_{diff}}{r_f}\right)^{\frac{1}{3}} \tag{1.26}$$

In contrast with diffractive scintillation, refractive scintillation is broadband in nature:

$$\Delta\nu_{ref} \approx 1 \tag{1.27}$$

This concludes the discussion of the different regimes in which interstellar scintillation can manifest itself. The information here gathered is essential for discriminating between source-intrinsic and source-extrinsic IDV models.

Intrinsic versus extrinsic models

In general, intrinsic explanations are more flexible in adapting to the observed variability characteristics. The diverse intrinsic mechanisms which have been proposed as possible origin of variability can fit observational evidences quite well; the problem with this scenario is always represented by the violation of the inverse-Compton limit. The solutions proposed up to now are causes of controversial discussion. On the other hand, ISS models have proven to work well in the case of fast scintillators, and an extension to type-II sources appears almost natural, given the small size of the objects involved. However, the basic physics of propagation effects is known well enough to allow solid predictions about the variability's frequency dependence, and how possible changes in the source (or the screen) conditions should reflect onto the modulation index, the time scales and the radiation polarization. For type-II sources, the predictions from ISS often fail, which is hard to understand, given the robustness of the models.

Time scales variations

Since our project is essentially based on the use of the Urumqi radio-telescope, for which just one receiver is suitable for IDV experiments, the multi-frequency approach to the investigation of the phenomenon is precluded in this work. We focused our attention on the study of the changes in time scales and modulation indexes which, in the case of intrinsic variability, can be related to a large variety of effects occurring in the source (geometrical changes, emission of bulks of plasma, etc.). According to ISS models, instead, such changes may be determined by variations either in the source size or in the properties of the scattering screen.

A special case is the one in which source and screen are not subject to any significant variation, but the relative velocity between the Earth and the screen changes with time.

Considering that the Earth moves around the Sun, and the Sun moves with respect to the Local Standard of Rest (LSR), this case is not only possible, but is necessary. If the velocity of the ISM cloud responsible for the scattering is constant over a time span of the order of years, the relative velocity to the Earth has to be 1-year periodic.

Annual modulation

The effect described above is the origin of the so-called 'annual modulation of the variability time scales', which explains the periodic variations seen in the characteristic time scales of an ISS-induced variability. An estimation of the effect can be obtained through a few steps: first of all we need to calculate the relative velocity $\mathbf{V}$ between the observer and the screen; afterwards, $\mathbf{V}$ has to be projected onto the Earth orbital plane, in order to find the observer's transverse velocity across the scintillation pattern; finally, the ratio between the characteristic scintles length scale and the transverse velocity gives the variability time scale.

Transverse velocity across the scintles

$\mathbf{V}$ can be expressed as the sum of the three vectors

$$\mathbf{V} = \mathbf{V}_\odot + \mathbf{V}_\oplus - \mathbf{V_m} \tag{1.28}$$

where $\mathbf{V}_\odot$: the velocity of the Sun in the LSR
$\mathbf{V}_\oplus$: the velocity of the Earth's orbital motion around the Sun
$\mathbf{V_m}$: the velocity of the scattering screen in the LSR

$\mathbf{V}_\odot$ and $\mathbf{V}_\oplus$ are known (see Qian and Zhang (2001) for a detailed description), while $\mathbf{V_m}$ is not; it can only be inferred from observations, or used as a fit parameter.

Let us express the vector in terms of an equatorial coordinate system having its origin at the center of the Sun, the X-axis directed towards the equinox, the Y-axis towards the point on the terrestrial equator at right ascension 6^h and the Z-axis towards the north pole: $\mathbf{V} = (V_x, V_y, V_z)$. Other important quantities are:

$V = \sqrt{{V_x}^2 + {V_y}^2 + {V_z}^2}$: the modulus of the vector
ζ: the angle between $\mathbf{V}$ and the line of sight towards the source
$V_\perp = V sin\,\zeta$: the transverse velocity of the Earth across the scintillation pattern

It should be noted that both V and ζ depend on the right ascension and declination of the source. Also in the case that two sources are scattered by screens with similar characteristics (e.g. two screens nearly at rest in the LSR), the resulting transverse velocities can be different.

Isotropic scintillation

In case of an isotropic scintillation pattern, following Goodman (1997), the characteristic variability time scale τ due to ISS can be expressed as

$$\tau[\mathrm{d}] = 0.58\,\frac{\theta_{eff}[10\,\mu\mathrm{as}]\,D_s[\mathrm{kpc}]}{V_\perp[30\,\mathrm{Km/s}]} \tag{1.29}$$

where θ_{eff}: the effective angular size of the source
D_s: the distance to the scattering screen

The quantity θ_{eff} is a function of the Fresnel angular size, the intrinsic angular size of the scintillating component and the scattering angle. An estimation of its value can be obtained using the formulas in Qian and Zhang (2001).

Equation 1.27 illustrates the meaning of the annual modulation effect. Assuming that $\mathbf{V}_\odot - \mathbf{V_m}$ in Eq. 1.26 is constant on a time scale of a few years, and that possible changes in θ_{eff} can be neglected too, variations in τ can only be caused by $\mathbf{V}_\oplus$ and ζ, which are both 1-year periodic. As a consequence, τ has to show a seasonal cycle. Note that such a periodic variation of the time scales, when detected, allows an estimation of the free parameters in the equations, which are the velocity and distance of the screen, $\mathbf{V_m}$ and D_s.

Anisotropic scintillation

When the scintillation pattern is not isotropic, Eq. 1.27 is not valid anymore. In fact, the scintles appear elongated in the direction of the anisotropy; θ_{eff} becomes a function of the direction, and the variability time scales change accordingly. Anisotropies in the scintillation pattern can be caused either by an anisotropic scattering medium or by an extended anisotropic source. The anisotropic case is not considered in Qian and Zhang (2001); we derived the formulas which allow to calculate the changes it introduces in the annual modulation effect by means of two new parameters: the angular ratio of the anisotropy r and its position angle γ, following the approach illustrated in Bignall et al. (2006) (see also Gabányi et al. (2007)).

The effect of the anisotropy can be calculated by introducing the vector $\mathbf{S}$, which defines the orientation of the elliptical scintillation pattern. It is also convenient to express the velocity $\mathbf{V}$ in terms of its projections onto the right ascension and the declination coordinates of the source:

$$V_\alpha = -V_x\, sin(\alpha_s) + V_y\, cos(\alpha_s) \tag{1.30}$$
$$V_\delta = -V_x\, cos(\delta_s) \cdot sin(\alpha_s) - V_y\, sin(\delta_s) \cdot sin(\alpha_s) + V_z\, cos(\alpha_s) \tag{1.31}$$
$$V_\gamma = -V_\alpha\, sin(\gamma) + V_\delta\, cos(\gamma) \tag{1.32}$$

where α_s: the right ascension angle of the source
δ_s: the declination angle of the source
γ: the anisotropy angle
V_α: the velocity projection onto α_s
V_δ: the velocity projection onto δ_s
V_γ: the modulus of $\mathbf{V} \times \mathbf{S}$

(the units are the same as in Eq. 1.27). The variability time scale of the source is then:

$$\tau[\mathrm{d}] = 0.58\, \frac{\theta_0\, D_s \cdot \sqrt{r}}{\sqrt{{V_\alpha}^2 + {V_\delta}^2 + (r^2 - 1)\, {V_\gamma}^2}} \tag{1.33}$$

The meaning of the angular scale θ_0 can be easily understood through its relation with the major/minor length scale of the scintles: $r_{major} = \theta_0\ D_s \cdot \sqrt{r}$, $r_{minor} = \theta_0\ D_s/\sqrt{r}$.

The modulation index

Since the annual modulation effect is not caused by changes neither in the scattering screen nor in the IDV sources, theoretically the modulation index of the variability should not be affected at all; its expression in terms of Eq. 1.18, 1.21 and 1.24 is always valid, and the effect does not play any role in them. However, in practice the situation is different, due to the limited duration of typical IDV experiments, such the ones we performed in Urumqi and Effelsberg.

The invariance of the modulation index is subordinated to the condition of a variability time scale which is smaller than the observation duration. If we have to deal with observing sessions of different durations, it may be that such condition is valid for some epochs, but not always. In the specific case of annual modulation, the characteristic time scale can vary by a factor ten or more, passing from few hours to several days. Consequently, the periods of slowest variability are expected to be characterized also by a significant decrease of the modulation index.

The investigation of the effects of annual modulation on both the time scales and the modulation index of intraday variable sources is the main purpose of this project.

Chapter 2

The Observations

The project for the monitoring of IDV sources at the Urumqi radio observatory has started in August 2005 and is still ongoing. In this chapter, it will be presented in detail by describing the main aims, the target sources and by summarizing the main characteristics of the 22 epochs of observations which span from August 2005 to April 2008[1]. Special attention will be payed to the description of the data calibration. The efficient implementation of this step is a *condicio sine qua non*, because the precision of data products is a necessity for obtaining reliable results.

2.1 The Urumqi (and Effelsberg) project

The Urumqi telescope is a 25-meter parabolic radio antenna, equipped with a 4.8 GHz state-of-the-art single horn receiver provided, as well as the new telescope driving program, by the MPIfR (Sun et al., 2006). The bandwidth of the receiver is 500 MHz. The aim of the intensive monitoring project at the Urumqi Observatory, both in total intensity and in polarization, is to study the *changes* – if any – in the variability pattern of selected IDV sources throughout the year. The ultimate goal is to confirm or disregard the prediction of the ISS models for the existence of an annual modulation in the variability pattern of IDV sources.

The key points of the project are the regularity and the short separation between consecutive observations, and the duration of each experiment, which has to be long enough to ensure a proper determination of the variability time scales. In the 22 epochs here presented, we collected a total observing time of 77.6 days. Realistically this could not be achieved at large and oversubscribed telescopes such as the Effelsberg one. The separation between consecutive observing epochs varies between 1 and 3 months, and almost all the months of the year are covered with at least one observing session. This way every phase of a possible seasonal variation of the time scales can be closely followed.

In order to check the reliability of the Urumqi antenna for IDV measurements, two simultaneous Urumqi-Effelsberg sessions have been carried out during the year 2006. These experiments allowed us to cross-check the results from the two observatories, which have very different properties. The main findings from this experiment are described in detail in chapter 6, but it may be worth to underline already that the degree of correlation between

[1]More observations have been performed since, but the data they provided will not be discussed in the present work because of the necessity to summarize and draw some conclusion about a project which, hopefully, will still go on for a long time.

the variability curves from the two telescope is remarkable, also in cases of faint and fast variations. This shows that the Urumqi telescope is well suited for IDV observations.

2.2 The main IDV-sources in the monitoring project

Below, we present some properties of the sources that comprise the sample of the main targets of our study.

- **S5 0716+714** (hereafter 0716+714) is a type II-IDV object whose redshift is still not definitely known – the recent attempt to measure it resulted an estimate of $z = 0.31 \pm 0.08$ through the detection of an underlying elliptical galaxy (Nilsson et al., 2008). It has been the target of many studies, with the consequence that nowadays 0716+714 is one of the best studied blazars in the sky. Several experiments have been devoted to the investigation of its IDV characteristics and led to important conclusions: the source shows strong IDV activity; no evidence for annual modulation has been detected so far (Qian and Zhang, 2001); remarkable interday variability has been observed at 86 GHz, which can not be explained by source extrinsic causes (Agudo et al., 2006); correlated radio-optical intraday variability has been detected in an experiment which involved a four-antenna subarray of the Very Large Array (VLA), the 2.2 m Calar Alto telescope (Spain) and the 0.71 m telescope of the Landessternwarte in Heidelberg (see Quirrenbach et al. (1991), Wagner and Witzel (1995), Wagner et al. (1996)). The last two points established 0716+714 as the best candidate to be intrinsically variable on IDV time scales.

- **S4 0917+624** (from now on, 0917+624) is a type II-IDV source at redshift $z = 1.45$. It has been one of the first objects to be included in regular IDV studies, which also lead to the discovery of the first annual modulation cycle in a type II-IDV source (Rickett et al., 2001). The variability features of 0917+624 have changed considerably over the years (Kraus et al., 1999b). After a long period of strong activity, around the year 2000, the source has entered a phase of quiescence which is still ongoing (Fuhrmann et al., 2002). These results imply that the origin of the IDV observed in 0917+624 is source-extrinsic; the change in the ISS-induced variability could be attributed to a change in the structure of the source – which may have caused a size increase and hence a quenching of the scintillation – or to interstellar weather.

- **S4 0954+658** (hereafter 0954+658) is a type II-IDV source at redshift $z = 0.368$. It is a well studied BL Lac object whose IDV features have been investigated since the early '90s (Wagner et al., 1993). The origin of the variability is still controversial: 0954+658 is the second source for which a radio-optical correlation has been claimed Wagner et al. (1990); however, the observation of an extreme scattering event in March 2000 Cimò et al. (2002) and the possible presence of a seasonal cycle in the variability time scales of 0954+658, revealed in a recent monitoring project (Fuhrmann, 2004), seem to shift the balance in favour of an extrinsic explanation.

- **J 1128+592** (hereafter 1128+592) is a recently discovered IDV source at $z = 1.795$. It is characterized by strong variability on short time scales, which places it in a peculiar position, in between a type II source and a fast scintillator. This characteristic, along with the discovery of a possible seasonal cycle in its variability time scales

Gabányi et al. (2007), makes 1128+592 a primary target for further IDV studies. It may provide precious information about similarities or differences between the two classes of IDV objects.

- **AO 0235+164** (hereafter 0235+164) is a 'historical' blazar at redshift 0.940, subject of an impressive number of studies since its discovery in the early '70s. Its IDV characteristics – which allow to classify it as a type II source – were investigated both in the optical and in the radio (Kraus et al. (1999a), Gupta et al. (2008)). A multi-frequency campaign during the years 2006-2007 detected a prominent outburst which could be observed over a large range of wavelengths (Raiteri et al., 2008). This made 0235+164 an ideal target for investigating how relevant changes in the features of an IDV source could affect its intraday variability.

- **OJ 287**, at redshift 0.306, is among the best studied blazars. Among the reasons for its popularity there is the discovery of a long-term periodicity in the optical frequencies (Sillanpaa et al., 1988). The source is known to vary on a scale from minutes to tens of years, but its IDV activity, in the radio, is mild and the characteristic time scales seem to suggest a classification as type I source.

- **Mrk 421** is one of the nearest BL Lac objects ($z = 0.030$) and thus among the brightest. It is a strong and highly variable TeV source. Despite the large number of publications about Mrk 421, no deep study of its radio IDV characteristics is available in literature.

- **1156+295** is a blazar at redshift 0.729, which has been identified as an IDV source in 2007 Savolainen and Kovalev (2008). Its IDV characteristics are extreme: the variations in the flux-density are as high as 40% while the time scales of the variability seem to indicate an IDV category between type II and fast scintillators as in the case of 1128+592. Since these discoveries are very recent, still no study for the existence of seasonal cycles in the variability time scales has been performed.

The core of the monitoring program is represented by four sources, namely 0716+714, 0917+624, 0954+658 and 1128+592, which were always included in the source list (*almost* always, in the case of 0917+624); instead 0235+164, OJ 287, Mrk 421 and 1156+295 have been observed less regularly. A large number of other sources, including the fast scintillator J 1819+384, have been sporadically included in our monitoring campaign; the complete list along with the basic variability characteristics is presented at the end of chapter 6.

2.3 The observations

The 22 IDV observing sessions so far performed with the Urumqi Telescope are summarized in Tab. 2.1. With an average separation of about 1.5 months, they cover all the months of the year – except for May – providing an excellent sample to search for a possible annual modulation in the time scales. Along with starting/ending date of the sessions, the table includes their duration, the average time sampling – which also reflects the conditions of the observation (the higher the sampling the better the weather, and/or the less the technical problems), the number of monitored sources (including the calibrators), and the mean duty cycle for IDV sources. This last piece of information is probably the most important since it represents the shortest time scale on which we can successfully search for variability.

A total of 77.6 days of observations comprise an exceptionally large amount of time for an IDV experiment. If the overall data quality is good enough – and this seems to be the case as will be shown in the following sections – the Urumqi project may be the ideal experiment for the study of the intraday variability. The average duty cycle of about one measurement per hour should suffice for detecting variability also on short (hourly) time scales.

Table 2.1: 22 epochs of observing sessions with the Urumqi telescope; in column 1 are reported the starting and ending dates of the experiments; in column 2 the duration; in column 3 the mean number of flux-density measurements per hour; in column 4 the number of observed sources; in column 5 the average number of measurements per hour for each IDV source (duty cycle).

Epoch	Duration (d)	Average sampling (h^{-1})	Number of observed sources	Duty cycle for IDV sources (h^{-1})
14.08−18.08.2005	2.9	7.4	24	0.3
27.12−31.12.2005	3.7	8.7	18	0.6
15.03−18.03.2006	3.0	10.0	18	0.7
27.04−01.05.2006	3.9	8.7	14	0.7
09.06−12.06.2006	3.2	10.9	11	1.2
14.07−18.07.2006	4.0	8.6	11	0.9
19.08−25.08.2006	6.4	11.3	12	1.3
23.09−28.09.2006	5.0	11.0	12	1.2
17.11−22.11.2006	4.7	12.0	14	1.2
18.12−21.12.2006	2.4	11.0	12	1.3
25.01−27.01.2007	2.3	11.2	14	1.1
12.02−16.02.2007	4.0	11.1	15	1.0
24.03−27.03.2007	2.8	11.0	16	0.9
20.04−24.04.2007	3.7	7.9	16	0.8
15.06−18.06.2007	2.4	10.1	16	0.9
19.07−22.07.2007	2.9	10.2	18	0.9
18.08−21.08.2007	3.1	9.1	15	0.9
13.10−16.10.2007	3.0	10.1	16	1.0
21.12−25.12.2007	3.2	11.3	15	1.1
24.02−27.02.2008	2.9	8.5	15	0.8
21.03−24.03.2008	3.0	11.0	15	1.1
21.04−24.04.2008	3.1	10.9	14	1.0
all the epochs	77.6	10.1	69	0.9

2.4 Standard data calibration procedure

All the flux-density measurements have been performed in 'cross-scan' mode. Each scan consists of 8 sub-scans in perpendicular directions over the source position – 4 sub-scans in elevation (ALAT) and 4 in azimuth (ALON). This observing mode allows the evaluation and correction of the pointing offsets; it turned out to provide accurate flux-density measurements also for the faintest sources in the our sample (~ 0.3 Jy). The comparison between elevation and azimuth sub-scans is an important consistency check for the data.

Differences due to extended source structures or confusion (i.e. undesired sources in the horn, which may alter the flux-density measurements depending on the relative position to the target source) would induce discrepancies in the results in the two scanning directions.

For each sub-scan, the received power is the convolution of the source brightness distribution and the antenna beam pattern. For an unresolved point-source, this convolution can be well approximated by a Gaussian profile. For the Urumqi telescope, the Full Width at Half Power (FWHP) is $\sim 600''$. The sub-scans extend though to a length of $1500''$, in order to allow the computation of the baseline level around the source position.

The data calibration procedure for total flux-density measurements follows a standard pipeline. After removing the average baseline, which is the background power, each sub-scan is fitted by a Gaussian profile, whose amplitude provides an estimate of the flux-density (see fig. 2.1). This part of the data calibration has been performed automatically via a python-based toolbox software package developed by P. Müller at the MPIfR. It leads to uncalibrated measurements of the sources brightness, expressed in arbitrary antenna temperature – hereafter, the **raw data**.

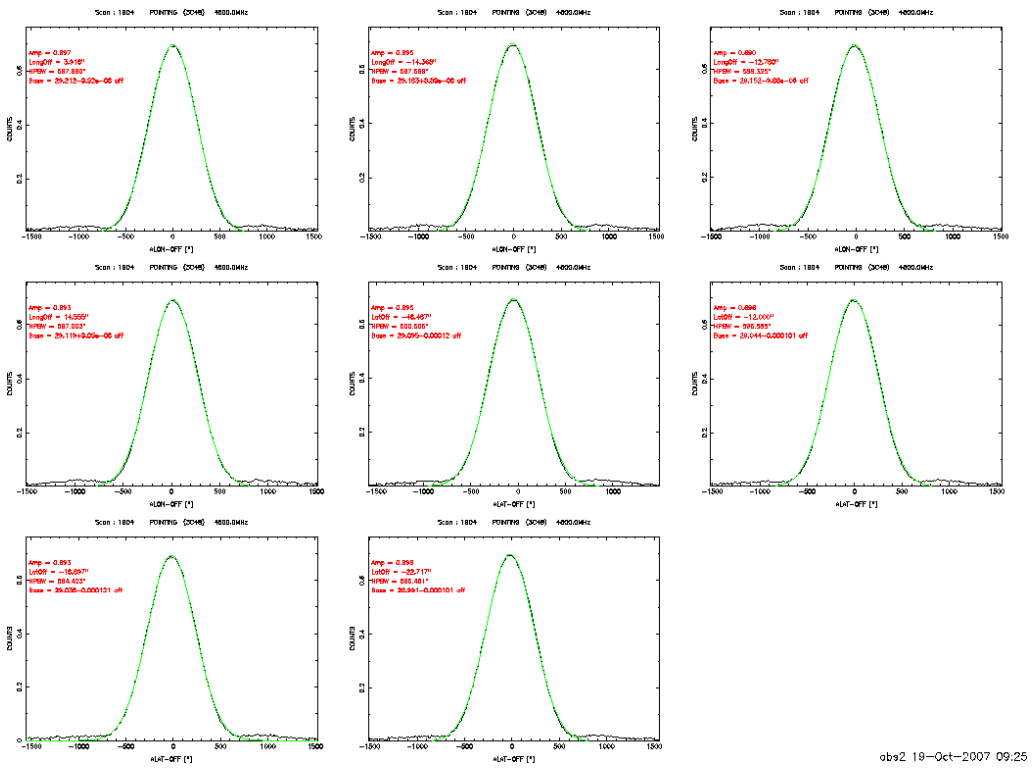

Figure 2.1: An example of individual scan, consisting of 8 sub-scans. The green lines are the Gaussian profiles fitted to the data.

2.4.1 The 'Redux' routine

The next step of the data calibration is the evaluation of the average flux-density value for each scan. This procedure, straightforward in theory, consists in practice of several

different operations. First of all, an **automatic quality check** has been applied to the individual sub-scans, removing the ones not matching the following standards:

1. FWHP between $450''$ and $750''$;
2. pointing offset (i.e. the offset of the Gaussian fit peak with respect to the expected source position) lower than $100''$;
3. error in the Gaussian fit estimate lower than 10% of the peak[2].

Optional condition, the comparison between the measurement of each *single sub-scan* and the *average of all the other ones* in the same scanning direction. This constrain, although potentially good for detecting anomalous jumps in the flux-density, has practically never been used because it is possibly dangerous when dealing with extremely fast variability or with faint sources for which the accuracy of the single sub-scans is low. After flagging the sub-scans not satisfying the above requirements, a weighted average is applied to the remaining ones, with a weight proportional to the inverse of the squared errors:

$$f = \frac{\sum_i f_i/(\Delta f_i)^2}{\sum_i 1/(\Delta f_i)^2} \tag{2.1}$$

$$\Delta f = \left(\sum_i 1/(\Delta f_i)^2 \right)^{1/2} \tag{2.2}$$

where f: the average flux-density
f_i: the flux-density measurement for the i-th sub-scan
Δf: the error in the average flux-density
Δf_i: the error in the flux-density measurement for the i-th sub-scan

An average FWHP and pointing offset is calculated *the same way*. This is because the sub-scans which give higher contribution to the average may also have a major influence on the pointing offset. This naturally leads to the **pointing correction**, which is described by:

$$A_{\parallel}{}^{corr} = A_{\parallel}{}^{meas} \cdot exp(4 \cdot ln2 \cdot \frac{\Delta p_{\perp}{}^2}{FP_{\perp}{}^2}) \tag{2.3}$$

where $A_{\parallel}{}^{corr}$: the corrected flux-density on scanning direction Azimuth (Elevation)
$A_{\parallel}{}^{meas}$: the measured flux-density on scanning direction Azimuth (Elevation)
$\Delta p_{\perp}$: the average pointing offset on scanning direction Elevation (Azimuth)
$FP_{\perp}$: the average FWHP on scanning direction Elevation (Azimuth)

The equation, whose meaning is illustrated in figure 2.2, assumes that the flux-density can be described by a two dimensional Gaussian profile in the azimuth-elevation space. Theoretically, in the very unfortunate case of $\Delta p \sim 100''$ – recalling that $FP \sim 600''$ – the pointing offset could be responsible for a flux-density underestimation of up to 8%; in practice, it seldomly affects the flux-density by more than $2-3\%$.

Once the data are corrected as explained above, an average flux-density for the azimuth scanning direction and one for the elevation are obtained to be averaged again with a

[2]This constrain proved to be effective in removing sub-scans for which bad atmospheric conditions, RFI or any other source of noise made the detection doubtful or particularly inaccurate.

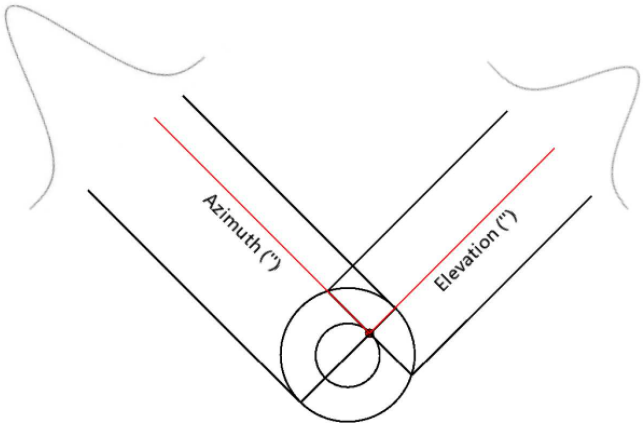

Figure 2.2: The effect of the pointing offset on the flux-density measurements. A large offset on the Elevation axis can cause a severe underestimation of the flux-density on scanning direction Azimuth.

natural weighting. This step concludes the first part of the data calibration; it allows obtaining a single flux-density measurement out of the 8 sub-scans. The procedure is automatically performed by a script called 'Redux' which we developed for the purposes of the project and which also includes the option to correct for atmospheric opacity. However, we decided to apply no such correction; first of all, because it requires the knowledge of the atmospheric temperature T_{atm}, which can not be accurately estimated. Moreover, considering that the opacity effect depends on the elevation of the observed source, it can be removed by the 'gain-elevation correction' which is the next step in the data calibration.

2.4.2 The 'Autoredux' routine

Because of their large size and inconceivable weight, the structure of radio-telescopes is subject to deformations that make the amount of radiation they collect a function of the elevation. This is called the 'gain-elevation' effect. The Urumqi antenna is optimized for maximum response at an elevation around 45°. When pointing higher or lower the gain decreases. As a consequence, following a source along its daily path in the sky the elevation dependence of the antenna gain induces variation in the measured flux-density, which can be of the order of $3 - 4\%$.

In order to remove this modulation of the flux-density – and for the correction of time-dependent effects, which will be described later on in this chapter – a significant part of the observing time has been spent in the observation of so-called 'calibrators'. The calibrators are classified in two categories:

- primary, characterized by highly stable and well known flux-density;
- secondary, whose main features are: a rather constant brightness for the typical duration of an IDV experiment (i.e. a few days at least); flux-density of the same order as the IDV sources; close proximity to IDV sources in the sky.

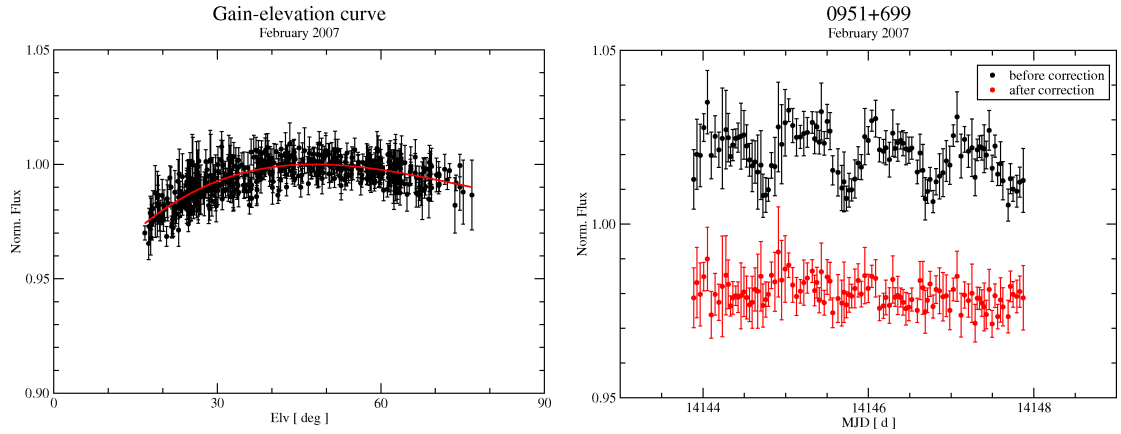

Figure 2.3: *Left panel*: the flux-density measurements of the calibrators plotted versus Elevation; a polynomial regression of the data (red curve) provides a good estimation of the gain-elevation effect. *Right panel*: the variability curve of a calibrator before (black points) and after (red points) the correction. The offset the two curves is arbitrary, for better visualization.

The primary calibrators are used for an accurate K-Jy conversion of the measurements (see Baars et al. (1977), Ott et al. (1994)). The secondary calibrators are more suitable for determining residual time-dependent effects, like changes in temperature and weather. Any source of spurious variability which affects the IDV sources should also appear in the light curves of the calibrators; for this reason, they provide a powerful tool for the correction of the data.

The gain-elevation correction, in particular, is done as follows: first of all, we plot the normalized flux-density measurements of the calibrators as a function of elevation. If we fit them via a polynomial regression, a good estimation of the average gain-elevation effect can be obtained and therefore be removed from the whole dataset (see fig. 2.3). The calculation of the gain-elevation curve from the calibrators data is automatically performed by a specific piece of software called 'Autoredux', which we developed. It allows to easily select the calibrators to be included in the calculation just by adding their names in a parameter file and to comment out the possible outliers in the data just by means of the mouse, without need of editing the ASCI data files. This considerably speeds up the operation. Therefore, it can be repeated several times, changing the list of calibrators till the best result is obtained, with very positive repercussions on the data quality. The correction of the data for the gain-elevation effect is performed by using the software 'Eff_flux', written by A. Kraus and embedded in 'Autoredux' in order to execute it automatically.

A further contribution to the variability observed in the calibrators comes from time-dependent factors. Some of them, as the temperature-induced changes in the antenna-receiver system (the day-night effect) introduce a rather regular modulation in the data; others, such as the weather conditions, determine variations which are simply unpredictable. One way for filtering them out is to estimate the average variations they produce on the secondary calibrators, parameterize them and apply the resulting correction to all the sources. That is the path we followed for our **gain-time correction**. The

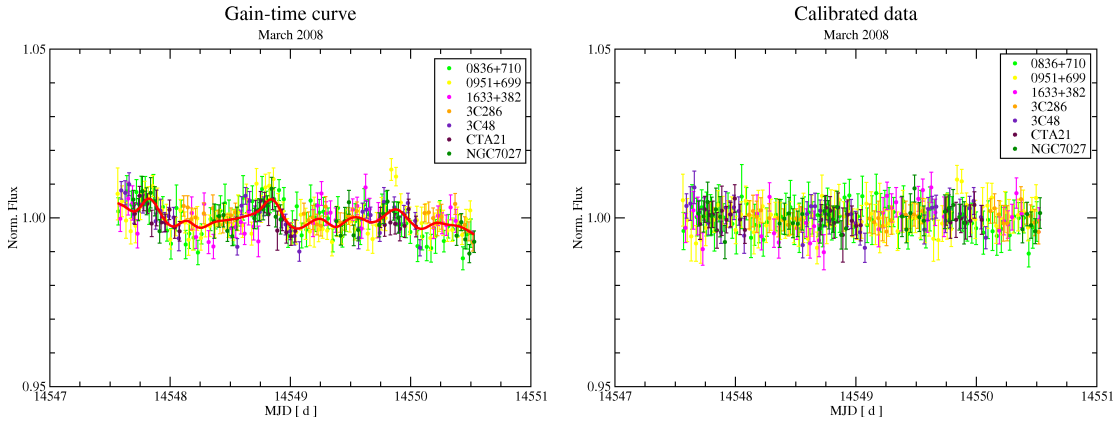

Figure 2.4: *Left panel*: the flux-density measurements of the primary and secondary calibrators plotted versus time; in red, the gain-time correction curve. *Right panel*: the variability curve of the calibrators after the correction.

parameterization of the time effect has been realized by means of the de-trending algorithm (see section 3.3), which averages the calibrators' normalized data in time bins of equal size (usually 0.08 days), fits a spline curve to the mean values and re-samples them with the time coordinates of the calibrators' scans obtaining a light curve which resembled the gain-time variability. This 'gain transfer function' is finally linearly interpolated, to provide an estimate of the gain-time variability for the data-points of all the sources (see Fig. 2.4). The division of the normalized flux-density measurements by the interpolated values completes the data correction. This procedure may sound complicated, but it is very effective. It is implemented in the 'Autoredux' code, as for the gain-elevation correction and it works in similar way: the calibrators to be used for the correction are listed in a parameter file; the outliers can be edited via a PGPLOT routine embedded in the software, so that no editing of ASCI files is needed. The linear interpolation and correction of the data is done by means of the software developed by A. Kraus, also embedded in 'Autoredux', in order to make the whole procedure very easy and fast.

The final step is the conversion of the flux-density measurements from K to Jy. The conversion factor is estimated as the average ratio of the primary calibrators' assumed flux-densities by the measured temperatures. This step is also included in 'Autoredux'. In principle, a preliminary calibration of a complete dataset can be performed within few minutes. For an accurate result, if we include also the editing of the ASCI files, one hour of work is usually enough.

Throughout all the data calibration steps the formal error propagation is done.

The data calibration procedure described above improves significantly the data quality; it guarantees a level of accuracy that, for the calibrators, is in the range between 0.2% and 0.7% of the measured flux-densities (see Fig. 2.5).

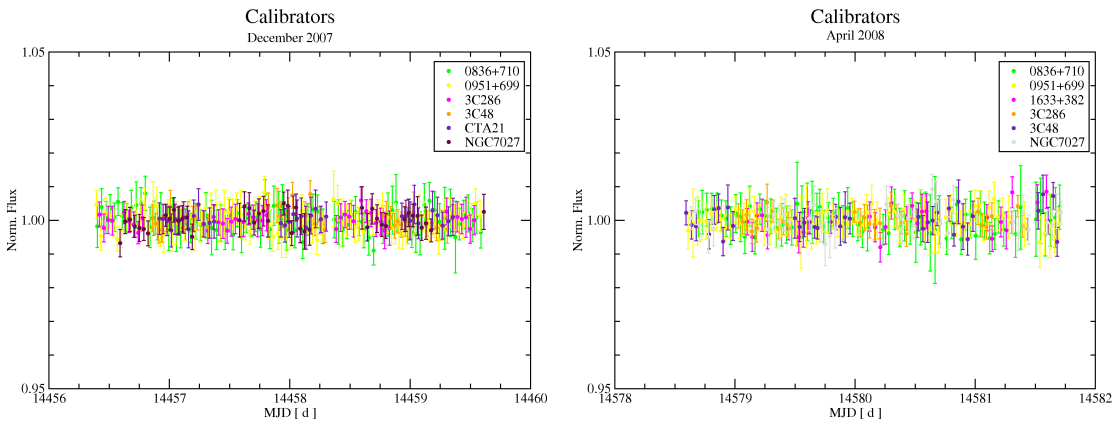

Figure 2.5: Two examples of calibrated data: the variability curves of the calibrators in December 2007 (left panel) and April 2008 (right panel). For both epochs, the residual variability is of the order of 0.3%.

Chapter 3

Time series analysis tools

The changes in the amplitudes and time scales of the variability represent the essential information for discriminating between the different models proposed to explain the IDV phenomenon. Once the data have been properly reduced and calibrated, a non-trivial part of the process is to choose the most efficient and reliable way to extract the variability characteristics. Here we try to explain the pros and cons of the standard tools of time series analysis, and the reasons why a new method has been developed and used besides the others. The reliability of the method has been checked by means of Monte Carlo simulations developed for the purpose.

3.1 The aims of the study

A fruitful discussion of the methods to be used for analyzing the data has to begin with the definition of the most relevant targets of the analysis itself.

An ISS-induced IDV is expected to be characterized by *annual modulation of the variability time scales and a rather constant variability amplitude.* The detection of clear signs of annual modulation in the time scales of a given source would be an almost unquestionable proof of the source-extrinsic origin of its variability. Unfortunately, the opposite is not always true, since erratic fluctuations of variability strength and time scales can not be unmistakably ascribed to source-intrinsic mechanisms. It would not be trivial, however, to explain the absence of annual modulation of the time scales in sources which are constantly characterized by a strong IDV activity, if we assume the variability to be induced by ISS.

Anyway, it is obvious that amplitudes and time scales of the variability provide a powerful tool for discriminating between different IDV models. Therefore, it is essential to find out which time analysis methods are most suitable for an accurate and transparent estimate of these features. Since the datasets to be analyzed do usually show variations on several time scales, it is also important that the analysis tools are able to deal with them. Finally, they should provide results with a reasonably low degree of dependence on the sampling and observation duration.

3.2 Standard tools for time series analysis

The standard approach to the evaluation of the variability characteristics in a time series is to use the modulation index m_i for the estimation of the amplitudes, while the time

scales are usually investigated by the first-order Structure Function (SF) and the Discrete Auto-Correlation Function ($DACF$).

The degree of correlation between two different data-sets is calculated by means of Cross-Correlation Function (CCF), while the existence of periodic signals in a time series is usually investigated by means of power spectrum analysis and Fourier transforms, or by periodogram. In cases of uneven sampling the standard periodogram is replaced by the modified version proposed by Lomb (1976) and extensively discussed by Scargle (1982). When applied to a stochastic signal, the same methods can also turn useful for the evaluation of the relative strength of variability components characterized by different time scales.

3.3 De-trending Function

Following the procedure presented in Villata et al. (2002) we developed an algorithm which:

- divides a variability curve in time segments of given duration (from now on, the 'bin');
- estimates the average flux-density within each bin;
- fits these averages with a spline curve.

Afterwards, if we re-sample the spline curve the same way as the original variability curve, we obtain an estimate of the variability on a time scale which is at least two times longer than the bin; from now on, we will call it the *long-term trend* in the curve. The difference between the flux-densities and the long-term trend provides the fast component of the variability – we will call it *the short-term variability*, or the 'de-trended variability curve'.

In general, the estimation of the fast and the slow variability component of a given time series is an ambiguous procedure, since it can be obtained in many different ways with different results. In our case, the change of the bin value leads to the change of the two components as well. However, if small changes of the bin induce negligible differences in the components, the use of the de-trending algorithm is rather justified.

The reasons which make this method extremely important for a successful time analysis are several and will become clear in the next chapters. The standard analysis methods mentioned above are quite sensitive to the presence of long-term trends, with the result that often the characteristics of the fast variability – the most interesting piece of information in the context of an IDV study – are either hidden or distorted. It also allows us to extract multiple time scale information using methods which are not meant for such applications.

Finally, it is necessary to underline that the algorithm does not suffer from the problems which may be expected when using a spline curve interpolation – such as the high-amplitude spurious fluctuations in correspondence to large gaps in the variability curves. This is because the spline is finally re-sampled according to the original data; in other words, it is used as a fitting instead of an interpolating procedure.

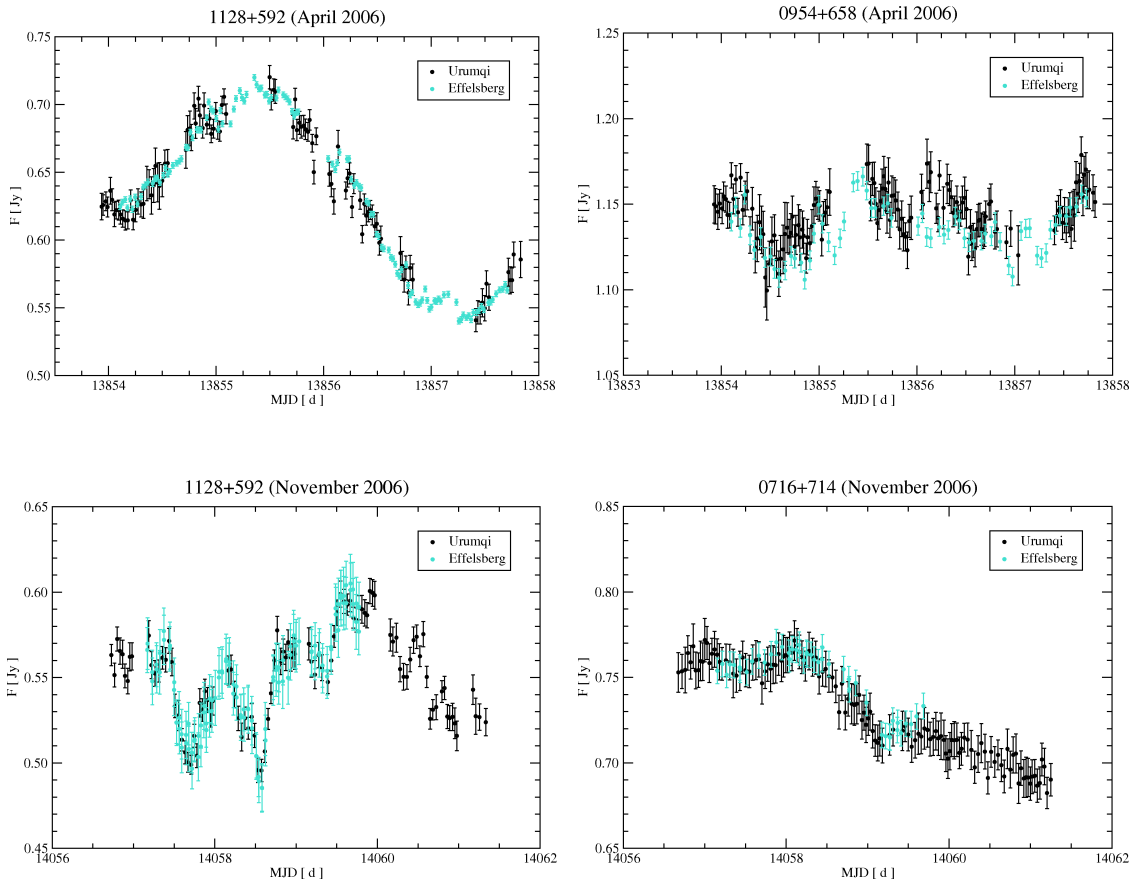

Figure 3.1: Examples of variability curves from simultaneous Urumqi (black points) and Effelsberg (turquoise points) observations. In clockwise order, starting from the upper left panel: 0954+658 (April 2006), 0716+714 (November 2006) and 1128+592 (November and April 2006) .

3.4 Modulation Index

The modulation index m_i of a time series x_i, with i=0, 1, ..., N, is given by the ratio between its standard deviation σ_x and the average flux $< x >$, expressed in percentage:

$$m_i[\%] = 100 \cdot \frac{\sigma_x}{< x >}. \tag{3.1}$$

The modulation index is possibly the most obvious way to estimate the scatter in a dataset. It does not account though for the intrinsic noise in the data (due to instrumentation, weather, etc.) which can be different from epoch to epoch. As a more uniform estimator of the variability strength, a new quantity is often used, namely the *variability amplitude*, which corrects the modulation index for the average residual noise and possibly even systematic scatter in the calibrators (m_0):

$$Y[\%] = 3\sqrt{{m_i}^2 - {m_0}^2}. \tag{3.2}$$

In order to be well defined, an estimate of the variability strength has to depend

only on the nature of the signal. Parameters like the data sampling or the observation duration should play no role in the result. An easy way to evaluate how much the m_i – and consequently the variability amplitude – varies with these features, is to apply the function to time series which are diverse realizations of the same signal differing in the sampling and the time interval they cover. The simultaneous Effelsberg-Urumqi variability curves of 0954+658 (April 2006), 0716+714 (November 2006) and 1128+592 (April and November 2006) comprise an excellent example of such realizations (see Fig. 3.1). The perfect match of the light curves ensures that they represent the same signal. The m_i has been applied to them and has been estimated over time windows which start with the first data point observed and go up to the Nth one, in order to understand if/when the function reaches a stationary value. In Fig. 3.2 and 3.3, we plotted the resulting values versus time and index, respectively.

Three major conclusions arise from these plots:

- **The role of the slow variability:** in order to be considered stationary, a time series has to cover a time interval much longer than the lowest time scale present in the data. If a time series is not stationary, its standard deviation – and consequently the modulation index – does not converge. This can be clearly seen in the upper-left panels of Fig. 3.2 and 3.3. A direct and serious consequence of this is the fact that the m_i of variability curves characterized by monotonically increasing/decreasing trends do not converge to a constant value (lower-right panel); therefore, the m_i has to be considered as a function of the observation duration. Moreover, a large contribution to it can come from slow variability which, strictly speaking, is not IDV.

- **The role of fast variability:** strong and fast changes in the flux density determine sudden and large variations in the m_i value (e.g. the large increase around day 5.5 in the August 2006 variability curve of 0716+714 in Fig. 3.4).

- **The role of the sampling:** the standard deviation of a time series does not preserve the time information – i.e. the standard deviation of a set of flux-density-vs-time measurements is completely determined by the flux-densities, while the time information can be completely disregarded. The upper left-panels of Fig. 3.2 and 3.3 show it clearly: the J1128+592 m_i curves of the Effelsberg and Urumqi datasets show a delay in the rising trends, due to the presence of gaps in the Urumqi observations. The two trends, however, match perfectly when plotted as functions of the index (see Fig. 3.3).

The tests demonstrate that the modulation index does not depend solely on the signal (both variability amplitude and time scales), but also on the time-sampling and the overall duration of the observations. Hence, the m_i can not be considered as a very reliable way to characterize the variability, since it does not allow a proper comparison of the results of different experiments, which may have different duration and number of data points. In the majority of cases though, it provides acceptably stable results (upper-right and lower-left panels in Fig 3.2 and 3.3). The modulation index will be often used throughout this work, but more reliable tools have to be investigated for a coherent evaluation of the variability strength in a time series.

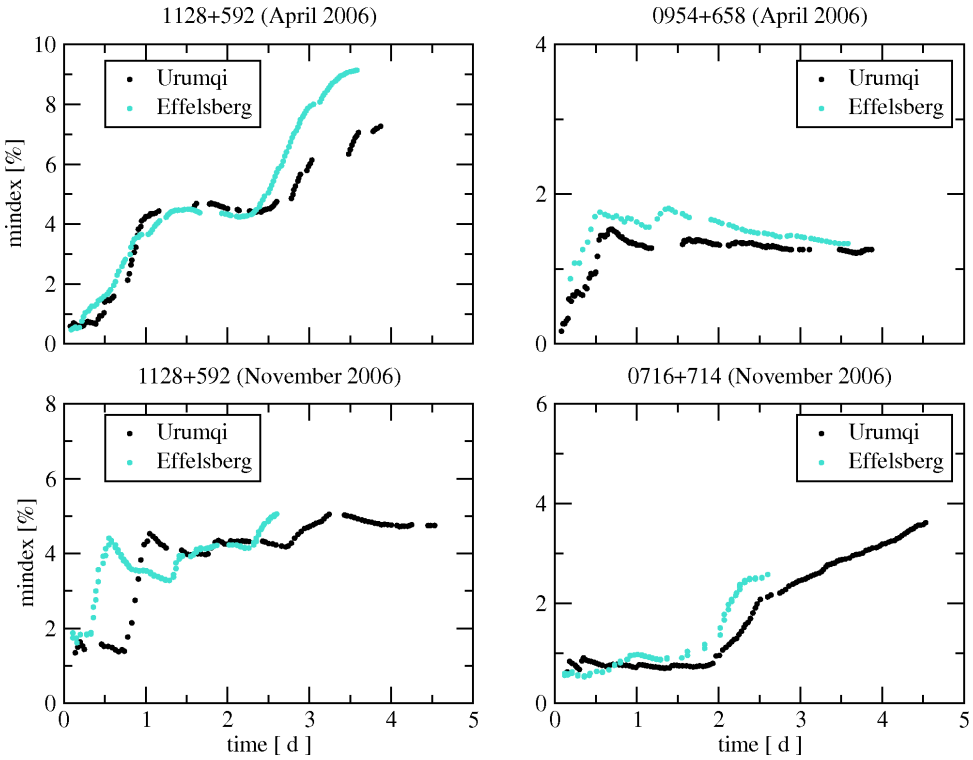

Figure 3.2: The modulation index of different variability curves estimated over time windows of the size indicated on the abscissa, starting from the first data point. The offsets between Urumqi and Effelsberg data is caused by the differences in the sampling.

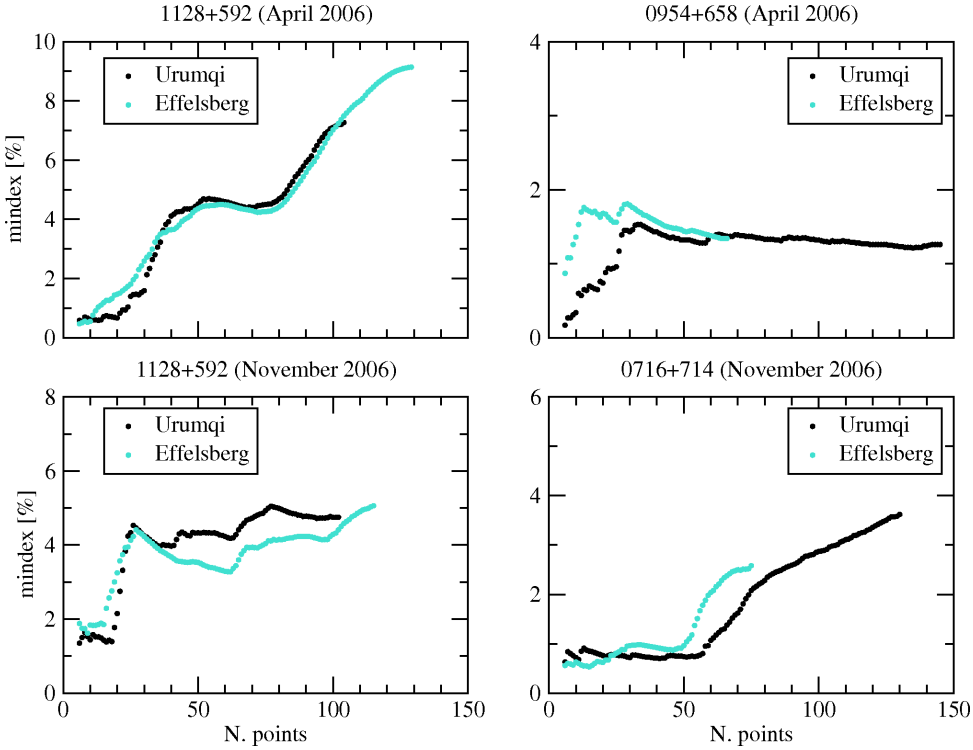

Figure 3.3: The modulation index of the same variability curves plotted in Fig. 3.2 estimated over windows containing the number of points reported on the abscissa. The offset between the Effelsberg and Urumqi variability curves of 0954+658 is due to a strong and fast variation in the flux-density which happens during the first day of observation.

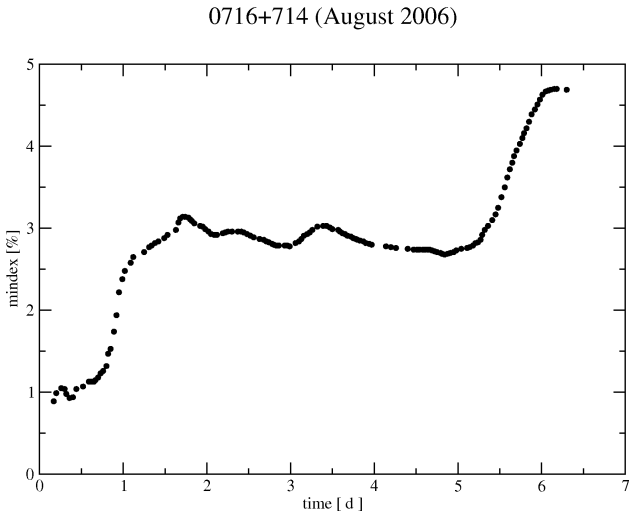

Figure 3.4: The modulation index of the August 2006 variability curve of 0716+714 evaluated over time windows of different durations. There is a large increase in the m_i during the last day of observations. The total duration of an IDV experiment can play a fundamental role in the estimated m_i value, which makes difficult to compare the results of different experiments.

3.5 Discrete Auto-Correlation Function, Cross-Correlation Function

When a signal $f(t)$ does not vary periodically, the determination of its variability time scales – if any – is usually subject to statistical tools. The *auto-correlation function* is a statistical method for estimating the time scales by calculating the average degree of correlation between all the pairs of data points $(f(t), f(t+\tau))$, for different values of the time lag τ:

$$\rho_f(\tau) =< [f(t+\tau) - \bar{f}][f(t) - \bar{f}] > . \tag{3.3}$$

In case the signal can not be described by a continuous function, but by a discrete sample of unevenly-spaced points (the time series $\{f(t_i)\}_i$) the evaluation of the correlation in the signal is often studied by means of the *Discrete AutoCorrelation Function* ($DACF$), which can be written as:

$$DACF(\tau) = \frac{1}{N\sigma^2} \sum_{ij} (f(t_i) - \bar{f})(f(t_j) - \bar{f}), \tag{3.4}$$

where σ: the standard deviation
N: the number of pairs (t_i, t_j) for which $t_i \neq t_j$ and $\tau - \frac{\Delta\tau}{2} \leq \| t_i - t_j \| \leq \tau + \frac{\Delta\tau}{2}$
$\Delta\tau$: the bin size.

The function is calculated for a discrete number of time lags τ, which are the multiples of a basic value τ_0. It is common to set $\Delta\tau$ equal to τ_0, so that every pair of points gives a contribution in the estimation of the $DACF$. The formal error in the $DACF$ is defined as:

$$\sigma_{DACF}(\tau) = \frac{1}{N-1}\Big\{\sum_{ij}[(f(t_i)-\bar{f})(f(t_j)-\bar{f}) - DACF(\tau)]^2\Big\}^{1/2}, \tag{3.5}$$

unless the values $(f(t_i)-\bar{f})(f(t_j)-\bar{f})$ falling into the same bin are strongly correlated, in which case it is necessary to substitute $(N-1)$ in the denominator with $[(N-1)(N'-1)]^{1/2}$, where N' is the number of uncorrelated couples within a bin.

The above equations can easily be modified to allow the calculation of the degree of correlation between two different sets of data. The *Cross-Correlation Function* (CCF) between two time series $\{f(t_i)\}_i$ and $\{f'(t_i)\}_i$ is given by:

$$CCF(\tau) = \frac{1}{N\sigma\cdot\sigma'}\sum_{ij}(f(t_i)-\bar{f})(f'(t_j)-\bar{f}'), \tag{3.6}$$

where σ': the standard deviation of $\{f'(t_i)\}_i$.

There is no unique way to define the characteristic time scale inferred from the $DACF$. Some authors define it as the 'first zero point' of the function, while others identify it with the lower values of τ for which $DACF(\tau) = DACF(0)\,e^{-1}$. A different approach is to determine the time scale by looking at the first minimum of the function. The difference between these definitions can sometimes be important. As long as $DACF$ is the only tool used, all the approaches can be equally valid, but when other methods are used to confirm the result, it is essential to check if the evaluation criteria are consistent. In the course of this work, the $DACF$ time scale will be inferred from the *first minimum of the function*. This will sustain the consistency between the results of the correlation function and the structure function, as it will be discussed further in the next section. Moreover, it is noteworthy that the $DACF$ version used for this project is modified with respect to the classical method. The differences are:

- the routine divides the time series in bins which have the same size of τ_0 and averages the points within each bin, providing 1 data point per bin. This way, $DACF(0)$ is always equal to 1 and the results of the analysis are not strongly influenced by large inhomogeneities in the data sampling.
- $\bar{f}$ and σ in Eq. 3.4 have been replaced by $\bar{f}_\tau$, and σ_τ, respectively, which are the average and variance of the data pairs which contribute to the time lag (see Lehar et al. (1992)). This modification helps filtering some unpleasant effects which affect the classical $DACF$, such as the tendency to show strong anti-correlations at high time lags when slow variability is present in the data.

The $DACF$ is widely used for the estimation of characteristic time scales in astronomy and can also be fruitfully utilized for detecting periodicities. It has the advantage that it is not strongly dependent on the data sampling, but also the disadvantage of a reduced capability to deal with multiple time scales – a problem common among all statistical methods that do not preserve time information.

3.6 Structure Function

The first order structure function (hereafter, simply the *Structure Function*, SF; see Simonetti et al. (1985))is probably the most popular among the methods used for time scale

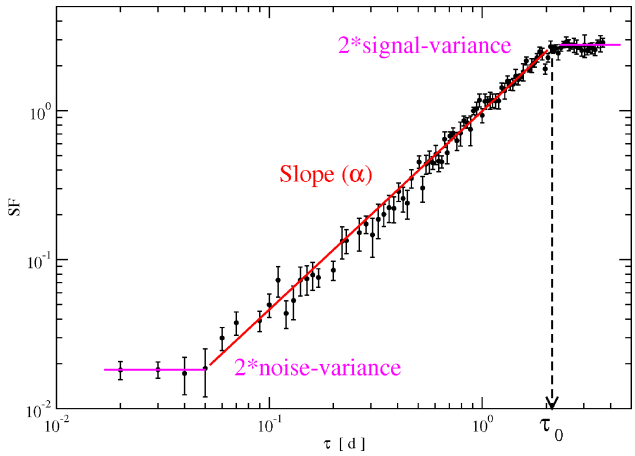

Figure 3.5: An ideal case of structure function analysis. It is possible to clearly localize both the noise variance and the signal variance level. The latter determines the plateau which allows the estimation of the characteristic time scale of the signal.

estimations. It is defined by:

$$SF(\tau) =< [f(t+\tau) - f(t)]^2 >, \tag{3.7}$$

or, in case f is represented by a time series $\{f_i\}_i$

$$SF(\tau) = \frac{1}{N}\sum_{ij}[f(t_i) - f(t_j)]^2, \tag{3.8}$$

where the sum is extended to the N pairs (t_i, t_j) for which $t_i \neq t_j$ and $\tau - \frac{\Delta\tau}{2} \leq \| t_i - t_j \| \leq \tau + \frac{\Delta\tau}{2}$. The error in the SF is given by

$$\sigma_{sf}(\tau) = \frac{1}{N-1}\sum_{ij}\{[f(t_i) - f(t_j)]^2 - SF(\tau)\}^{\frac{1}{2}}. \tag{3.9}$$

Let us consider the case of a time series which is the superposition of a generic signal and white noise. Ideally, on short time scales, the structure function of the time series will have a nearly constant value around the *noise variance* (see Fig. 3.5). For larger time scales, when the signal variability becomes dominant over the noise, the SF will show a rising trend – a power law slope, with scaling exponent varying between 0 (for white-noise-like signal) and 1 (for red-noise-like signal). At the time lag τ_0 which corresponds to the coherency time of the signal, the structure function will show a plateau. Therefore τ_0 can be considered as an estimate of the signal characteristic time scale.

It can be shown that, theoretically, SF and $DACF$ are bound by the simple equation

$$SF_f(\tau) = 2{\sigma_f}^2[1 - DACF_f(\tau)]. \tag{3.10}$$

Practically, sampling effects and/or a non-stationary signal makes this equation less strict, therefore the results provided by SF and $DACF$ can not be considered perfectly equiva-

lent. Nevertheless, an important consequence of the equation above is that *the plateau of a structure function – corresponding to a local maximum – is equivalent to a minimum of the discrete autocorrelation function.* This justifies the choice of defining the $DACF$ time scale as the point of the first (relevant) minimum in the function.

As for the $DACF$, also the structure function owes probably its popularity to the modest sensitivity to the data sampling – an important advantage in dealing with astronomical data. Additionally, through the power law slope, it also provides information about the nature of the signal. The SF, though, is less efficient than the $DACF$ in revealing weak periodicities hidden in the data and suffers the same limitations when the signal consists of a superposition of two or more time scales.

3.7 Lomb-Scargle Periodogram

The classical periodogram is a function defined by:

$$P_f(\omega) = \frac{1}{N} \mid FT_f(\omega) \mid^2. \tag{3.11}$$

where ω: the pulse angular frequency
FT: the Discrete Fourier Transform of the time series $\{f_i\}_i$
It can also be expressed written as:

$$P_f(\omega) = \frac{1}{N}\Big[\big(\sum_i f(t_i)cos(\omega t_i)\big)^2 + \big(\sum_i f(t_i)sin(\omega t_i)\big)^2\Big]. \tag{3.12}$$

Given a series of N terms, there are N/2 values $P_f(\omega_j)$ which are independent – half of the information contained in the series is lost (see Scargle (1982), Appendix D). It is a convention to compute the periodogram for a set of frequencies spreading from $\frac{1}{T}$ to $\frac{N}{2T}$, where T is the maximum time interval of the series; $\frac{N}{2T}$ is called *the Nyquist frequency*, and represents the maximum frequency for which it is possible to extract meaningful information from a N-term time series of an overall duration T.

The periodogram is a powerful tool for the detection of periodic or quasi-periodic components in a signal but it strongly depends on the data sampling. A modified version of the algorithm, suitable for unevenly sampled data, has been proposed by Lomb (1976) and improved by Scargle (1982) . It is known as the Lomb-Scargle periodogram, and is defined as follows:

$$P_f(\omega) = \frac{1}{2}\left\{\frac{\Big[\sum_i f(t_i)cos\omega(t_i-\tau)\Big]^2}{\sum_i cos^2\omega(t_i-\tau)} + \frac{\Big[\sum_i f(t_i)sin\omega(t_i-\tau)\Big]^2}{\sum_i sin^2\omega(t_i-\tau)}\right\}, \tag{3.13}$$

where τ is defined as the value for which $tan(2\omega\tau) = \frac{\sum_i sin(2\omega t_i)}{\sum_i cos(2\omega t_i)}$. $P_f(\omega)/\sigma^2$, known as the Lomb-Scargle normalized periodogram (see Press and Rybicki (1989)), defines the version of the algorithm we used for our study.

The modification of the classical formula leads to some improvement in the sampling dependence of the periodogram and has significant effect in the estimation of the false-alarm probability. Given a pure-noise signal, the probability of finding a value of the periodogram z between z_0 and $z_0 + dz$ is:

$$p_z(z_0)dz = Prob(z_0 < z < z_0 + dz) = exp^{-z_0}dz. \tag{3.14}$$

This equation, which for a classical periodogram can not be used in the case of uneven sampling, is instead valid for the Long-Scargle algorithm. Hence, it allows the calculation of the probability that a periodogram value z_0 hides a false-alarm detection, as follows:

$$p(z_0) = 1 - (1 - e^{-z_0})^n, \tag{3.15}$$

where n is the number of investigated frequencies. Unfortunately, the formula strictly describes the case of false alarms due to white-noise. When red-noise is present, the probability distribution of the periodogram values can not be expressed as in equation 3.15 anymore, as the false alarm probability becomes a function of ω.

Along with the frequency, the periodogram is also able to reconstruct information about the amplitude and phase of a periodic signal. This can easily be demonstrated in the case of the classical formula. If we consider a time series $X_i = X_0 \cdot cos(\omega t_i + \phi)$, for i=1, 2, ..., n, following equation 4.11, the periodogram at angular frequency ω will be:

$$P_f(\omega) = \frac{1}{N}\Big[\big(\sum_i X_0 cos(\omega t_i + \phi) cos(\omega t_i)\big)^2 + \big(\sum_i X_0 cos(\omega t_i + \phi) sin(\omega t_i)\big)^2\Big] \tag{3.16}$$

which, with the help of elementary trigonometric formulae, can be re-written as:

$$\begin{aligned} P_f(\omega) = \frac{1}{N}\Big[&\big(\sum_i X_0 (cos^2(\omega t_i) cos(\phi) + sin(\omega t_i) cos(\omega t_i) sin(\phi))\big)^2 \\ &+ \big(\sum_i X_0 (cos(\omega t_i) sin(\omega t_i) cos(\phi) - sin^2(\omega t_i) sin(\phi))\big)^2\Big] \end{aligned} \tag{3.17}$$

$$\simeq \frac{1}{N}\Big[\big(\sum_i X_0 cos^2(\omega t_i) cos(\phi)\big)^2 + \big(\sum_i X_0 sin^2(\omega t_i) sin(\phi)\big)^2\Big] \tag{3.18}$$

$$= \frac{1}{N}\Big[\big(X_0 cos(\phi) \sum_i cos^2(\omega t_i)\big)^2 + \big(X_0 sin(\phi) \sum_i sin^2(\omega t_i)\big)^2\Big]. \tag{3.19}$$

The terms with products of sine and cosine, in the first equation, have an average value of zero, so they should give no contribution if the period is short enough – compared to the total length of the time series – and the sampling is dense. In this case the terms $\sum_i cos^2(\omega t_i)$ and $\sum_i sin^2(\omega t_i)$ should both converge to N times the average value 0.5. Therefore:

$$P_f(\omega) \simeq \frac{N {X_0}^2}{4}\big(sin^2(\phi) + cos^2(\phi)\big), \tag{3.20}$$

which, of course, is equal to $\frac{N {X_0}^2}{4}$. The amplitude of the sinusoidal signal can be estimated as:

$$X_0 \simeq 2\sqrt{\frac{P_f(\omega)}{N}}. \tag{3.21}$$

Still, in the case of short period and dense sampling, it is easy to reconstruct information about the phase of the periodical signal, using the ratio between the two quadratic terms on the right-hand part of equation 4.15:

$$R(\omega) = \frac{\left(\sum_i X_0 cos(\omega t_i + \phi) cos(\omega t_i)\right)^2}{\left(\sum_i X_0 cos(\omega t_i + \phi) sin(\omega t_i)\right)^2} \tag{3.22}$$

$$\simeq \frac{\left(\sum_i X_0 cos^2(\omega t_i) cos(\phi)\right)^2}{\left(\sum_i X_0 sin^2(\omega t_i) sin(\phi)\right)^2} \tag{3.23}$$

$$= \frac{cos^2(\phi)}{sin^2(\phi)} \tag{3.24}$$

$$= cot^2(\phi), \tag{3.25}$$

which leads immediately to the estimate of the angle ϕ as the arccot of $\sqrt{R(\omega)}$.

3.8 The Sinusoidal Regression

Formally, the periodogram analysis is equivalent to least-squares fitting of sinusoids to the data. The sampling rate, though, can cause this statement to be less solid; a comparison with a real least-squares fitting function may turn useful for testing the results. For this reason, besides the classical time series analysis methods described above, we implemented two algorithms which fit sinusoidal waves of different amplitudes, frequency and phase-shifts to the given time series $\{f(t_i)\}_i$, evaluating the most important time scale according to different criteria. From now on, we will refer to both of them as the *Sinusoidal Regression* (SR). The two algorithms, which will be described in the next section, lead to slightly different results, providing a useful comparison tool.

The procedure for estimating the most prominent period in a time series can be repeated iteratively: once we subtract the 'best sinusoid' to the signal, we can fit the residuals in a similar way, till the standard deviation approaches the noise level. For each iteration, the SR provides four pieces of information:

- the *amplitude* of the best fit sinusoid
- its *frequency*
- its *phase-shift*
- an estimate of the significance of the detected period in the overall signal (hereafter, simply the *significance*)

The significance of the period is defined by:

$$R_f = 100 \cdot \frac{var_a - var_b}{var_a}, \tag{3.26}$$

where var_a: the signal variance
var_b: the residual variance after subtracting the sinusoid

Therefore R_f represents the fraction of variance of the periodic component to the total signal, in percentage.

There has been a very strong assumption implied in the use of a 'periodicity detector' in the analysis of a generic variability curve: *the characteristic time scale is identified*

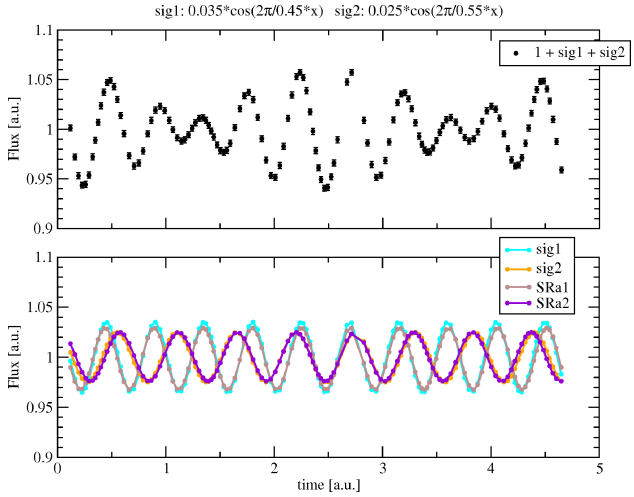

Figure 3.6: Example of a superposition of two periodic signals. The SR analysis allows to recover both of them with fairly good accuracy.

with the period of a sinusoidal wave – or, less strictly, the signal can be described, in first approximation, as the superposition of sinusoidal components. The concept is definitively not new, being the fundamental idea at the base of the Fourier analysis, but the fact that *any* signal can be interpreted as the superposition of sines and cosines does not necessarily attribute a physical meaning to the inferred periods. The question is – and will remain – open and there is no definitive answer to it. Below are presented the main arguments for which, eventually, SR and periodogram have been widely used in the estimation of the time scales in a variability curve:

- the concept of *characteristic time scale* is quite nebulous – still no rigorous definition exists for it; each time-analysis method provides its own formula for its evaluation, with results which can appear extremely inhomogeneous. The SR/periodogram approach gives the time scale a clear meaning: it is the most prominent period in the data. Given the fact that the resulting sinusoid is determined in frequency, amplitude and phase, it can always be compared to the data, in order to check the consistency between the periodic modulation and the fitted signal.

- The presence of multiple time scales can be immediately and unambiguously handled by the functions as some simple tests can demonstrate. Problems can arise when the analyzed signal consists of a superposition of sinusoids with similar amplitudes and frequencies, leading to the appearance of beats, but also in this case important piece of information about the original signal can be reconstructed (see fig. 3.6); other analysis tools, generally, do not perform equally well.

- The ability of the functions to find strictly periodic components turns out to be extremely useful in finding out and removing any residual variability that is of systematic nature, such as gain-elevation or day-night (see fig. 3.7). This is a great advantage on the SF and $DACF$, for which the contribution of small, but not negligible, spurious periodic components can significantly change the estimation of the

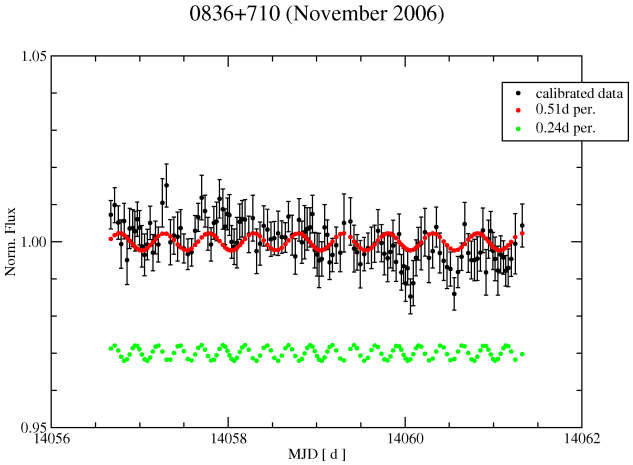

Figure 3.7: The SR analysis for the data of a calibrator. The method is able to detect residuals of spurious variability with very low amplitude. Their removal improves the results of the time analysis of the data.

time scales, in unpredictable ways.

- SR and periodogram provide an alternative for evaluating the variability strength, by means of the amplitudes of the best-fit sine waves. These amplitudes depend neither on sampling (unless the data are affected by large frequent gaps; but this is not our case), nor on duration.

- Last, but not least, any detection of strictly periodic components in the variability of an intraday variable source would be an important discovery, with relevant implications for all the variability models attempting its explanation.

The arguments presented above, all together, can assist understanding the reasons why the main role in the data analysis has been played by a techniques like SR; the most convincing argument comes though directly from its application to the datasets.

3.8.1 The algorithms

The first SR algorithm we implemented is nothing but than a least-squares cosine fit ($LSCF$). It generates a number $N_a \cdot N_f \cdot N_\phi$ of sinusoidal waves – where N_a, N_f and N_{phi} are, respectively, the numbers of evenly separated amplitudes, frequencies and phases. The main difference from a standard periodogram is the possibility of shifting the time series average over a given range of values. This peculiarity minimizes the effect of a bad sampling on variability curves which present long-term trends – a case that the periodogram difficultly handles. The amplitude ranges between $\frac{A}{N_a}$ and A (being A the peak-to-peak flux-density difference in the light curve); the frequencies run from $\frac{1}{n}$ to $\frac{2T}{3}$ (where n is the number of points in the curve, T is the total duration of the observations[1]). The phase

[1]For the case of long-term trend in the data, an option for extending the maximum investigated period to $2 \cdot T$ as been implemented

range runs from 0 to 2π. The criterion for the best fit to the data is the minimization of the χ^2.

The method turned out to be extremely effective in detecting periods in noisy data as will be discussed in more details in section 3.9. It is clear however, that in order to have enough amplitude, frequency and phase resolution, high values of N_a, N_f, N_ϕ are needed, making the algorithm rather slow. The execution of the calculations can be speeded up by sacrificing amplitude and/or angular-phase resolution. If we keep high the number of investigated frequencies, we do not lose the most important piece of information, which is the time scale. However, this solution is not optimal, because a poor resolution (e.g. in angular-phase) can decrease the capability of the function to find weak periodicities. This issue led to the development of the second version of the sinusoidal regression (hereafter, *SRb*).

The *SRb* generates a number of sinusoidal waves with N_f and N_ϕ different frequencies and angular-phases as the *LSCF* does. Contrary to this, the former has *fixed amplitude*. In order to explain how exactly the algorithm works, it is necessary to develop some equations.

Let us consider a signal which is given by the superposition of a stochastic component $X(t)$, and a periodic component $A\,sin(\omega t + \phi)$. A n-point sample of the signal can be expressed as:

$$\{W_i\}_i = \{X(t_i) + Asin(\omega t_i + \phi)\}_i. \tag{3.27}$$

The product of the time series $\{W_i\}_i$ with a sample function $\{V_i\}_i = \{A'sin(\omega' t_i + \phi')\}_i$ will be:

$$W \cdot V = \sum_i \Big[\big(X(t_i) + Asin(\omega t_i + \phi)\big) \cdot A'sin(\omega' t_i + \phi')\Big]. \tag{3.28}$$

If V and X are uncorrelated and if the time series has enough data-points, the first term on the right-hand side of the equation gives a contribution close to 0:

$$\sum_i \Big[A'sin(\omega' t_i + \phi') \cdot X(t_i)\Big] \approx 0 \tag{3.29}$$

and then equation 3.28 can be written as

$$W \cdot V \sim \sum_i \Big[Asin(\omega t_i + \phi) \cdot A'sin(\omega' t_i + \phi')\Big]. \tag{3.30}$$

It is straightforward then to define a new way of determining which sinusoidal wave V_b fits the data better. The product $W \cdot V$ is in fact maximum for values of ω' and ϕ' which approximate ω and ϕ best; for such values, the previous equation can be written as:

$$W \cdot V_b \approx \sum_i \Big[A \cdot A'sin^2(\omega' t_i + \phi')\Big]. \tag{3.31}$$

It is worth to note that *the maximization of the function does not depend on the product* $A \cdot A'$ which can be moved out of the sum. For this reason, an arbitrary value can be assigned to A' – it is not a **variable** anymore, but a **parameter**. This way, the estimation of the best fit speeds up remarkably, without losing resolution. The information about the

amplitude of the best-fit sine wave can be immediately reconstructed, as follows:

$$A = \frac{W \cdot V_b}{A' \sum_i \left(sin^2(\omega' t_i + \phi')\right)}. \tag{3.32}$$

This concludes the formal exposition of the SR algorithms. The next step is to determine how efficient is the function in its two different versions and how reliable are the results – which, in turn, should be compared to what the periodogram returns.

3.9 Monte Carlo simulations, testing the reliability of the methods

In order to investigate the weaknesses and the strengths of the algorithms, we are going to use for our data analysis, we developed a piece of software which simulates stochastic signals, by the superposition of 1000 sinusoidal waves S_n, with frequency ν_n and amplitude $A_n \propto Const^{-\alpha\nu_n}$. The slope α is generated randomly, with uniform distribution, in the range [0 - 1] (i.e., the signal is in between white and brown noise). A synthetic variability curve $\{N_i\}_i$ is produced by sampling the signal the same way as a real light curve – in order to account for possible sampling effects. A second curve $\{P_i\}_i$ is produced by summing up the stochastic signal and a periodic component, with randomly generated amplitude, frequency and phase-shift. The two curves are then analyzed by means of $LSCF$, SRb, and the Lomb-Scargle periodogram. Aim of the simulations is to study how the methods respond to stochastic and periodic signals.

Two sets of time-series have been generated, counting respectively 2000 and 10000 curves – the first one for comparing the efficiency of $LSCF$ and SRb, the second one, which excludes the time-consuming computation of $LSCF$, for comparing SRb and the periodogram. A periodic signal has been successfully detected when $\mid \nu_{det} - \nu_{sig} \mid < 0.1 \cdot \nu_{sig}$ (with ν_{det} the detected frequency and ν_{sig} the frequency of the periodicity), and $\mid \phi_{det} - \phi_{sig} \mid < \frac{\pi}{3}$. No constrain has been put to the amplitude estimate – which is more sensitive to the features of the underlying noise. For a more accurate evaluation of the frequency by means of the periodogram, the number of checked frequencies has been extended to $2 \cdot N$, i.e. oversampled by a factor of 4.

The main results of the test are:

- The three tools are almost equally effective in finding periodicities. The function $LSCF$ counted 80.8% of detections, SRb 80.4% and the periodogram 80.1%. The comparable efficiency of the first and third algorithm was expected by theoretical arguments, since they are formally similar. Concerning the SRb algorithm, which is different, it is important to note that the increase in the computational speed led to no loss of efficiency. If we compare the $LSCF$ and SRb results, it is remarkable that SRb is more precise in estimating amplitudes and phases for high-frequency waves, while $LSCF$ resulted more accurate for low-frequency waves. Consequently, during the data analysis, we will make use of the algorithm which has higher chances to provide the most accurate result, according to the variability characteristics of the datasets.

- The amplitude of the real sinusoid is reconstructed with similar accuracy by the three methods. In 95% of the cases (considering the detections only), the difference

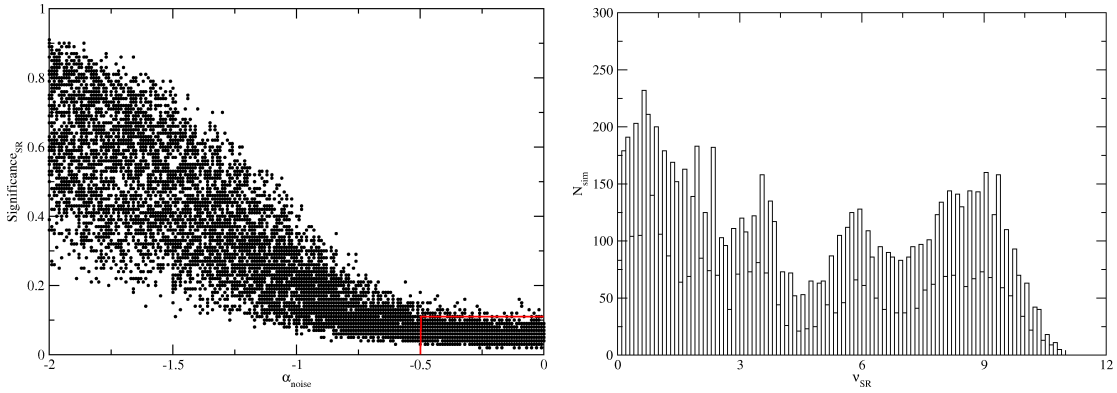

Figure 3.8: SR analysis of 10000 datasets generated through Monte Carlo simulations. For each dataset, the variability is purely stochastic and the sampling is extrapolated from a real light curve. *Left panel*: if we plot the significance of the most prominent sinusoidal waves detected in the synthetic light curves versus the slope α, we can see that, for white/flicker noise ($\alpha < 0.5$), in 95% of the case the significance remains below below the limit of 9%. *Right panel*: the histogram of the time scales detected in the synthetic light curves; the short time scales appear preponderant, which is probably due to the fact that their contribution can be strong for any value of α, while the longest time scales become important only when $\alpha \leq 1.0$. Apart from that, the distribution is rather homogeneous, which demonstrates that the SR is not strongly biased by sampling or duration effects.

between real and estimated wave amplitude is within 20% of the real amplitude. This result give us the chance to provide an error estimation in the computed amplitudes.

- For 95% of the detected sinusoids, the error in the estimation of the phase-shift turns out to be smaller than $\frac{\pi}{5}$. We can use the result for determining a 'standard error' in the evaluation of ϕ for the real data.

- After applying the functions to the purely stochastic signals, three main findings have to be mentioned. First: the estimator of false periodic detections provided by the periodogram is not effective – in almost all of the supposed periods, it claimed a false-alarm probability under 5%! This result just confirms what was anticipated above: the formula is not valid when dealing with brown/red noise. Second: when the SR points out a periodicity in a purely stochastic signal, its significance (equation 3.26) depends on the colour of the noise. In particular, for noise in between white and flicker, the significance is usually lower than 9% (see Fig. 3.8, left panel). This suggests that, when using the function with real data, detections with significance below this limit should be regarded as marginal. Third: the false periods that the SR pointed out are reasonably well spread among all the investigated frequencies, without any suspicious concentration of values around a single frequency. This means that there is no observable sampling/duration effect.

3.10 An actual example

At the end of the current chapter, it may be useful to present an actual example for explaining how precisely the time information can be extracted from a variability curve.

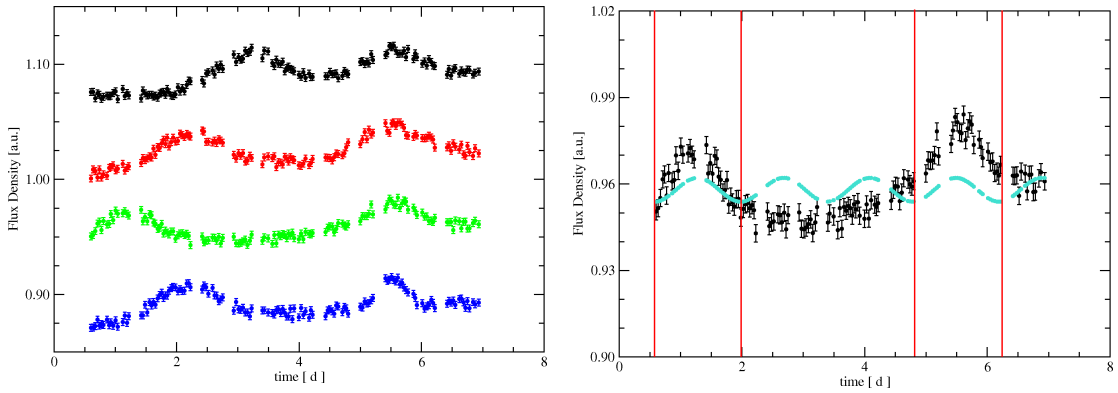

Figure 3.9: *Left panel*: the synthetic variability curves generated using the parameters in Table 3.1. *Right panel*: one of the synthetic light curves (black points) is plotted along with the sinusoidal signal detected via SR (turquoise points), which seems to evaluate quite well the duration of the flares.

It is straightforward that, in case of periodic/quasi-periodic signal in the data, the most useful tool for its detection is the SR or the periodogram. It is obvious as well that when a variability curve shows a single 'flaring event', structure function and $DACF$ provide the most reasonable way for estimating the time scale. The question then, is what kind of information can be reconstructed in a more complex situation. It is interesting to investigate, for example, how the different methods respond to a case that is just one step beyond the previous – two flaring events, separated by random time, in a variability curve (see Fig. 3.9). The case has been analyzed by simulating curves as a superposition of white noise, a long-term trend (linear increase of the flux-density) and two flares, with Gaussian shape. Two kinds of time information are contained in the curves: the separation between the peaks (pk) and the average coherence time (the rising-falling time of the flares, $\bar{\tau}$). The estimation of a coherence time via SR can be obtained by dividing by 2 the corresponding period. The estimation of the peaks separation via SF ($DACF$) is done by looking at the first strong minimum (maximum) in the function plot (see Fig. 3.10).

Four variability curves have been generated. The main parameters are reported in Table 3.1: the peaks separation (column 1), the coherence time of the first (column 2) and of the second peak (column 3). In the columns from 4 to 9 we present the two dominant time scales provided by SF (col. 4 and 5), $DACF$ (col. 6 and 7) and SR (col. 8 and 9).

All the methods are able to determine, with reasonable approximation, the separation between the peaks. It is worth to note that τ_{SF} and τ_{DACF} are characterized by values which are much higher than the effective coherence-time. The reason is that SF and $DACF$ tend to identify the characteristic time scale with the min-to-max separation. As far as the ratio between τ_{SF} (τ_{DACF}) and $\bar{\tau}$ remains constant, this should not be considered a problem. The third example, though, shows that the estimated coherence time does sometimes depend on the peaks separation. It may be surprising, on the other hand, that the SR is able to recover $\bar{\tau}$ with good accuracy. It can be explained by considering that the function recognizes the time scales as the periods which carry the most of the variance. Therefore, for isolated flares, the most of the variance is in the short time scales (see fig. 3.9, right panel). Finally, it has to be underlined that none of the tools found

Table 3.1: The time scales provided by SF, $DACF$ and SR analyses (column 4-9) of the synthetic light curves, compared to the real time scales (columns 1-3), which are the peaks separation (col. 1), and the coherence times of the two flares (col. 2 and 3). The methods show an acceptable capability to recover the time scales.

signal			SF		$DACF$		SR	
pk	τ_1	τ_2	pk	τ_{SF}	pk	τ_{DACF}	pk	τ_{SR}
2.3	0.70	0.70	2.7	1.6	2.7	1.5	3.0	0.9
3.3	0.70	0.70	3.3	1.3	3.4	1.7	3.2	0.8
4.3	0.70	0.70	4.6	2.2	4.4	2.7	4.2	0.7
3.3	0.70	0.35	3.3	1.3	3.4	1.6	3.3	0.8

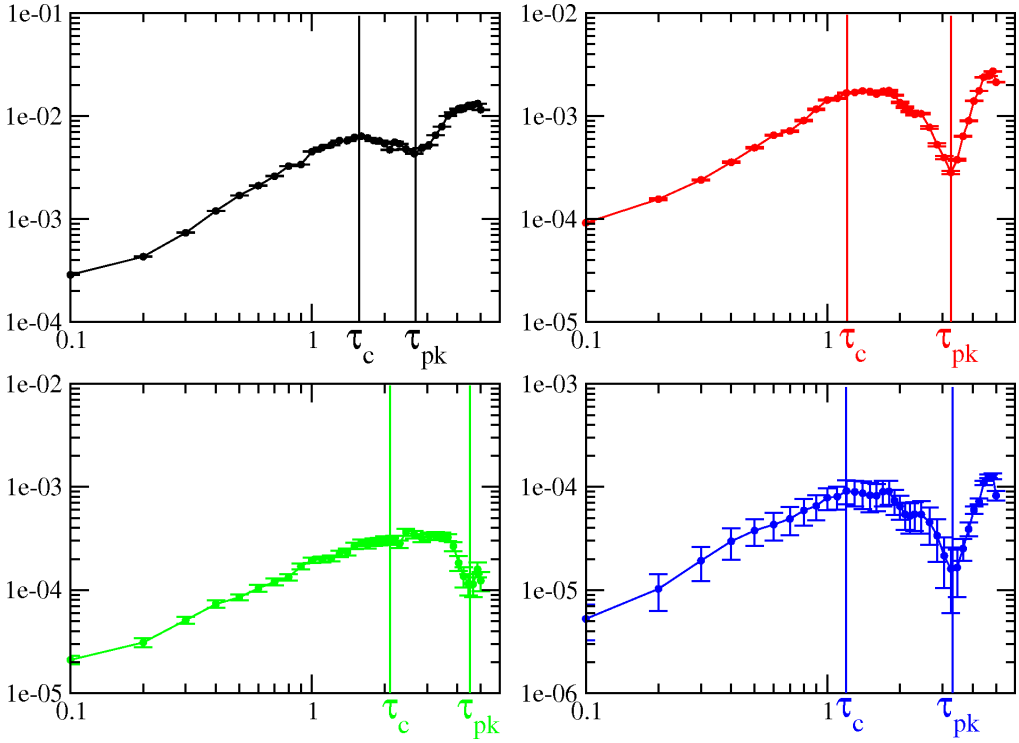

Figure 3.10: Structure function analysis of the synthetic light curves plotted in Fig. 3.9. Two different time scales can be recovered: the coherency time (from the plateau), and the peak-to-peak separation (from the first deep minima).

any difference between the second and fourth variability curve, characterized by different coherence times for the two flares.

3.11 Notes about the standard time analysis procedure

All the methods described above will be used for the time analysis of the variability curves.

The de-trending algorithm will be applied whenever a clear distinction between a slow and a fast component is possible. The separate analysis of the two does usually allow a much more accurate evaluation of the variability characteristics.

SR and periodogram provide the same kind of information; due to a more flexible code,

and a straightforward way of evaluating the significance of the signal, SR will be the main tool, while the periodogram will be called to confirm/discard the results. Their ability to estimate multiple time scales will be capitalized for checking whether it is possible to trace the behaviour of single variability components across the epochs.

Finally, SF and $DACF$ are both suitable for evaluating a single time scale for a dataset. On the one hand, this represent a loss of information with regard to the SR results; on the other, it allows an easier interpretation of the variability evolution. The use of SF and $DACF$ is also important as a trait-d'union with previous IDV studies, which usually did not distinguish between different variability components, and were only making use of these methods for their time series analysis.

Chapter 4

Periodic variability in the light curves: I. Main Findings

The efforts put in removing the known sources of noise from the data ensure an accuracy which is amazing for a relatively small antenna such as the Urumqi one. After the calibration, the modulation index of primary and secondary calibrators is generally between 0.2% and 0.7% .

Despite these flattering results, it turns out that **several data-sets are characterized by the presence of a daily-periodic variability component, with a peak-to-peak amplitude ranging from 1-2% up to almost 20%! The periodicity** – this is an essential point – **only affects the variability curves of IDV sources, being negligible in the calibrators**. We investigated the nature of this contribution as thoroughly as possible, with the results of the investigation being at the focus of chapters 4 and 5. Below we discuss the essential characteristics of the effect. In the next chapter, we present other aspects of the variability – which are either supported by weaker evidence or appear less important for the interpretation of the phenomenon – and we propose a possible explanation.

It is reasonable to expect that the periodicity can not be classified as a proper IDV phenomenon. Therefore, for a rigorous IDV study it is essential to remove such a component, in order to reach a correct estimation of the variability parameters. On the one hand, the regular character of the contribution is an advantage for the data analyzer, because it is more easily recognizable than a stochastic noise; on the other hand, if not detected, it may cause a severe distortion of the data, due to the introduction of a regular time scale which has many chances to be mistakenly identified as *the* time scale of the variability. The nature of this periodic component itself is a puzzle which seems to have extremely important implications.

4.1 The periods

The existence of a regular pattern in the Urumqi data was identified for the first time in August 2006 in the data of 0716+714 (see fig. 4.1). After separating the long from the short time scale variability by means of the de-trending function, the fast component was found to show maxima and minima regularly separated in time. A periodogram analysis of this signal identified two dominant frequencies, $1.0\,\mathrm{d}^{-1}$ and $2.0\,\mathrm{d}^{-1}$, corresponding, obviously, to 24-hour and 12-hour periods.

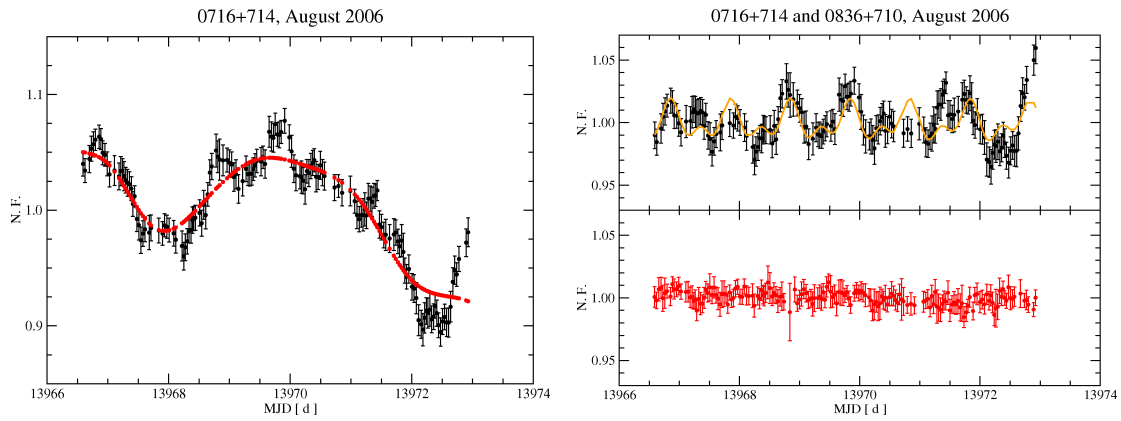

Figure 4.1: *Left figure*: the August 2006 variability curve of 0716+714 and its long-term trend (red curve). *Right figure*: The de-trended 0716+714 variability curve (upper panel), along with its periodic component (orange curve). In the lower panel, the variability curve of the calibrator 0836+710.

The identification of the modulation origin is a challenging task. In principle, all the effects discussed in chapter 2 – pointing offset, gain-elevation, day-night effect – can introduce 24-hour and 12-hour periodic modulations. At first glance, the 24-h period could be ascribed to the regular variations of the parameters on which each effect depends (note that also the pointing offsets follow a 1-day regular pattern). The 12-h period could be due to the ~ 0.5 d separation of the gain-elevation peaks, or be considered as a second-order contribution of the day-night or pointing effect. It is intuitive, in fact, that a non-sinusoidal periodic signal can be described at best as a superposition of harmonics. In order to preserve the signal symmetry, these harmonics have to be characterized by a *well defined phase correlation*[1].

To begin with, the most obvious hypothesis would be to consider the two periods as harmonic components of the same origin – possibly caused by a wrong correction of the known effects. In order to confirm it, the most direct approach is to check if the two periods have the expected phase correlation ('in-phase') or no ('out-of-phase'). For this purpose we need a time analysis method which can provide information about both the frequency and the phase of the signal. The tool we utilized is the *sinusoidal regression function.*

Our approach to the problem is straightforward: *for all the epochs in which the effect has been detected* (i.e., whenever clear periods between 0.95 d and 1.05 d or 0.48 d and 0.52 d have been found) we analyzed the calibrated data of the observed objects by means of sinusoidal regression. In order to determine a precise phase relation between the different curves, 1.000 d (0.500 d) sinusoidal signals were fitted to the variability curves, obtaining an estimate for the best amplitude and phase [2].

The main findings of this investigation can be summarized as follows:

- The 0.5-d period seems to be elevation-dependent: the flux-density minima are usu-

[1]Specifically, the second harmonic peaks have to correspond either to a maximum or to a minimum of the first harmonic; a similar behaviour is also expected for the higher order harmonics.

[2]Due to the short duration of the observations, the difference between the best-period sinusoid and the fitted 1.000 d (0.500 d) is generally negligible.

ally close to the elevation maxima and minima – the peaks happen in correspondence to the crossing of the 40 °-elevation.

- The 1.0-d period shows a correlation with the elevation as well, though not so strict. The flux-density peaks fall often close to the elevation maxima, but delays up to 6 h have been observed between them; in two cases (November 2006, July 2007), the flux-densities turned out to peak close to the minima in elevation. The correlation, we shall conclude, is loose, and difficult to decipher. Given the importance of the issue, a deeper investigation in unavoidable: the whole section 4.6 will be devoted to this point.
- Periods of 0.33 d are also frequently present in the data, often stronger in amplitude than the 0.5-d period.

Concerning the question of whether the periodicities are correlated or not, the results do not lead to a solid answer. The signals are mostly out-of-phase, which suggests that the periods can not be identified with different harmonics of a same signal. Still it may well be that they represent different manifestations of the same phenomenon. We will return to this topic in section 5.3, after a deeper investigation of the 1.0-d period – which, among others, is by far the strongest.

4.2 Recurrence of the 1d-periodicity in the Urumqi data

Strong evidence for 1-d periodic variability with amplitude of a few percent have been found in 35 curves of IDV sources out of 86. In Table 4.1, we reported a list of all the performed observations, with the corresponding day of the year (DoY). For each of the main targets of our monitoring program, we marked the affected epochs with a number which is a conservative estimate of the amplitude of the oscillations (in percent of the average flux-density). *In the same epochs, the amplitude of 1-d periodicities in the calibrators' curves oscillates between 0.0% (no detection) and 0.2%*, which demonstrates that the effect acts differently on IDV sources and calibrators. All the amplitudes are calculated via SR analysis. The label 'N' means that the object was not observed during the session; in brackets, we reported the cases of periodicities which are present in the gain-corrected data but not in the fully calibrated ones. A question mark is given for the August 2007 data of 0716+714; the detection, in this case, is doubtful.

The table does not fully give the idea of the extension of the phenomenon, since it focuses on the 1-day period, disregarding the higher order harmonics.

For each of the 86 variability curves, we checked for the three strongest time scales in a range which was different from case to case, depending on the average time sampling, the total duration of the observation and the presence of long term trends. In average the range of the investigated time scales is ~ 3 days, which means ~ 30 intervals of 0.1d. If we assume every time interval to be equally probable, we have all the elements to estimate the number of times in which a 1-d period would be expected to appear by chance:

$$N_{exp} \sim \frac{86 \cdot 3}{30}, \tag{4.1}$$

which means 9, approximately.[3]. If we subtract this number from the 35 detections, we obtain 26 occurrences, which means that the effects showed up, in average, at least once

[3]This represents a large overestimate. With the exception of the August 2007 0716+714 case, the effect

Table 4.1: The recurrence of the 1-day period in the Urumqi data: in column 1, the epochs, in col. 2 the day of the year, in col. 3-6 the amplitude of the 1-day period (in percent of the average flux-density) for 0716+714, 0917+624, 0954+658 and 1128+592.

Epoch	DoY (d)	0716+714 (%)	0917+624 (%)	0954+658 (%)	1128+592 (%)
14.08.2005	228	1.5	-	-	-
27.12.2005	363	-	1.7	-	-
15.03.2006	76	0.9	-	-	-
27.04.2006	119	1.0	-	-	-
09.06.2006	162	2.7	-	-	-
14.07.2006	198	-	-	-	2.5
19.08.2006	235	1.2	0.6	-	1.6
23.09.2006	269	(1.3)	(0.7)	0.5	1.9
17.11.2006	324	1.0	-	0.7	1.5
18.12.2006	354	0.6	N	1.4	3.2
25.01.2007	26	1.2	-	-	-
12.02.2007	45	-	1.0	-	4.6
24.03.2007	85	0.7	0.6	-	-
20.04.2007	113	-	-	0.6	-
15.06.2007	168	-	-	1.4	-
19.07.2007	202	2.7	-	-	(1.9)
18.08.2007	232	1.8 (?)	N	(0.9)	-
13.10.2007	286	-	-	-	-
21.12.2007	357	-	-	0.8	-
24.02.2008	57	1.0	-	0.9	-
21.03.2008	82	-	0.8	-	-
21.04.2008	113	-	-	-	3.2

every observing epoch. It is interesting to examine the results source by source: for 0716+714 the number of affected curves is 13 out of 22 (59%); for 0917+624, 6 out of 20 (30%), for 0954+658, 8 out of 22 (36%); for 1128+592, finally, 8 out of 22 (36%). While for the last three sources the probability of finding traces of the 1d-effect is similar, 0716+714 represents a clear exception.

The table provides further interesting information: the period in which the effect appeared more frequently is between August 2006 and March 2007. There is no clear indication for a dependence on the the day of the year, although the detections seem to be more probable between August and November (see Fig 4.2). The periodicity seems to occur independently in different objects, in the sense that the probability of observing the periodicity simultaneously in more than one object appears to be close to the product of the single probabilities. This result, if confirmed, would be quite surprising, because it implies that the effect is not triggered by any special condition which is common to all the sources. Therefore, it can not be explained as a calibration error.

is always characterized by at least two conditions: the 1d-period and a significant correlation with raw data of the closest calibrator. This second condition causes the probability of a false-alarm to drop significantly.

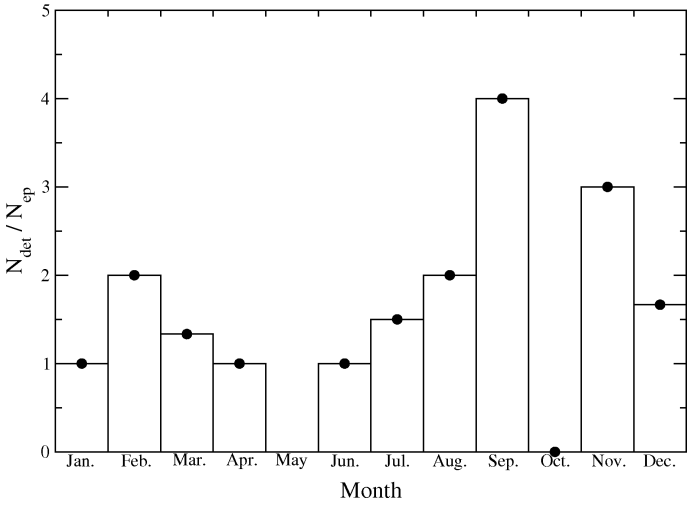

Figure 4.2: The recurrence of the 1-d period month-by-month: the columns show the ratio between the number of detections and the number of observing sessions.

4.3 About the hypothesis of a gain-elevation effect

In order to exclude beyond any doubt that the periodic modulation is due to an inefficient correction of the gain-elevation effect, it is necessary to return to the de-trended August-2006 variability curve of 0716+714. Comparing the uncalibrated data of the source with the ones of 0836+710 (Fig. 4.3), a few important points clearly stand out:

- both the source and the calibrator show minima and maxima regularly separated, but the former shows peak-to-peak variations much larger than the latter (9% against 3%). Considering that 0836+710 has slightly lower declination, we would expect the calibrator to show a little more elevation-induced variability than the source, which is obviously not the case.
- **The maxima in the source curve seem to correspond to the expected gain-elevation peaks** (turquoise curve in the figure), **but the amplitudes** (this is an essential point) **change with time**.
- A fit of the flux-density with the sum of a 1.0 d and a 0.5 d sinusoid (orange curve in the figure) reveals a significant asymmetry in the 0716+714 data. If we plot the flux-density versus elevation (see Fig. 4.4, left panel), this asymmetry appears as a hysteresis: the flux-density generally takes a higher value when the source is setting than when it is rising in elevation. *No gain-elevation curve could ever correct for this.* In principle, tracking errors in the drive program may cause such an effect. However, given the fact that the calibrators do not show it, this hypothesis can be disregarded.

It is important to point out that the gain-elevation curves of all the calibrators (see Fig. 4.4, right panel) are consistent at least within a 1%-confidence level.

Given these facts,we can finally state that *the periodic variability can by no means be explained in terms of a wrongly corrected gain-elevation effect.*

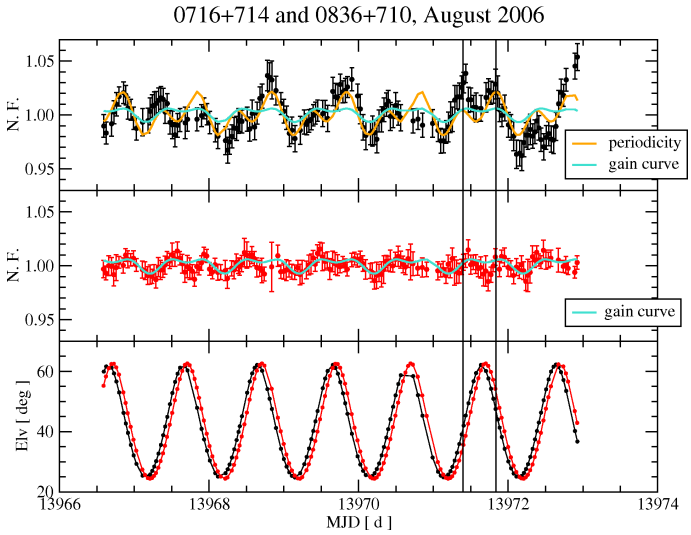

Figure 4.3: The uncalibrated variability curves of 0716+714 (black circles) and 0836+714 (red circles). In orange, the periodic component detected via *SR*, whose maxima occur close to the ones in the gain-elevation curves (in turquoise). In the lower panel, the elevation curves of the objects.

While in August 2006 the unexplained 1.0-d period is particularly prominent for the 0716+714 light curve, for other IDV sources the situation is slightly different. The sinusoidal regression detects relevant periodic modulation in both 0917+624 and 1128+592 with maximum peak-to-peak variations of respectively 5% and 7%. In the case of 1128+592 however, the periodicity is partially hidden by the strong activity of the source on short time scales (see Fig. 4.5). The three periodicities show delays up to $\sim 5\,\mathrm{h}$.

4.4 About the hypothesis of other systematic effects

Once the gain-elevation effect has been accounted for, a few other options have to be examined. Among them: day-night effect, pointing offset and confusion[4]. The last hypothesis can immediately be discarded by considering the presence of the modulation in several different IDV sources almost simultaneously – definitely an unrealistic coincidence.

4.4.1 The pointing offset

The pointing offset represents a more likely concern:

- the offsets in the two scanning directions follow patterns which are similar, with a time-shift of 6 hours, hence their effects can possibly sum up and induce stronger variability.

[4] *Id est*, the presence of one or more sources in the telescope beam along with the observed one; this produces variations in the flux-density measurements which depend on the relative position of the confusing source relative to the center of the feed.

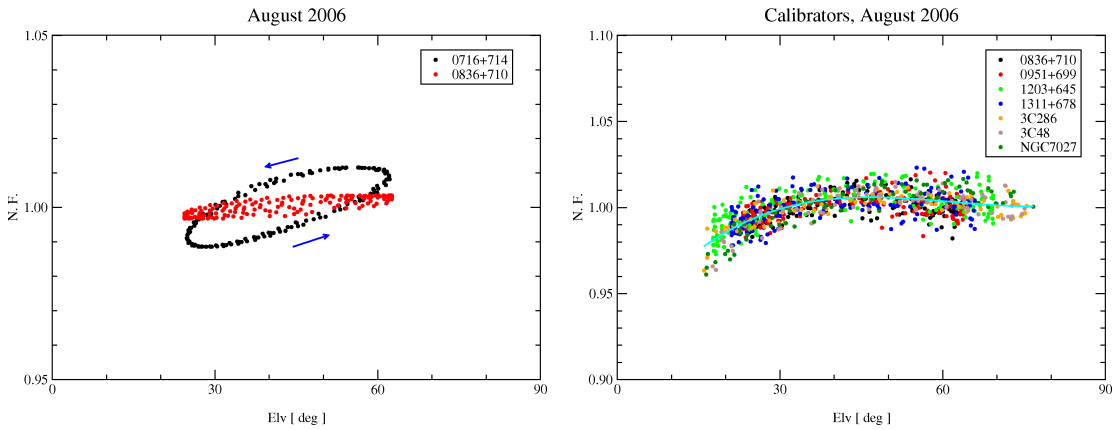

Figure 4.4: *Left panel*: the hysteresis pattern in the periodic variability of 0716+714 (black circles): the flux-density generally assumes a higher value when the source is setting than when it is rising in elevation. The calibrator 0836+710 (red circles) appears to be much less affected. *Right panel*: the clear agreement between the calibrators' gain curves in August 2006.

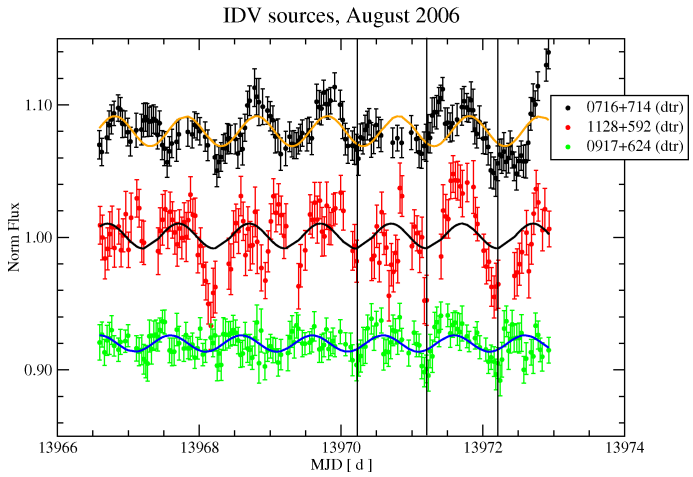

Figure 4.5: The de-trended variability curves of 0716+714 (black circles), 1128+592 (red circles) and 0917+624 (green circles); the 1-d periodicity appears in the three curves with a time delay of 0.2-0.3 d.

- The pointing offset may affect each source differently; this would explain why the effect is prominent in some cases and almost absent in other ones.
- It depends on the source position, which of course changes with a period of 1 day.

Therefore, it seems to match the characteristics expected for causing a spurious 1-day modulation, in case of imperfect pointing correction. Nevertheless, there are several arguments against this hypothesis:

1. First of all, the efficiency of the correction can be evaluated by comparing the ALON and ALAT data separately. In case of a pointing offset problem, we should see a phase difference of 6 h between the ALON and ALAT variability curves. This is not observed (see Fig. 4.6, left panel), therefore it is rather unlikely that the pointing offset is the reason for the modulation.
2. The average pointing offset in our observations can account for a flux-density variability of the order of $3-4\%$; in order to cause variations two or three times larger, the offset should be significantly larger than our estimates. This can only happen if the zero-point of the pointing offset is severely displaced. A piece of software has been written for evaluating this displacement. It assumes that the source is placed at a generic p_0, in the range [-50 arcsec, +50 arcsec]. Then the actual pointing offset is $p - p_0$, and the pointing correction changes accordingly. We give to p_0 all the values in the range (with a 5-arcsec step), and estimate which one minimizes the variance. This value is then the best estimate of the real position of the source. The results show that the source positions are accurate within 10 arcsec (see Fig. 4.6, right panel), which would require corrections of less than 1%.
3. The variations in the pointing offset repeat on a 24-hour time scale, but they are not smooth. They are instead characterized by large abrupt changes. This is in contrast with the features of the 1d-period: it varies very smoothly, but is not self-similar on a 24-hour time scale.

These considerations should be sufficient for excluding the pointing offset from the list of the possible causes of periodic variability. Moreover, in April 2007 the pointing model for the Urumqi telescope was modified, with the addition of several new parameters. The result is that the offsets became smaller, and almost constant in time (see Fig. 4.7). Despite this, the modulation can still be seen in the later observations. It therefore removes every remaining doubt.

4.4.2 The day-night effect

The last obvious candidate for contributing a periodic signal to the variability pattern is the day-night effect. The most solid argument against it comes from the fact that when periodicities are observed in more than one object during the same epoch, sometimes clear delays can be seen between them (see Fig. 4.5). This point should also cross out a possible influence of the weather.

We conclude that none of the factors described above can alone explain the characteristics of the observed modulation. It seems unlikely that it is the result of a complicated combination of them. The fundamental problem is that none of the systematic sources of noise can account for a periodicity which affects IDV sources more than calibrators. This fact, however, is observed throughout all the epochs. Probably, it is necessary to look for a completely new phenomenon.

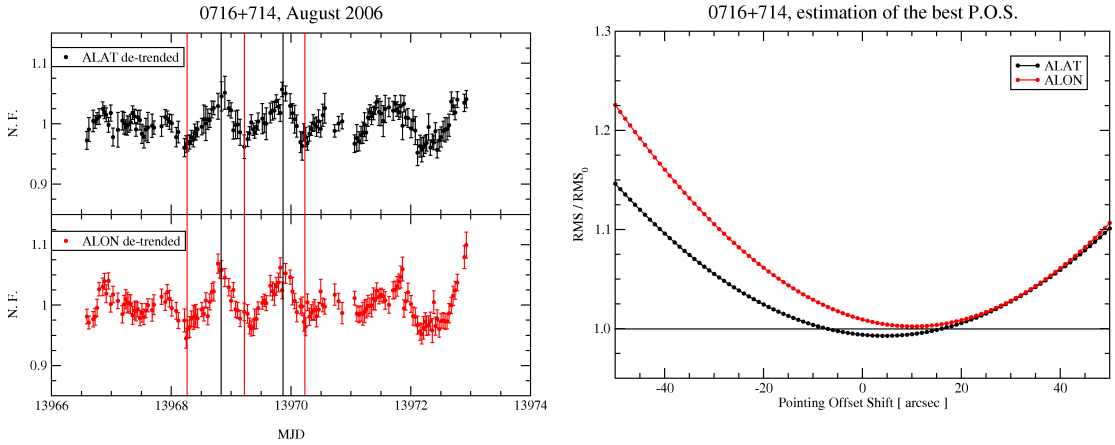

Figure 4.6: *Left panel*: the excellent agreement between the ALAT (black circles) and ALON data (red circles) of 0716+714 seems to exclude the possibility of a pointing problem. *Right panel*: the minimum of the RMS of the pointing-corrected data is reached when we assume that the zero-point of the telescope is shifted by 5-10 arcsec with respect to the real position; this excludes the existence of a large misalignment of the zero-point.

4.5 The 1-d period in Effelsberg

The April 2006 epoch was our first attempt to perform simultaneous Effelsberg-Urumqi observation. The comparison of the variability curves obtained at the two sites (see, e.g., Fig. 3.1, upper panels) provides a strong confirmation of the efficiency of our data calibration. The calibrated data of the IDV sources are in excellent agreement, even on the very short time scales. The only exception has been the light curve of 0716+714. While, at first sight, in April 2006 **the 1-d effect** can not be detected in the Urumqi variability curves, it **is distinctly present in the 0716+714 data obtained in Effelsberg** (see Fig. 4.8, left panel).

A thorough investigation of archival Effelsberg data demonstrated that the April 2006 session is not a unique case. In September 1998, for example, a clear 1-d period can be observed in the variability curve of 0716+714 (see Fig. 4.8, right panel), and in that of 0917+624, although much lower in amplitude. Periodicity with frequencies $1\,\mathrm{d}^{-1}$, $2\,\mathrm{d}^{-1}$ and $3\,\mathrm{d}^{-1}$ turned out to be as frequent in the Effelsberg data as in the Urumqi ones. Therefore, we can unquestionably state that the effect can not be regarded as a problem concerning solely the Urumqi telescope.

4.6 Elevation dependence: evidence and exceptions

The most puzzling issue concerning the 1-d periodicity is its relation with elevation:

- In the **Urumqi** data, the periodicity often appears correlated to elevation, in the sense that the minima in the periodic signal correspond to minima in the elevation pattern (see Fig 4.9). In **Effelsberg** it often happens the opposite. A sinusoidal regression analysis of 0716+714 data obtained between January and February 1990 at the **VLA** demonstrates the presence of a prominent 1-day periodicity during the

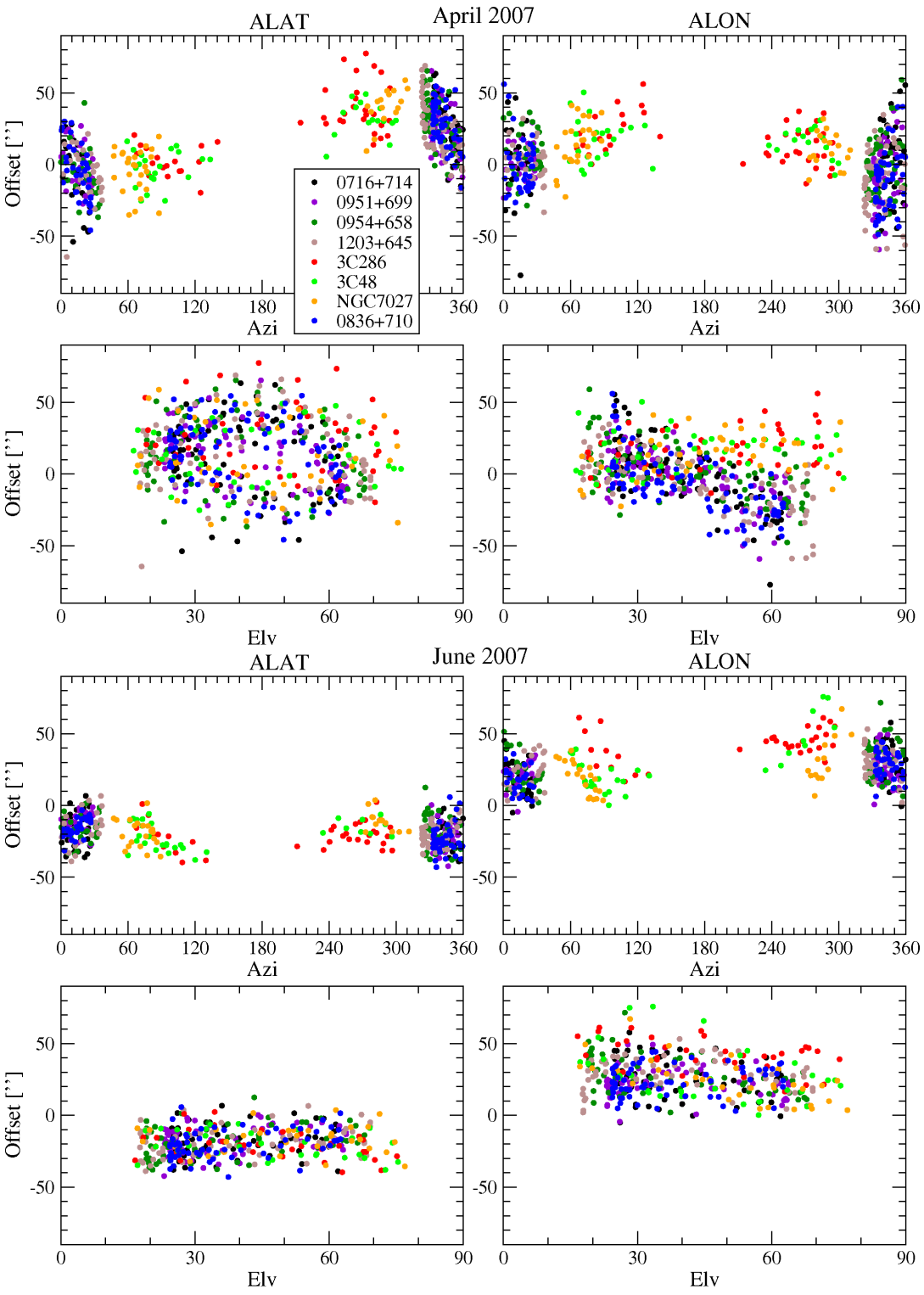

Figure 4.7: The pointing offsets plotted versus Azimuth and Elevation, for the April 2007 (4 upper panels) and June 2007 (4 lower panels) observing sessions, i.e. before and after the change of the pointing model. Offset variations of $\sim 100''$, as observed in April 2007, can cause a flux-density modulation of the order of 3-4%. In June 2007, the pointing offset is almost constant: the flux-density modulation it can introduce is of the order of 1%.

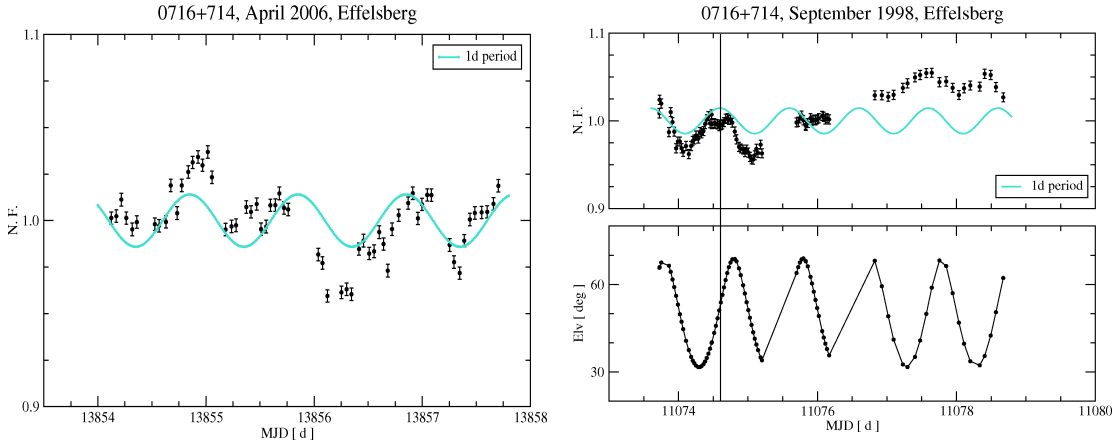

Figure 4.8: Two examples of 1-day periodicities in the Effelsberg data: the 0716+714 variability curves of April 2006 (left panel) and September 1998 (right panel). In the latter case, note the absence of correlation with the elevation (lower plot).

whole three weeks of observations, which appears anti-correlated with elevation (see Fig. 4.10).

- When the periodicity is detected in different IDV sources during the same observing session, it sometimes appears delayed according to their Right Ascension (see Fig. 4.11).

For both the statements we found important exceptions. For example, concerning the Effelsberg data, the maxima in the 0716+714 variability curve of September 1998 appear at an elevation around 50° (see Fig. 4.8, right panel). In August 2006, the periodic variability in 0917+624 peaks before the one in 1128+592, in agreement with the difference in the Right Ascension of the two sources. The variability detected in 0716+714, instead, *follows* the others. Below we extensively discuss two cases which appear particularly important for investigating the relation between the effect and elevation.

4.6.1 Anti-correlation with elevation, in Urumqi

Differently from usual, the 1-d periods detected in the Urumqi calibrated data of November 2006 are *anti-correlated* with elevation (see Fig. 4.12). Finding the difference between this epoch and the others may be helpful for the solution of the enigma.

During this session, 0.5 d/1.0 d periodic variations show up in the 0716+714 light curve, with peak-to-peak variations of up to 5% of the average flux-density; they are detected also in 0954+658 and 1128+592, although less pronounced.

Let us take a step back to the raw data, in order to check whether there is any relation between the variability of the source and of the calibrator. The 0716+714 and 0836+710 raw data are strongly correlated. There is no time delay between the peaks in the curves of the two objects, but the peak amplitudes are very different. This correlation provides a very important clue: in this epoch, the effect is inverted, but also the gain-elevation curve is in some way inverted, showing minima at high elevations, rather than at low elevations. It looks as if the effect tends to amplify the variations shown by the gain-elevation curve.

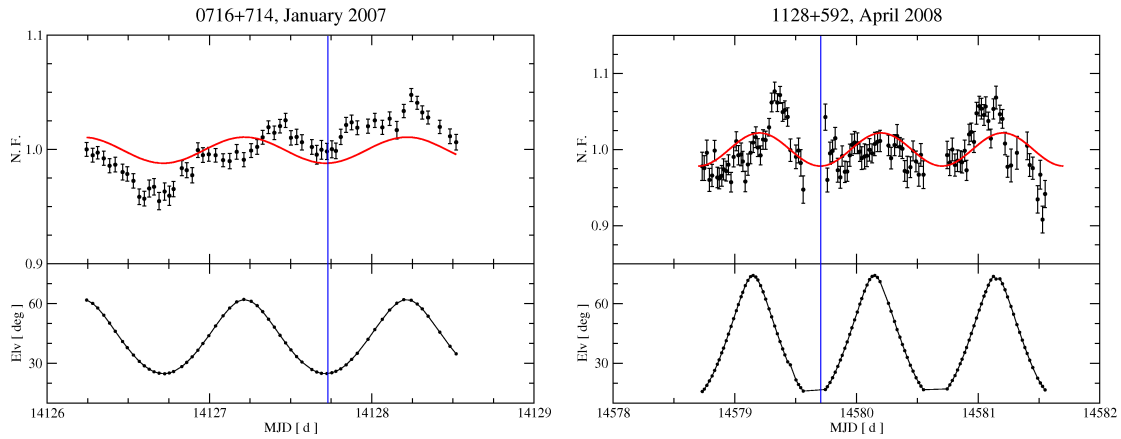

Figure 4.9: Two examples of elevation-correlated periodic variability in the Urumqi light curves.

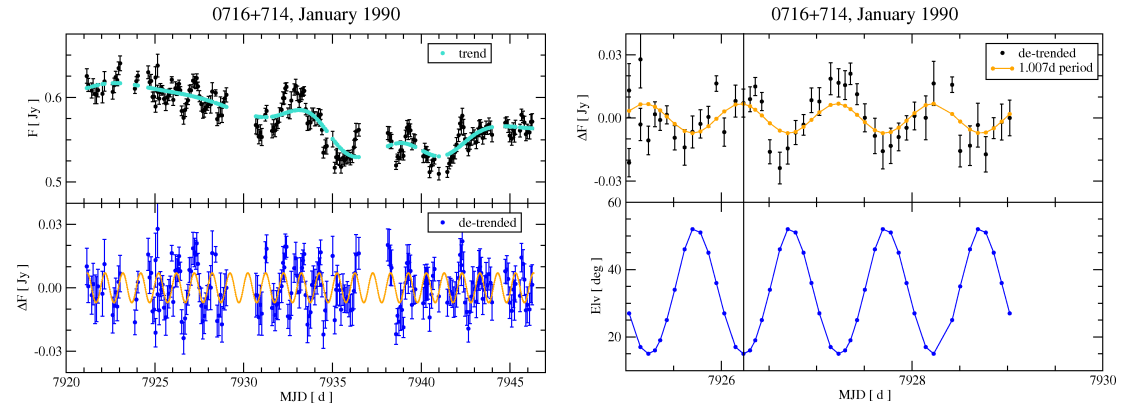

Figure 4.10: The 0716+714 data from observations performed between January and February 1990 at the VLA. *Left panel*: the variability curve (black circles), the long-term trend (turquoise line), the de-trended curve (blue circles) and the 1-day periodicity detected via *SR* (orange line). *Right panel*: the de-trended curve (black circles) and the fit of the periodicity are compared with the elevation curve of the source (blue line).

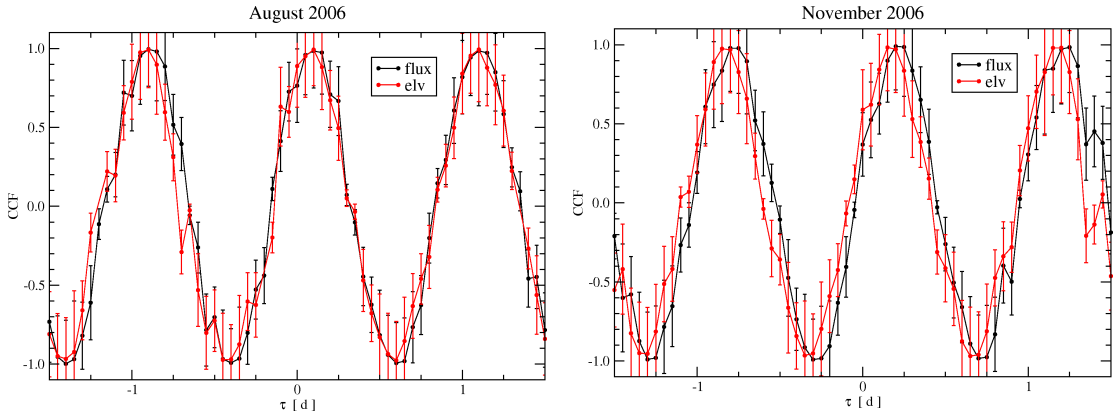

Figure 4.11: The delay in the 1-d periodic variability detected in the light curves of two IDV sources (black circles), plotted along with the delay in their elevation patterns (red circles). On the left panel, the case of 0917+624 and 1128+592 (August 2006); on the right panel, the case of 0716+714 and 1128+592 (November 2006). There is evidence that the flux delay agrees with the elevation delay.

More importantly though, we could paradoxically say that *the gain-elevation curve does not behave as a gain-elevation curve*, since its shape does not stay constant from epoch to epoch. In principle, exceptional weather conditions (snow, for example) can justify a different curve shape, but the log file of the observations states that the weather was very good.

The only alternative is that *more than one effects merge into the gain-elevation curve*. If this is the case, **it might well be that the 1-d effect is a phenomenon which affects all the objects, both IDV-sources and calibrators, though much more significant in the former than in the latter case**. This conclusion has important implications: if a regular pattern appears in the calibrators, the gain-elevation correction should partially remove it; this means that the effect may be present in more epochs than we expect, remaining undetected just because we correct for it *by chance*; the gain-elevation correction, on the other hand, may introduce (weak) regular patterns in the variability curves of sources – if any – which are less sensitive to the effect than the calibrators.

4.6.2 Effelsberg-Urumqi simultaneity

April 2006: first simultaneous Effelsberg-Urumqi observations

As reported above, the April 2006 observations surprised us with a 1-d periodic modulation appearing in the calibrated data of 0716+714 obtained in Effelsberg. Using the *SR*, which allows to fit to the data a sinusoid with a given period, we find that a weak 1-d periodic signal (its amplitude is 0.5% of the average flux) can be detected also in the calibrated Urumqi data. The periodic modulations at the two observatories are in-phase (see Fig. 4.13).

The comparison of the gain-elevation corrected curves of 0716+714 for Effelsberg and Urumqi (see Fig. 4.14) provides important information:

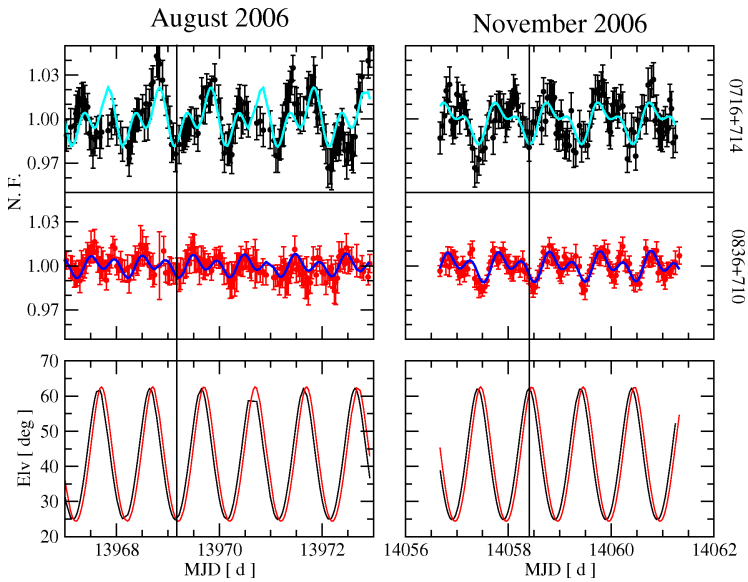

Figure 4.12: Comparison between the August 2006 and the November 2006 raw data of 0716+714 (upper plots) and 0836+710 (middle plots): in August, for both the sources, the flux-density minima correspond to minima in elevation; in November, they correspond to maxima in elevation.

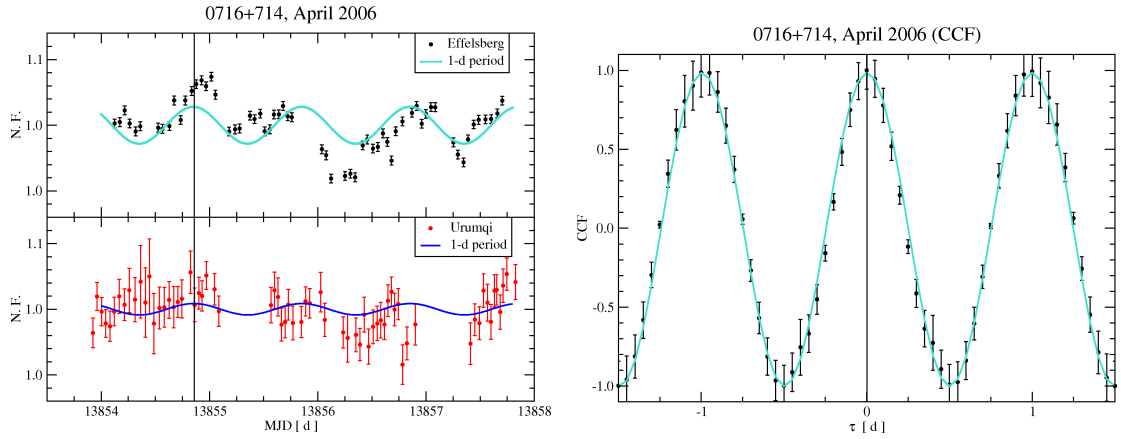

Figure 4.13: *Left panel*: The calibrated data from the Effelsberg (black circles) and from the Urumqi (red circles) observations in April 2006. In turquoise and blue, the respective 1-d periodicities. *Right panel*: The results of a CCF analysis of the periodic signals in the Effelsberg and the Urumqi data: the time delay between the two is 0.00 ± 0.05 d.

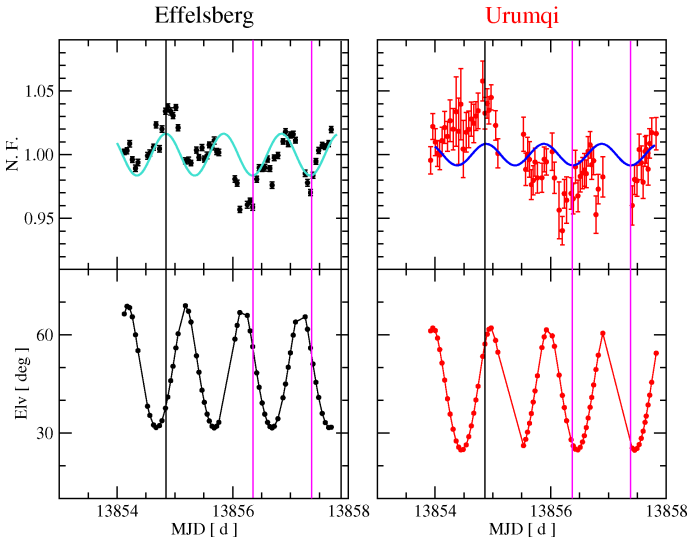

Figure 4.14: The gain-elevation corrected data from the Effelsberg (black circles) and from the Urumqi (red circles) observations in April 2006. In turquoise and blue, the respective 1-d periodicities, which are out-of-phase with respect to the elevation curves, plotted in the lower panels).

- The Urumqi gain-elevation corrected curve is affected by a strong 1-d periodicity, which is in-phase with the one detected in the calibrated data. We shall conclude that *this periodicity is real*. The reason why the amplitude of the periodic modulation decreases dramatically after the gain-time correction is because *the calibrators are affected almost as much as 0716+714* (see Fig 4.15).
- The periodic modulation in Effelsberg can not be due to an elevation-dependent effect, since the 1-d period and the elevation curve are out-of-phase by more than 0.2 d.

These facts lead to remarkable conclusions:

1. The hypothesis of an instrumental problem, or a calibration error, affecting at the same time both Effelsberg and Urumqi observations is not realistic. We can definitely disregard it.
2. In-phase 1-d periodicities, with different amplitudes, simultaneously detected at the two telescopes suggest that the 1-d period may be caused by a physical phenomenon, able to affect the results from telescopes which are thousands of kilometers away from each other.
3. The detection of the periodicity in the calibrators' curves obtained in Urumqi confirms our hypothesis that the effect may be partially removed by chance throughout the data calibration procedure.

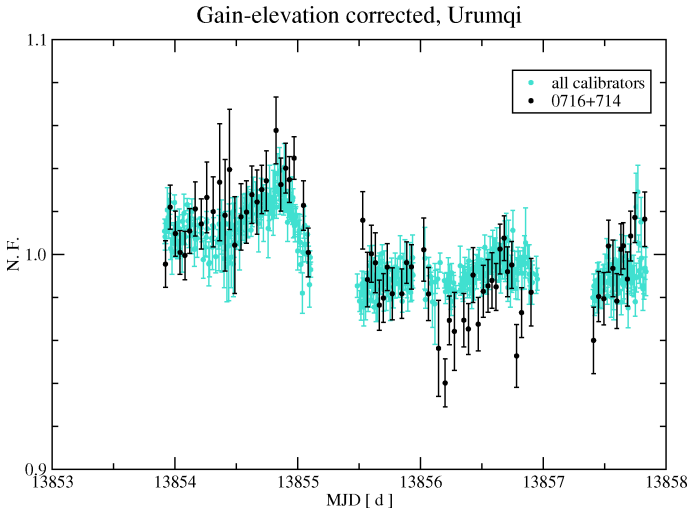

Figure 4.15: The gain-elevation corrected data of both 0716+714 (black circles) and all the calibrators (turquoise data), from the Urumqi observations. A considerable part of the variability which we observe in the source affects also the calibrators.

November 2006: second simultaneous Effelsberg-Urumqi observations

Both the variability curves of 0954+658 obtained in Effelsberg and Urumqi in November 2006 show 1-d periodic modulations (see Fig. 4.16, left panel). The modulation in the Urumqi data (magenta curve) seems to occur slightly before the one detected in Effelsberg (red curve); the time-shift between the two sinusoids is $\sim 0.05 \pm 0.05$ d. However, if we cross-correlate the two variability curves (see Fig. 4.16, right panel) we obtain a best time-shift estimate of $\sim 0.00 \pm 0.05$ d.

Evidence of a 1-d period has been found also in the Effelsberg and Urumqi variability curves of 0716+714 (see Fig. 4.17). Also in this case, the periodic signals detected at the two telescopes appear approximately in-phase (the time-shift estimate resulted by CCF is 0.00 ± 0.05 d). The black arrows in the figure show the flux-density peaks which seem to be common to the 0716+714 and 0954+658 variability curves. The black vertical lines correspond to the flux-density minima of 0954+658. The minima in the 0716+714 curves seem to occur slightly ahead of the ones in 0954+658 ($\sim 0.10 \pm 0.05$ d, according to the CCF).

The November 2006 observations confirm the main findings of the April 2006 observing session. There is strong evidence that the 1-d period occurs in Urumqi and Effelsberg with no time delay. An important conclusion supported by these data is that sources with different Right Ascension peak at different time. This characteristic seems to point towards an elevation dependent effect. Simultaneity at the two sites and elevation dependence of the periodicity are two facts which seem almost in contradiction between each other. In the next section, we investigate this issue further.

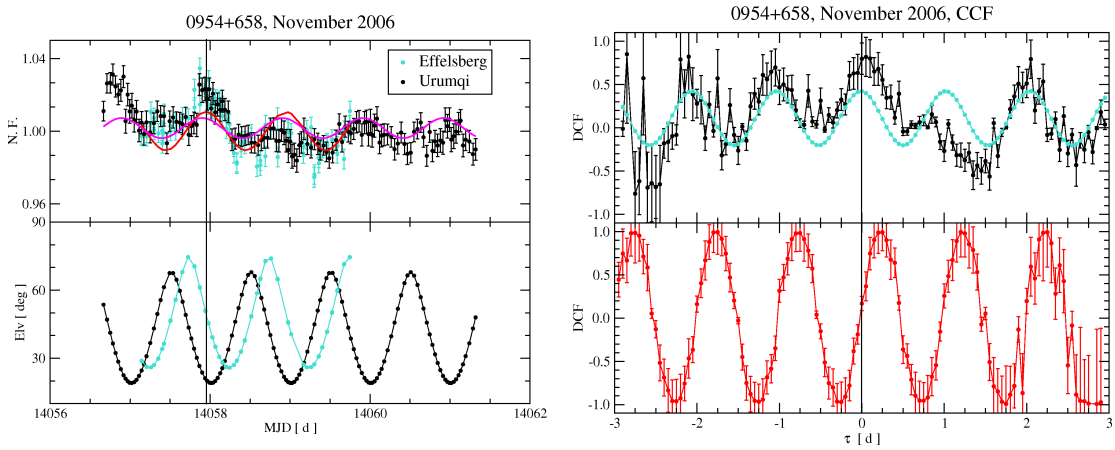

Figure 4.16: *Left panel*: Calibrated flux-density data of 0954+658 from Effelsberg (turquoise points), compared to the Urumqi data before gain-time correction (black points); in the lower panel, the elevation patterns. *Right panel*: *CCF* analysis of the Effelsberg and Urumqi flux-density data (black points) and of the elevation patterns (red points). The flux-densities at the two sites seem to vary simultaneously, despite the delay in elevation.

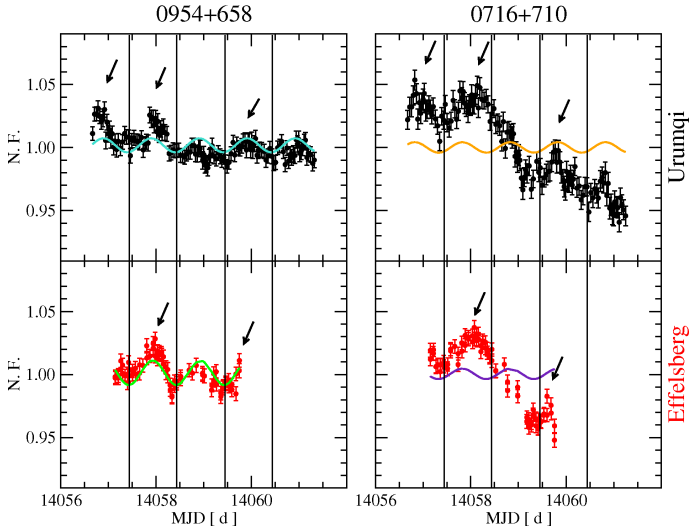

Figure 4.17: Calibrated variability curves of 0954+658 (left panels) and 0716+710 (right panels), in Urumqi (black circles) and Effelsberg (red circles), for the simultaneous observations performed in November 2006. There is evidence for 1-d periodic variations in all the light curves. The periodicities detected in Urumqi and Effelsberg (turquoise and green curve, respectively) seem to be in-phase. Note that the periodic signal in the 0716+714 variability curves (orange and violet curves, respectively) seem to be slightly ahead of the one in the 0954+658 curves.

Table 4.2: The manifestations of the 1-day period between August 2005 and April 2008. In column 1, the observing session; in col. 2, the time of the day (in UT) in which the source peaks in elevation; in col. 3 and 4 the timing of the flux-density peaks in the gain-elevation corrected data of the IDV source and in the ones of the closest calibrator, respectively. In col. 5 and 6 the consistency of the data with the hypotheses of an elevation dependent or a time dependent effect. In col. 7, we show in which epochs the 1-d effect is present in both the IDV source and the closest calibrator.

Epoch	τ_e (d)	τ_p (d)	τ_c (d)	elev. dep.	time dep.	effect in cal.
14.08.2005	0.7	0.0	0.8	no	yes	no
15.03.2006	0.1	0.1	0.1	yes	yes	yes
27.04.2006	0.0	0.9	0.0	yes	yes	yes
27.04.2006E	0.2	0.9	0.7	no	yes	no
09.06.2006	0.9	0.0	0.9	yes	yes	yes
14.07.2006	0.8	0.1	0.9	no	yes	no
19.08.2006	0.7	0.9	0.7	no	yes	no
23.09.2006	0.8	0.9	0.0	yes	yes	yes
17.11.2006	0.4	0.9	0.9	no	yes	yes
17.11.2006E	0.6	0.9	0.2	no	yes	no
18.12.2006	0.5	0.3	0.3	no	no	yes
25.01.2007	0.2	0.2	0.2	yes	no	yes
12.02.2007	0.3	0.3	0.4	yes	no	yes
24.03.2007	0.1	0.9	0.0	no	yes	yes
19.07.2007	0.8	0.1	0.9	no	yes	no
18.08.2007	0.7	0.3	0.9	no	no	no
21.12.2007	0.4	0.6	0.5	no	no	yes
24.02.2008	0.2	0.8	0.9	no	no	yes
21.03.2008	0.2	0.1	0.1	yes	yes	yes
21.04.2008	0.2	0.2	0.2	yes	no	yes

4.6.3 Time/elevation dependence of the 1-d effect

A simple way to cast some light on the complicated relation between the effect and both time and elevation is to check, for each epoch, the time of the day in which the 1-d period peaks in the most affected IDV source (τ_p) and in the closest calibrator (τ_c). We can compare τ_p with the time of the day in which the IDV source culminates in elevation (τ_e). If $|\tau_p - \tau_e| \leq 0.1\,\mathrm{d}$, we can consider the 1-d effect to be compatible with an elevation dependence.

The estimation of τ_c allows us to understand how often the effect is present in the calibrators: if $|\tau_p - \tau_c| \leq 0.1\,\mathrm{d}$ we can conclude that the source and the calibrators are both affected. Since the gain-time correction often removes any trace of variability from the calibrators, the evaluation of τ_c must be done on the gain-elevation corrected data. For consistency, also τ_p is estimated on the gain-elevation corrected data (note, however, that the difference with the τ_p values obtained from fully calibrated data is negligible).

The values are presented in Table 4.2. It immediately appears that τ_p preferably occurs at a given time of the day, namely around 0.0 d (i.e. 0 UT; we will refer to it as τ_t). In the last three columns of the table, we show which epochs are compatible with an elevation

dependent effect, which ones are compatible with a time dependent effect ($|\tau_p - \tau_t| \leq 0.1$ d) and, finally, in which epochs the closest calibrator is affected by the 1-d effect too.

Table 4.2 provides several clues about the nature of the 1-d effect:

- In 13 epochs out of 20 (11 out of 18, if we exclude the Effelsberg observations), the 1-d period appears in the time range 0.9-0.1 d (see Fig. 4.18, red lines). The correlation of the 1-d effect with time is preponderant.
- The 1-d effect appears strongly correlated with elevation in 8 epochs out of 20 (see Fig. 4.18, black lines). If we look at the 7 epochs in which the time dependence is not observed, 3 times we find the a strict correlation with elevation ($|\tau_p - \tau_e| = 0.0$ d), 2 times a weak correlation ($|\tau_p - \tau_e| = 0.2$ d). The elevation dependence of the 1-d effect seems to be weaker than the time dependence, and complementary to it.
- In 12 epochs out of 20, the appearance of a 1-d period in an IDV source coincide with the presence of a weak 1-d periodic modulation in the closest calibrator (blue line in Fig. 4.18).
- There is only one case in which τ_p does not peak close to τ_e, τ_t or τ_c. It is likely that here the variability has nothing to do with the effect.

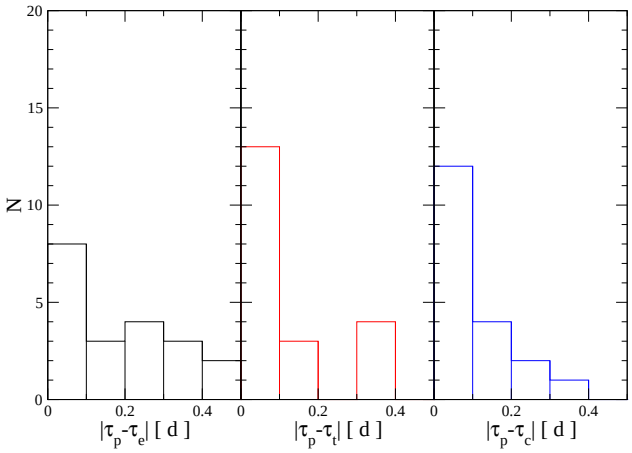

Figure 4.18: In the histograms, the distribution of the 1-d effect as a function of $|\tau_p - \tau_e|$ (black), $|\tau_p - \tau_t|$ (red) and $|\tau_p - \tau_c|$ (blue).

4.7 Summarizing the findings about the 1-day effect

Let us summarize the main findings of our investigation so far:

- The effect appears as a regular modulation – a superposition of a 24 h periodicity plus higher order harmonics (above all, 0.5 d and 0.33 d periods).
- It strongly affects IDV-sources (the maximum peak-to-peak variation so far observed is of the order of 15%), while its contribution to the calibrators' variability is small or none.

- The amplitude of the modulation changes significantly from epoch to epoch, but also within a single observing session. From one day to the next, the peak-to-peak variation can vary from several percent to zero.
- The periodic modulation affects data from Effelsberg, Urumqi and the VLA.
- It can not be explained through any of the standard sources of noise (gain-elevation, pointing offset, day-night effect, confusion).
- The high-order harmonics do not strictly follow the phase correlation we would expect with the 24 h period. All the components, though, have in common the properties listed above; therefore, they are likely different manifestations of the same phenomenon.

Considered all together, these features clearly illustrate how important it is to understand the origin of the periodic modulation. Due to its strength, it can seriously affect the estimation of the IDV characteristics of the sources; the variation in the peak amplitude during the observations makes difficult to trace it and remove it; the fact that it is present in data from different telescopes (including an interferometer) suggests that it may be influencing or have influenced other IDV experiments as well. The key-point, though, is probably the discrimination it exerts between IDV sources and calibrators. It shows, on the one hand, that some characteristic must be common among these sources (maybe the small size). This may lead to the conclusion that, for all of them, the variability has the same origin. The 1-d effect itself then, becomes a powerful tool in the study of intra-day variability and, at the same time, of the physical properties of the sources. On the other hand, it raises more than one question about the possibility to achieve a 'proper' calibration of the data and to discriminate between 'real' and systematic variability.

4.8 Possible interpretations

Below, we propose some hypotheses about the nature of the effect, along with pros and cons:

1. **A combination of a time dependent effect and a gain-elevation effect:** the elevation dependence may results from the contribution of two independent components to the 24-h periodic oscillations: a time dependent '1-d effect' and the gain-elevation effect which *must* provide a contribution. Depending on their relative strength, the time analysis points out the existence of either simultaneous or elevation-dependent variability. The impossibility of disentangling them, moreover, would make the gain-correction ineffective and potentially wrong, causing the components to merge unpredictably in a periodic pattern. *Main downside*: the contribution from the gain-elevation effect should be approximately constant in time; therefore, the epochs in which the periodic oscillations are larger should be the ones in which the effect is stronger. These ones, consequently, should be the epochs in which no clear elevation dependence should appear. According to our data, though, this is not the case.
2. **A time-dependent gain-elevation effect:** we could hypothesize that a time-dependent gain-elevation effect may explain several characteristics of the 1-d period.

If the amount of radiation that a telescope collects depends, for instance, on atmospheric conditions (such as the temperature) we would expect the gain curve to be a function of elevation as well as time. In this case, though, the effect should appear almost identical, in shape, in objects which are very close in both Right Ascension and Declination, because the telescope would find them in the same position at the same time. The existence of time lags between the periodicities in 0716+714 and 0836+710 (see, for example, the experiment of September 1998), does not support this idea. The simultaneity of the effect in Urumqi and Effelsberg, moreover, would not be explained, and neither the different sensitivity of IDV sources and calibrators to the periodic signal.

3. **A completely independent effect:** the 1-d effect may depend on time, source position and source characteristics. If the amount of radiation which the telescope collects depends on all these parameters, it is reasonable to expect a preferential time for the peaks of the 1-d effect, but also time-lags between the periodicities detected in different objects, which would emulate an elevation dependence. This scenario – which seems to fit the best the characteristics of the effect – would also account for the changes that the periodic pattern often shows within the same observing session. The problem, in this case, is that the effect should arise in a region close enough to the Earth to be influenced by its 1-d periodic rotation, and far enough to allow simultaneity between Effelsberg and Urumqi.

Chapter 5

Periodic variability in the light curves: II. Further Evidence

5.1 Similarities between variability curves of different sources

In chapter 4, we focused our attention on some essential aspects of the 1-d period. Here we present some other peculiarities emerging from a deeper investigation of the Effelsberg and Urumqi data-sets, which, if confirmed, could provide important clues for better understanding the phenomenon.

The similarities among variability curves of different objects is probably the most intriguing aspect. The similarities can regard limited parts of the variability curves or extend to the whole duration of the observation. In order to establish whether these analogies are incidental or not, a proper statistical study would be required, aiming at estimating the recurrence of apparent correlations between independent time series. Unfortunately, this kind of study turns out to be more difficult than expected: first of all, because of the inadequacy of the cross-correlation function to compare signals which show variability on both short and long time scales. The contribution from the long time scales, in fact, will always be dominating. Secondly, the result could be influenced by the fact that our time series are not really independent, being affected by the same systematic effects and passing through the same correction procedures.

An example of a possibly correlated variability between light curves is plotted in Fig. 5.1 (left panel); it refers to the Effelsberg observations performed in August 2004. The similarity regards the large peak around MJD 13232 observed in both 0716+714 and 0954+658. It seems that it starts, peaks and reaches again a minimum simultaneously for both the sources. Also the amplitude of the variation is similar. The suspicion of correlated variability increases when we consider the raw data: apart from the first peak in 0716+714, the two variability curves follow identical patterns. A sinusoidal regression analysis reveals the presence of a residual 1-d period in the 0716+714 data; if we remove it, the CCF reveals a degree of correlation close to 85%, at a time lag of 0.05 d (right panel).

Other examples are provided by the observations of June and October 2007 (see Fig. 5.2), where some evidence of correlated variability seem to appear in the curves of 0917+624 and 0954+658 – two objects which frequently show similar behaviour. Two interesting characteristics are in common between the two epochs: 0917+624 and 0954+658 show regular variability on the same time scale – 0.33 d in June, 0.40 d in October; 0954+658 shows further variability on a time scale of 0.93 d (June) and 0.94 d (October).

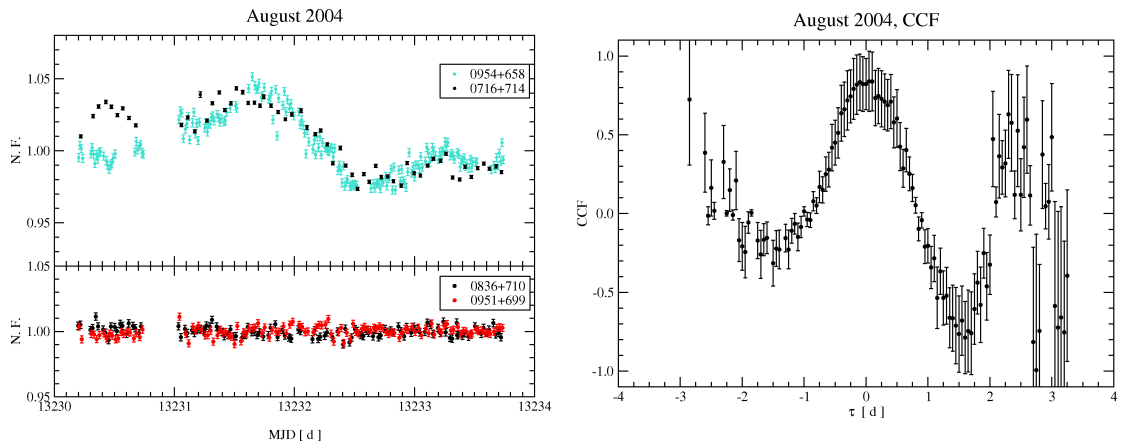

Figure 5.1: Similarities between the variability curves of different IDV sources. In the left panel, the curves of 0716+714 (black circles) and 0954+658 (turquoise circles) – on the bottom, the calibrators 0836+710 and 0951+699. In the left panel, the CCF analysis of the data-sets of the two IDV sources.

Therefore, this may be a case of 'disguised' 1-d periodicity, with the period appearing, for some reason, shorter than usual and the 'third harmonic' (0.33 d period) particularly strong.

Another case of astounding similarity between light curves can be explained in the same way: in June 2006 (see Fig. 5.3, left panel), 0716+714 and 1128+592 followed the same variability pattern for about two days. In the former case, we detected a strong 1-day modulation, which seems to account for most of the fast variability. In the latter case, the attenuation of the variability in the second part of the observation hides the effect – our estimate of the time scale is 1.28 d.

If our interpretation is correct, the examples of correlation between 0917+624 and 0954+658 and between 0716+714 and 1128+592 do not add anything new to our knowledge about the 1-d effect. However, they clearly illustrate a very important problem. Time scales of the order of 0.9 d or 1.3 d may be distorted expressions of our usual 1-day oscillation; moreover, it can not be excluded that the range of the affected time scales may be significantly larger than this. The 1-d day effect, consequently, can be much more common than we estimated (another example in Fig. 5.3, right panel).

5.2 Evidence for a two-day periodicity

The observations performed in April 2008 illustrate another case which deserves being mentioned. The variability curves of 0716+714, 0954+658 and 1128+592 (see Fig. 5.4, left panel) are characterized by two large peaks, separated by ~ 1.8 d, which are almost simultaneously occurring in the different objects. A cross-correlation analysis of the three datasets reveals that the degree of correlation is very high, and the maximum time lag is 0.1 d. It is hard to believe that the analogies occur just by chance. The analysis of the 1128+592 raw data reveals the presence of structured variability, with double peaks regularly repeating on daily scale. The same pattern is also present in the calibrator's curve, and may be explained with an elevation dependent effect, where each peak corresponds

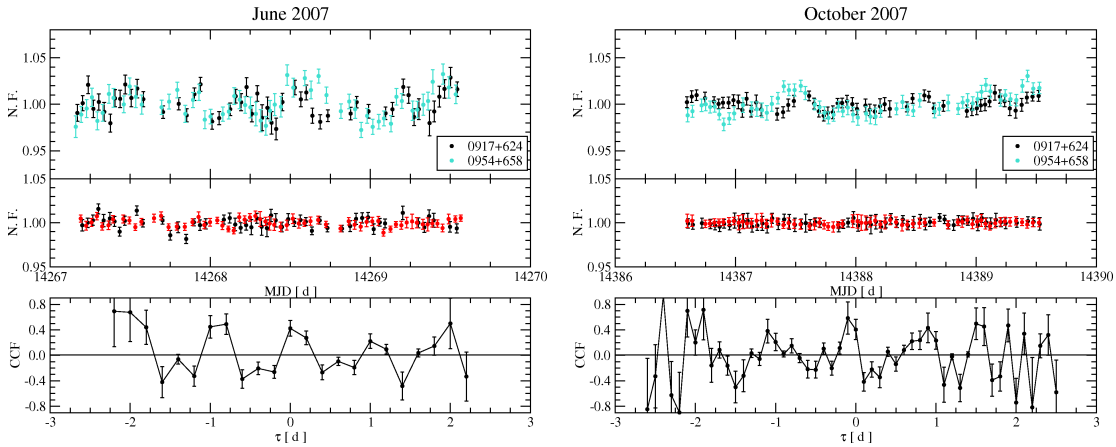

Figure 5.2: Similarities between the variability curves of 0917+624 and 0954+658 in June 2007 (left panel) and October 2007 (right panel); on the lower panels, the results of the CCF analysis of them.

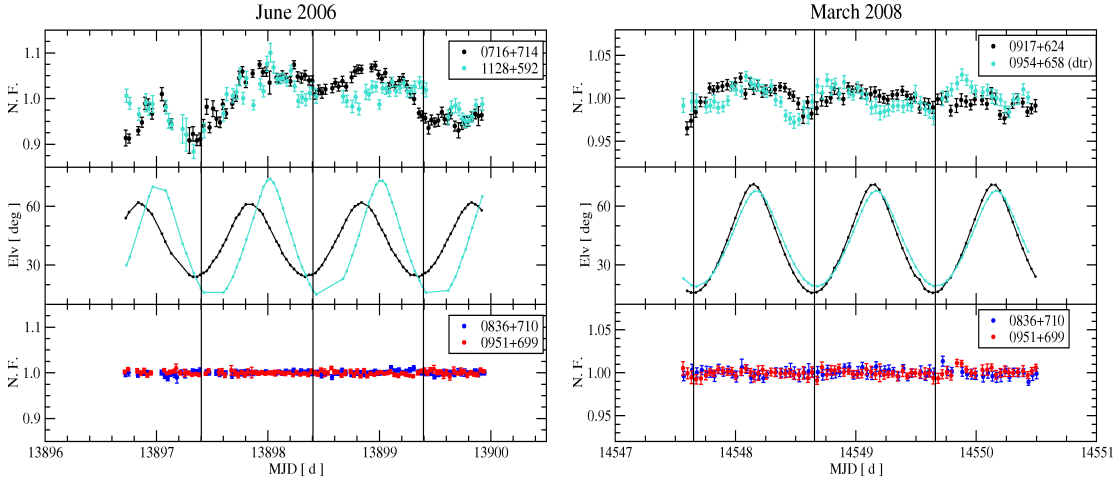

Figure 5.3: Possible cases of 'disguised' 1-day effect: the variability curves of 0716+714 and 1128+592 (left panel) are very similar, but only in the first one a 1-d period is detected. Same situation for 0917+624 and 0954+658 (right panel). In the middle and lower panels, the elevation of the sources and the variability curves of two calibrators, respectively.

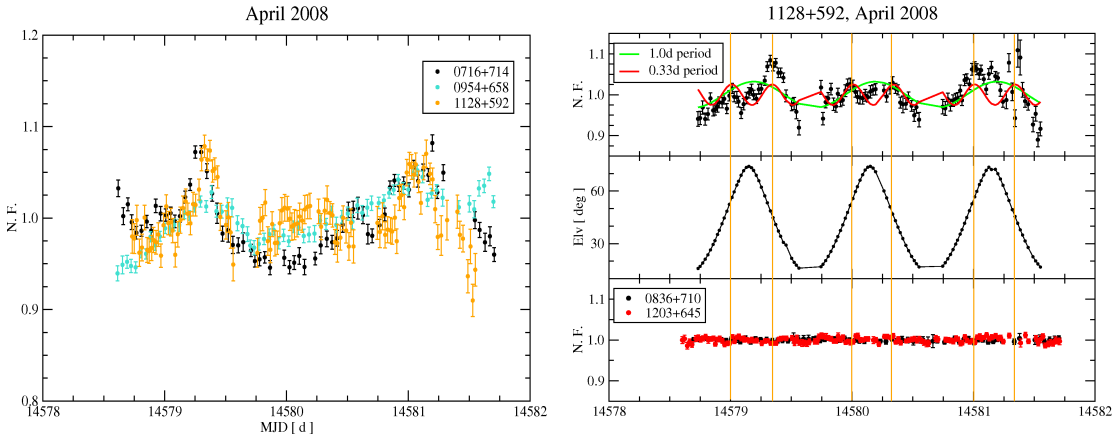

Figure 5.4: Similarities between variability curves in April 2008: in the left panel, the curves of 0716+714 (black circles), 0954+658 (turquoise circles) and 1128+592 (orange circles). The two common maxima may be related to a 1-day period in the 1128+592 variability curve (right panel).

to the source crossing the 50 deg elevation line (see Fig. 5.4, right panel). The two major peaks in the calibrated data appear like strongly amplified versions of the elevation peaks in the calibrators. Whatever is the nature of this amplification, the simultaneity of the peaks in the three IDV sources points towards a time dependent phenomenon, with a time scale close to two days.

5.2.1 Cross-correlated 2-day periodicity in archival Effelsberg data

Periodic oscillation with two-day time scales have been detected several times in the Urumqi data but, due to the short duration of the observations, the estimate of the period could not be accurate. The last example we want to present here is the extraordinary result of an IDV experiment performed in Effelsberg, in December 1997. After combining two epochs of observation (05-08 December 1997 and 25-30 December 1997), a sinusoidal regression analysis confirms what a visual inspection already reveals: the light curve of the 0917+624 exhibits an extremely strong periodicity (peak-to-peak: 13% of the mean flux-density), which persists unmodified for the whole 25-day interval (see Fig. 5.5, left panel). Our estimate of the period is 1.99 days. The amplitude and the regularity of the modulation, themselves, represent a very remarkable characteristic. A similar periodic signal is moreover detected in the light curve of 0716+714 as well, slightly time-shifted with respect to 0917+624. Unfortunately, 0716+714 was not observed between 5 and 8 of December, which makes more difficult to determine the exact period and phase of the signal. The SR estimate of the period is 2.01 days. While the first peak of the periodicity is clear, the following ones are hard to see by eye. The sinusoidal regression, though, ascribes 24% of the total variability to it, which makes the detection rather significant. A cross-correlation analysis of the 0917+624 and 0716+714 data confirms both the strongly correlated variability (with estimated time-lag of 0.1 days) and the periodicity (see Fig. 5.5, right panel).

The cases discussed above do not allow a unique interpretation. Several of them may

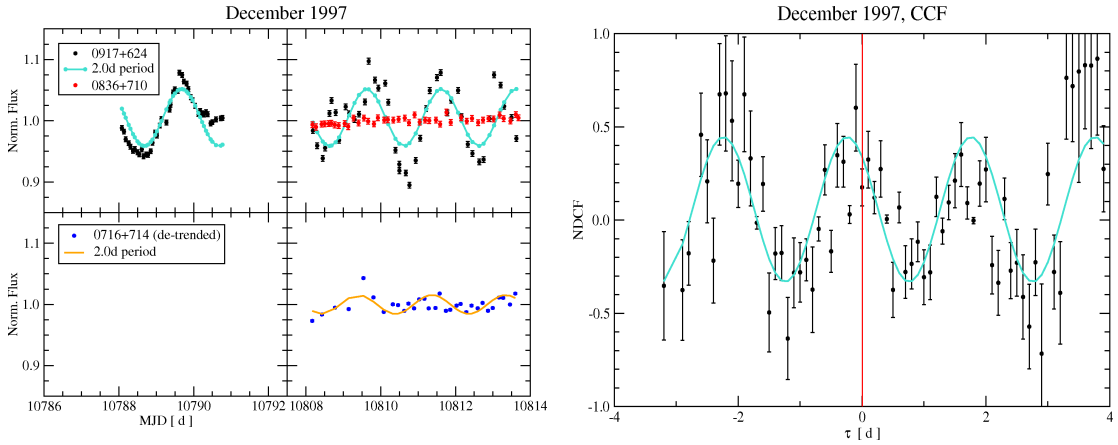

Figure 5.5: *Left figure*: The variability curve of 0917+624 (upper panels, black circles), and the clear two-day periodicity detected via SR (turquoise line). In red, the calibrator 0836+710. Evidence of a two-day periodicity has been found also in the data of 0716+714 (lower panels, blue circles). *Right figure*: results of a CCF analysis of the 0917+624 and 0716+714 data; the variability in 0716+714 is slightly ahead than in 0917+624.

simply be considered as peculiar manifestations of the 1-d effect, for which the presence of higher order harmonics or the absence of one of the peaks does not allow a clear detection. Other ones, like the 2-d period in the December 1997 Effelsberg data, seem to have a different origin and require further investigation. In section 5.4, we will propose a possible interpretation in terms of atmospheric variability.

The existence of correlated variability in different sources, independently of its origin, has fundamental implications for the study of IDV. If demonstrated, it would imply that *the origin of the variability is non-intrinsic*. In a ISS scenario, moreover, the maximum angular separation between the objects showing correlations (in our case, $\sim 30°$) would allow to fix a higher limit to the distance of the scattering screen originating the variations, by means of causality arguments:

$$D_{max} \sim \frac{c \cdot t}{sin(30°)}. \tag{5.1}$$

Given a time scale of the order of 1 day, the expression leads to a distance of the order of light-days, by far smaller than commonly hypothesized.

5.3 The 0.33-day period

While the 0716+714 variability is largely dominated by the 1-d periodicity, the time scale most frequently detected in 0917+624 and 1128+592 is in the range between 0.32 d and 0.35 d.

The origin of this time scale has not been clarified yet. Here below we discuss the three simplest explanations:

- It may be an elevation-dependent effect; if this is correct, the signal should be in-phase with the source elevation. The data, though, seem not to support this

hypothesis.

- The detected 0.33 d periodicity may be the third harmonic of a 1-day period. The hypothesis has two main downsides: if this is indeed the case, it is hard to understand how, for some source, the 0.33-d period could appear more often than the 1-d one; the hypothesis also requires that the two appear in-phase, which is not confirmed by the investigation of the affected light curves.

- The 0.33-day and 1-day periodicities may be two independent phenomenon, although, likely, caused by the same physical mechanisms.

The data we collected so far do not allow a definite answer about the nature of the 0.33-d period. In order to test the proposed hypotheses, an accurate estimation of the phase of the signal is essential. However, given the relatively low amplitude of the 0.33-day periodicity (generally of the order of 1-3%, peak-to-peak), this condition is difficult to fulfill. A possible explanation of the origin of the phenomenon is proposed in the next section.

5.4 An ionospheric contribution to IDV?

All together, the evidences we collected about the 1-d effect seem to point towards an atmospheric contribution to IDV. The arguments in favour of such a hypothesis will be discussed in the present section. Below, we introduce some basic notions of atmospheric physics which are essential for evaluating the possibility of a correlation between atmospheric variability and the periodicities we detected in our light curves.

5.4.1 Atmospheric variability

The characteristics of the atmosphere are affected by periodic variations of different origin. Earth's rotation causes daily-periodic oscillation of the total electron content (TEC) in the ionosphere. Atmospheric parameters such as wind, temperature, density and pressure are characterized by regular oscillations, mostly induced by two phenomena: **the atmospheric tides** and **the planetary waves**.

Atmospheric tides Atmospheric tides refer to the oscillations in the atmosphere with periods which are integral fractions of a lunar or solar day (Lindzen (1979); see also Chapman and Lindzen (1970)).

- The *solar tides*, as the variability of the ionospheric TEC, are primarily forced by the regular cycle in the insolation of the atmosphere. This induces two main types of oscillations: a 24-hour component, which is referred to as the *diurnal tide*; a 12-hour oscillation, known as the *semidiurnal tide*. *Terdiurnal tides*, i.e. 8-hour periodic components, are also known in literature (see, e.g., Thayaparan (1997) and Zhao et al. (2005)), although still very few studies are available on this topic.

- *Lunar tides* are caused by both the gravitational pull of the Moon on the atmosphere and the motion of the oceans. The amplitude of lunar tides is much lower than the one of solar tides.

One distinguishes between *migrating* solar tides (which propagate westward with the apparent motion of the Sun) and *non-migrating* tides (which are non-Sun-synchronous and depend on both local time and longitude).

An important parameter for the differentiation of the waves is the zonal wavenumber, i.e. the wavenumber along a line of constant latitude. Migrating tides are characterized by zonal wavenumbers which are equal to their frequency, expressed in cycles per day (i.e., the diurnal tide has wavenumber 1, the semidiurnal tide has wavenumber 2; see Oberheide et al. (2005)). The situation is more complicated when we deal with non-migrating tides, which are forced by a variety of mechanisms (e.g. the latent heat release in the tropical troposphere, see Hagan and Forbes (2002), and non-linear interaction between quasi-stationary planetary waves and the migrating tide, see Hagan and Roble (2001)). They are characterized by different zonal wavenumbers and can propagate in different directions.

It is worth to mention that the amplitude of atmospheric tides increases exponentially with height (Volland, 1997). The reason lies in the fact that the density of the atmosphere decreases with increasing height. As far as the kinetic energy is conserved, the density decrease must be compensated by an increase of the amplitude of the tide. The high layers of the atmosphere, therefore, may be the ones that more strongly affect the incident radiation from the sources.

Planetary waves Planetary waves – or Rossby waves, in acknowledgment of the pioneer studies by C. G. Rossby (Rossby, 1939) – are quasi-periodic oscillations with periods near 2, 5, 10 and 16 days which affect the atmospheric dynamics at a height between 80 and 150 km (Voiculescu et al., 2000). They are caused by the latitude variation of Coriolis force in the atmosphere (Gavrilov and Prodanov, 2008).

Particularly interesting is the case of the so-called quasi-two-day wave, a planetary-scale disturbance in the atmosphere (upper stratosphere, mesosphere and thermosphere) which is widely testified in literature (see, e.g., Muller (1972), Beard et al. (1997), Jacobi et al. (2001) and Chshyolkova et al. (2005)). It is also suspected to play a decisive role in the quasi-two-day periodicity characterizing the variability in the structure of the F layer, which is the top most layer of the ionosphere (Altadill et al., 1998).

5.4.2 Evidence for an atmospheric contribution to IDV

Demonstrating the involvement of the atmosphere in the variability of IDV sources is a difficult task. Likely, the aim can be reached only through dedicated experiments, which combine atmospheric physics and radio observations. Nevertheless, some results of the present study seem to fit fairly well the hypothesis of an atmospheric contribution to fast variability:

- Atmospheric variability could easily account for the dependence of the 1-d effect on both time and source position hypothesized in section 4.8, since atmospheric parameters vary with time and change according to the pointing direction.
- The periodic variations induced by atmospheric tides seem to match the characteristics of the variability due to the 1-d effect. Diurnal, semidiurnal and terdiurnal tides appear as natural candidates for the introduction of the 1-day, 0.5-day and 0.33-day oscillations observed in the flux density of IDV sources. The relative strength be-

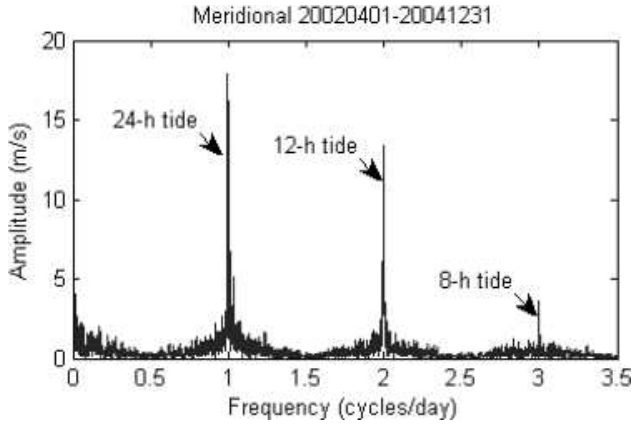

Figure 5.6: An estimation of the relative strength of the solar tides. The figure shows the Lomb periodogram of meridional winds at 90 km in the interval April 2002 to December 2004. From Zhao et al. (2005).

tween the tides (see Fig. 5.6) seems to be in agreement with the increasing amplitude of the effect with the period.

- The evidence we found for a possible 2-day periodicity in the variability curves of some IDV sources (see section 5.2) could be naturally explained as a consequence of the quasi-two-day wave.

A comparison between the variability characteristics of the atmosphere and the 1-d effect highlights a number of similarities which can not be ignored. To assume a correlation between the two seems to be plausible. The major problem is to find out *how* the atmosphere can significantly influence the flux-density measurements of IDV sources at 5 GHz. The most simple idea would be to hypothesize an atmospheric scintillation, affecting the radiation in a similar fashion as ISS does. This would explain the discrimination that the 1-d effect exerts between IDV and non-IDV sources.

The idea of an atmospheric scattering of radio waves is definitely not new. Ionospheric scintillation, for example, is known to severely affect radio experiments, expecially the ones involving interferometry at low wavelength. The effect, which introduces random temporal fluctuations in both the amplitude and the phase of radio signals, should be important on a time scale of *seconds*. It is a fact, though, that the TEC of the ionosphere varies significantly on daily time scales (see Fig. 5.7). Therefore, if we assume that changes in the TEC can cause considerable variations in the amount of scattered radiation, the correlation between the 1-d effect and ionospheric scattering would be obvious. *At 5 GHz, however, the effect is generally assumed to be negligible.* A further downside of this scenario is that the 1-d effect would not be expected to appear almost simultaneously in Effelsberg and Urumqi. However, since the time delay at the two sites also depends on the source position, and given the largeness of the region of the sky which is interested by high electron content due to insolation (see Fig. 5.7), a quasi-simultaneity must be regarded as possible. The time shift, moreover, should decrease with the height of the atmospheric layers where scintillation takes place.

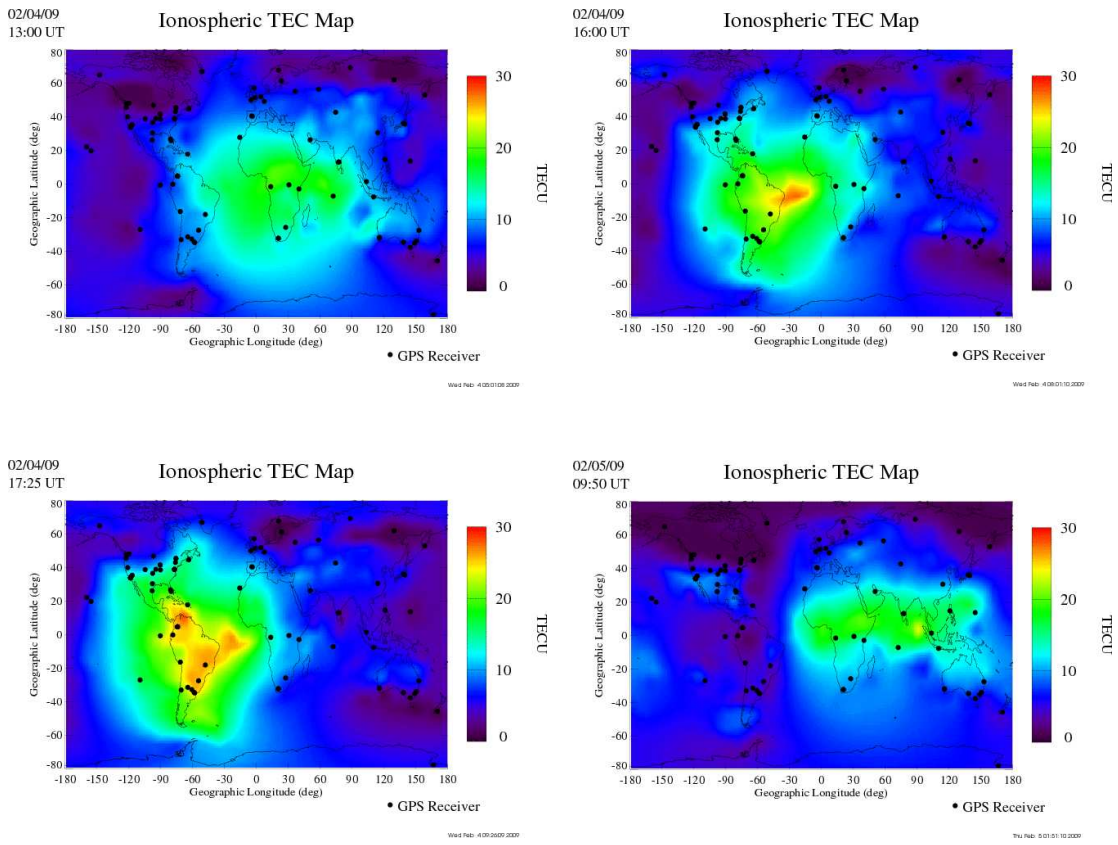

Figure 5.7: Global maps of ionospheric total electron content (TEC) produced by mapping GPS observable collected from ground stations. From the website *http://iono.jpl.nasa.gov*

On the same topic, it is worth to mention that standing waves would easily account for in-phase variability observed at different telescopes. The amplitude of the oscillation of such a wave would vary depending on the longitude of the site. We could roughly say that in correspondence with the nodes of the wave, the amplitude of the oscillation would be close to zero, while elsewhere it would assume a value between the maximum peak of the wave and its opposite. This implies that the phase difference between the oscillations observed at different sites should be close either to 0 or to π. Consequently, non-migrating atmospheric tides would provide a possible explanation for the simultaneity between the 1-d periodicities observed in Effelsberg and Urumqi. However, it is hard to say if and how much similar phenomena can affect the ionosphere. If this was the case, we could postulate that radio waves passing through the ionosphere could be affected too.

Looking at the remarks reported above, it should be evident that the scenario is far from being completely defined. There are many questions still waiting for an answer. Also assuming that the hypothesis of an atmospheric contribution to IDV is correct, it still must be established whether it is caused by changes in the ionospheric TEC, or by atmospheric tides, or if they all contribute to the variability. Atmospheric tides and TEC variations are both influenced by insolation; some of the time scales which characterize them are similar. Nevertheless, they are not the same phenomenon. While the TEC seem to provide a more

natural explanation for the scattering of radio waves, the simultaneity between Urumqi and Effelsberg peaks of the 1-d effect would be better explained by atmospheric tides.

The issue requires deeper investigation. Anyway, the existence of a correlation between atmospheric phenomena and IDV seem to be supported by several indirect arguments.

5.5 An alternative way for calibrating the data

The demonstration of the existence of a periodic signal in the variability curves of IDV sources leads immediately to a fundamental issue – should the data be analyzed as they are or is it better to isolate the periodic component in them and remove it? And, in this case, how can we do that?

It is very likely that the variability we detect after the standard data calibration procedure is a superposition of the 1-d effect and other components – due to ISS, for example, or to source intrinsic processes, or maybe both. Each component can provide us with very important information. An accurate estimate of the 1-d effect would help to conclusively define its nature, and possibly lead to interesting by-products (such as some characteristics of magnetosphere and/or ionosphere). Given the fact that the effect is distinctly source dependent, it may also provide useful information about the sources themselves. With regard to the other variability components, the importance of a proper estimation of their features does not need further discussion, being the usual arguments for the study of IDV.

It is straightforward that the best accuracy in the estimation of both the periodic and non-periodic components can be reached by disentangling them. For this reason, we have been looking for a method capable to isolate any variability which appears regularly, on daily basis, in a light curve. The procedure we developed is based on a very simple idea: if a pattern occurs regularly every day, it can be determined by dividing a variability curve into segments of 24 hours[1] and folding them on top of each other. Afterwards, if we fit a spline curve to the data, we can obtain an estimation of the 'average daily behaviour' of the variability. Expanding this pattern to the whole duration of the observation, finally, we can remove it from the original data, and obtain an approximation of the non-regular component. Since the presence of strong variability on long time scales can make the estimation particularly difficult, it may be necessary, before applying the procedure, to remove the long-term trend from the light curves.

An advantage of the procedure, is that it requires no preventive hypothesis about the shape of the periodic component. No need for approximations or sinusoidal decomposition; therefore, the 1 d, 0.5 d and 0.33 d plus any higher order harmonic can be removed in a single step, independently of their intensity and phase relations.

An example of how the technique works is showed in Fig. 5.8, for the light curve of 0716+714 in January 2007; the superposition of the variability patterns in the three days of observation (upper right panel) demonstrates the regularity of the effect during this epoch. The removal of the daily average modulation (lower right panel) determines a significant drop of the variability on short time scales, which shows how fundamental it is to take the 1-d effect into account for a proper study of annual modulation in IDV sources.

The evaluation of the average daily pattern has several applications. When plotted along with the source elevation, it provides a useful tool for determining if and how much

[1] Alternatively, we can opt for 23.93 hours segments – i.e. split the curves in sidereal days. Unfortunately, the duration of the observations and the sampling do not allow to see any clear difference between the two options, otherwise they could be used to discriminate between a solar-related and a sidereal effect.

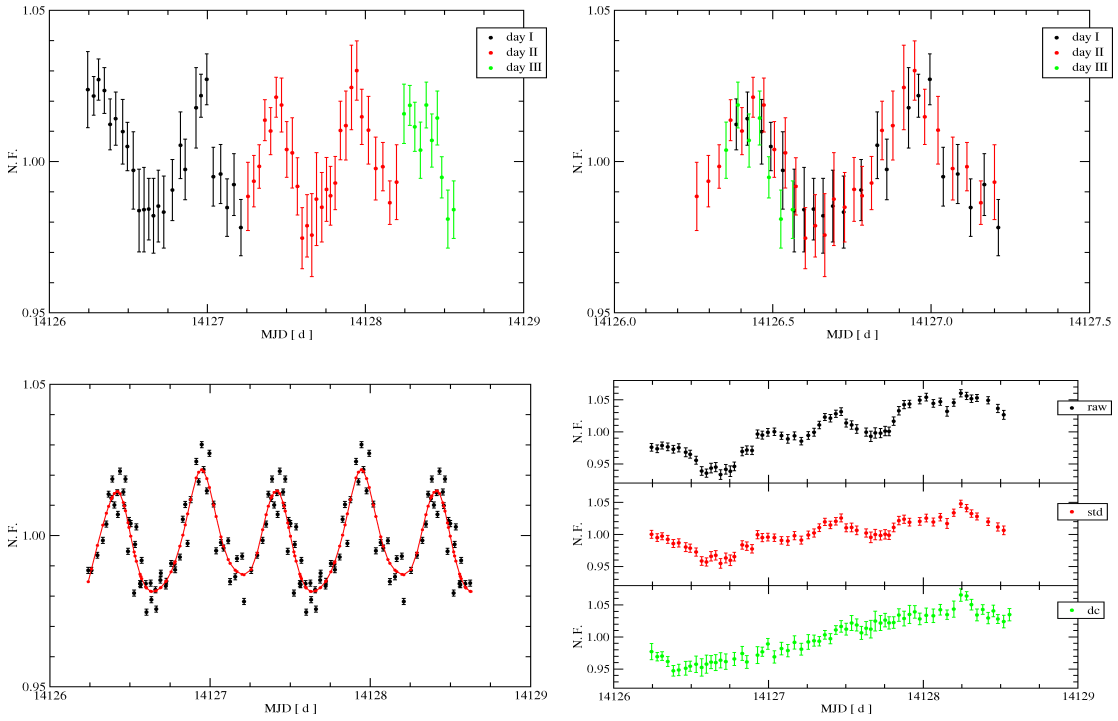

Figure 5.8: Different steps of the data calibration procedure which was developed for removing spurious periodic modulation. Upper left panel: the variability curve of 0716+714, observed in January 2007, after de-trending; upper right panel: the superposition of data obtained on different days of observation; lower left panel: the 'daily average modulation' extended to the total duration of the experiment; lower right panel: the variability curves before calibration (black), after the standard procedure for data calibration (red), and after the new calibration procedure (green).

the flux-density and elevation are correlated. A critical review of the procedure showed that a gain-elevation curve is not sufficient for reproducing the effect.

Interesting by-product is the possibility to compare the gain-elevation corrections, obtained in the standard way, with the daily average pattern, providing an evaluation of the efficiency of the gain-elevation correction and opening the way to the study of other sources of regular variability (instrumental, or due to day-night effect, etc.), which the procedure can trace. The removal of the 1-d periodic variability from the calibrators should reveal the non-regular variability component (mainly weather), which is supposed to be the same for all of them. In this sense, the method also provides an independent estimate of the gain-time variability.

Chapter 6

Time Analysis Results

The discussion of the variability characteristics of IDV sources is the main topic in this thesis project. In this chapter we are going to illustrate, source by source, the results we obtained for the observations performed between August 2005 and April 2008.

We will introduce the standard procedure we used for the data analysis and show how we removed any residual variability related to the 1-d effect. For all the IDV objects in our monitoring program, we will discuss the changes in the variability characteristics, and compare them with the predictions of the standard annual modulation model.

6.1 Time series analysis: from theory to practice

The application of the methods of time series analysis to real data suffers from some limitations. When the variability of the analyzed light curves has a non-negligible contribution from very slow components – with time scales longer than the duration of the observation – the estimated variability time scales may turn out to be proportional to it.

6.1.1 Two examples

We applied the sinusoidal regression (SR) and the structure function analysis (SF) to some data sub-samples from the August 2005 and August 2006 light curves of 0716+714. The sub-samples have different duration and number of points. In Fig. 6.1 we plot both light curves and results provided by the functions, while the time scale estimates are shown in Table 6.1. For the SR, the estimated time scales increase with duration – considerably for the August 2005 observation, less dramatically in the August 2006. The situation is more complicated when the analysis is performed by means of SF: for the August 2005 observation, again, the differences are very important. The shortest data-set almost does not allow a proper estimation of the time scale due to the absence of a clear trend in the function. In the case of the August 2006 data, three different plateaus can be identified in the plots, depending on the investigated sub-sample.

Apparently, the duration of the observation plays an important role in the evaluation of the time scales, with the consequence that the results for different epochs are not really comparable. When computed by applying directly SF and SR to the data-sets, the time scales of sources like 0716+714 and 1128+592 – which do often show strong long-term trends – turn out to be partially correlated with the duration of the observations, which makes the results useless for investigating the existence of annual modulation.

Table 6.1: SR and SF time scale estimates for the 0716+714 variability curves of August 2005 and August 2006. The application of the analysis methods to data sub-samples of different duration (column 2) demonstrates that the time scales (column 3 and 4) depend on the duration of the observation.

Sample	Duration (d)	SF (d)	SR (d)
August 2005			
1	2.7	2.0	4.7
2	2.4	1.4	4.3
3	2.1	?	3.3
August 2006			
1	6.3	5.0	4.0
2	5.4	1.4-3.0	3.5
3	4.4	1.4-3.0	3.3
4	3.5	3.0	3.1

There is no easy way to resolve the problem. On the one hand, it can not be considered a drawback of the analysis tools, since it is obvious that, for slow variability, the duration of the observation is a quite reasonable estimate of the lower limit of the variability time scale. On the other hand, lower limits do provide only limited information for our purposes. The removal of a long-term trend, calculated with a reasonably long time bin, may be a solution. However, it is not obvious how to chose a time bin which is suitable for all the epochs. Using different time bins will introduce serious and unpredictable biases in the results. The truncation of all the variability curves to the duration of the shortest, finally, would be an unacceptable loss of information and would raise the question of where to place the eligible time window within each curve.

6.1.2 Time scale estimation by Sinusoidal Regression

About SR, the resolution we finally adopted is the following. We obtained from the original light curve 13 de-trended curves, one for each de-trending time bin in the range from 0. 8d to 2.0 d. For each de-trended curve, and for the original light curve, we estimated the time scales. Finally, we plotted them as a function of the time bin (see Fig. 6.2). When a time scale was detected in most of the de-trended curves, we considered it significant. Often, the period and the amplitude of the fitted SR components for different bins showed small fluctuations. Therefore, we took the average as the best estimate, while the standard deviation provided us with a measure of the uncertainty.

In Fig. 6.2 we show the results for the August 2006 observations of 0716+714. In the rectangles are two time scales which have been discarded: the first, around 0.8 d, is apparently less significant than the others. The strong component around 10 d has been ignored because the time scale is too long to allow any comparison with the results of all the other observations, which have shorter duration.

6.1.3 Time scale estimation by Structure Function

Due to the difficulty of automating the evaluation of the time scales, this method could not be applied for the SF analysis. In an alternative approach, we decided to remove a

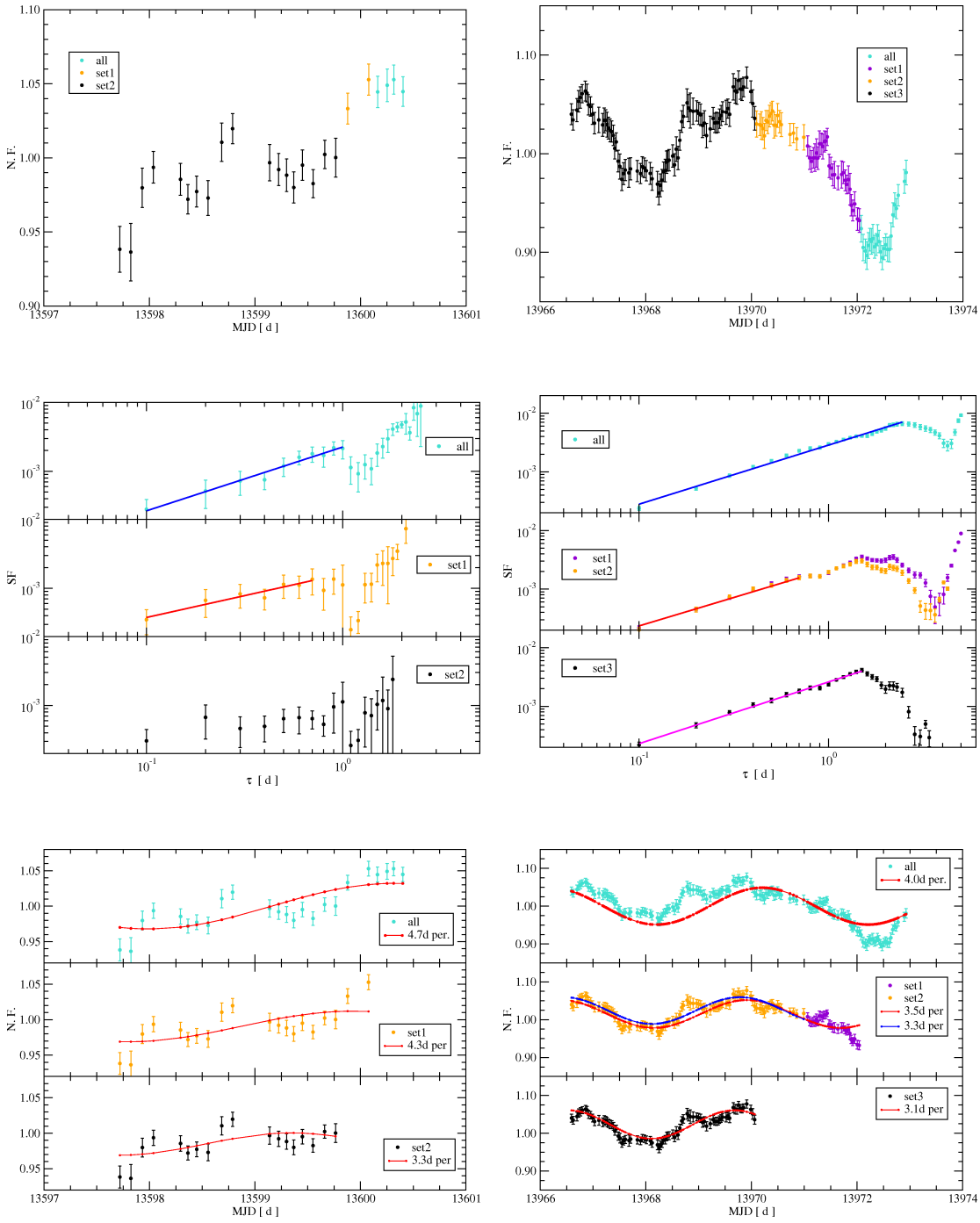

Figure 6.1: Upper panel: the August 2005 and August 2006 variability curves of 0716+714 (all the points), and the data sub-samples – in different colors – used for checking the dependence of the SF and SR on the duration. The middle and the lower panels give an idea of how the analysis tools are affected by the duration of the observations.

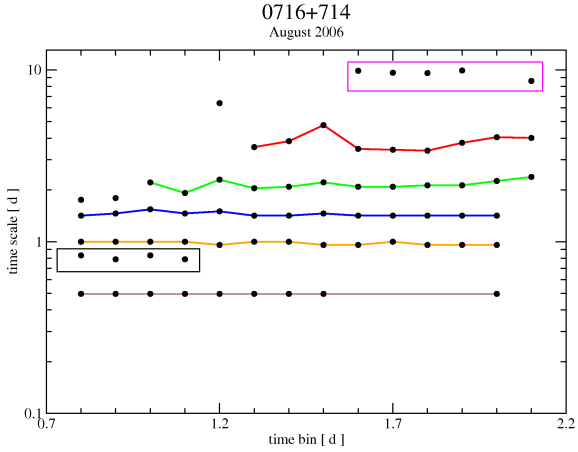

Figure 6.2: After de-trending the August 2006 variability curve of 0716+714, we de-trended it with different time bins. In the figure, we show the SR estimates of the time scales for the de-trended curves, plotted versus the de-trending time bins.

trend with a 2.5 d time bin, which is slightly smaller than the duration of the shortest observation. The results show that this approach is sufficient to make the SF results reasonably independent of the duration of the observation without modifying the IDV characteristics in the variability curves.

6.2 Standard procedure

Before presenting the results of the time analysis, we should briefly discuss the standard procedure which we used for the estimation of the variability characteristics.

- For each variability curve, we estimated the SR time scales. It is convenient to perform this step at first because it can reveal the presence of the 1d-periodicity, or its high-order harmonics.
- In the case that periodicities in the ranges 0.95-1.05 d, 0.47-0.53 d, 0.31-0.35 d and 0.23-0.27 d are detected, they are removed from the original data by subtracting the corresponding sinusoids.
- All the remaining time scales are averaged, using the amplitude of the sinusoids as weights. This way, SR can also provide a single time scale value for each variability curve.
- In an alternative approach, the variability curves are finally analyzed by means of the SF analysis.

All the variability curves of the IDV sources discussed in this chapter are plotted in Appendix B (upper panels of each figure) along with the dominant SR components; in the

lower panels, the corresponding structure functions. When the SF results are suspected to be affected by sampling, a scaled version of the sampling curve[1] is plotted as well.

The complementary use of SR and SF offers a very promising approach to the time analysis of a variability curve: it allows to 'clean' the data from undesired effects, it gives the possibility to look for independent variability components – and possibly trace their evolution – and provides two completely independent ways to determine the characteristic time scale in a data-set. The presentation of the results will demonstrate that, also practically, this approach pays off.

6.2.1 Annual modulation fit

The final step of the analysis is to search for a possible annual modulation of the variability time scales, as described in section 1.3.2. Using the equation presented there, we developed an algorithm for estimating the values of the five free parameters in the anisotropic annual modulation model which best fit the characteristic time scales. The free parameters are listed below (in brackets, we specify the ranges in which they are allowed to vary, which have been chosen according to the estimates given in Qian and Zhang (2001)):

- The screen distance (allowed to vary between 0.1 and 1 kpc);
- The screen velocity projected onto the right ascension of the source – hereafter, v_{RA} (between -20 and 20 km/s);
- The screen velocity projected onto the declination of the source – hereafter, v_{DEC} (between -20 and 20 km/s);
- The anisotropy degree (between 1 and 10);
- The anisotropy angle (between 0 and 180 degrees[2]).

The best fit is obtained through a least-square fit method.

Generally, the anisotropy does not play a very important role in the fit, and the screen distance acts on the time scales as a proportionality coefficient. The most important parameters, therefore, are the two screen velocities v_{RA} and v_{DEC}. In order to evaluate the most probable range of values for the velocities, for each pair (v_{RA}, v_{DEC}) we calculated the minimum variance obtained by letting the other parameters to vary freely in the given ranges. The results are then shown in a v_{RA}-v_{DEC} plot. Different level of variance are shown in different colors. An example is given in Fig. 6.3: on the left panel, an artificial set of time scales – a random sequence of two values, 1.3 d and 1.6 d, simulating a complete absence of annual modulation – along with the best fits. On the right panel, we show the plot of the variances. In order to refine the results, we repeated the fit three times, iteratively restricting the ranges of parameters closer to the best values obtained from the previous run. In the example, the best fits converge to (v_{RA}, v_{DEC}) in the ranges (3.5 - 8.0 km/s, 13.0 - 17.0 km/s). The red triangle represents the sun velocity in the Local Standard of Rest (LSR) projected onto the right ascension and declination axes of the source, respectively (v_{Sr}, v_{Sd}).

[1] For each time bin τ, the sampling is the number of data pairs which are used for the computation of $SF(\tau)$.

[2] Note that the anisotropy is π-periodic with respect to the angle.

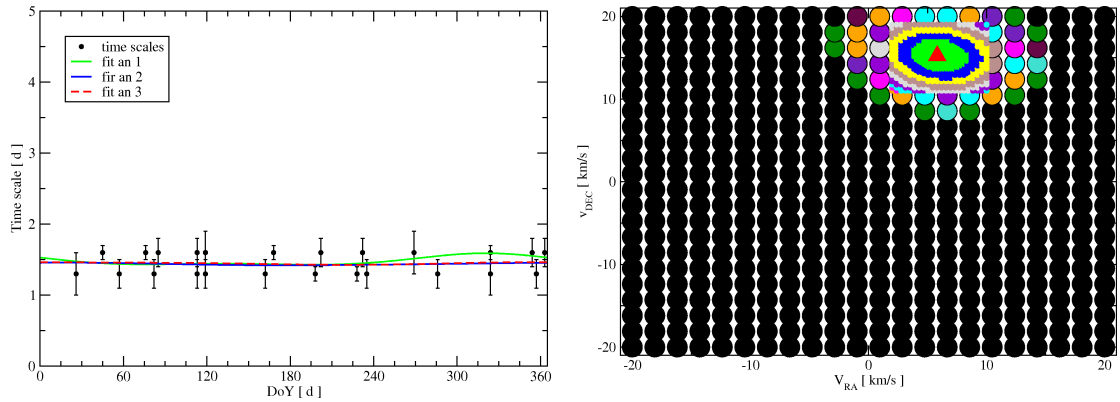

Figure 6.3: Examples of annual modulation plots obtained by an algorithm developed for the purpose; on the left panel, we show the variability time scales and the best fit. On the right panel, we plot the variances as a function of the velocity vector ($v_{\rm RA}$, $v_{\rm DEC}$); the black dots represent the highest variances, the light-green dots the lowest. The red triangle indicates the sun velocity in the LSR projected onto the right ascension and declination axes of the source position.

The example highlights an important aspect: when no annual modulation is present in the time scales of an object, $v_{\rm Sr}$ and $v_{\rm Sd}$ should fall into the region of most probable screen velocities. The plot can be used for judging the significance of the detected annual modulation pattern: the closer the location of the triangle to the region of most probable $v_{\rm RA}$ and $v_{\rm DEC}$, the less significant the fitted annual modulation.

6.3 0716+714

6.3.1 SR analysis

In Fig. 6.4, left panel, we plotted the *SR* estimates of the time scales as a function of the modified Julian date – where day 0 is set to January 1st, 2005. The plot includes the sinusoidal components with a significance[3] higher than 14%. The periodicities in the ranges 0.95-1.05 d, 0.47-0.53 d, 0.31-0.35 d and 0.23-0.27 d have been excluded. The size of each point in the plot is proportional to the amplitude of the corresponding sinusoidal component. In the right panel, same figure, the time scales are plotted as a function of Day of the Year (DoY), in order to investigate the presence of annual modulation. The time scales, along with the most important characteristics of the variability curves, are shown in Table 6.2.

In the plots, it is impossible to notice a clear trend in the evolution of *individual* variability components. From one epoch to the following, the most significant time scales – as well as their amplitudes – change considerably. Despite this fact, the plots of the averaged values obtained by *SR* (see Fig. 6.5) demonstrate the presence of a regular trend in the overall variability: the time scales tend to slow down, reaching a maximum around day 600 (September 2006), then they speed up till day 900 (April 2007). Later, a new raising trend appears, peaking close to day 1090 (December 2007), followed by a new

[3]For the definition of the significance of a period estimated by means of *SR*, see Eq. 3.26.

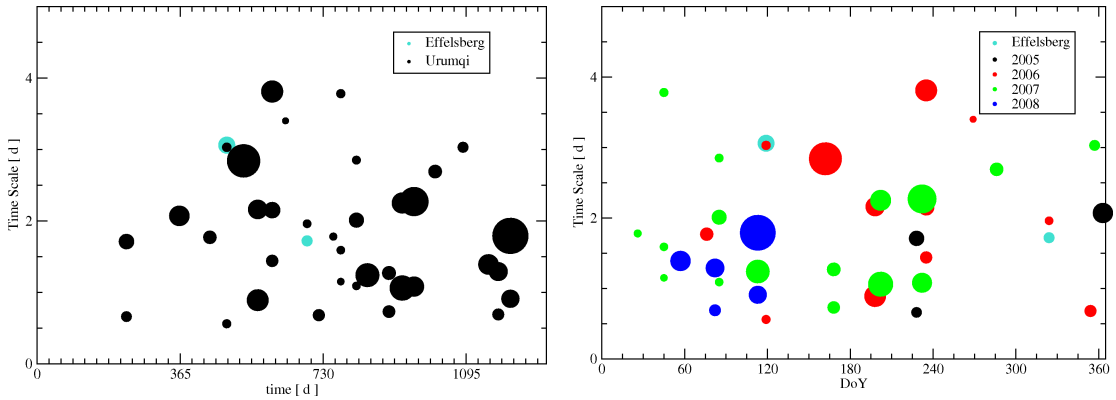

Figure 6.4: The SR variability components with significance higher than 14%, plotted versus modified Julian date – with day 0 being set to January 1st 2005 – (left panel), and Day of the Year (DoY) (right panel), for 0716+714. The size of the symbols is proportional to the amplitude of the sinusoidal components.

minimum at the beginning of 2008. Summarizing, we may say that the variability time scales tend to be higher in the second part of the year (June-November), although the plot versus DoY does not show it very clearly.

The presence of a trend in the time scales is a fact which deserves attention: it tells us that the variability changes slowly from epoch to epoch, and somehow coherently, therefore it makes us confident that the SR values are meaningful. It also means that sources of random noise, such as the sampling, do not significantly affect the results.

6.3.2 SR time scales histogram

An interesting by-product of the SR analysis is the histogram of the occurrence of each time scale in the 22 epochs under investigation (see Fig. 6.6). For the computation, we used all the sinusoidal components with significance higher than 9%[4], including the periods related to the 1-d effect. Our aim is to understand if there is any time scale which systematically repeats during the monitoring of a source, independently of its contribution to the total variability. Potentially, this could reveal spurious variability and give hints for possible periodicities, which could be intrinsic to a source.

According to the plot, in the 0716+714 variability curves two time scales occur more often than others: one is in the range between 0.95 and 1.05 d, the second one between 0.65 and 0.75 d. The former is a consequence of the 1-d effect. Our alternative way of data reduction has not been applied to all the data-sets, but only to those for which the 1-d period could be removed 'safely', with small risk of altering the characteristics of the rest of the variability. Therefore, residuals of the 1-d period were expected. The second time scale, instead, is less easy to explain. It is even more common than the former, and can not be a high-order harmonic of it. If we restrict our bin to 0.033 days, the recurrent time scale appears confined in the range between 0.65 and 0.683 days.

A fascinating hypothesis is that the time scale can be identified with a 0.666-d peri-

[4]According to our Monte Carlo simulations (see section 3.9), a periodic signal with 9% significance has to be regarded as real.

Table 6.2: The main parameters of the 0716+714 variability curves. In column 1 the epoch, in columns 2 and 3 the Day of the Year (DoY) and the modified Julian date (starting at January 1st, 2005); in column 4 the duration of the observations; in columns 5 and 6 the SR time scales and relative errors; in columns 7 and 8 the SF time scales and errors; in columns 9 and 10 the Modulation Index (m_i) and the average flux-density, respectively.

Set	DoY (d)	day (d)	Duration (d)	t_{SR} (d)	Err (d)	t_{SF} (d)	Err (d)	m_i (%)	$< S_{5\,GHz} >$ (Jy)
14.08.2005	228	228	2.9	1.1	0.1	1.4	0.3	3.27	0.880
27.12.2005	363	363	3.7	2.0	0.2	1.0	0.2	5.28	0.823
15.03.2006	76	441	3.0	1.5	0.1	1.6	0.2	1.94	0.638
27.04.2006	119	484	3.9	1.8	0.2	2.6	0.3	1.43	0.644
27.04.2006E	119	484	3.6	2.0	0.3	2.6	0.3	1.75	0.641
09.06.2006	162	527	3.2	2.6	0.2	3.0	0.3	4.93	0.736
14.07.2006	198	563	4.0	1.4	0.1	1.0	0.2	2.85	0.749
19.08.2006	235	600	6.4	3.2	0.2	1.4	0.2	4.53	0.838
23.09.2006	269	634	5.0	3.5	0.3	> 4.5	-	1.83	0.816
17.11.2006	324	689	4.7	2.2	0.1	1.6	0.3	3.63	0.742
17.11.2006E	324	689	2.6	2.5	0.3	1.8	0.3	2.61	0.751
18.12.2006	354	719	2.4	0.9	0.2	0.8	0.2	1.81	0.701
25.01.2007	26	756	2.3	1.6	0.3	2.0	0.2	2.18	0.786
12.02.2007	45	775	4.0	2.0	0.1	1.2	0.2	2.27	0.754
24.03.2007	85	815	2.8	2.6	0.2	3.0	0.3	2.16	0.738
20.04.2007	113	843	3.7	1.6	0.2	1.4	0.2	4.35	0.740
15.06.2007	168	898	2.4	0.9	0.1	0.6	0.2	2.09	0.834
19.07.2007	202	932	2.9	1.8	0.2	2.4	0.3	4.07	0.776
18.08.2007	232	962	3.1	2.1	0.2	3.0	0.2	4.05	0.779
13.10.2007	288	1018	3.0	3.2	0.2	2.8	0.3	2.62	0.802
21.12.2007	357	1087	3.2	3.6	0.2	> 2.3	-	3.04	0.689
24.02.2008	57	1152	2.9	1.1	0.2	1.0	0.2	2.09	0.818
21.03.2008	82	1177	3.0	1.2	0.2	1.4	0.3	2.99	0.786
21.04.2008	113	1208	3.1	1.5	0.2	1.6	0.5	3.40	0.853

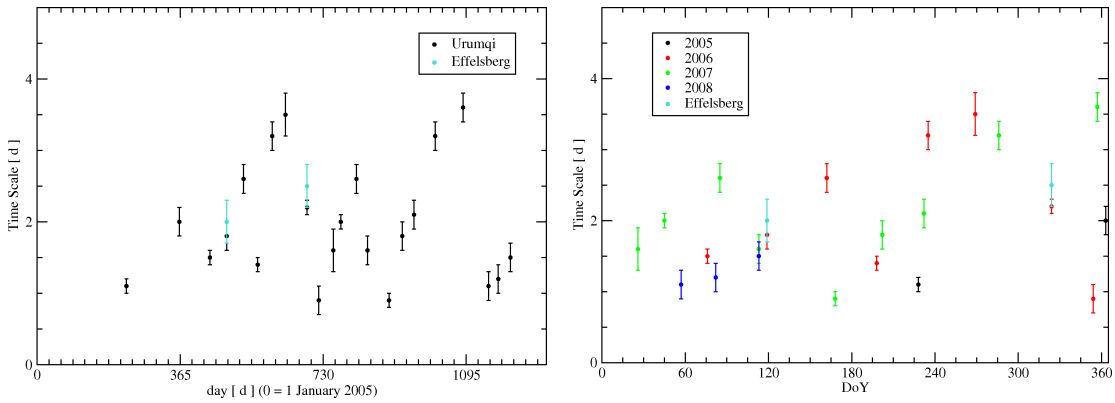

Figure 6.5: The weighted average of the 0716+714 variability components provided by SR, plotted versus modified Julian date (left panel) and DoY (right panel). The averages have been estimated excluding all the components with significance lower than 5%.

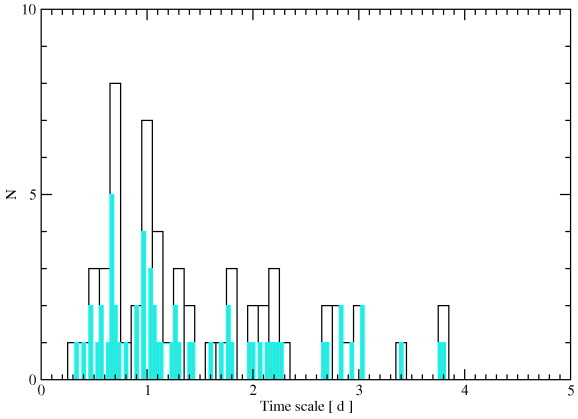

Figure 6.6: The histogram of the 0716+714 variability components provided by the SR analysis of 22 light curves. The time scales close to 0.66 d and 1.00 d occur more frequently than any other.

Table 6.3: The number of time bins N_τ (column 2) characterized by n_{det} detections (column 1), compared with the expectations from the model (N_{exp}, column 3).

n_{det}	N_τ	N_{exp}
0	26	25
1	17	18
2	7	6
3	0	1
4	0	0

odicity, namely *the 3rd harmonic of a two-day period*. If this is the case, it would support the hypothesis that the 1-d effect is related to Earth-rotation.

In order to understand how significant the result is, we can estimate the probability of a time scale in the interval 0.65-0.683d to occur 5 times *by chance*. The simplest way is to assume that all the time bins have the same probability to host a detection, and evaluate the probability according to a binomial distribution. Looking at the histogram, we can see that the assumption is reasonable if we limit the investigation to the time bins in the range between 0.25 and 2.12 days, and if we exclude the ones falling between 0.95 and 1.05 days – because their probability is higher than that of the others. This leads to 51 bins, which include 36 events . Therefore, the probability p for one detection to fall in a given bin will be $\frac{1}{51}$, and the number N of events will be 36. The binomial distribution gives the probability of m detections in a single bin as

$$P(m) = \frac{N!}{m!(N-m)!} p^m (1-p)^{N-m}, \tag{6.1}$$

which, in our case, means

$$P(5) = \frac{36!}{5!\ 31!} \Big(\frac{1}{51}\Big)^5 \Big(1 - \frac{1}{51}\Big)^{31} \tag{6.2}$$

which can be worked out to be $\sim 0.06\%$. We can again use a binomial distribution for estimating the probability that 'the event' of finding 5 recurrences in the same bin occurs in 1 or more bins out of 51, obtaining a value of 3%.

Before any further discussion, we ought to make sure that the simple model we used, including the assumptions, is reliable. For doing so, we can check whether the number of time bins N_τ characterized by n_{det} detections is consistent with the expectations from the model (N_{exp}). In Table 6.3, we report n_{det} (column 1), N_τ (column 2) and N_{exp} (column 3).

The table demonstrates that the model works fairly well, and that it is very improbable that the time interval between 0.65 and 0.683 days occurs that often by chance. It must instead have a special meaning for the variability of 0716+714. This, of course, does not necessarily mean that it is a high-order harmonic of a two-day period, as we hypothesized. Such an explanation, however, seems to be the simplest. Combined with the evidence illustrated in section 5.2 it strongly supports the idea that what the so-called 1-d period is just one aspect of a complex phenomenon, whose contribution to IDV can also appear on time scales longer than 1 day. If this is true, the implications in the study of IDV can be very important, since it becomes almost impossible to separate the contribution of the phenomenon to the variability from any other.

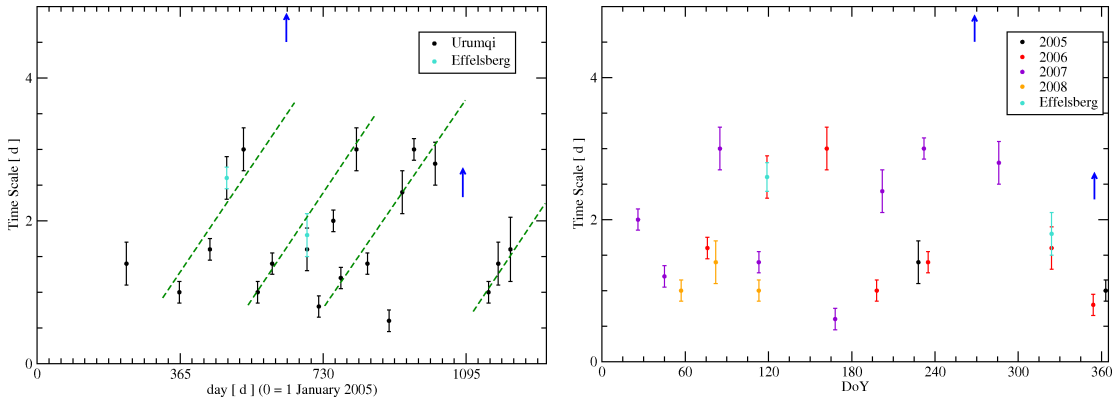

Figure 6.7: The variability time scales of 0716+714 obtained by SF analysis, plotted versus MJD (0=January 1st, 2005; left panel) and day of the year (right panel). At first look, no strong evidence in favour of a seasonal cycle can be seen in the plots. The dashed lines highlight four possible phases of coherent slow down in the time scales.

An objection could be raised: in Fig. 6.6, we do not see a high concentration of time scales close to two days, as expected in case of a two-day period in the data. A possible explanation is that the limited duration of the observations does not allow to find it. In most of the variability curves, we could not see more than one complete cycle of a two-day period, and this implies a large uncertainty in its estimation. Only three observations have durations long enough for a better evaluation of the periodicity: August, September and November 2006 (with respectively 6.4, 5.0 and 4.7 days of observation). In the second epoch (see Fig. B.10) there is no hint of a two-day period, while in the other two we found periodicities of 2.15 ± 0.12 d (August, see Fig. B.12) and 1.96 ± 0.12 d (November, see Fig. B.13). The explanation, therefore, is reasonable. The histogram, moreover, shows a large number of detected time scales between 1.95 and 2.28 days, which also could be due to an inaccurate estimation of a two-day period.

6.3.3 SF analysis

Further interesting information is provided by the results from a Structure Function analysis (see Fig. 6.7 and Table 6.2).

It is difficult to see a clear pattern in the variations of the SF time scales, when they are plotted versus time. The variability seems to slow down coherently in time intervals of about 6 months. Later, it speeds up quite abruptly: it fastly reaches a minimum, and then it starts again to gradually slow down. This peculiar behaviour appears 4 times during our monitoring campaign: in December 2005 - June 2006, July 2006 - March 2007, December 2006 - December 2007, February 2008 - April 2008 (see Fig. 6.7, left panel). Three of these trends are fully confirmed by the SR results, while the fourth appears less certain. Between the end of 2006 and the beginning of 2007, the slow and the fast time scales appear alternatively. This behaviour is hard to explain; we may hypothesize that the variability of 0716+714, during this time interval, is characterized by the co-existence of two variability components. Changes in the relative strength of the two may determine which one is detected as the dominant by the SF analysis.

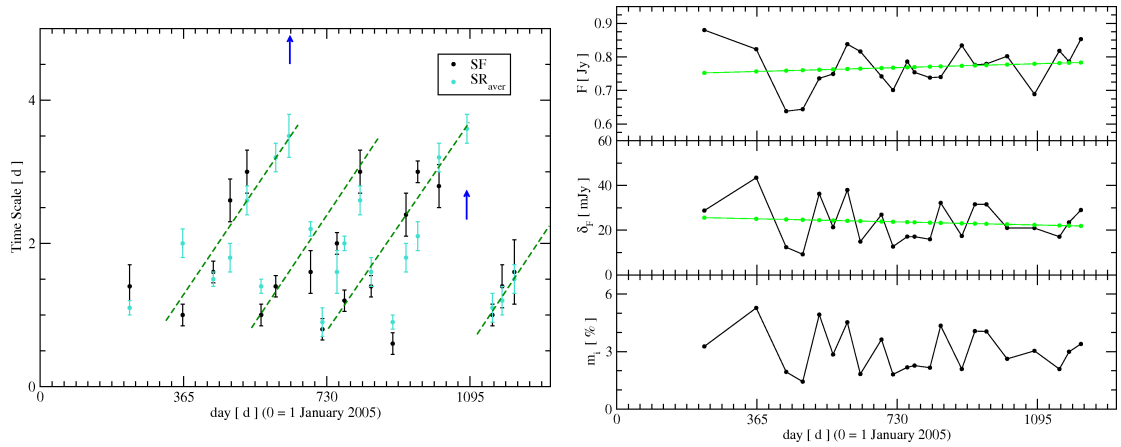

Figure 6.8: *Left figure*: comparison between the 0716+714 time scales provided by SF (black circles) and SR (turquoise circles); despite small differences, the agreement looks fairly good. *Right figure*: the average flux at 6 cm (upper panel), the modulation index (middle panel) and the standard deviation of 0716+714 during the three years of our monitoring project.

Important information is provided by the comparison of the SR and SF time scales (see Fig. 6.8, left panel). Despite a small discrepancy, the degree of overlap is fairly good: in five cases (December 2005, April and August 2006, February and August 2007) the difference between the time scales is larger than 0.7 d. The fact can be explained by the existence of more than one time scale in the variability curves.

Let us briefly discuss the results of the simultaneous Effelsberg-Urumqi observations Despite the differences in the sampling and duration, the time scales provided by both SF and SR for the two sites are in excellent agreement (see Table 6.2, and Fig. 6.5 and 6.7); this confirms the capability of the analysis methods to provide information about the *signal*, independently of its different *realizations*.

During the three years of monitoring, the average flux of 0716+714 varied considerably, with peak-to-peak variations of the order of 30%, but without following a regular trend (see Fig. 6.8, upper right panel). No correlation is seen between the amplitude of the flux variations and the corresponding variability time scales. A similar conclusion can be drawn for the variations in the modulation index, which almost looks like the result of a random process (see Fig. 6.8, lower right panel).

6.3.4 Annual modulation

Although the plots of the SR and SF time scales versus DoY (see Fig. 6.8, left panel) do not reveal any obvious seasonal variation in the 0716+714 variability, the results of the annual modulation fitting software leads to different conclusions. In Fig. 6.9 we show the variability time scales derived with the SR (upper panel) and the SF (lower panel) method, along with the best fits, and the variances versus screen-velocity plots. The fits to the SR and the SF results both reveal a prolongation of the variability time scales which peaks between DoY 250 and 300. The SF annual modulation plot[5] shows a second

[5]The plot includes the lower limits in order to take into account the epochs of very slow variability.

peak around DoY 90. The best fit parameters are reported in Table 6.4.

The comparison between the SR and SF results reveals an excellent agreement in the v_{DEC} (see section 6.2.1) and screen distance estimations, while the difference between the v_{RA} values is larger, but still within the error bars. Some discrepancy is seen in the anisotropy parameters: the SR results are compatible with isotropic scattering, while the SF ones are fitted better if we introduce some degree of anisotropy.

If we project the sun's velocity with respect to the LSR onto the Right Ascension and Declination axes for 0716+714 we obtain $v_{Sr} = 5.8\,\mathrm{km/s}$ and $v_{Sd} = 15.2\,\mathrm{km/s}$, respectively. These values are outside the velocity range obtained from the annual modulation fits, which means that the detected seasonal cycle is significant. Further evidence in favour of annual modulation comes from the fact that the most prominent peak in the time scales falls between DoY 250 and 300. Unless the LSR screen velocity is very high, we expect the sun's motion to play the major role in the variation of the time scales. For example, assuming the screen velocity to be close to zero, the time scale peak would fall around DoY 270, which is consistent with our results.

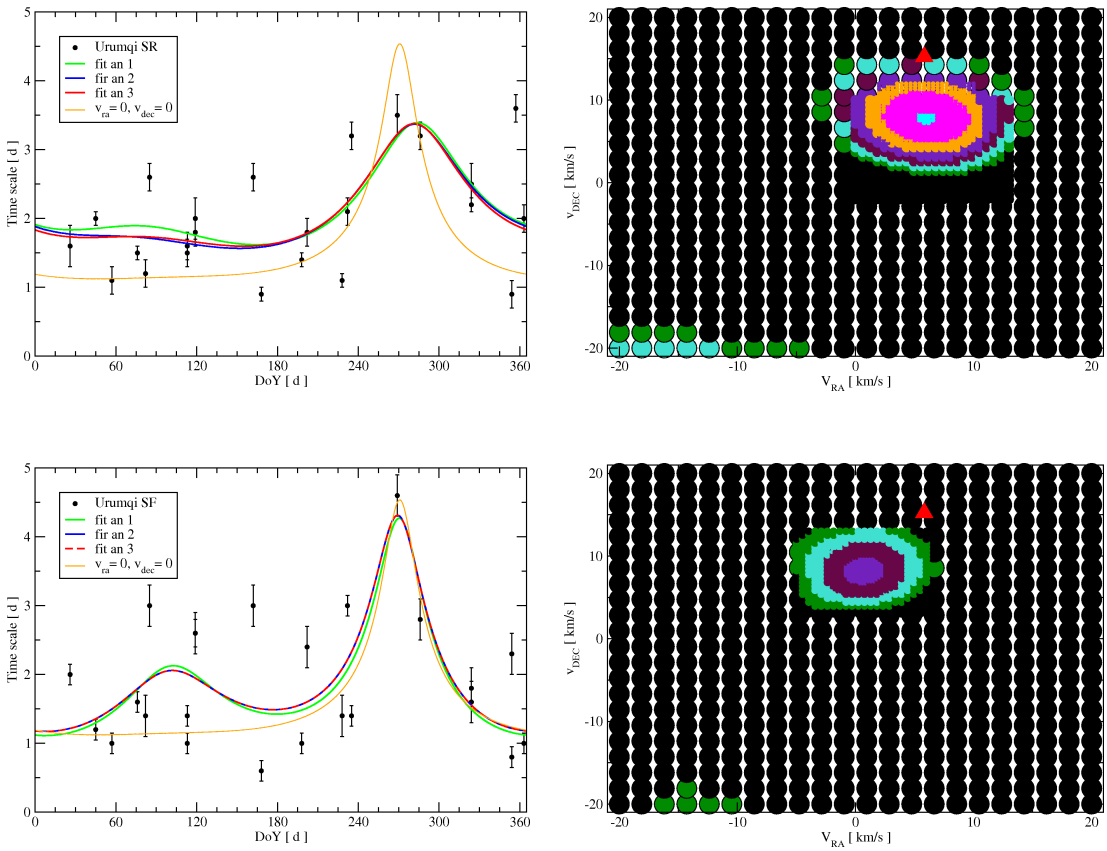

Figure 6.9: *Left panels*: Annual modulation plots for the variability time scales of 0716+714. The slowdown between September and October is detected by both the SR (upper panels) and the SF (lower panels) analysis, while the March-April peak appears only in the latter ones. *Right panels*: In turquoise and in violet, the regions of lowest variance in the annual modulation fit of the time scales derived by SR and SF, respectively. In black, the regions of highest variance.

Table 6.4: The best fit screen parameters deduces from the 0716+716 time scales.

Analysis method	v_{RA} (km/s)	v_{DEC} (km/s)	Screen distance (kpc)	Anisotropy degree	Anisotropy angle (degrees)
SR	6 ± 4	8 ± 3	0.22 ± 0.03	1.1 ± 0.1	-
SF	1 ± 3	8 ± 3	0.21 ± 0.02	1.5 ± 0.2	80 ± 10

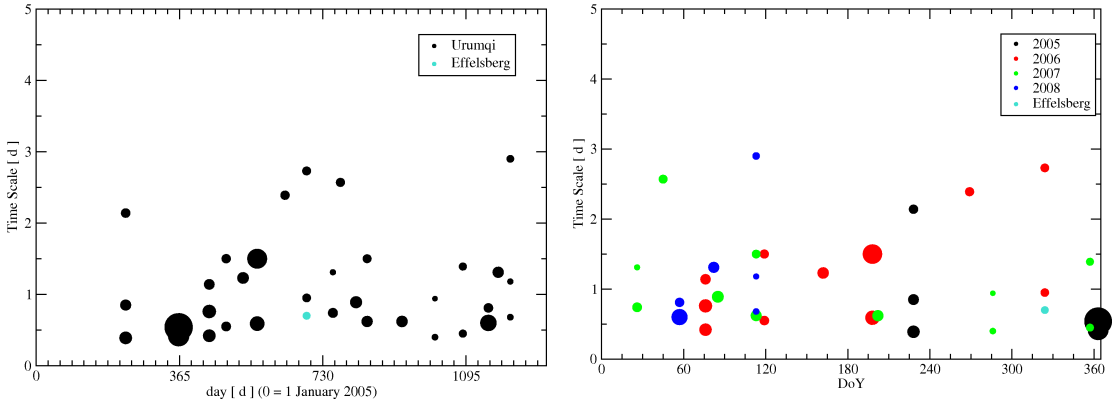

Figure 6.10: The 0917+624 variability components with significance higher than 9%, as computed by *SR* analysis. When plotted versus modified Julian date (left panel), the time scales appear to undergo a gradual slowdown during the year 2006. It seems to culminate between October and November. When plotted versus DoY (right panel), the time scales appear preferably concentrated in a small range of values during the first half of the year. In the second half, they seem to spread over a larger interval.

6.4 0917+624

6.4.1 Variability time scales

Between 1999 and 2000, the previously very pronounced IDV in 0917+624 stopped and up to now did not reappear (Fuhrmann et al. (2002), Bernhart et al. (2006)). A glance at the variability curves observed during the Urumqi monitoring campaign (see Appendix B) confirms that the object is still in quiescent state. The variability detected in the light curves is so low that the *SF* analysis is able to provide proper time scale estimations only for 9 out of 20 observing sessions. In all the other cases only lower limits could be found. Under these circumstances the *SR* analysis shows its advantages, being able to provide useful information for all the curves (see Fig. 6.10). A summary of the most important characteristics of the variability curves can be found in Table 6.5.

If we plot the sinusoidal components with significance higher than 9%[6] versus modified Julian date, we see a clearly increasing trend, which peaks in November 2006; afterwards the time scales decrease reaching a minimum in October 2007. This epoch marks the beginning of a new phase of slower variability, which is still ongoing. The plot of the time scales versus DoY shows two remarkable features:

- While in the first part of the year most of the variability time scales are concentrated

[6]We set a lower threshold than for 0716+714, because of the fewer variability components.

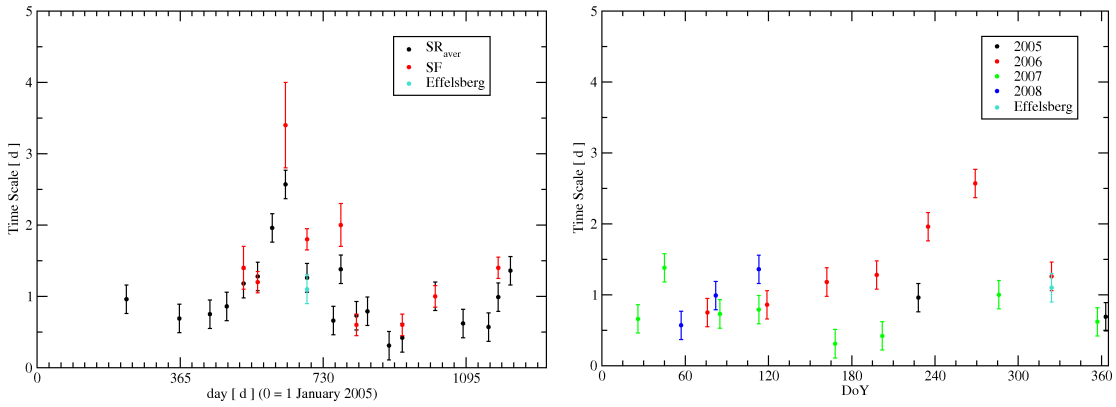

Figure 6.11: The average values of all the SR components with significance higher than 5%, plotted versus modified Julian date (left panel) and DoY (right panel). The 0917+624 time scales follow a regular pattern, with a clear maximum (September 2006) and a clear minimum (June 2007).

between 0 and 1 day, in the second part they spread over a larger range of values.

- Between DoY 200 and 350 the fast time scales seem characterized by lower significance than those in the rest of the year. This means that the contribution of the slow variability components in this time interval is higher than on average.

6.4.2 Annual modulation

The picture above is fully confirmed by the plot of the averages of the sinusoidal components (see Fig. 6.11). The very regular slowdown of the time scales, peaking in November 2006, emerges clearly from the data, and is confirmed in the few SF values (turquoise points). The plot of the time scales versus DoY gives the impression that the variability becomes slower between DoY 210 and 300. It has to be mentioned, though, that this impression is mainly caused by two points, both associated to the same year of observation (2006).

The results of the annual modulation fitting program appear consistent with the presence of a seasonal cycle, with the time scales peak around DoY 260 (see Fig. 6.12, left panel). This is in excellent agreement with the conclusions of the 0917+624 IDV studies by Rickett et al. (2001) and Fuhrmann et al. (2002), in the end of the 90s – when the source was still showing strong IDV activity – which predict the period of slowest variability to occur around DoY 250. The range of values which best fit the annual modulation plot are reported in Table 6.6. Due to the limited number of reliable time scale estimates, no meaningful fit could be obtained from the SF data.

The comparison of the extrapolated screen velocities with the LSR velocity of the sun ($v_{\rm Sr}$=11.74 km/s, $v_{\rm Sd}$=11.39 km/s) seems to confirm the significance of the detected annual modulation (see Fig. 6.12, right panel). As mentioned earlier, the evidence in favour of a seasonal cycle comes mostly from the observations performed in the year 2006. In the course of the year 2007 the variability appears considerably faster (see Fig. 6.13,left panel). Nevertheless, the overall trend agrees with the behaviour of our annual modulation fit: the

Table 6.5: The main parameters of the 0917+624 variability curves. In column 1 the epoch, in columns 2 and 3 the Day of the Year (DoY) and the modified Julian date (starting at January 1st, 2005); in column 4 the duration of the observations; in columns 5 and 6 the SR time scales and relative errors; in columns 7 and 8 the SF time scales and errors; in columns 9 and 10 the Modulation Index (m_i) and the average flux-density, respectively.

Set	DoY (d)	day (d)	Duration (d)	t_{SR} (d)	Err (d)	t_{SF} (d)	Err (d)	m_i (%)	$< S_{5\,GHz} >$ (Jy)
14.08.2005	228	228	2.9	1.0	0.2	-	-	1.50	0.885
27.12.2005	363	363	3.7	0.7	0.2	-	-	2.09	0.981
15.03.2006	76	441	3.0	0.75	0.2	-	-	1.13	1.046
27.04.2006	119	484	3.9	0.9	0.2	-	-	0.88	1.075
09.06.2006	162	527	3.2	1.2	0.2	1.4	0.3	1.08	1.090
14.07.2006	198	563	4.0	1.3	0.2	1.2	0.2	1.58	1.082
19.08.2006	235	600	6.4	2.0	0.3	-	-	1.61	1.088
23.09.2006	269	634	5.0	2.6	0.3	3.4	0.6	0.92	1.092
17.11.2006	324	689	4.7	1.3	0.2	1.8	0.2	1.00	1.093
17.11.2006E	324	689	2.6	1.1	0.2	-	-	0.93	1.086
25.01.2007	26	756	2.3	0.7	0.2	-	-	0.84	1.130
12.02.2007	45	775	4.0	1.4	0.3	2.0	0.3	1.15	1.144
24.03.2007	85	815	2.8	0.7	0.2	0.6	0.2	0.85	1.168
20.04.2007	113	843	3.7	0.8	0.2	-	-	0.89	1.211
15.06.2007	168	898	2.4	0.3	0.2	-	-	1.30	1.229
19.07.2007	202	932	2.9	0.4	0.2	0.6	0.2	1.23	1.268
13.10.2007	288	1018	3.0	1.0	0.2	1.0	0.2	0.87	1.253
21.12.2007	357	1087	3.2	0.6	0.2	-	-	0.77	1.282
24.02.2008	57	1152	2.9	0.6	0.2	-	-	0.97	1.317
21.03.2008	82	1177	3.0	1.0	0.2	1.4	0.2	1.12	1.319
21.04.2008	113	1208	3.1	1.4	0.2	-	-	0.65	1.342

Table 6.6: The best fit screen parameters deduced from the 0917+624 time scales. The SF results, unfortunately, do not provide enough information for a proper annual modulation fit.

Analysis method	$v_{\rm RA}$ (km/s)	$v_{\rm DEC}$ (km/s)	Screen distance (kpc)	Anisotropy degree	Anisotropy angle (degrees)
SR	-1 ± 4	8 ± 2	0.11 ± 0.02	2.0 ± 0.1	10 ± 10
SF	-	-	-	-	-

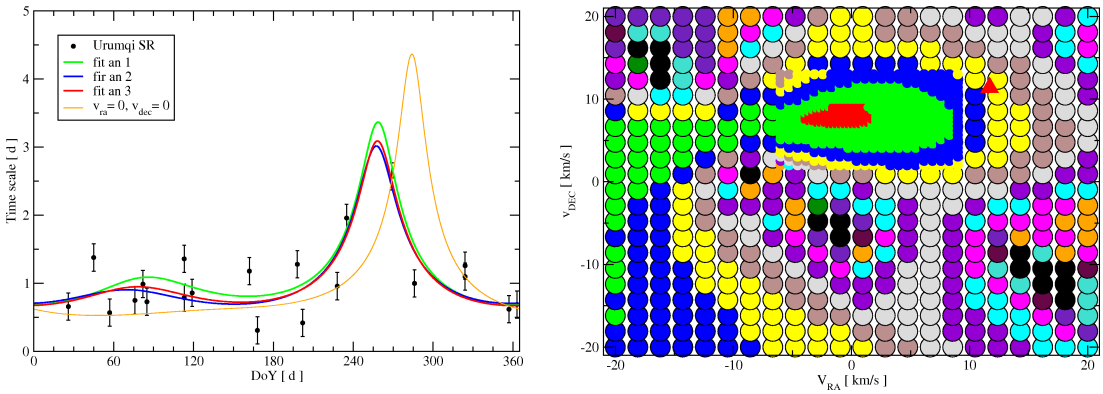

Figure 6.12: Annual modulation plots for the variability time scales of 0917+624, as estimated by means of SR. The screen velocities for which the variance is lower are the ones represented in red and green (right panel).

slowest time scale occurs in October, as expected from the model. It is really unfortunate that in August 2007 (when the variability was expected to be considerably slow) the source was not observed. It would have been an excellent probe for the seasonal cycle.

6.4.3 Further characteristics

The variability curves from the simultaneous Effelsberg-Urumqi observations performed in November 2006 are in good agreement. The few features which appear in the variability curve obtained in Urumqi seem to be confirmed by the Effelsberg data, which implies that, despite the weakness of the IDV activity shown by 0917+624, our experiments are able to detect it (see Fig. 6.13, right panel).

The histogram of the SR sinusoidal components of 0917+624 (see Fig. 6.14, left panel) shows important differences to that of 0716+714. The predominant periodicities are between 0.25 and 0.35 days, and between 0.45 and 0.55 days. The time ranges are consistent with high-order harmonics of a 1-d period; it is unclear, however, why these do reoccur more often than the 1-d period itself. If we narrow the histogram bins to 0.033 d, we realize that the interval centered on 0.333 days is by far predominant over all others.

The plot of the average flux-density versus the modified Julian date (Fig. 6.14, right panel) shows an almost-linear increasing trend during the three years. Over the same period, the modulation index of 0917+624 seems to follow an opposite trend: the variability gradually fades away, reaching its minimum in March 2008. As in the case of 0716+714, no evidence for a correlation between time scales and flux-density and/or modulation index

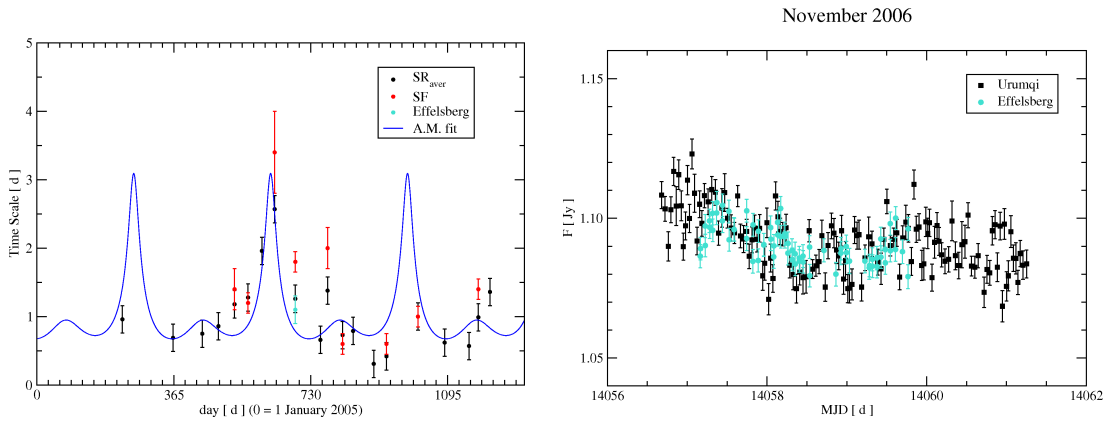

Figure 6.13: *Left panel*: The best fitting annual modulation model follows very well the changes in the variability time scales of 0917+624 during the year 2006. In 2007, the variability appears to be generally much faster than before. *Right panel*: the variability curves from the simultaneous observations performed in Urumqi (black circles) and Effelsberg (turquoise circles) in November 2006.

is apparent.

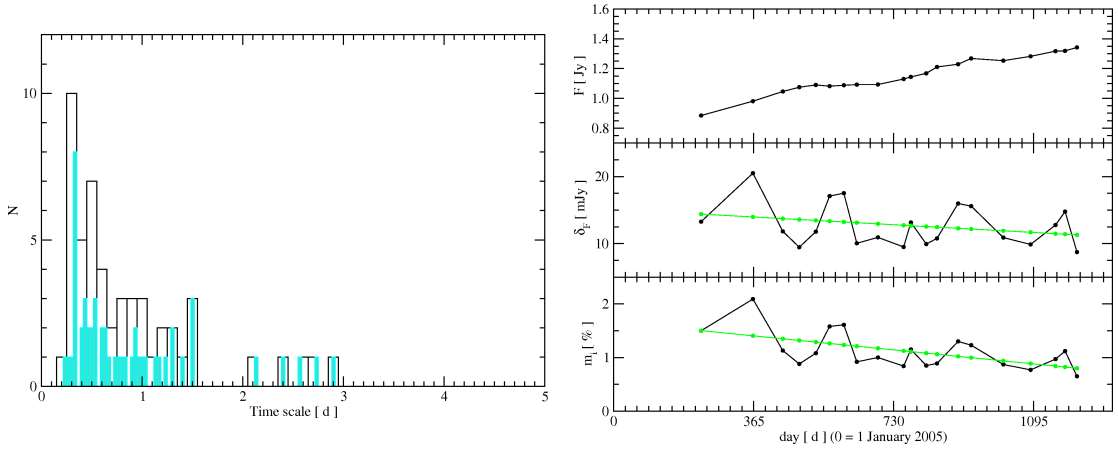

Figure 6.14: The histogram of the SR time scales of 0917+624 (left panel) reveals the predominance of the time scale centered around 0.33 d, most likely a by-product of the 1d-effect. The plots of the flux and modulation index versus modified Julian date (respectively upper and lower panels on the right) seem to show an anti-correlation between the two quantities. The anti-correlation, however, appears weaker looking at the plot of the standard deviation (middle panel).

6.5 0954+658

Being the target of several IDV campaigns over the last years, 0954+658 did never show a seasonal cycle strong enough to claim beyond any doubt an ISS origin of its variability.

Table 6.7: The main parameters of the 0954+658 variability curves. In column 1 the epoch, in columns 2 and 3 the Day of the Year (DoY) and the modified Julian date (starting at January 1st, 2005); in column 4 the duration of the observations; in columns 5 and 6 the SR time scales and relative errors; in columns 7 and 8 the SF time scales and errors; in columns 9 and 10 the Modulation Index (m_i) and the average flux-density, respectively.

Set	DoY (d)	day (d)	Duration (d)	t_{SR} (d)	Err (d)	t_{SF} (d)	Err (d)	m_i (%)	$< S_{5\,GHz} >$ (Jy)
14.08.2005	228	228	2.9	1.9	0.2	2.2	0.3	1.93	0.912
27.12.2005	363	363	3.7	1.4	0.2	> 3.5	-	2.03	1.143
15.03.2006	76	441	3.0	1.6	0.1	1.0	0.2	1.60	0.919
27.04.2006	119	484	3.9	1.4	0.2	0.8	0.2	1.22	1.146
27.04.2006E	119	484	3.6	1.6	0.2	1.8	0.2	1.33	1.135
09.06.2006	162	527	3.2	1.9	0.2	1.4	0.3	1.99	1.110
14.07.2006	198	563	4.0	1.8	0.2	> 3.5	-	0.90	1.016
19.08.2006	235	600	6.4	2.5	0.3	1.6	0.2	1.06	1.092
23.09.2006	269	634	5.0	2.0	0.2	1.6	0.2	1.26	1.213
17.11.2006	324	689	4.7	2.3	0.2	2.0	0.3	1.16	1.065
17.11.2006E	324	689	2.6	2.0	0.2	2.0	0.3	1.23	1.051
18.12.2006	354	719	2.4	0.8	0.1	1.4	0.2	0.95	0.959
25.01.2007	26	756	2.3	1.0	0.1	1.2	0.3	1.12	1.083
12.02.2007	45	775	4.0	1.8	0.1	1.8	0.2	2.28	1.060
24.03.2007	85	815	2.8	1.1	0.2	1.4	0.6	1.27	1.293
20.04.2007	113	843	3.7	2.3	0.2	3.6	0.5	1.95	1.301
15.06.2007	168	898	2.4	0.5	0.1	0.6	0.2	1.50	1.017
19.07.2007	202	932	2.9	1.1	0.2	1.8	0.3	1.73	0.899
18.08.2007	232	962	3.1	1.8	0.3	> 3.0	-	1.62	0.860
13.10.2007	288	1018	3.0	1.0	0.2	1.2	0.2	1.08	0.937
21.12.2007	357	1087	3.2	1.7	0.2	1.4	0.3	1.03	1.129
24.02.2008	57	1152	2.9	1.0	0.2	0.6	0.2	1.43	0.950
21.03.2008	82	1177	3.0	1.7	0.2	3.6	0.9	2.26	0.901
21.04.2008	113	1208	3.1	1.3	0.2	1.2	0.3	2.63	0.978

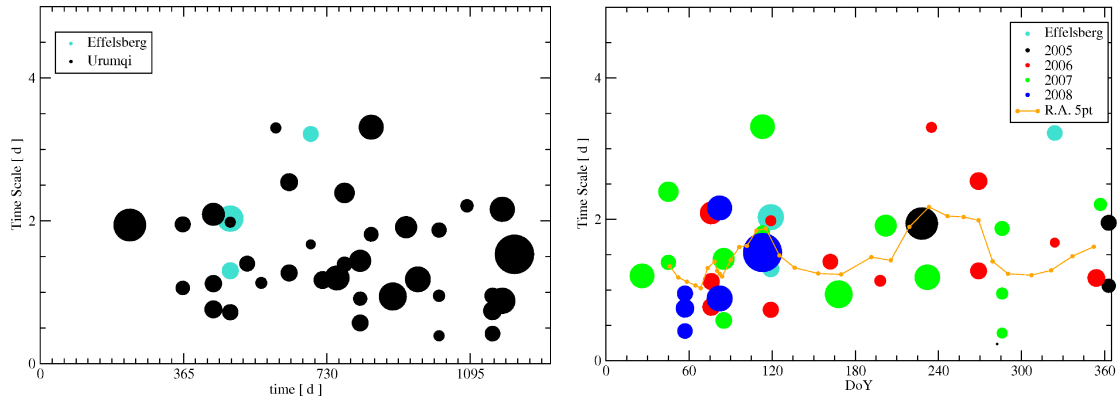

Figure 6.15: No regular or systematic pattern is seen in the variability components of 0954+658, derived by SR. The plot versus DoY (right panel) seems to give clues for the existence of two slowdown periods for the time scales: between April and May (DoY 120), and between September and October (DoY 240-270), as a 5-point running average (orange line) seems to highlight.

Our results confirm that the variability time scales of this source can not be easily modeled by annual modulation. Its variability characteristics are summarized in Table 6.7.

6.5.1 SR analysis

Figure 6.15, left panel, shows the plot of the SR-estimated variability components versus modified Julian date. The 0954+658 time scales seem to reach a minimum around March 2006. Afterwards, a phase of slower variability begins, which leads to a maximum around summer 2006, followed by a slow decrease till January 2007. In March 2007 the variability time scales drop to lower values than the year before, and a new slowdown phase begins. From October 2007 on, it becomes difficult to find a coherent pattern in the data.

If we plot the SR time scales versus DoY (Fig. 6.15, right panel), we found some (weak) evidence for a seasonal cycle. The source reaches the fastest variability between February and March (around DoY 60), while the slower time scales seem to fall between September and October (DoY 240-270). There is also a hint for a peak in the time scales around April (DoY 120), which becomes more evident when a 5 point-running averaging of the data is applied. Given the small amplitude of the variations under examination, though, it is hard to tell if this is significant.

The averages of the SR time scales agree partially with the description given above (see Fig. 6.16, upper panels). The slowdown trend between March and November 2006 is clearly visible in the data, while in the following epochs the variability pattern appears more scattered.

The superposition of the Urumqi and Effelsberg results reveals a very good agreement (see Table 6.7, and Fig. 6.16) the difference in the estimates of the time scale from the two telescopes is 0.2 d for the April 2006 experiment, 0.3 d for November 2006 – when the duration of the Urumqi experiment was considerably longer than the Effelsberg one (4.7 d versus 2.6 d).

No significant indication comes from the histogram of the SR values: the time scales

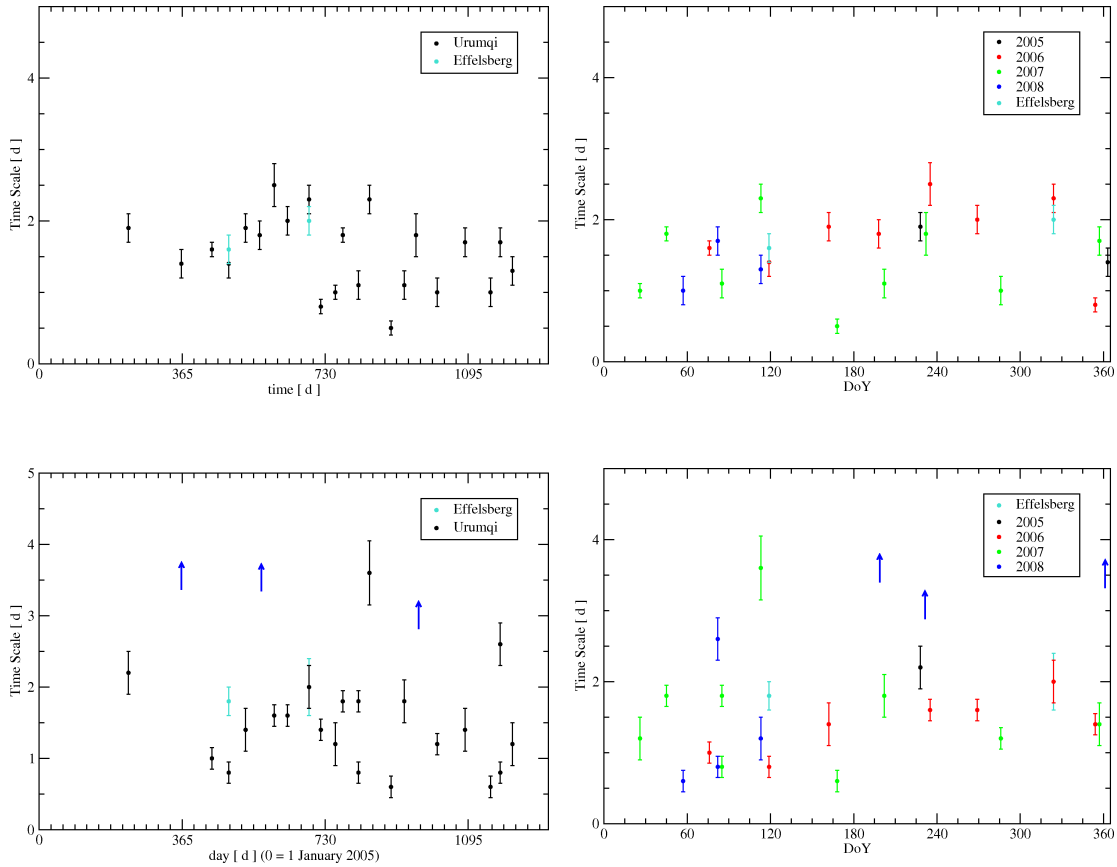

Figure 6.16: The variability time scale estimations obtained from SR and SF analyses (upper and lower panels, respectively), plotted versus MJD (0=January 1st, 2005; left panels) and DoY (right panels). No clear evidence for a seasonal cycle is seen in the data.

appear distributed almost homogeneously between 0 and 2 days, and even the ones typically related to the 1-d period seem to be as common as any other. Among the main sources in our monitoring project, 0954+658 is the one which suffers the less by a contamination of the 1-d effect.

6.5.2 SF analysis

For 0954+658, the agreement between the SF results and the SR average values is not very satisfactory. The latter are usually larger than the former. Nevertheless, what is important is that the *variability trends* that we obtain from the two methods are very similar. Therefore the same considerations expressed above apply to the SF estimates, plotted in the lower panels of Fig. 6.16. Slow variability seems more common in the summer than in the winter, but sometimes it also appears dominant between March and April, and even in December (note that in December we found one of the three lower limits we detected; the others occur in July 2006 and August 2007).

There is perfect agreement between the November 2006 time scales as estimated from the Urumqi and the Effelsberg light curves (see Table 6.7, and Fig. 6.16); less satisfactory are the results for the April campaign, for which the variability time scale derived from

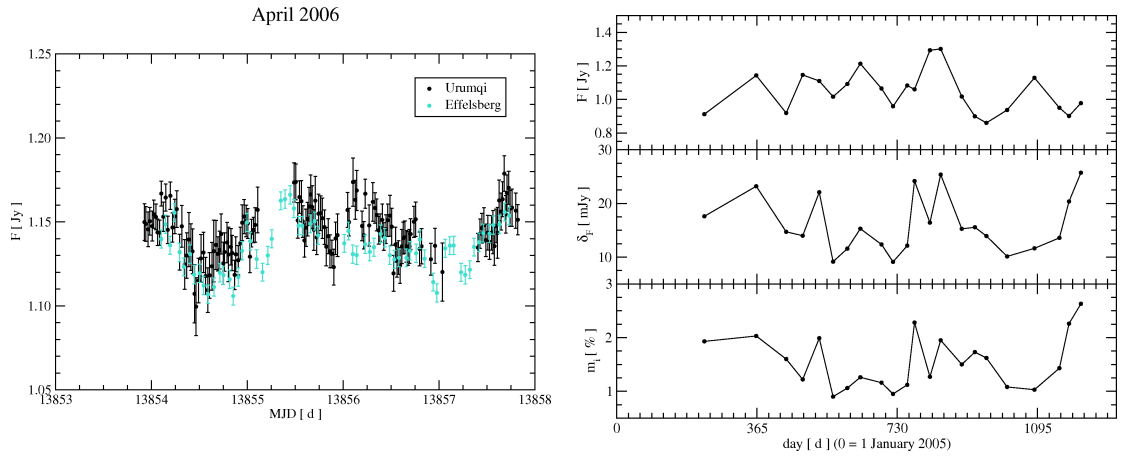

Figure 6.17: *Left panel:* The variability curves of 0954+658 obtained in Urumqi (black circles) and Effelsberg (turquoise circles) in April 2006. *Right panel:* flux-density and modulation index/standard deviation of the variability curves of 0954+658, plotted versus MJD. The modulations seem not to follow any regular trend.

the Effelsberg observation is more than twice the one from the Urumqi observation (1.8 d versus 0.8 d). If we consider that the two light curves overlap very well (see Fig. 6.17, left panel), and that the duration of the observations at the two sites is similar, we shall conclude that the reason for such a large discrepancy has to be associated with the presence of two large gaps in the Urumqi variability curve. Therefore, the most trustworthy time scale results from the Effelsberg data. The comparison with the SR results seem to confirm it.

The plots of the average flux and the modulation index (see Fig. 6.17, right panel) versus modified Julian date show that both quantities are characterized by fast variations, apparently not correlated with the observed changes in the time scales or between each other.

6.5.3 Annual modulation

The results provided by the annual modulation fitting program confirm that there is very weak evidence in favour of a seasonal cycle in the time scales of 0954+658. When applied to the SR values, the program highlights the possibility of a mild annual modulation (see Fig. 6.18, upper panels), peaking around DoY 260. We notice that the sun velocity in the LSR ($v_{\mathrm{RA}} = 13.01$ km/s, $v_{\mathrm{DEC}} = 9.38$ km/s) is not in the range of values which minimize the fit variance (see Table 6.8), but it falls very close to it. This means that the observed annual modulation is probably not significant. The usage of the fitting procedure on the SF time scales supports this conclusion: the seasonal changes are minimal, while the sun velocity in the LSR is consistent with the fitted screen velocities (Fig. 6.18, lower panels).

6.6 1128+592

The quasar 1128+592 is a special IDV source: the amplitude of its variability is very high and the time scales are faster than for other type-II IDV sources. Past IDV studies (see

Table 6.8: The best fit screen parameters deduced from the 0954+658 time scales. The SR and SF results seem compatible with a very mild annual modulation, if at all.

Analysis method	$v_{\rm RA}$ (km/s)	$v_{\rm DEC}$ (km/s)	Screen distance (kpc)	Anisotropy degree	Anisotropy angle (degrees)
SR	9 ± 3	9 ± 3	0.16 ± 0.02	1.3 ± 0.1	160 ± 15
SF	11 ± 3	9 ± 3	0.16 ± 0.02	1.05 ± 0.05	160 ± 30

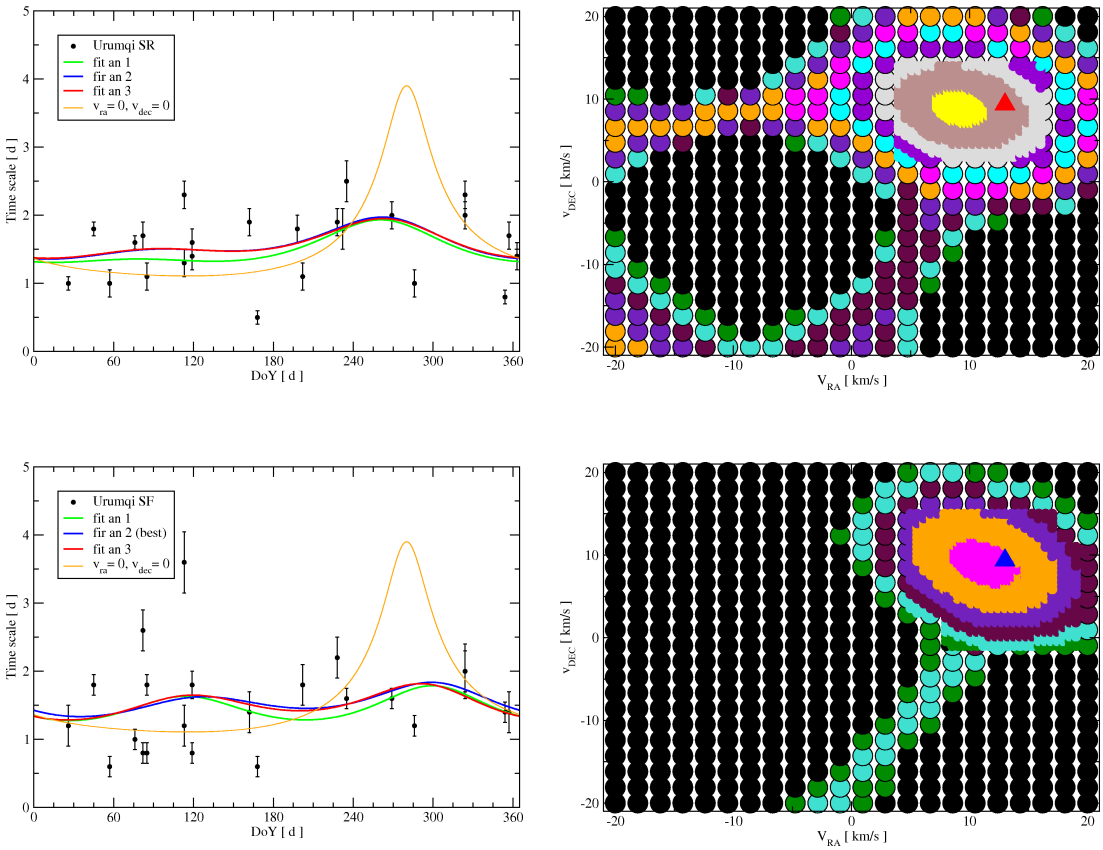

Figure 6.18: Annual modulation plots for the variability time scales of 0954+658.

Gabányi et al. (2007), from now on G07) found evidence in favour of annual modulation of the time scales, which makes 1128+592 more similar to fast scintillators. These facts suggest that this source may be the missing link between the two classes of objects.

6.6.1 SR analysis

The characteristics of the variability curves are given in Tab. 6.9. We start the discussion of the results, as usual, by presenting the variability components detected by the SR analysis (Fig. 6.19). If we exclude for a moment the exceptional result obtained for the April 2006 epoch (MJD 484, DoY 119), the plot of the most significant time scales versus modified Julian date seems to reveal the existence of a regular pattern – a gradual slowdown of the variability, which peaks in the second half of 2006. Afterwards, the time scales decrease

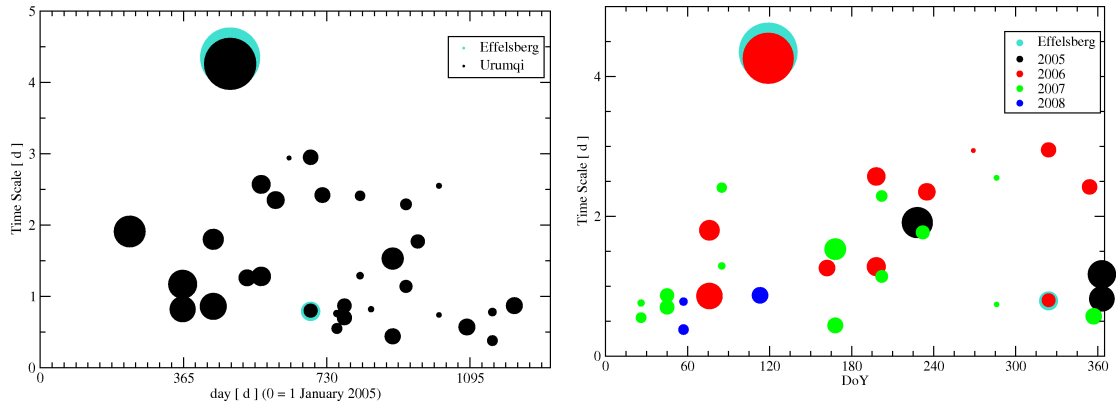

Figure 6.19: SR estimations of the variability components for 1128+592. The time scales seem to increase regularly from spring to autumn, strengthening the impression of a seasonal cycle in the variability of the source.

again reaching a minimum at the beginning of 2008. When we plot them versus DoY, the hypothesis of seasonal variations seems to be fully confirmed. With the exception of some data points between March and April, the slower variability occurs in the second half of the year, while the first half is characterized by much faster variability. It is remarkable that when the time scales increase to ~ 3 d, fast variability becomes visible again – still weak around DoY 290, but getting gradually stronger until December, when it becomes dominant. In January, the slow components are not detectable anymore, and the cycle seems to start again. The scenario is similar to the one described in G07, which explains the abrupt change in the time scales around April and the later slow variability – peaking around November – by means of an anisotropic annual modulation model. According to our results, however, the most important feature of the variability modulation in 1128+592 is the slowdown in the second part of the year. It repeats in 2006 and 2007 with very similar characteristics. Moreover, the two observations in 2005 provide time scales which fit perfectly with the other ones. The strong and slow component observed in April 2006, instead, does not repeat in other epochs. It should be noted, though, that the annual modulation plot is poorly covered during April and May, and that a slow time scale characterizes the March 2007 observation. This seems to testify that also the spring slowdown hypothesized in G07 is probably seasonal.

In the average SR values plot (see Fig. 6.20), the regularity of the time scale variations appears clearly. The variability reaches its slowest phase between DoY 240 and 280 (better coverage is needed for a more precise estimation). In the left panel the time scales corresponding to the April 2006 and the March 2007 observations appear unusually high.

A last remark about the recurrence of the SR time scales. Only the one in the interval between 0.317 and 0.35 days occurs much more often than the others. Most likely, it is related to the 1-d effect.

6.6.2 SF analysis

The agreement between SR averaged values and SF results (see Fig. 6.21) is very good. Despite the fact that sometimes the differences are larger than the error bars, the trends

Table 6.9: The main parameters of the 1128+592 variability curves. In column 1 the epoch, in columns 2 and 3 the Day of the Year (DoY) and the modified Julian date (starting at January 1st, 2005); in column 4 the duration of the observations; in columns 5 and 6 the SR time scales and relative errors; in columns 7 and 8 the SF time scales and errors; in columns 9 and 10 are reported the SF time scale estimated by K. E. Gabanyi (part from G07, part from private communication); in columns 11 and 12, the Modulation Index (m_i) and the average flux-density, respectively.

Set	DoY (d)	day (d)	Dur. (d)	t_{SR} (d)	Err (d)	t_{SF} (d)	Err (d)	t_{G07} (d)	Err (d)	m_i (%)	$< S >$ (Jy)
14.08.2005	228	228	2.9	1.8	0.1	2.0	0.3	1.8	0.5	6.62	0.674
27.12.2005	363	363	3.7	1.0	0.1	0.6	0.2	0.7	0.2	7.88	0.713
15.03.2006	76	441	3.0	1.2	0.1	0.8	0.2	0.7	0.2	5.66	0.668
27.04.2006	119	484	3.9	3.7	0.2	3.6	0.3	3.2	0.4	7.03	0.648
27.04.2006E	119	484	3.6	3.9	0.2	2.4	0.2	3.0	0.3	9.16	0.638
09.06.2006	162	527	3.2	1.7	0.1	1.4	0.3	1.0	0.2	4.08	0.595
14.07.2006	198	563	4.0	2.0	0.2	1.4	0.2	1.2	0.3	5.77	0.601
19.08.2006	235	600	6.4	2.4	0.1	2.0	0.2	2.4	0.3	4.67	0.586
23.09.2006	269	634	5.0	3.3	0.1	> 4.8	-	2.6	0.6	2.28	0.613
17.11.2006	324	689	4.7	2.0	0.2	1.6	0.6	-	-	4.73	0.551
17.11.2006E	324	689	2.6	1.9	0.1	1.6	0.6	-	-	5.12	0.553
18.12.2006	354	719	2.4	1.7	0.2	2.0	0.2	0.7	0.1	3.89	0.529
25.01.2007	26	756	2.3	1.1	0.1	0.6	0.2	0.8	0.3	2.54	0.488
12.02.2007	45	775	4.0	1.1	0.1	0.8	0.2	0.8	0.2	4.23	0.480
24.03.2007	85	815	2.8	2.0	0.2	2.0	0.3	-	-	3.46	0.462
20.04.2007	113	843	3.7	0.7	0.1	0.8	0.2	-	-	2.21	0.437
15.06.2007	168	898	2.4	1.1	0.1	1.2	0.3	-	-	4.48	0.417
19.07.2007	202	932	2.9	1.4	0.1	1.6	0.3	-	-	4.53	0.402
18.08.2007	232	962	3.1	1.3	0.2	1.6	0.3	-	-	3.72	0.389
13.10.2007	288	1018	3.0	3.0	0.2	2.6	0.6	-	-	2.92	0.366
21.12.2007	357	1087	3.2	0.6	0.1	0.6	0.2	0.6	0.2	3.71	0.374
24.02.2008	57	1152	2.9	1.0	0.2	0.8	0.3	-	-	2.48	0.369
21.03.2008	82	1177	3.0	1.3	0.2	> 2.8	-	-	-	1.85	0.357
21.04.2008	113	1208	3.1	0.8	0.2	1.0	0.2	-	-	3.10	0.361

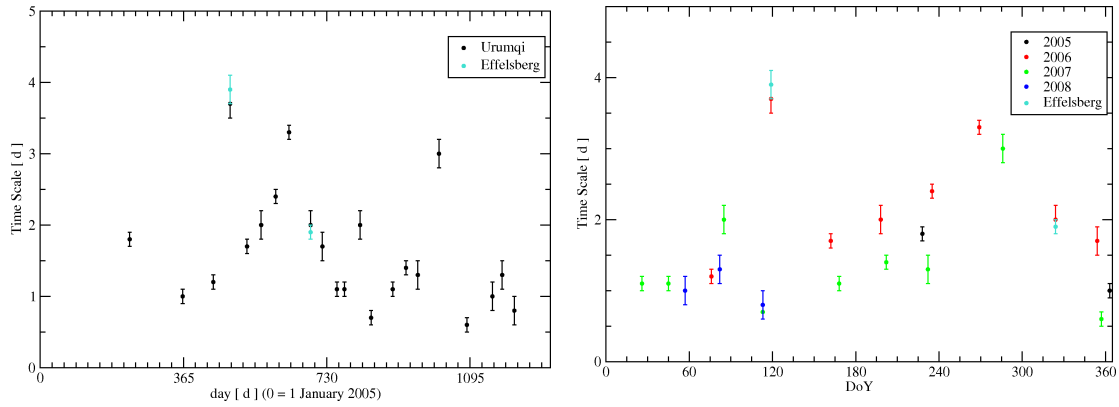

Figure 6.20: The average time scales of the 1128+592 variability, obtained by SR analysis. Two features are clearly visible in the plots: the large slowdown peaking in September 2006 (left panel) and the probable presence of a seasonal cycle in the time scales of 1128+592 (right panel).

that the time scales follow are always similar. The annual modulation plot of the structure function results (see Fig. 6.21, right panel) shows that the behaviour of the source is very regular. The time scales repeat from year to year within the error bars. Interestingly, in the last part of the year the SF analysis often reveals two time scales, a slow one and a very fast one, in perfect agreement with the variability components detected by SR. Concerning the March 2008 observations, the time scale estimate by SF is > 2.8 d: a further indication that between April and March the variability time scales can increase dramatically.

In Table 6.9 – columns 9 and 10 – we report the SF time scale estimates by K. E. Gabányi; part of the results are published in G07, others come from private communication. The agreement is generally remarkable – the differences between the time scales lie within the error bars. There are two exceptions: in September 2006, we replace the 2.6 d value in G07 with a lower limit of 5 days, with no consequence for the resulting annual modulation models; in December 2006, the 0.7 d value in G07 increases to 2.0 d in our analysis. The differences are explained by the fact that both the variability curves are affected by the 1-d effect. Since our estimations refer to 'cleaned' curves – i.e. the curves after the removal of 1-d related periodical components – the time scales change consequently. A more detailed discussion can be found in the annual modulation subsection (see 6.6.5).

6.6.3 Simultaneous observations at Effelsberg and Urumqi

The estimated time scales from the simultaneous Effelsberg-Urumqi observations are in good agreement (see Table 6.9, Fig. 6.20 and 6.21). The only exception is the April 2006 SF results. In the case of the Urumqi variability curve, the SF reveals two distinct time scales, a fast one and a very slow one. The analysis of the Effelsberg curve instead leads to an average of the two. The difference, although large, does not significantly alter our conclusions. Two different time scales are also detected in the November 2006 variability curves, both for Effelsberg and Urumqi – the obtained time scales are identical (2.4 and

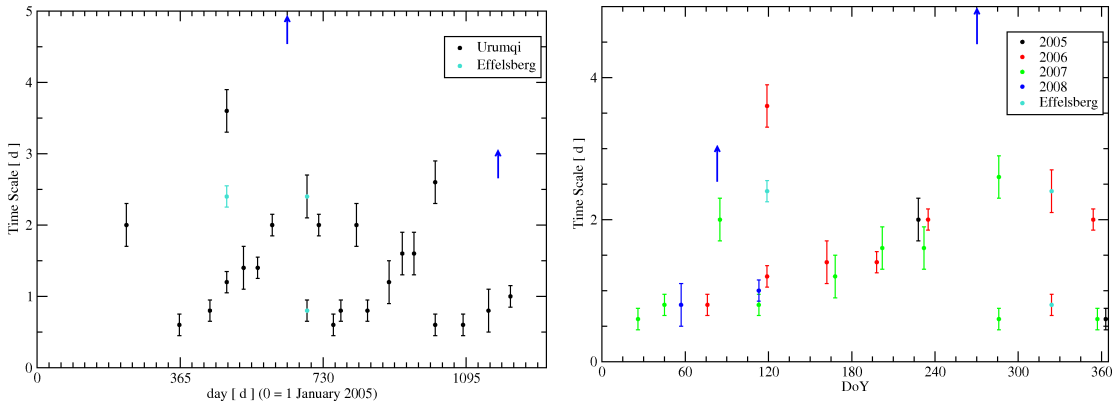

Figure 6.21: The SF analysis results strongly support the hypothesis of annual modulation in the time scales of 1128+592. It is remarkable how regularly the changes in the time scales repeat from year to year (right panel).

0.8 d).

6.6.4 A correlation between flux-density and modulation index?

The flux-density average of 1128+592 follows an almost monotonically decreasing trend between 2005 and 2008 (Fig. 6.22, top panel), which matches the pattern observed in the modulation index plot. Therefore, there is a correlation between the two quantities. In terms of ISS-induced variability, this could be explained by hypothesizing that the flux in the scintillating component is decreasing.

The correlation here observed is opposite to the one we mentioned in the case of 0917+624 (see section 6.4.3). In order to find out whether there is a connection between flux-density and modulation index in IDV sources, it is necessary to compare the behaviour of one of the quantities when the other inverts its trend – if they present quasi-simultaneous inversion points, the quantities are very likely correlated. Since neither of the flux-density trends of 1128+592 and 0917+624 show a proper trend inversion during the period of monitoring, no definite conclusion can be reached. It is interesting, though, that the trends of both flux-density and modulation index in 1128+592 seem to get flat at the same time, namely around December 2008, as pointed out by a cubic regression (green lines in the plots).

6.6.5 Annual modulation

The annual modulation fit provides evidence in favour of a seasonal cycle in the time scales of 1128+592. The SR time scales (see Fig. 6.23, upper panels) are characterized by two slowdown periods – in spring (around DoY 130) and autumn (around DoY 280). Two peaks characterize the fit of the SF time scales[7], which though show some differences with respect to the SR results: the peaks occur around DoY 110 and 270, with the latter being

[7]Lower limits are also included. In case that more than one time scale has been detected in a light curve, only the strongest has been taken into account.

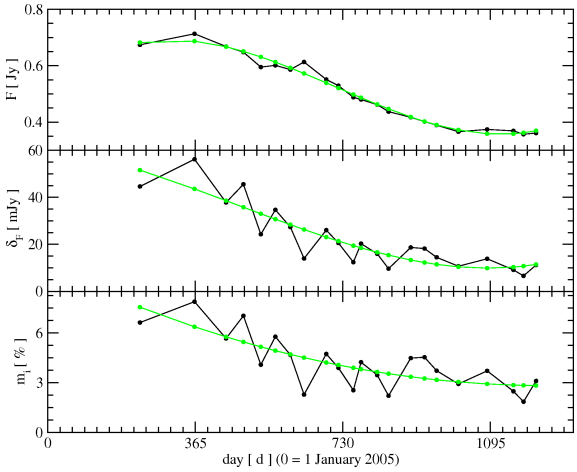

Figure 6.22: A possible correlation between the flux-density (upper panel) and the modulation index (lower panel) of 1128+592. Apparently, the standard deviation (middle panel) decreases much faster than the flux-density. The green curves are the results of cubic regressions.

considerably higher than the former. This leads to some discrepancy in the estimations of v_{RA} and v_{DEC} from SR and SF data. The values, however, still fall within the error bars.

Table 6.10: The annual modulation parameters obtained from the 1128+592 time scales, compared with the results of G07.

Analysis method	v_{RA} (km/s)	v_{DEC} (km/s)	Screen distance (kpc)	Anisotropy degree	Anisotropy angle (degrees)
SR	8 ± 3	9 ± 3	0.19 ± 0.01	1.9 ± 0.2	20 ± 10
SF	3 ± 4	7 ± 3	0.18 ± 0.02	2.1 ± 0.2	0 ± 10
SF Gabanyi	18 ± 6	16 ± 3	0.11 ± 0.02	3.8 ± 0.5	0 ± 10

6.6.6 Comparison between annual modulation models

Here, we propose a slightly modified model, which differs from the one proposed by G07 (see Fig. 6.24, left panel). In the paper (which includes measurements from 6 Urumqi observing sessions, between August 2005 and July 2007), the time scales are modeled with an annual modulation fit with two maxima – one around DoY 120 and another around DoY 240. Both our fit and the one in G07 need an anisotropic annual modulation model in order to successfully reproduce the data. However, two important differences emerge: the position of the second time scales slowdown – which we place about one month later than G07 – and the height of the peaks: according to our estimations, the dominant feature in the annual modulation plot is the second slowdown. As a consequence, the values of the screen parameters which we obtained do not agree very well with the ones in G07 (see

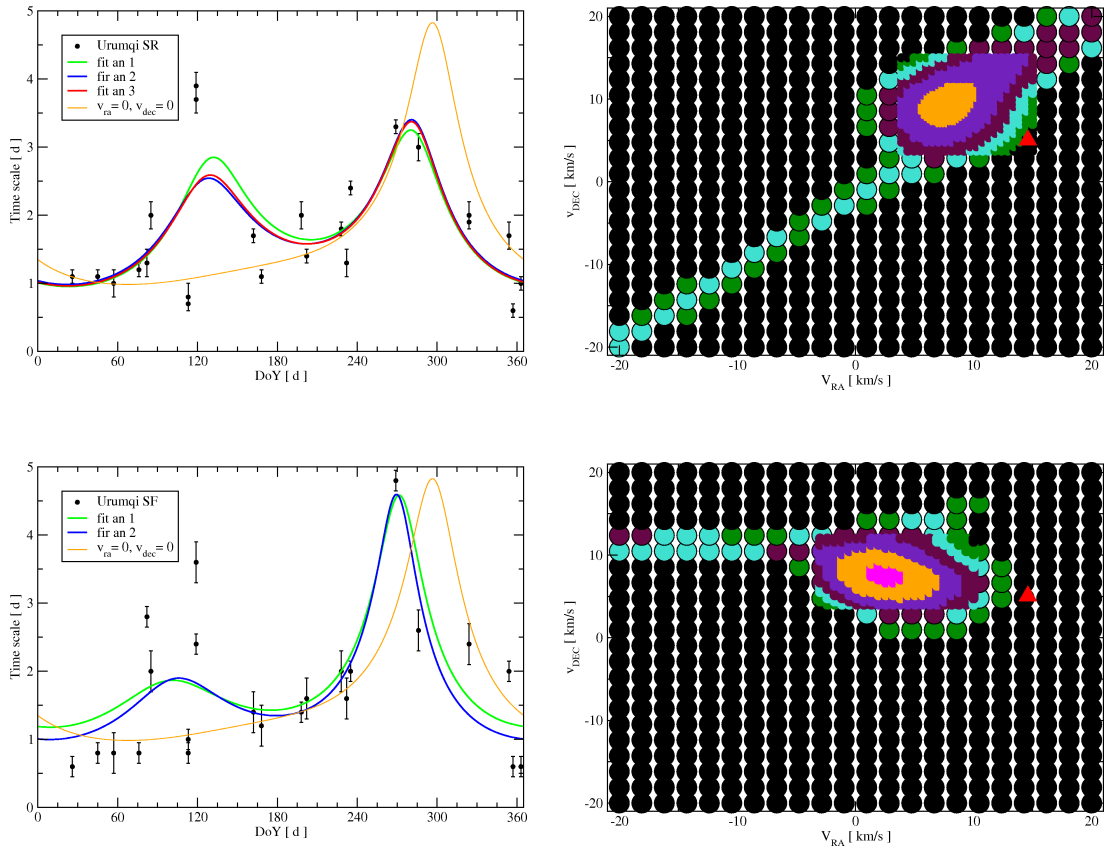

Figure 6.23: The annual modulation plots obtained from the *SR* and *SF* results (respectively, upper and lower panels). Despite some differences, both analysis tools lead to the same conclusion: there is a significant seasonal cycle in the variability time scales of 1128+592.

table 6.10[8]).

Considering that several time scales in G07 have been obtained from the same variability curves we analyzed, it is of great importance to understand the origin of the discrepancies. We noted earlier that there is a satisfactory agreement between our *SF* time scale estimates and the ones in G07 (see Table 6.9). *This excludes the possibility of inconsistency between the time analysis results.* Therefore, the differences between the annual modulation fits must be caused by the different data-sets used in the present study (from now on, M08) and in G07.

If we look at the plots in Fig. 6.24, we notice three main differences:

- The spring slowdown, which is the most important feature in G07, appears much weaker if we consider also the time scales from the observations performed between the end of 2006 and April 2008, as in M08.

- The autumn slowdown is covered much better in M08 than in G07. This considerably

[8]It shall be noticed that although the values we report in the table look different from the ones which can be found in G07, the discrepancy is only apparent. It is due to the fact that we evaluate the screen motion with respect to the LSR, while in the paper it is calculated with respect to the Sun.

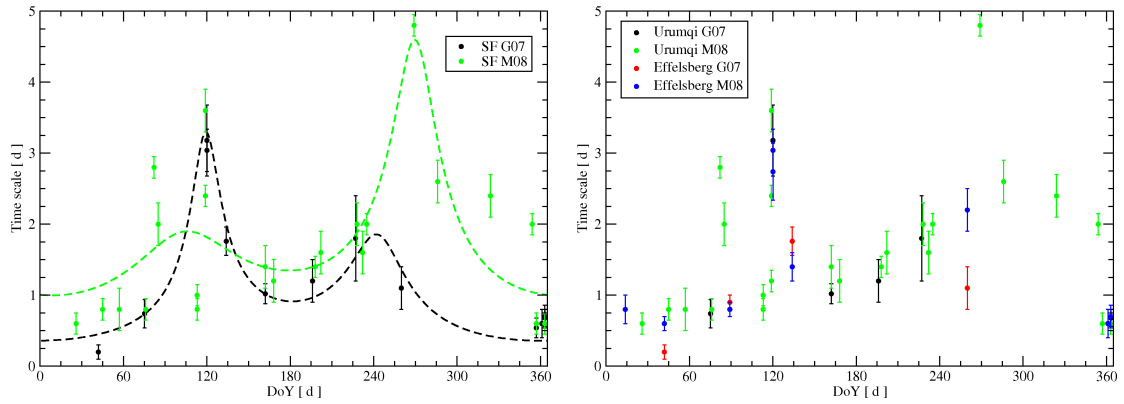

Figure 6.24: Comparison between our results (M08) and the ones in G07. In most cases, the time scales estimated from the same variability curves are in excellent agreement, which shows that the differences in the annual modulation plots are not caused by different approaches to the analysis of the data.

increases its importance for the estimation of the best annual modulation fit.

- G07 includes several time scales obtained from Effelsberg observations, which are not included in M08. We repeated the analysis of these data-sets. The results are generally consistent; in two cases, however, the time scales we found are different from G07. The results of the new analysis seem in good agreement with our annual modulation fit.

Concerning this last point, the differences in the time scale estimations play a marginal role for the annual modulation fits. If we repeat the fit of our time scales for all the epochs included in G07, the resulting best fit parameters become very similar to the ones in G07. This leads to an important conclusion: something has changed in the variability pattern of 1128+592 during the last two years.

6.6.7 Evolution of the 1128+592 variability

The presence of data in the period October-November, which led to the discovery of the autumn slowdown, is not indicative of a *change* in the variability of the source. It simply adds data points in a period of time which previously was not covered at all. The changes in the spring slowdown, instead, comprise a concern. The variability observed in April 2006, characterized by a time scale of more than 3 d, may have been a *unicum*. It is a matter of fact, though, that the corresponding modulation index is the highest we found during the whole campaign (9% for the Effelsberg observation, 7% for the Urumqi one), which makes the result unquestionable; if we want to explain the intraday variability of 1128+592 purely in terms of interstellar scintillation, we have to find an argument which could explain this unusual behaviour. Moreover, the slow time scale obtained for March 2007 and the *SF* lower limit for March 2008 (not confirmed though by the *SR* analysis), represent the only other 'outliers' in a picture which finds the time scales of 1128+592 increasing very regularly from December to September/October, and then suddenly drop again to a very fast mode. It seems as if the spring peak is very narrow and has been

shifted in the last two years from April to March. The fast time scales observed in April 2007 and 2008 seem to support this conclusion.

It is not possible to tell whether the change in the variability has to do with the screen or with the source itself. According to our picture, the spring slowdown is probably caused by some anisotropy, which can be localized either in the interstellar medium or in the source. This means that the change in the variability should be related to a variation in the anisotropy characteristics. In order to understand the origin of the variation further investigation is needed. A new VLBI study of 1128+592 may help to clarify this point. Some information, though, may also come from the comparison of the 1128+592 results with those for other sources. We will return to this point in chapter 7.

6.7 Other sources

In this section we will briefly summarize the time analysis results for other objects which were occasionally included in the source list of our monitoring project, namely 0235+164, OJ 287 (0851+202), Mrk 421 (1101+384) and 1156+295. Besides the limited number of available epochs, all the sources are characterized by a relatively low declination, which determines large gaps in the variability curves and also affects the total duration of the observations. Therefore, the study of these objects is characterized by two serious problems: the poor statistics makes a proper annual modulation investigation difficult; the bad sampling and short length of the light curves may lead to incorrect estimations of the time scales. These limits have to be kept in mind while considering the results presented below.

All the variability curves can be found in Appendix B.

6.7.1 0235+164

The source has been observed 12 times in the course of our monitoring program[9], in a period that goes from December 2006 to March 2008. In 7 occasions the structure function analysis was able to provide estimations of the time scales. The sinusoidal regression allowed the evaluation of time scales for all the epochs, but it is debatable whether they are all meaningful. A visual inspection of the individual variability curves, the regular trend of the changes and the agreement with SF results (see Fig. 6.25) argues in favour of their reliability. Only for one epoch the two analysis methods diverge considerably: in July 2007 the obtained values are 2.4 d (SF) and 3.2 d (SR), which seems to have no implication for the modeling of the variability.

Despite the limited amount of observations, the results look very interesting. Two remarkable elements emerge from the plots of the time scales versus MJD ((see Fig. 6.25; as usual, 0 corresponds to January 1, 2005) and versus DoY. *In primis*, the time scales of 0235+164 are characterized by pronounced variations during the monitoring period. Secondly, the April 2007 data point (see Fig. B.23 for the variability curve) is an exceptional one for the source, both because it is by far the slowest time scale in the sample and because of the large difference from the March 2007 value. The exceptional character of this epoch is also confirmed by the corresponding modulation index (see Table 6.11), which is much higher than for any other observation. A comparison between the time scales, the flux-densities and the modulation index (Fig. 6.26, left panel) reveals a

[9]Actually 13, but in the 13th epoch the source was too close to the sun for providing useful data.

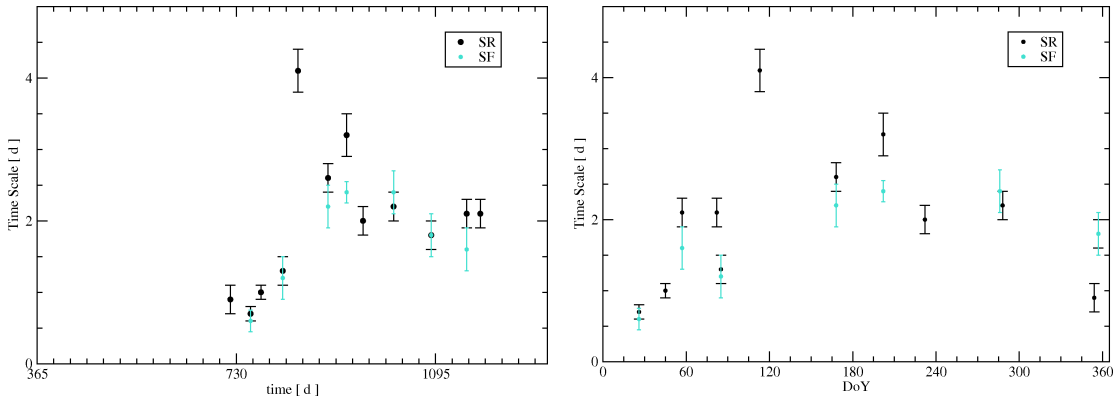

Figure 6.25: The SR and SF time scales of 0235+164 plotted versus MJD and DoY. The source's variability undergoes a remarkable change during the 15 months of observations, characterized by a slowdown which culminates around April 2007.

significant correlation between these quantities; this result is confirmed by means of a correlation function (same figure, right panel). The CCF is applied to two different sets of data – one includes all the epochs, the other excludes the April 2007 data point, which strongly influences the results. In the first case, time scales and modulation indices appear to peak simultaneously, while the flux-densities are delayed by 30-60 days; the correlation coefficients, for all the data pairs, reach values between 0.75 and 0.80. In the second case, flux-densities and modulation indices peak almost simultaneously (correlation coefficient: 0.65), while the time scales follow with a delay of ~ 30 days. The correlation coefficients between flux-densities or m_i vs time scales show peaks between 0.80 and 0.90. Due to the limited number of data points, the time delays can not be determined very accurately; the existence of a correlation between the variability time scale and the modulation index, however, appears unquestionable.

The result becomes even more interesting when we consider the recent flux density evolution of 0235+164. In Raiteri et al. (2008), the data from a multi-wavelength campaign performed between 2005 and 2007 are presented. During the second half of 2006 and the first half of 2007 the object undergoes an outburst phase, which is observed in the optical as well as in several radio frequencies. The maximum flux in the optical is reached around February-March 2007, while at 37-43 GHz it can be clearly located in April 2007 (see Fig. 6.27). The flux-density maximum which we observe at 6 cm, around June, is most likely the effect of the propagation of this outburst to lower frequencies. The outburst could be explained in terms of a shock propagating along an inhomogeneous jet (see e.g. Marscher and Gear (1985), Hughes et al. (1989a), Hughes et al. (1989b), Valtaoja et al. (1992)) – a phenomenon which may lead to a temporary change in the source size θ.

Testing an ISS-induced variability We know how the time scale τ and the modulation index change with the source size θ, in case of scintillation-induced IDV. For quenched scattering, the equations are the followings (see Beckert et al. (2002), Fuhrmann (2004)):

$$\tau = \frac{2\,D \cdot \theta}{v} \tag{6.3}$$

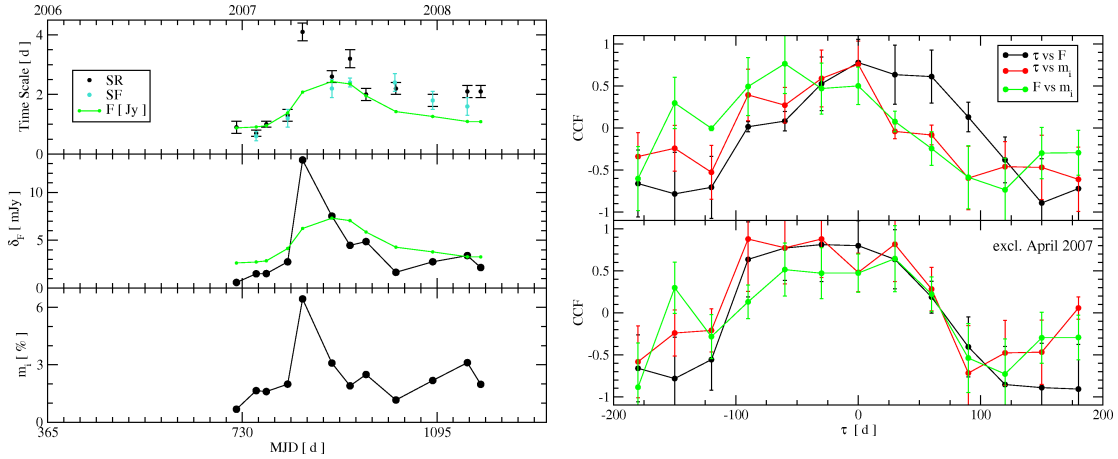

Figure 6.26: Left figure: Variability time scales (upper panel) and modulation indeces (lower panel) of 0235+164, compared with the flux-density curve (green line). The existence of a similar pattern emerges clearly from the data; this is confirmed by the results of a CCF analysis (right figure). On the top, the black curves shows the results of a CCF between time scale and flux-density, the red curve between time scale and m_i and the green curve the between flux-density and m_i. The lower panel shows the CCF results after excluding the April 2007 values, which are unusually high.

Table 6.11: The main parameters of the 0235+164 variability curves during the period which runs from December 2005 to March 2008. In column 1 the epoch, in columns 2 and 3 the Day of the Year (DoY) and the modified Julian date (starting at January 1st, 2005); in column 4 the duration of the observations; in columns 5 and 6 the SR time scales and relative errors; in columns 7 and 8 the SF time scales and errors; in columns 9 and 10 are given the Modulation Index (m_i) and the average flux-density, respectively.

Set	DoY (d)	day (d)	Duration (d)	t_{SR} (d)	Err (d)	t_{SF} (d)	Err (d)	m_i (%)	$< S_{5\,GHz} >$ (Jy)
18.12.2006	354	719	2.3	0.9	0.2	-	-	0.68	0.877
25.01.2007	26	756	2.0	0.7	0.1	0.6	0.2	1.65	0.910
12.02.2007	45	775	4.0	1.0	0.1	-	-	1.60	0.951
24.03.2007	85	815	2.2	1.3	0.2	1.2	0.3	1.99	1.380
20.04.2007	113	843	3.2	4.1	0.3	-	-	6.44	2.078
15.06.2007	168	898	2.2	2.6	0.2	2.2	0.3	3.09	2.436
19.07.2007	202	932	2.3	3.2	0.3	2.4	0.2	1.90	2.351
18.08.2007	232	962	2.5	2.0	0.2	-	-	2.49	1.954
13.10.2007	288	1018	2.4	2.2	0.2	2.4	0.3	1.16	1.425
21.12.2007	357	1087	2.4	1.8	0.2	1.8	0.3	2.18	1.262
24.02.2008	57	1152	2.9	2.1	0.2	1.6	0.3	3.11	1.093
21.03.2008	82	1177	2.4	2.1	0.2	-	-	1.98	1.088

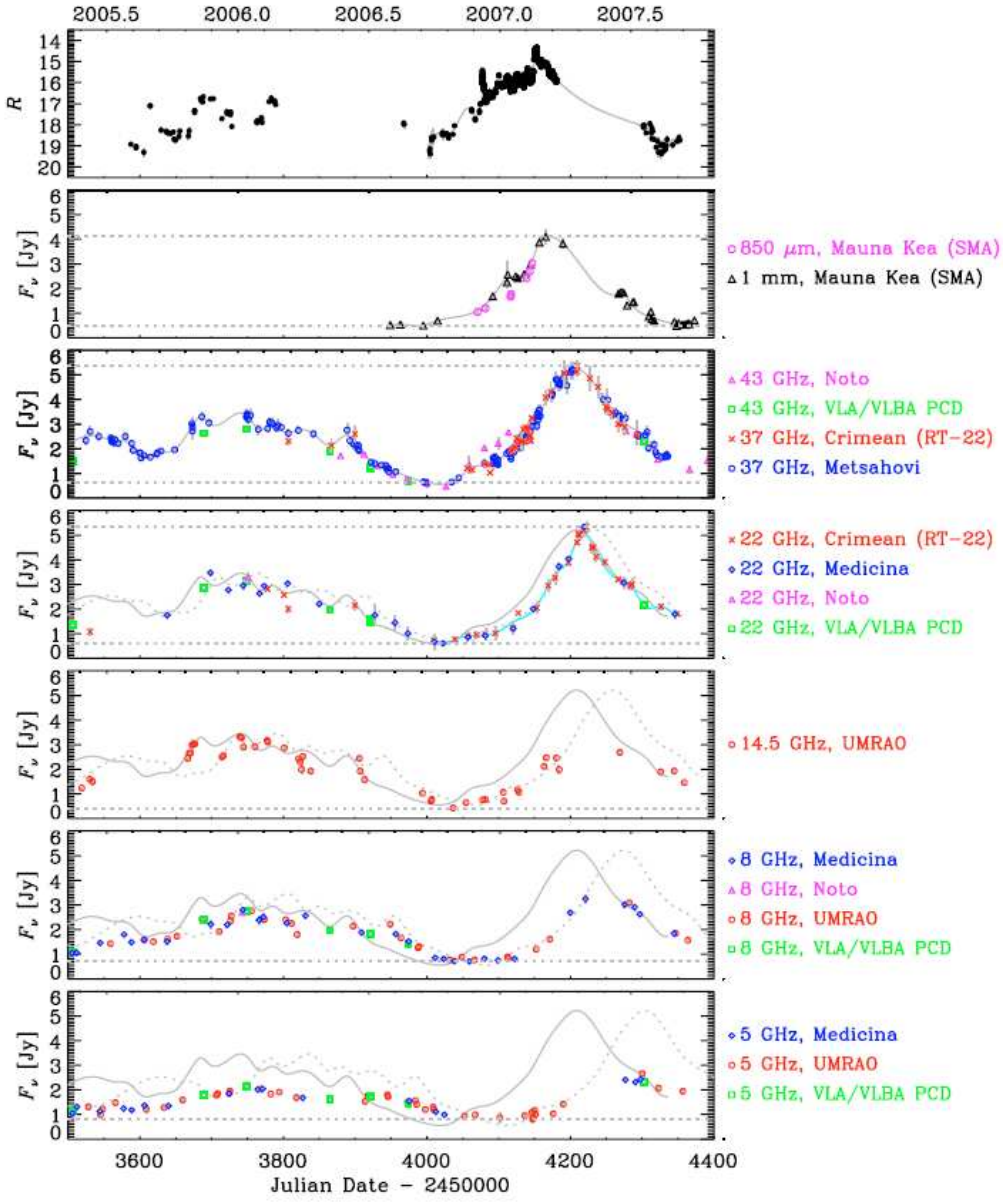

Figure 6.27: The variability curves of 0235+164 from the 2006-2007 multi-wavelength campaign described in Raiteri et al. (2008). The figure is taken from the cited publication.

$$m_i = \sqrt{2\Big(\frac{r_e}{D\,\theta^2}\Big)^2 \lambda^4 \Big(D\theta\Big)^{\beta-2} SM \cdot F_1(\beta)} \tag{6.4}$$

where v: the relative velocity between the screen and the Earth
r_e: the electron radius
D: the screen distance
λ: the observing wavelength
β: the spectral index of the electron density fluctuations in the ISM
SM: the scattering measure

The function $F_1(\beta)$ depends only on β and is of the order of unity. Assuming that the properties of the screen did not change considerably during the monitoring campaign and that the fluctuations in the ISM can be described by a Kolmogorov spectrum, $\beta = 11/3$, Eq. 6.4 leads to:

$$m_i \propto \theta^{-7/6} \tag{6.5}$$

or, given the proportionality between θ and τ

$$m_i \propto \tau^{-7/6} \tag{6.6}$$

As the time scale increases, m_i must decrease. This is opposite to what we observe in Fig. 6.26.

The situation does not substantially improve if we hypothesize that the IDV of 0235+164 is caused by the scattering of two or more emitting sub-components of different angular size θ_1, θ_2, θ_3, ..., θ_N. Let us assume that the observed modulation index m_{i0} and time scale τ_0 are given by

$$\tau_0 = \Big(\frac{\sum_n F_n\,\tau_n}{\sum_n F_n}\Big) \tag{6.7}$$

$$m_{i0} = \Big(\frac{\sum_n F_n\,m_{in}}{\sum_n F_n}\Big) \tag{6.8}$$

where F_n: the flux-density of the n-th component
m_{in}: the modulation index of the n-th component
τ_n: the time scale of the n-th component

Applying Eq. 6.6 to all the components, we can re-write Eq. 6.8

$$m_{i0} \propto \Big(\frac{\sum_n F_n\,{\tau_n}^{-7/6}}{\sum_n F_n}\Big) \tag{6.9}$$

It is straightforward that a change in the flux of one or more components (i.e. in their relative weight) would cause variations of m_{i0} and τ_0 which are anti-correlated. A change in the angular size of one or more components would have the same effect.

In order to have variations of the same sign in m_{i0} and τ_0, we have to postulate a simultaneous change of both flux-density and angular size of some component. Using a very simple model – a system of two components, with relative fluxes F_1, ($F_2 = 1 - F_1$) and angular sizes θ_1, θ_2 – we can derive a rough estimate of the state of system at the beginning of the flare (December 2006-January 2007) and at the peak of it (April-June 2007). Assuming that θ_2 is nearly constant (i.e., the variation in the angular size of one

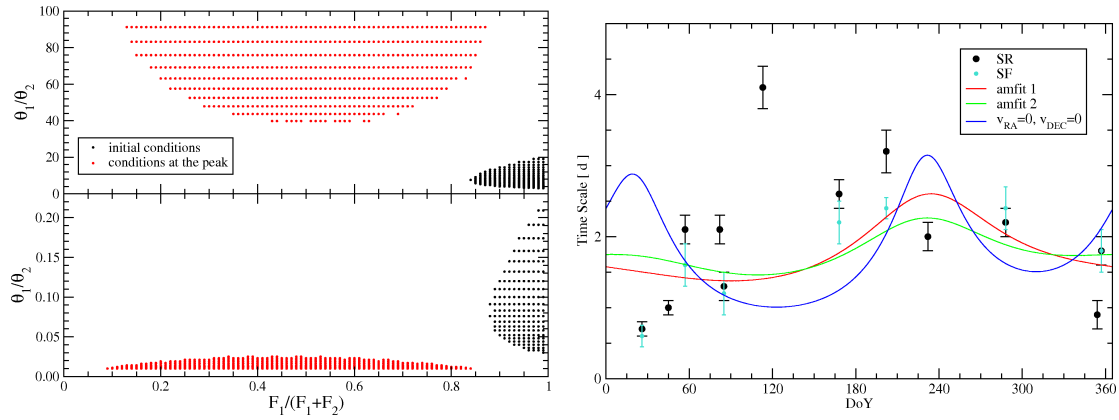

Figure 6.28: *Left panel*: The values of the parameters θ_1 and F_1 which are necessary for explaining the changes of m_i and τ observed during the outburst of 0235+164, according to a simple two-component model. In black the initial conditions, in red the conditions at the flux peak. *Right panel*: The variability time scales of 0235+164, along with the two best annual modulation curves (green and red lines). Very large screen velocities are needed for fitting the data due to the particular shape of the curve for a screen at rest in the LSR (blue curve).

of the components is negligible compared to the other), the values of F_1 and θ_1 which are consistent with an increase of m_{i0} by a factor 3 and of τ_0 by a factor 4 are reported in Fig. 6.28, left panel (in black are the initial conditions, in red the conditions at the peak). The probability of such a combination is very low ($\sim 3 \cdot 10^{-4}$ %). Note the preponderance of F_1 at the initial state and the large difference between θ_1 and θ_2, which becomes even more prominent at the time of the peak.

In conclusion, an ISS-induced variability can not be ruled out. It requires, though, the simultaneous occurrence of a series of variations in different components of the source, which appear very improbable.

The variability characteristics of 0235+164 would be described better – and more easily – in terms of a source-intrinsic mechanism. The advantage of source-intrinsic models is that they do not imply a strict correlation between τ and m_i. The emission of a new plasmon of relativistic electrons in the jet of an AGN, for example, would cause a variability whose intensity and time scale would be correlated either to the changes occurring in the blob or to the trajectory it follows. Therefore, a simultaneous increase of F, τ and m_i is absolutely plausible.

About the hypothesis of an annual modulation effect Whether the variability is due to mechanisms intrinsic to the source or to structural changes in the its scintillating components, the result would be anyhow important. The hypotheses we proposed, however, may not be the only ones which are suitable for explaining the variability. Assuming that the correlations between flux-density, m_i and time scale happen by chance we could also hypothesize that the time scale variations are simply due to annual modulation.

The plot of the time scales versus DoY (see Fig. 6.25, right panel) is not really meaningful, due to the fact that the source has been observed only for 15 months – which implies

that any variation of the time scale could be interpreted as part of a seasonal cycle. Nevertheless, the annual modulation fit routine provided additional information: 0235+164 is the only source in our monitoring project for which no good fit could be obtained. It turns out that there is no way to reproduce the slowdown peak between April and July, not even by assuming extreme values for the screen velocities $v_{\rm RA}$ and $v_{\rm DEC}$ ($> 50\,{\rm km/s}$) and for the anisotropy degree (> 25). The reason for this can be understood if we consider the annual modulation curve which the source would show in case of a screen at rest in the LSR (see Fig. 6.28). There would be two maxima (blue line), one in January (when the data reach a minimum), one in August; in April, instead, the time scales would be very fast. The best fits, obtained with the extreme values mentioned above, are denoted with the green and red lines. This result strongly supports the idea that the variability of 0235+164 can not be explained in terms of annual modulation and is probably due to changes in the structure of the source.

6.7.2 OJ 287

The fame of OJ 287 is mainly due to its long-term optical activity. From observations covering more than one century, Sillanpaa et al. (1988) postulated the existence of a $\sim$ 12-year periodicity in the optical flux variability, which makes of OJ 287 a possible prototype of a binary black-hole system. This peculiarity motivated the germination of a number of studies about the source. Still little is known, however, about its intraday variability characteristics.

OJ 287 has been included 8 times in our observations, during a period from November 2006 to February 2008. Due to the sparseness of the data and the low degree of variability (see Fig.B.13, B.18, B.22, B.24, B.26, B.30, B.32, B.34), the structure function did not provide any useful data (one time scale, one lower limit and six values which are irreparably biased by the sampling). Also the *SR* had problems in estimating the time scales – for the April 2007 observation e.g. the poor data quality and the huge gaps in the light curve made any evaluation impossible; about the remaining epochs, the results have to be considered carefully. The plots of the time scales versus MJD and DoY are given in Fig. 6.29. The number and reliability of the data points do not allow a meaningful use of the annual modulation fit routine. Nevertheless, it is interesting to compare the time scales with the annual modulation curve for a screen at rest (orange curve in the right panel). There seems to be no significant evidence for correlation between the two.

Despite the difficulties in establishing the variability time scales, it is evident that the source shows some activity over a time interval of 3-4 days. Therefore, OJ 287 can be considered as a proper IDV source. The comparison between the variability time scales and the modulation indices (see Fig. 6.29, right panel) provides interesting pieces of information. If we exclude the November 2006 observations, the two quantities look very well correlated.

Note that the two epochs showing faster variability (January and June 2007) are also the ones for which the duration of the observations was the shortest. They are both characterized by small m_i values. It is therefore very likely that the short duration of the experiments caused a wrong estimation of the time scales. The drop in the modulation index can be explained, then, as a consequence of the fact that the largest contribution to the variability of OJ 287 comes from the slow components (with time scales of a few days), which in these two session could barely be detected. If this interpretation is correct, then the variability of the source is speeding up following a quite regular trend, during the

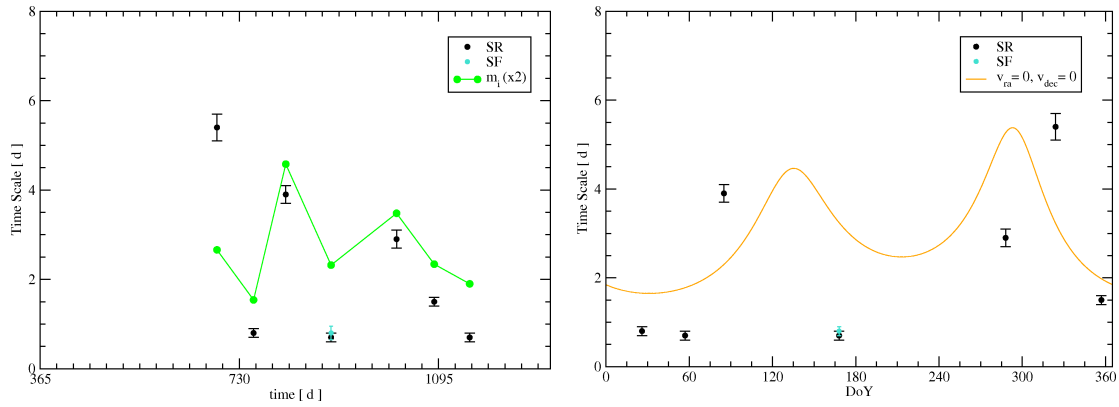

Figure 6.29: Variability time scales of OJ 287. In the left panel, the green line represents the modulation index. In the right panel, the time scales are plotted along with the annual modulation curve for a scattering screen at rest in the LSR.

Table 6.12: The main parameters of the OJ 287 variability curves during the period which runs from November 2006 to February 2008.

Set	DoY (d)	day (d)	Duration (d)	t_{SR} (d)	Err (d)	t_{SF} (d)	Err (d)	m_i (%)	$< S_{5\,GHz} >$ (Jy)
17.11.2006	324	689	4.7	5.4	0.3	> 4.0	-	1.33	2.09
25.01.2007	26	756	2.1	0.8	0.1	-	-	0.77	2.18
24.03.2007	85	815	2.5	3.9	0.2	-	-	2.29	1.92
20.04.2007	113	843	3.4	-	-	-	-	0.97	1.78
15.06.2007	168	898	1.4	0.7	0.1	0.8	0.15	1.16	1.67
13.10.2007	288	1018	2.9	2.9	0.2	-	-	1.74	1.76
21.12.2007	357	1087	3.1	1.5	0.1	-	-	1.17	1.76
24.02.2008	57	1152	2.4	0.7	0.1	-	-	0.95	1.73

$\sim$ 1.5 years of monitoring, while, at the same time, the modulation index is decreasing.

6.7.3 Mrk421

Markarian 421 has been observed 5 times throughout our project, between February 2007 and February 2008. The few observations and their concentration on the first half of the year do not allow the investigation of the existence of a seasonal cycle in the variability time scale. Nevertheless, the time analysis of the data resulted some interesting information about the source. First of all, Mrk421 showed always a low, but non negligible degree of variability ($m_i > 1.0\%$, see Table 6.13). Secondly, the time scales never exceeded 2 days. The results of *SR* and *SF* analysis are shown in Fig. 6.30. The time scales of both the February observations are the fastest among the 5 epochs. This would fit with the annual modulation curve been produced by a scattering screen at rest in the LSR. The slower value obtained from the June light curve would be in agreement with the same hypothesis. The March 2007 data point, instead, does not fit with the curve. Any interpretation would be useless, given the lack of further data points. We may just notice the similarity with

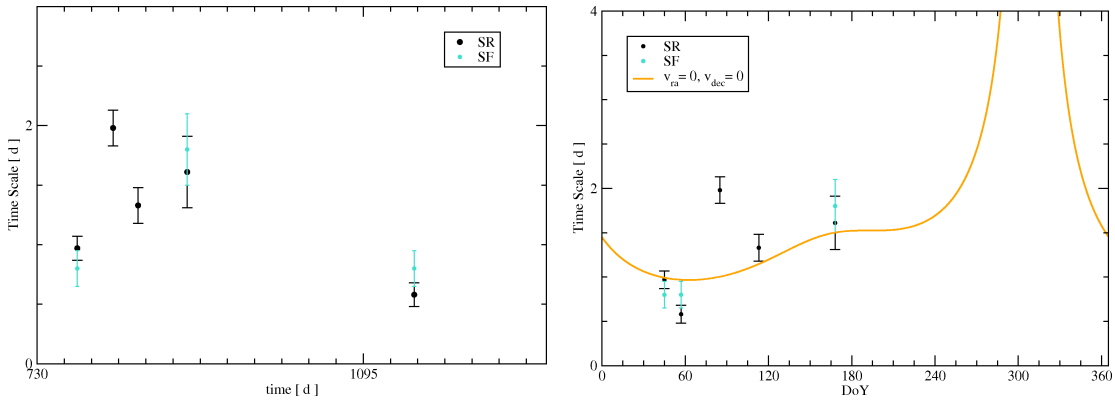

Figure 6.30: The Mrk 421 *SR* and *SF* time scales versus MJD and DoY. Given the lack of data points in the second half of the year, it is not possible to investigate the existence of annual modulation in the time scales.

Table 6.13: The main features of the variability curves of MRK 421 during the period which runs from February 2007 to February 2008.

Set	DoY (d)	day (d)	Duration (d)	t_{SR} (d)	Err (d)	t_{SF} (d)	Err (d)	m_i (%)	$< S_{5\,GHz} >$ (Jy)
12.02.2007	45	775	3.5	0.97	0.10	0.80	0.15	1.51	0.70
24.03.2007	85	815	2.5	1.98	0.15	-	-	1.61	0.69
20.04.2007	113	843	3.5	1.33	0.15	-	-	1.40	0.68
15.06.2007	168	898	2.1	1.61	0.30	1.80	0.30	2.19	0.65
24.02.2008	57	1152	2.5	0.58	0.10	0.80	0.15	1.38	0.65

the results obtained for the main sources in our monitoring campaign: again a slowdown around March-April.

No apparent correlation is seen between time scales, modulation indices and flux-densities. The source undergoes a slow flux decrease during the period of the monitoring, which seems to have no correlation with the estimated time scales.

6.7.4 1156+295

The intense IDV activity of the source 1156+592 has been discovered quite recently Savolainen and Kovalev (2008). This is the reason why the source has been integrated in our monitoring catalogue starting only from December 2007. The four epochs until April 2008 do not allow any discussion about the IDV characteristics of the object. Given the large amplitude and the short time scales of the variability, we decided to extend the data analysis – exceptionally for this source – to the latest available epoch (September 2008). The main variability parameters are reported in Table 6.14.

The estimated time scales, plotted versus MJD and DoY (see Fig. 6.31), reveal a peculiar behaviour. After December 2007, when the source's variability is dominated by a very slow component, the time scales undergo an extremely rapid change. The following epochs are characterized by strong and fast variability. From February 2008 on, the time

Table 6.14: Variability characteristics of 1156+295 between December 2007 and, exceptionally, September 2008.

Set	DoY (d)	day (d)	Duration (d)	t_{SR} (d)	Err (d)	t_{SF} (d)	Err (d)	m_i (%)	$< S_{5\,GHz} >$ (Jy)
21.12.2007	357	1087	3.2	3.1	0.2	-	-	6.56	0.98
24.02.2008	57	1152	2.4	0.8	0.2	0.6	0.2	4.48	0.96
21.03.2008	82	1177	2.5	1.0	0.2	-	-	6.75	1.03
21.04.2008	113	1208	2.5	0.9	0.2	0.6	0.2	5.89	1.05
21.06.2008	174	1269	3.4	0.5	0.1	0.5	0.2	6.29	1.25
18.07.2008	201	1296	4.7	0.5	0.1	0.4	0.2	2.96	1.43
20.08.2008	234	1329	4.9	0.8	0.1	0.8	0.2	2.98	1.57
12.09.2008	257	1352	3.4	1.3	0.2	1.4	0.2	3.93	1.68

scale changes appear gradual and regular: a minimum is reached around July 2008, and afterwards a new slow down phase starts again. This behaviour shows no correlation neither with the modulation index, nor with the flux-density. Despite the fact that the short time coverage of the monitoring does not allow a proper investigation of a season cycle, it is interesting to note that the annual modulation curve for this source – given, as usual, a scattering screen at rest in the LSR – is characterized by a time scale peak very high and narrow. Assuming a minimum time scale of 0.4-0.5 days, similar to the observed one, the maximum – around DoY 323 – reaches 67 d. It is quite easy to reproduce the estimated values by means of the annual modulation fit program (blue curve in Fig. 6.31, right panel). The inferred fit parameters are reasonable: $v_{RA} = 0.95$ km/s, $v_{DEC} = -0.95$ km/s a screen distance of ~ 0.11 kpc, a degree of anisotropy of 3.3, with an angle of 155°. Naturally, the significance of this result is low, due the limited number of data points; nevertheless, it allows a very simple cross-check: according to the model, if we observe 1156+295 around mid-November (DoY $\sim$ 326, when our fit curve peaks) we should obtain a completely flat variability curve, or – assuming that weaker and faster variability components can appear when the strongest gets too slow – a unusually low modulation index. The next months of observation will be an important test for proving the annual modulation in the 1156+295 time scales.

6.7.5 Notes about other sources

Along with the sources presented above, a number of other objects have been observed in Urumqi between 2005 and 2008. The few observations collected do not allow a meaningful characterization of their IDV features. Nevertheless, they still provide some information about the existence of variability on IDV time scales. A source-by-source description of these results is shown in Table 6.15. More information can be found in Appendix C, where we show the MINDEX tables[10] for all the observing sessions.

[10]The MINDEX tables contain important information about the variability of the observed objects: for each source, they show the number of data-points, the average flux-density, its standard deviation, the modulation index, the variability amplitude (see section 3.4), the χ^2 and the reduced χ^2.

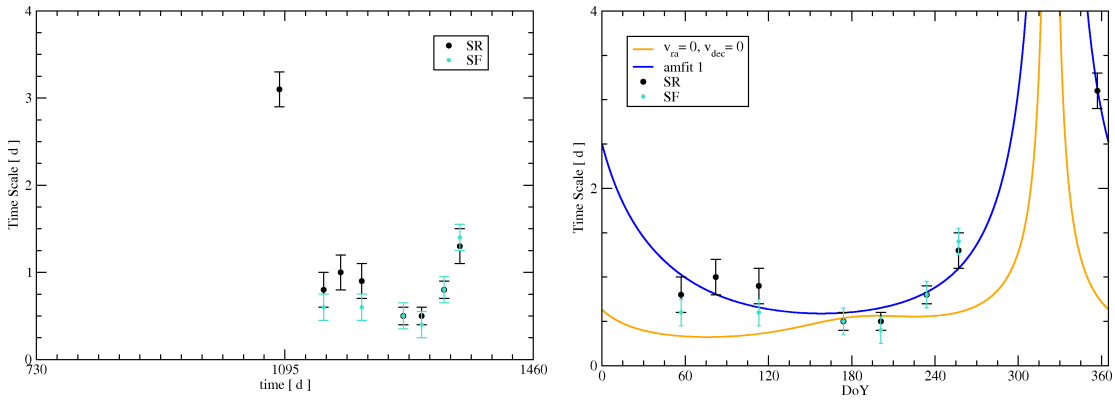

Figure 6.31: The time scales of 1156+295. A mid-November IDV experiment would be ideal to investigate whether the proposed annual modulation model is correct. The unusually high peaks of the fit curves are cut, in order to make the plot more readable.

Table 6.15: Short notes about other sources: in column 2 the number of observations collected; in column 3, the minimum and maximum m_i.

Source	N Obs.	m_i
0340+362	1	2.79
0346+800	3	2.22 – 2.60
0403+768	3	0.39 – 0.44
0454+844	1	1.31
0459+135	1	1.10
0602+672	2	1.14 – 1.81
0633+593	1	1.63
0639+732	1	0.90
0723+679	2	0.56 – 0.71
0804+499	2	1.19 – 1.69
0809+483	2	0.46 – 0.49
0827+243	1	1.05
0827+378	2	0.60 – 0.72
0835+580	3	0.81 – 1.25
0839+187	4	0.44 – 1.32
0954+556	1	0.95
1017+611	3	1.16 – 1.31
1035+562	1	1.36
1101+624	1	1.30
1127+565	3	0.82 – 2.03
1128+455	2	1.04 – 1.14
1131+437	2	1.14 – 1.89
1148+592	3	0.94 – 1.28
1153+59	1	0.32

Continued on next page

Source	N Obs.	m_i
1156+312	3	0.62 – 0.83
1311+678	9	0.41 – 0.95
1633+382	2	0.42 – 0.53
1634+628	1	0.55
1739+522	1	0.66
1749+701	1	3.06
1800+384	1	0.73
1803+784	1	0.60
1807+698	1	0.69
1808+454	1	1.08
1813+430	1	1.03
1814+411	1	1.08
1816+345	1	0.85
1819+384	1	29.54
1821+394	1	0.94
1829+395	1	1.15
1830-211	1	0.54
1840+390	1	3.29
1845+354	1	0.54
1852+401	1	0.45
1908-201	1	1.45
1921-293	1	0.73
1928+738	1	1.80
3C 454.3	3	0.35 – 0.41
CTA 102	2	0.54 – 0.62
CTA 21	12	0.24 – 0.90
Mrk 501	2	0.40 – 0.72
NRAO530	1	1.12

Chapter 7

Discussion

Now that the results for the main sources have been presented, it is necessary to discuss them in the light of the standard annual modulation model. In this chapter, we will focus only on the four IDV sources which have been regularly included in the monitoring project. For three of them (0716+714, 0917+624 and 1128+592) we found significant evidence in favour of a seasonal cycle, while the variability of 0954+658 seems to show no seasonal change. For the former ones the slowdown of the time scales is always seen in the range between September-October (DoY 270-285), which is in agreement with the predictions of scattering screens whose velocities in the LSR are small compared to the motion of the Earth. Assuming the screen velocities to be equal to zero, the peaks should fall in the range between DoY 270 and 300. The time scales, hence, get slower in the expected period. Despite this, the analogies between the changes in the time scale observed during the monitoring seem to go even further:

- The time scale peaks fall within a range which is smaller than that in the case of 'stationary' screens. For 0716+714 and 1128+592 – which are on different sky locations – the annual modulation patterns should show some differences (see Fig. 7.1). The peaks, instead, occur simultaneously. It is as if the screens in front of the objects have velocities which tend to make them behave similarly – a rather strange coincidence.

- All the objects show evidence for a fast increase of the time scale between March and April. In the case of 1128+592 we explained this in terms of an anisotropy in the screen or in the source. The occurrence of the same effect in other objects can not be a coincidence. This would lead to discard the hypothesis of a source-intrinsic anisotropy, and claim that the radiation from all the sources is in fact scattered by screens with similar characteristics. Reasonably, we should conclude that the screen is the same for all of them. The maximum distance between the sources is of the order of 30°. Hypothesizing such a large screen is not unrealistic: if the scattering screen is the prominent loop structure known as Loop III (see Berkhuijsen et al. (1971), Berkhuijsen (1971)), as suggested by Fuhrmann (2004), its extension is sufficient to cover both 0716+714 and 1128+592. The anisotropy, however, is still a major problem. If we look at the annual modulation plots of the sources (see Fig. 7.1), obtained using identical parameters (the ones which best fit the SR time scales of 1128+592; see Table 6.10), we realize that the spring peak – caused by the anisotropy of the screen – embraces a period of time of ∼100 days. This is not consistent with the results of our analysis. We should conclude that the anisotropy

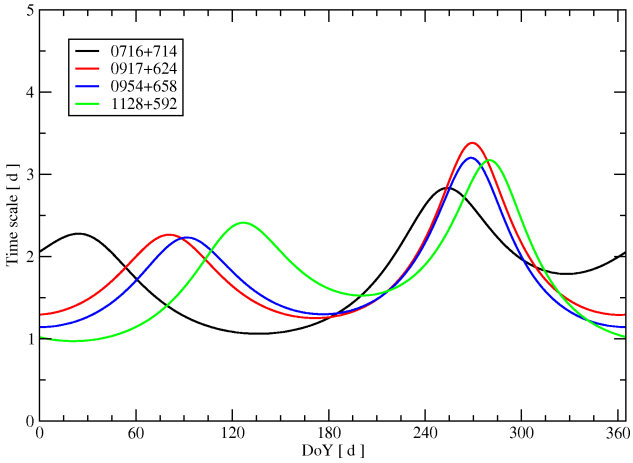

Figure 7.1: The annual modulation plots of 0716+714 (black line), 0917+624 (red line), 0954+658 (blue line) and 1128+592 (green line), obtained using the parameters which best fit the SR time scales of 1128+592. The peaks caused by the anisotropy of the screen fall within a time range of ∼100 days.

changes in such a way that the separation between the anisotropy peaks of different sources is minimized.

- A very peculiar case is that of 0954+658; we already mentioned that the object shows no trace of annual modulation of the time scale. The statement, though, is not completely correct. Between January 2006 and August 2007 it follows a trend which is very similar to all the other objects, compatible with a double-peaked seasonal cycle, with maxima around March and October. Again, it seems that the changes occurring in the variability characteristics of different sources show surprising similarities.

The analogies between the observed variability characteristics appear clearer when we plot the SR time scales of the four objects together (see Fig. 7.2, left panel). From August 2005 to the end of 2006 the behaviour of all sources is similar. The slowest variability

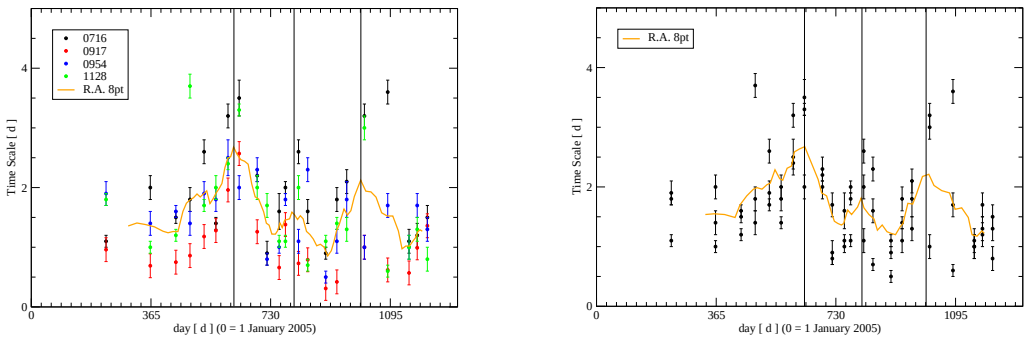

Figure 7.2: The clear analogies between the time scales obtained for different sources.

is detected in September 2006 (except for 0954+658, which reaches the peak in August). Afterwards, the time scales drop quite rapidly to reach a minimum between December and January 2007. There seems to be a new fast increase peaking in March/April 2007, then a new minimum in June 2007 and a slowdown phase, till October 2007. In 2008, all the sources – except for 0954+658 – start from the same level of fast variability. Afterwards, the time scales decrease in a similar fashion. An 8-point running average of the data (orange line) denotes the common pattern. Three peaks emerge neatly: one in September 2006, one in March 2007 and one in October 2007. Considering the absence of observations between August and October 2007, the picture is perfectly consistent with a seasonal cycle. If we plot together all the time scales excluding the ones of 0917+624 (Fig. 7.2, right panel), we can trace more clearly the general slowdown of the time scales between March and April. It is remarkable that the difference between consecutive peaks is close to 6 months. According to these data, *the annual modulation pattern first seen in 1128+592 may be common to all the most observed sources in our monitoring campaign.*

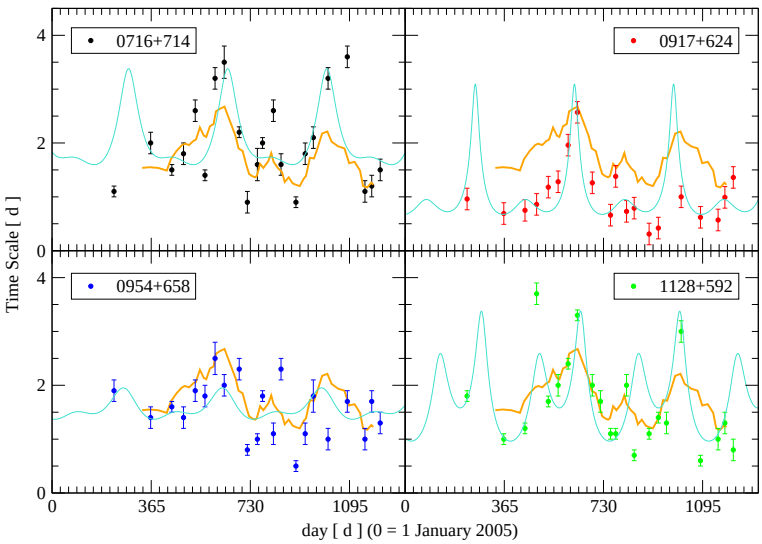

Figure 7.3: The variability time scales of 0716+714 (black circles), 0917+624 (red), 0954+658 (blue) and 1128+592 (green). In each panel, the turquoise line shows the best fit of the annual modulation model for the given source. In orange, the average behaviour.

The agreement between the 'average behaviour' (i.e. the curve given by the running average) and the time scales of the single sources can be evaluated by looking at Fig. 7.3. There, for comparison, we add also the annual modulation curves which best fit the data-set (turquoise curves). It is noteworthy that the minima and maxima in different sources occur at the same time, and that the March/April peak does not appear in any source in 2006, but in 2007 it is present in all. The annual modulation curves, instead, have some problems in resembling the time scales variations (see, for example, the cases of 0716+714 and 0954+658). It may be a futile exercise, but we could notice that the agreement between the average behaviour and the time scales of the sources, considered separately, improves by simply shifting and re-scaling the average curve from case to case (see Fig. 7.4; the re-scaling factors are given in table 7.1) – as if the differences in the variability changes

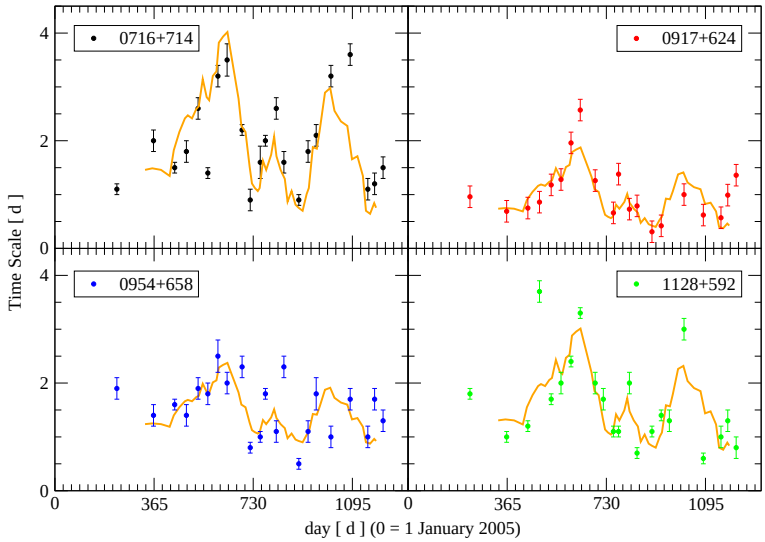

Figure 7.4: In orange, we show the average behaviour of the time scales, shifted and re-scaled from source to source (see Table 7.1 for the shifting/re-scaling factors). This considerably improves the agreement with the obtained values.

could be reduced to a simple proportionality factor.

Table 7.1: The average variability curve fits the time scales of the individual sources much better if we shift and re-scale it. In the table, for each source (column 1) we show the re-scaling factors (column 2).

Source	Re-scaling factor
0716+714	2.2
0917+624	1.0
0954+658	1.0
1128+592	1.5

7.1 SR versus SF results

So far, we took into account only the time scales derived by SR analysis. A fundamental issue is whether the discussed analogies are also confirmed by the SF time scales. In case they are not, we should start considering the possibility that in our analysis something did not work properly. If we plot together the SF time scales of the IDV sources – except 0917+624, for which we mainly obtained lower limits – a high degree of correlation is still visible, although less obvious than in the case of the SR values (see Fig. 7.5, left panel). The slowdown that peaks in autumn 2006 and autumn 2007 is easily recognizable, while the spring 2007 peak is characterized by a large scattering. It is interesting to notice that the major difference in SF and SR results is that the peak in the 0716+714 time scales

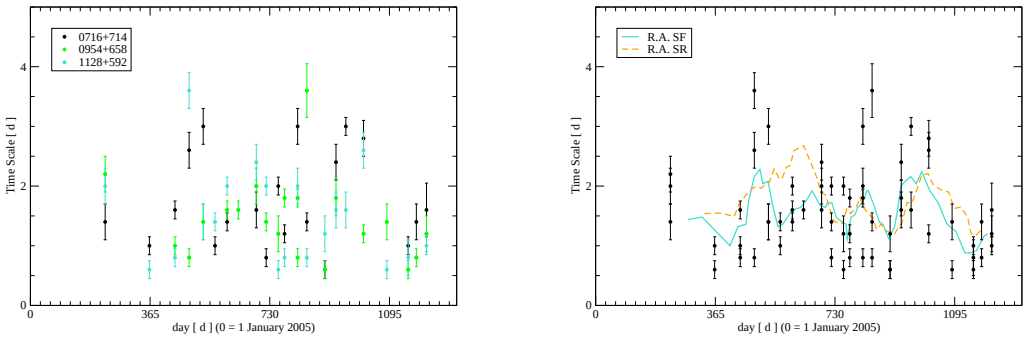

Figure 7.5: The superposition of the SF time scales for all the sources. The existence of a common pattern is less evident than in the case of the SR values, but careful investigation reveals significant similarities.

occurs between April and June 2006. This feature resembles the spring 2007 slowdown. According to the SF analysis, the March-April slowdown emphasized by SR may be part of a seasonal cycle, as the autumn one.

A 5-point running average of the data may help to underline some characteristics (see Fig. 7.5, right panel): strong peaks appear in April 2006, April 2007 and August 2007. The remarkable slowdown in Autumn 2006 is almost hidden after the high peak in April. The running average, though, does not take into account the September 2006 epoch, in which SF only provides lower limits both for 0716+714 and 1128+592.

The main difference with the running average of the SR time scales is the prominent slowdown in April 2006, which is due to the different time scales provided by the two methods for 0716+714. Apart from that, the agreement is fairly good.

Concerning individual data points, during the discussion of the 0716+714 SF results we discussed the possible existence of a rising trend in the time scales, which repeats several times during the monitoring. How does it correlate – if at all – with the average SR pattern? The minima in the SF values occur in December 2005 and 2006, July 2006, June 2007 and February 2008, matching well the minima in the SR running average (only exception is the July 2006 SR value, where no minimum is observed, but *it would be expected* if we believed the variations to be seasonal). The September 2006 lower limit could be the peak of the rising trend started in December 2005; the other SF maxima (March and August-October 2007) occur when the SR maxima are detected. A major difference between SR and SF results concerns the August 2006 time scales: 3.0 d in the first case, 1.4 d in the second. In section 6.1.1, we showed that the SF result for this variability curve oscillates between two specific values, 1.4 d and 3.0d., which is indicative of the presence of two time scales with comparable intensities. The existence of two distinct kinds of variability – a fast and a slow one – in the light curves of 0716+714 between November 2006 and April 2007 would also explain the peculiar way in which low and high values do systematically alternate.

In conclusion, the differences between the results of SR and SF are not a reason of concerns, they instead demonstrate the possibility to highlight different characteristics of the examined variability curves. The hypothesized correlation between time scales of different sources, which is so clear in the SR plots, is reliably confirmed also by the SF analysis – although with somewhat larger scatter in the data.

7.2 Real or spurious variability?

The results we have just discussed allow some very important conclusion to be drawn: the variability of 0716+714 can mainly be attributed to extrinsic mechanisms, differently from what is commonly thought; the variability in 0917+624 and 1128+592 is consistent with the evidence of annual modulation found in previous studies; 0954+658 is characterized by two different variability modes – in the first part of the monitoring campaign (till mid-2007) it is dominated by changes which are consistent with a seasonal cycle, whereas in the second part these regularities completely disappear, which indicates a mixture of different IDV mechanisms. These are important findings. It is crucial to spend some more time in establishing their reliability.

Let us discuss the different hypothesis about the origin of the common features which we observe.

- They may simply be caused by ISS, as a consequence of the similarities in the features of the scattering screen/screens in front of the objects.
- We can hypothesize that the variability is real, but not due to ISS: the analogies could be better justified by a single screen placed much closer to us than has been usually thought according to standard ISS models.
- They may be due to a spurious effect: the variability tools may be influenced by features which are common for all the objects – inefficient data reduction, sampling, duration – and could determine the similarities.

7.2.1 Calibration

We can start discussing the last hypothesis. The assumption of bad data calibration is not realistic. Residuals of spurious variability, as a result of an inefficient reduction, would not affect only IDV sources, but also the calibrators. Our calibrators, though, are flat within an uncertainty of less than 1%; moreover, it is hard to imagine how this presumed contamination could have the same influence both on sources characterized by very low modulation indeces, as in the case of 0917+624, and on 1128+592, which is usually very active. Consequently, this possibility has to be discarded.

7.2.2 Sampling and duration of the observations

More concerns arise from the sampling/duration of the variability curves: we have noted in section 6.1.1 that time analysis tools are easily influenced by the duration of the observations, and it is known in literature that the effect of sampling can not always be removed. The fact that we are discussing a systematic variation of the time scales similar, in certain ways, to a seasonal cycle, makes the hypothesis of a strong sampling effect rather improbable. The sampling, affected by erratic events such as bad weather, system failures and – in the last year – interruptions due to the Chinese Lunar Project, can not justify the existence of a regular and approximately yearly-periodic pattern in the time scales. We can safely exclude it from the list of possible problems. The last candidate for causing the analogies in the variability features is the duration of the observations. Despite being precautious for minimizing its effect on the results, we can not exclude that it still influences them in some way. When we plot the duration of the observation along with the estimated time scale (see Fig. 7.6), the suspicion increases. The large peak

in summer/autumn 2006 corresponds to the three longest experiments in the monitoring project (August, September and November 2006). Three of the minima in the time scales occur during periods of short observation. However, there are some arguments which speak against this hypothesis:

1. During the year 2006, the time scales of all the sources show a monotonic (and quite regular) slowdown till September 2006, while the durations in the same period do oscillate.

2. By far, the longest observations are the ones in August 2006, but all the maxima in the time scales (apart for 0954+658) appear in September 2006.

3. The slowdown in Autumn 2007 seems to faithfully repeat the one of the year before, supporting the impression of a seasonal cycle, but the duration of the observation is rather constant during the whole year 2007.

4. The peak in March 2007 (0716+714 and 1128+592) is revealed during one of the shortest observations of the whole project.

5. The SF time scales, which support the hypothesis of double-peaked seasonal cycle rising from the SR results, show their maxima during the period March-April, when the duration of the observation is usually short.

6. Finally, and most importantly: the annual modulation of 1128+592, which can be considered as a paradigm of the variability seen in all the other objects, can not be caused by the duration of the observations, because this is not yearly-periodic (see Fig. 7.6, right panel). Moreover, the annual modulation in 1128+592 is confirmed by the results of previous experiments.

It is useful to mention that the longest duration of the 2006 summer observations did not happen *by chance*, but as a consequence of the fact that all the main sources in our sample were expected to show the slowest time scales between summer and autumn. Therefore, longer observations were required for a better evaluation of the time scales. The fact that the summer 2007 slowdown shows larger scattering is probably due to the shorter duration of these experiments.

Anyhow, the best way to the definitely resolve any suspicion on the influence of the duration of the experiments to the variability time scales is to divide the data into *sub-samples* of equal duration and investigate the changes in the results. About November 2006, the existence of simultaneous Effelsberg data makes the investigation quite easy, because these observations lasted only 2.6 days (to be compared with the 4.6 d in Urumqi). As was discussed in chapter 6, the agreement between the results at the two sites is very satisfying: this epoch is surely not affected by the duration of the observations. September 2006 is the epoch of the peak in the slowdown. The variability curves of 0716+714, 0917+624 and 1128+592 (see Appendix B) leave no room for interpretation: almost no fast variability can be seen. The numbers confirm it: if we cut the light curves down to 3.5 d (approximately the average duration of our experiments) and estimate again the time scales, we can compare the new estimations with the results for the complete curves. The old and new values, reported in table 7.2, show only marginal differences. The only remarkable variation between the analysis results for the 4.7 d and the 3.5 d curves is the substitution of the lower limits with values which confirm the September time scales as the slowest in 2006. The same procedure can be repeated for the August 2006 data (see Table

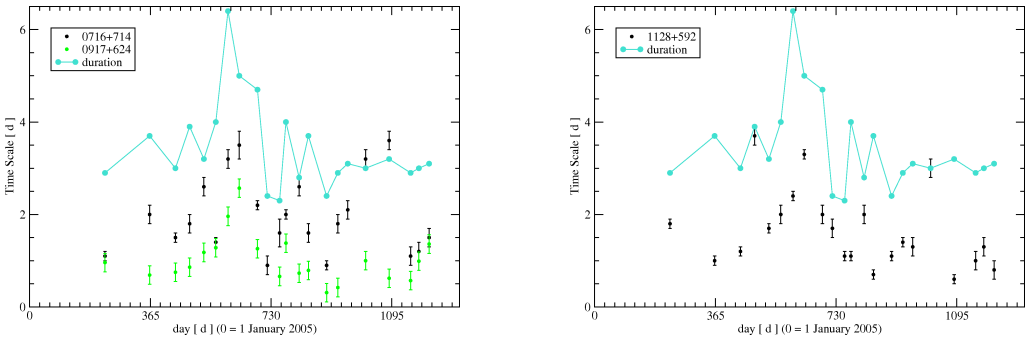

Figure 7.6: The duration of the observations (turquoise circles) compared, in the left panel, with the time scales of 0716+714 (black circles) and 0917+624 (green circles); on the right panel, the black circles are the 1128+592 time scales.

Table 7.2: Time scales estimations for the September 2006 variability curves of all the sources. The 2nd and 3rd column report the estimations for the complete curves, the 4th and 5th for a sub-sample having duration of 3.5 days. The agreement between the results for the complete curves and the ones for their sub-samples is very satisfying.

Source	4.7d		3.5d	
	SR (d)	SF (d)	SR (d)	SF (d)
0716+714	3.5	> 4.0	3.3	3.8
0917+624	2.6	3.4	3.0	3.4
0954+658	2.0	1.6	1.8	1.6
1128+592	3.3	> 4.0	2.9	2.6

7.3). For 0917+624 and 0954+658 the agreement between the results for the complete and the partial curves is quite good; about 1128+592, the SR analysis does not reveal significant differences, while the SF value for the 3.5 d window is considerably *higher* than that for the rest of the data-set. Similar is the situation for 0716+714. The reason is the variability in the first part of both the light curves, which is considerably slower than in the last part. This is demonstrated by repeating the estimations on the second half of the data: for 1128+592 the time scale drops to 1.8 d, for 0716+714 to 1.4 d. Here we find the origin of the double time scales already mentioned for this variability curve. In Fig. 7.7 we plot the time scales of 1128+592, after substituting the values obtained for the August, September and November 2006 variability curves with the ones from the sub-samples. Apparently, *the effect of the duration of the observations on the results of the time-series analysis is only marginal.*

7.2.3 Source-extrinsic variability

Once we excluded spurious effects as a possible cause of the observed variations in the variability time scales, the most likely conclusion is that the IDV observed in the four IDV sources has source-extrinsic origin.

The main time scale peaks, around September-October, are in excellent agreement with

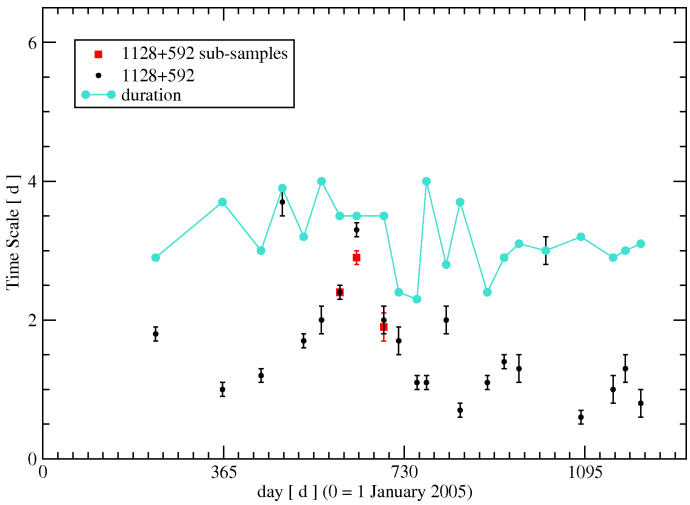

Figure 7.7: The difference between the variability time scales derived from the original light curves (black circles) and the ones obtained from data sub-samples (red squares) is negligible. This implies that the results can not be significantly affected by the duration of the observations.

Table 7.3: Same as Table 7.2, but this time for the variability curves of August 2006. Again, the differences are negligible.

Source	6.5d		3.5d	
	SR (d)	SF (d)	SR (d)	SF (d)
0716+714	3.2	1.4	2.9	3.0
0917+624	2.0	> 4.0	1.9	> 2.5
0954+658	2.5	1.6	2.6	1.6
1128+592	2.4	2.0	2.4	2.8

the idea that the major contribution to the annual modulation is due to the Sun's motion in the LSR. The nature of the March-April peak is puzzling: the peak is very prominent and narrow, and less regular than the other; it is not detected in all the sources every year, and seems to range between March and April. An explanation in terms of anisotropic annual modulation is not very convincing. Moreover, the fact that the two slowdown phases are separated by about 6 months gives rise to the suspicion of a strict correlation between the two and the revolution of the Earth around the Sun. The similarities between the time scale trends of different sources would be easier to explain in the hypothesis that the variability has its origin very close to the Earth. It would be natural, then, to think to an involvement of the atmosphere, whose parameters are also affected by large seasonal variations (see, e.g., Wu and Jiang (2005)).

The information we have does not allow a definite conclusion; further observations are needed in order to establish whether the slowdown between March and April is seasonal or not. In case of a seasonal phenomenon, we would have a strong argument against the annual modulation models currently used.

Conclusions

At the focus of the present thesis is the Urumqi monitoring project, an ongoing observational campaign for the investigation of the changes in the variability characteristics of a sample of IDV sources. We discuss the results of the first 22 observing sessions, from August 2005 to April 2008, for a total observing time of 77.6 days. The main achievements are summarized below:

Data calibration: We developed the software for the calibration of the flux-density measurements obtained at the Urumqi telescope. The complete procedure, which is highly automated, allows to reach a level of accuracy in the range between 0.2% and 0.7% of the average flux-density. Simultaneous Effelsberg-Urumqi observations fully confirms the reliability of the data, demonstrating that the Urumqi antenna is well suitable for IDV research.

A new analysis tool: We developed a new time analysis method, the *sinusoidal regression*. Its capability to provide information about both amplitude and time scale of the variability in a time series turned out to be extremely helpful for tracing the evolution of the variability characteristics of IDV sources. The agreement with the results from a classical time analysis method such as the structure function is very satisfactory.

The 1-day effect: We discovered a periodic contribution to the variability of IDV sources, which can not be ascribed to any known systematic effect.

- The frequency of the signal is $1\,\mathrm{d}^{-1}$, but high order harmonics have been detected as well. The origin of the variability can not be intrinsic to the sources.
- The amplitude of the signal changes from epoch to epoch, but also from one day to another, during the same observing session. This can make it hard to identify and to remove.
- The signal has been detected in variability curves from Urumqi, Effelsberg and the VLA. The problem, therefore, is not limited to a single facility, and may concern a considerable amount of IDV experiments.
- The effect seems to depend on both time and source position.
- We found evidence for a simultaneous appearance of the periodicity in Effelsberg and Urumqi, which seems to support the idea of a phenomenon acting on a large spatial scale.

We hypothesize that the 1-day effect may be caused by a global atmospheric effect; plausibly, it can be related to variations in the total electron content of the ionosphere. This hypothesis is supported by the evidence of a two-day periodicity in some light curves,

which would find a natural explanation in terms of the planetary wave known as the quasi-two-day wave. The issue, however, is still open.

Time series analysis results: We analyzed the variability curves of 8 IDV sources.

- For 0235+164 we found evidence that the evolution of the variability characteristics may be correlated with changes in the structure of the source.
- For 1156+295, the variability time scales seem to follow a trend which is consistent with annual modulation, pointing towards an extrinsic explanation of its IDV.
- The four main targets of our monitoring campaign show variability of the time scales which seem to be consistent with annual modulation cycles. For 0716+714, 0917+624 and 1128+592 the results strongly support this conclusion, while for 0954+658 the evidence is weaker. The peaks of the seasonal cycles all fall between DoY 260 and DoY 285, which is consistent with a screen nearly at rest in the LSR. For 0917+624 and 1128+592, the results confirm the conclusions of previous IDV studies. For all the four sources, it is very likely that the nature of the IDV is source extrinsic. The similarities between the changes in the variability characteristics of the different sources, however, raise the suspicion that part of the variability may raise at shorter distances than postulated by classic interstellar scattering models. A local contribution, e.g. from the ionosphere, can not be excluded. A series of rigorous tests demonstrated that the similarities are real. They can not be caused by instrumental errors or biases in the results of the time-series analysis.

7.3 Future developments

The natural evolution of the present thesis project is to establish the origin of the 1-d effect. A deep investigation of the phenomenon is essential for separating its contribution to the variability from any other.

The most straightforward way to test the hypothesis of an atmospheric effect would be via a combined IDV/atmospheric-physics experiment aiming to measure, simultaneously and with high degree of accuracy, the variations both in the flux-density of IDV sources and in geomagnetic and solar parameters (e.g. the TEC, but also sun-spots and sun activity).

Multi-frequency observations may also be useful for understanding if (and how strongly) the ionosphere may affect flux-density measurements at radio wavelengths. In case of an ionospheric contribution to the variability detected in IDV sources, we would expect that the effect would be larger at longer wavelengths.

Another important issue, which our results do not clarify, is the nature of the March-April slowdown which we detected in the variability time scales of different sources. This feature is not consistent with classic ISS models. It is still unclear, though, if it has to be regarded as a seasonal or an episodic phenomenon. The issue may be resolved by performing a series of IDV observations densely covering the time interval between February and May. The characteristic time scales are expected to vary considerably during this period; the change from a fast to a slow variability mode, and back, is expected to be very fast. The results should then be compared with both annual modulation and atmospheric variability models.

Appendix A

In this Appendix, we give some examples of the 1-day effect. Each page consists of two figures: on the top, we show the raw and the calibrated data; on the bottom, the gain-elevation corrected data.

A.1 Raw and calibrated data

The upper figure contains 4 panels: on the top are the raw (left panel) and the calibrated data (right panel) of the affected source. The orange curve is a fit to the 1-d periodicity. On the bottom, the raw (left panel) and the calibrated data (right panel) of the closest calibrator (red circles) and of 0951+699 (blue circles)[1]. The green curve is a fit to the residual 1-d periocity, if any, of the closest calibrator. The vertical lines show the time in which the elevation of the source (black line) and of the closest calibrator (red line) peak. Our aim is to give an exhaustive description of the main characteristics of the effect:

- The comparison between the raw data of the source and of the two calibrators shows that 1-d periodicities are usually present in both, nearly in-phase. However, they are stronger in the former than in the latter ones. Also, the existence of the effect in the source's raw data demonstrates that the 1-d effect is not *introduced* in its variability curve by a wrong calibration procedure.
- The comparison between the calibrated data of the source and of the two calibrators shows that despite the complete (or almost complete) disapparence of the 1-d period from both calibrators, the source is still affected.
- The superposition of the variability curves of two calibrators, at the beginning and at the end of the calibration procedure, shows the level of agreement between them, demonstrating the efficiency of the data calibration.
- The vertical lines, related to the elevation peaks of source and closest calibrator, illustrate the controversial relation between the 1-d effect and elevation. Sometimes the 1-d period peaks almost simultaneous to elevation, sometimes it does not.

A.2 Gain-elevation corrected data

In the lower figure, we plot the gain-elevation corrected data of the source (black circles) and of all the primary and secondary calibrators (turquoise circles). The blue curve shows the 1-d periodicity in the former, the red curve the 1-d periodicity (if any) in the latter.

[1] In the case that the closest calibrator is 0951+699, the blu circles refer to the data of 0836+710.

With this figure, we aim to show how the 1-d effect responds to the gain-elevation correction. It should be noted that:

- The uniform behaviour of the all-calibrator's curve demonstrates the agreement between the calibrators data;
- The residual variability in the all-calibrator's curve is always weaker than in the source's curve;
- Sometimes also the calibrators show evidence of a weak periodical oscillation, despite the removal of the gain-elevation effect. Such a periodicity is more remarkable if we consider that the curve includes data-points for sources which have very different celestial coordinates.

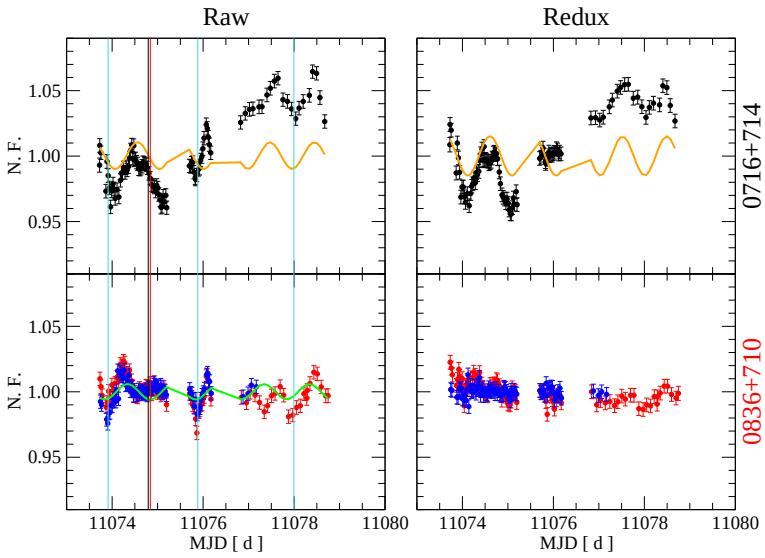

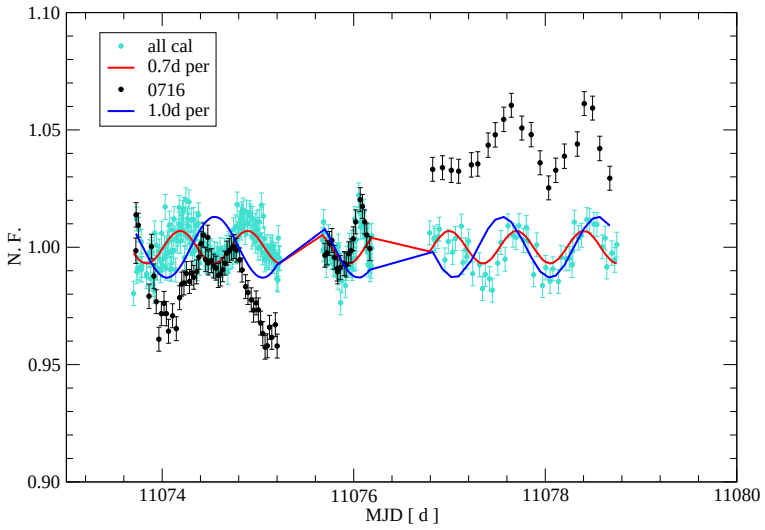

Figure A.1: 1998-09

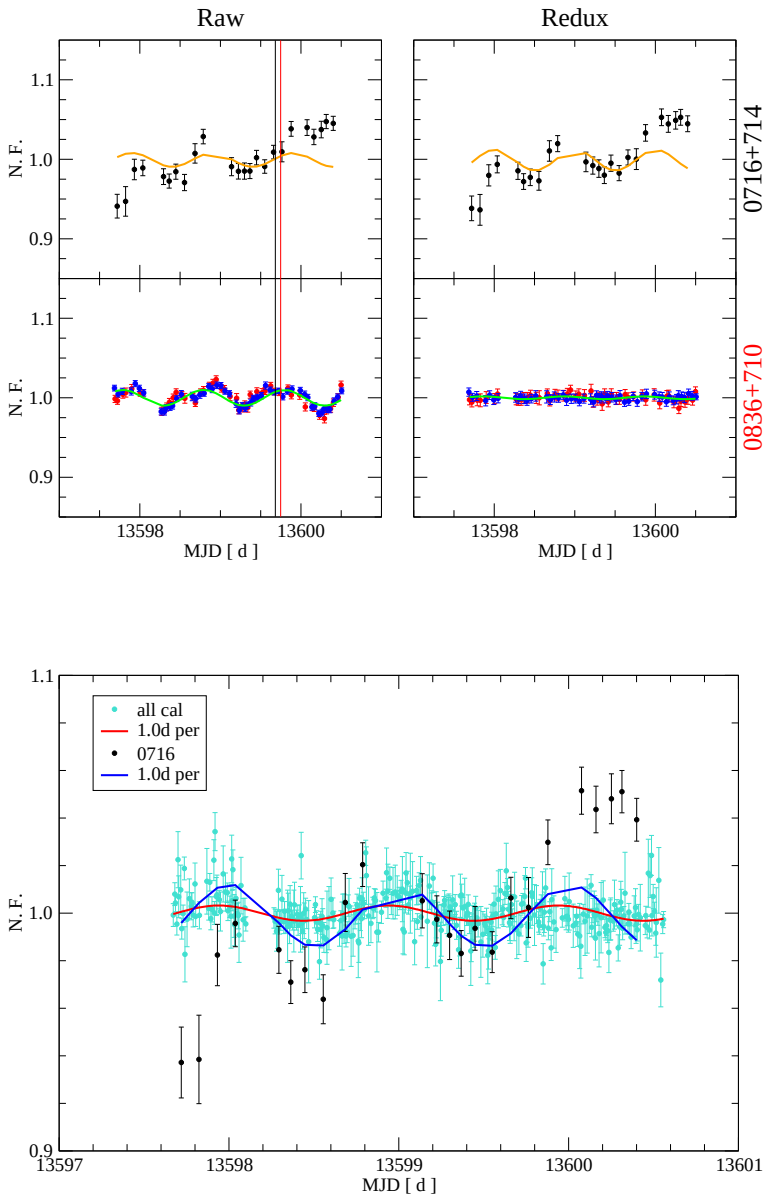

Figure A.2: 2005-08

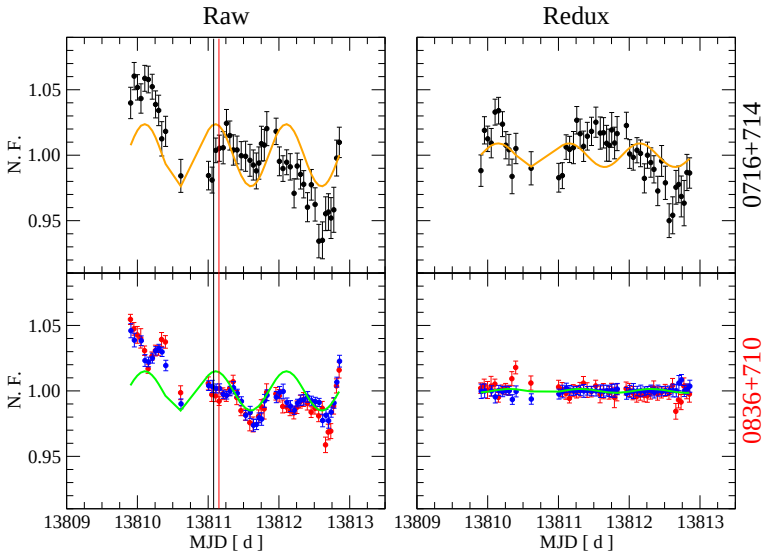

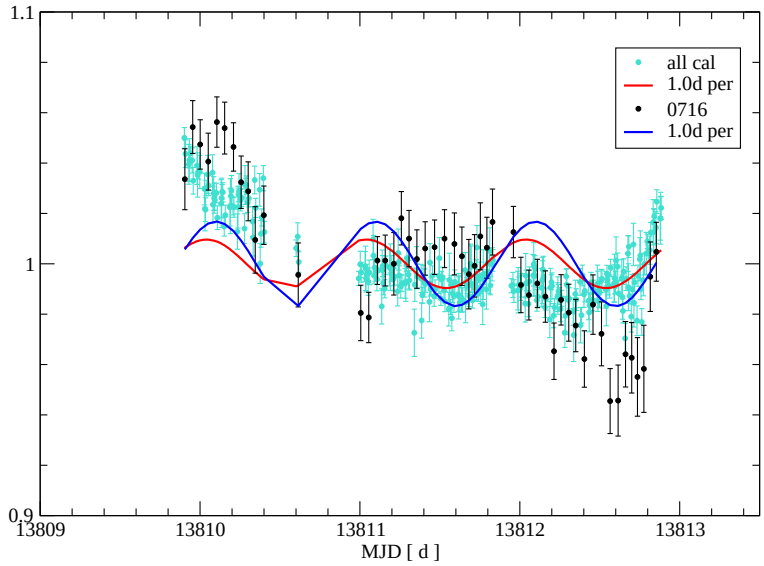

Figure A.3: 2006-03

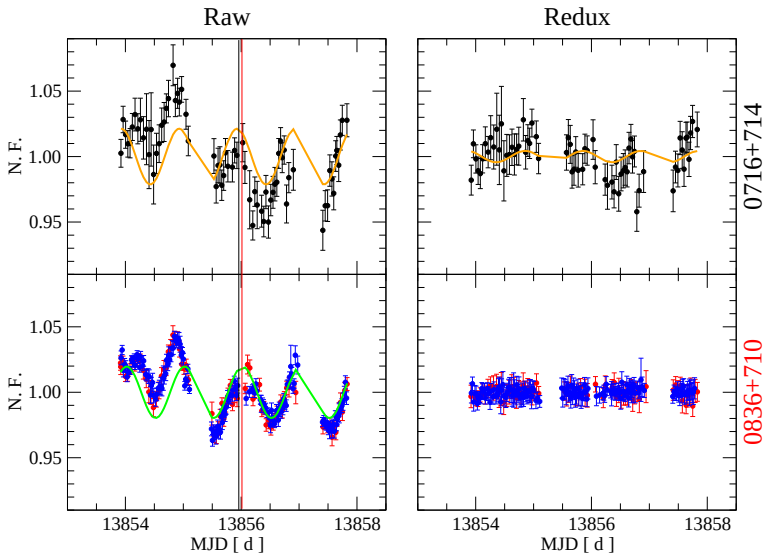

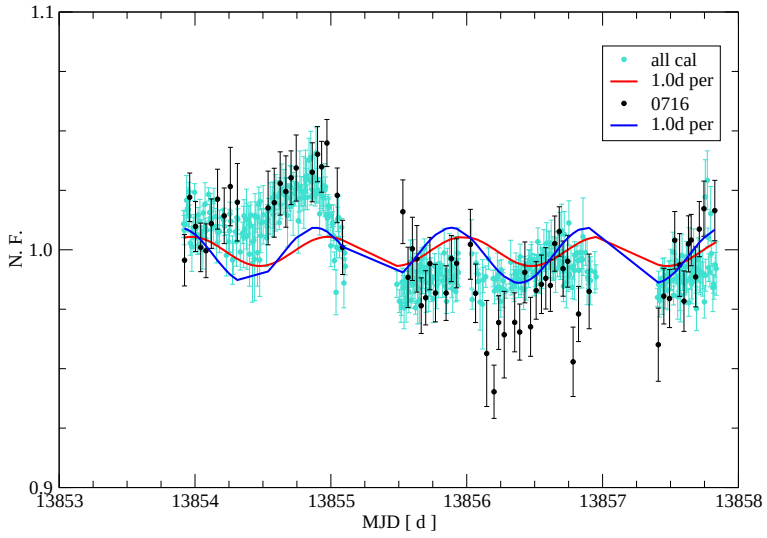

Figure A.4: 2006-04

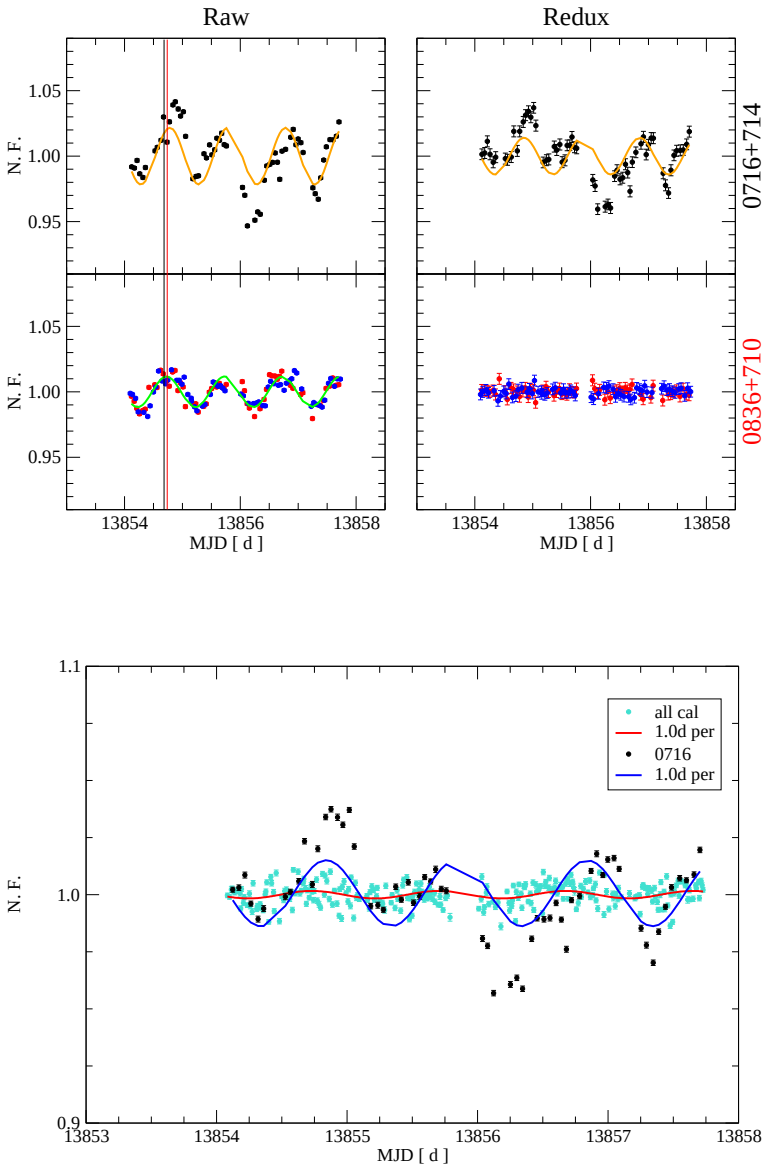

Figure A.5: 2006-04 eff

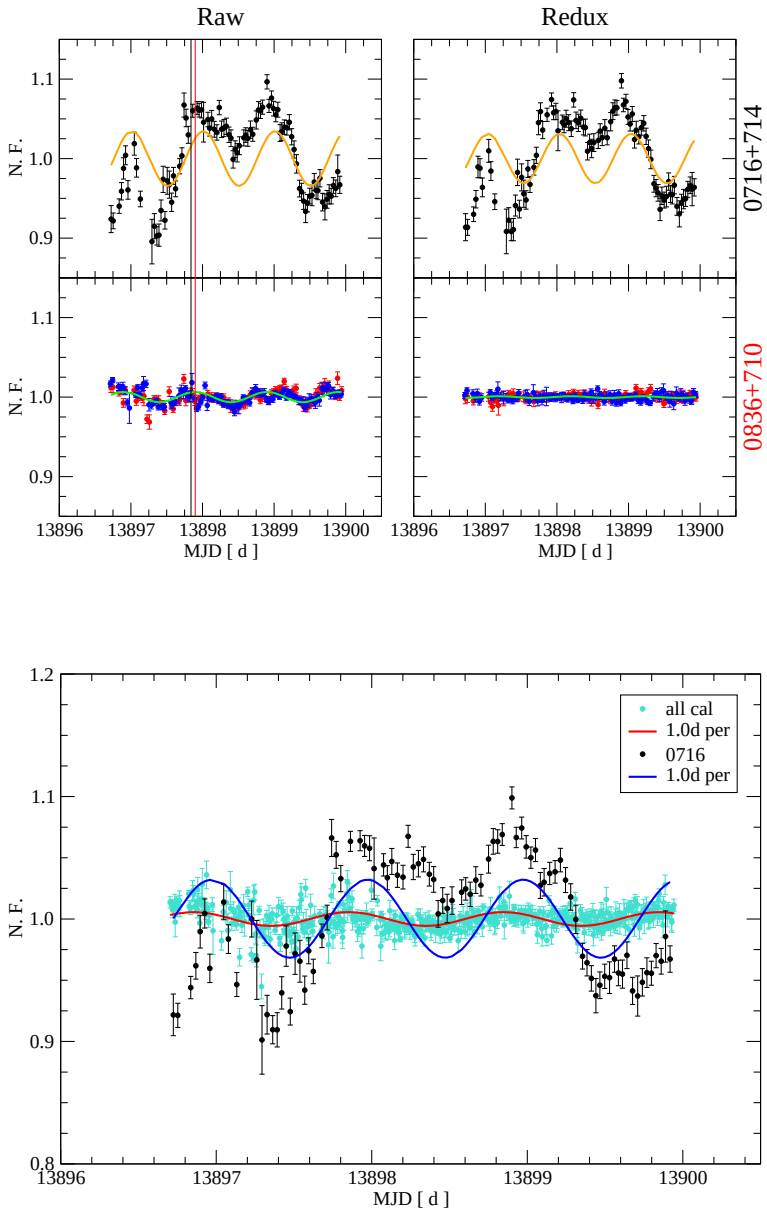

Figure A.6: 2006-06

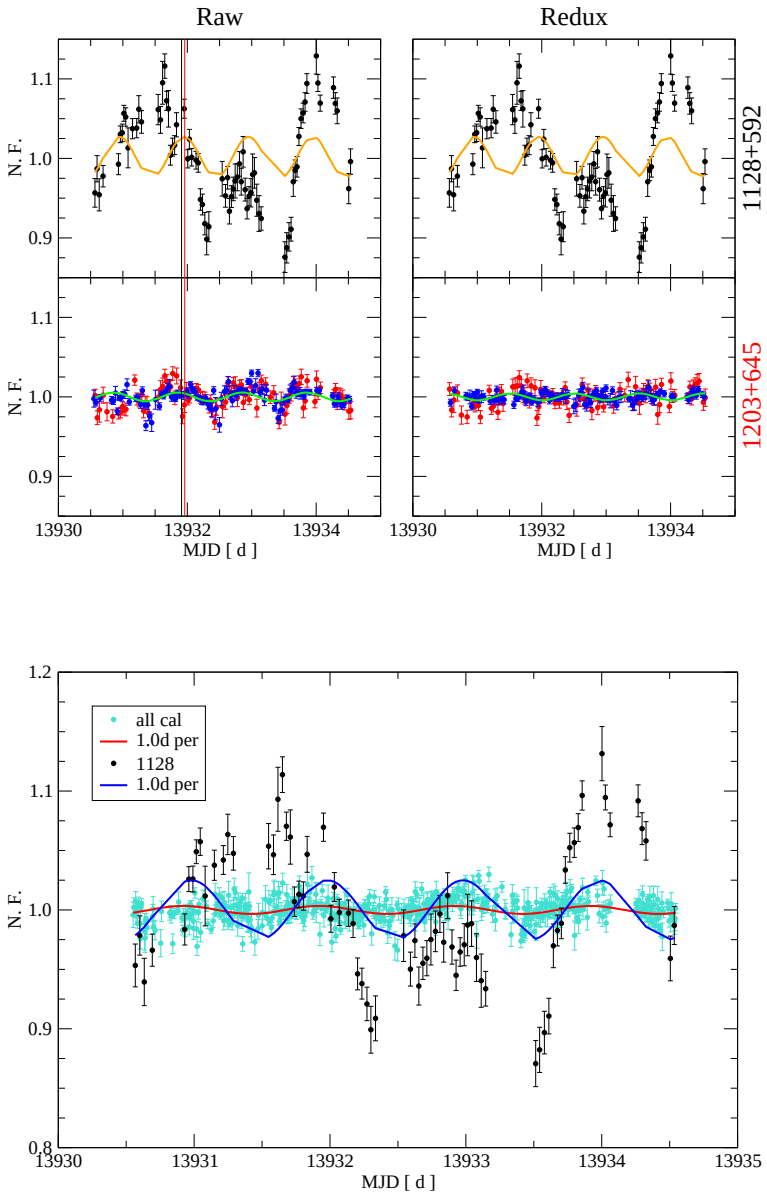

Figure A.7: 2006-07

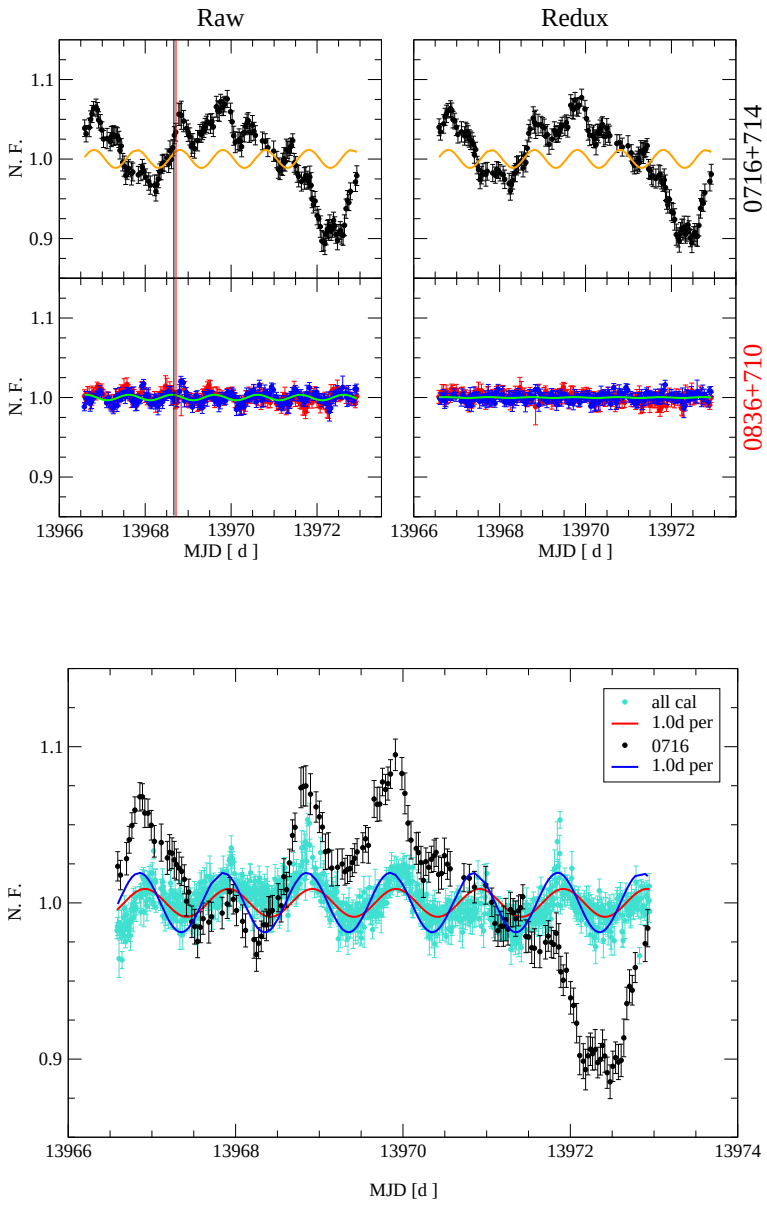

Figure A.8: 2006-08

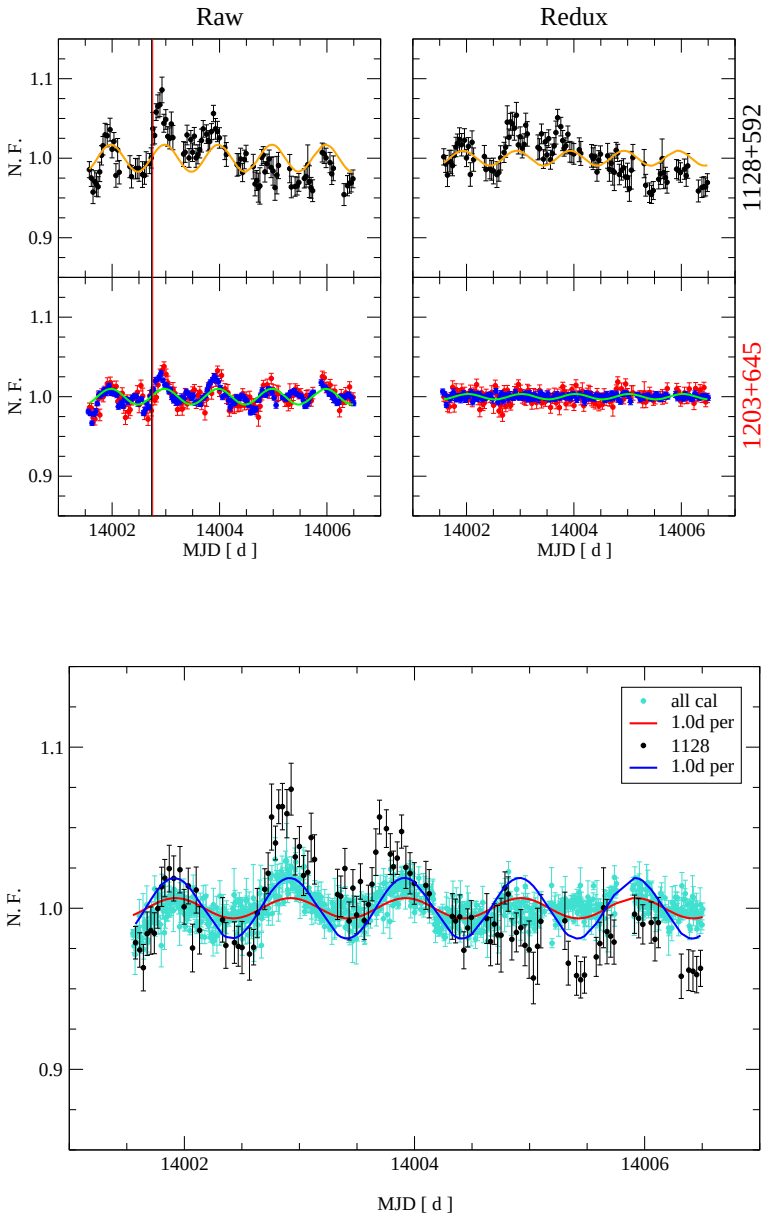

Figure A.9: 2006-09

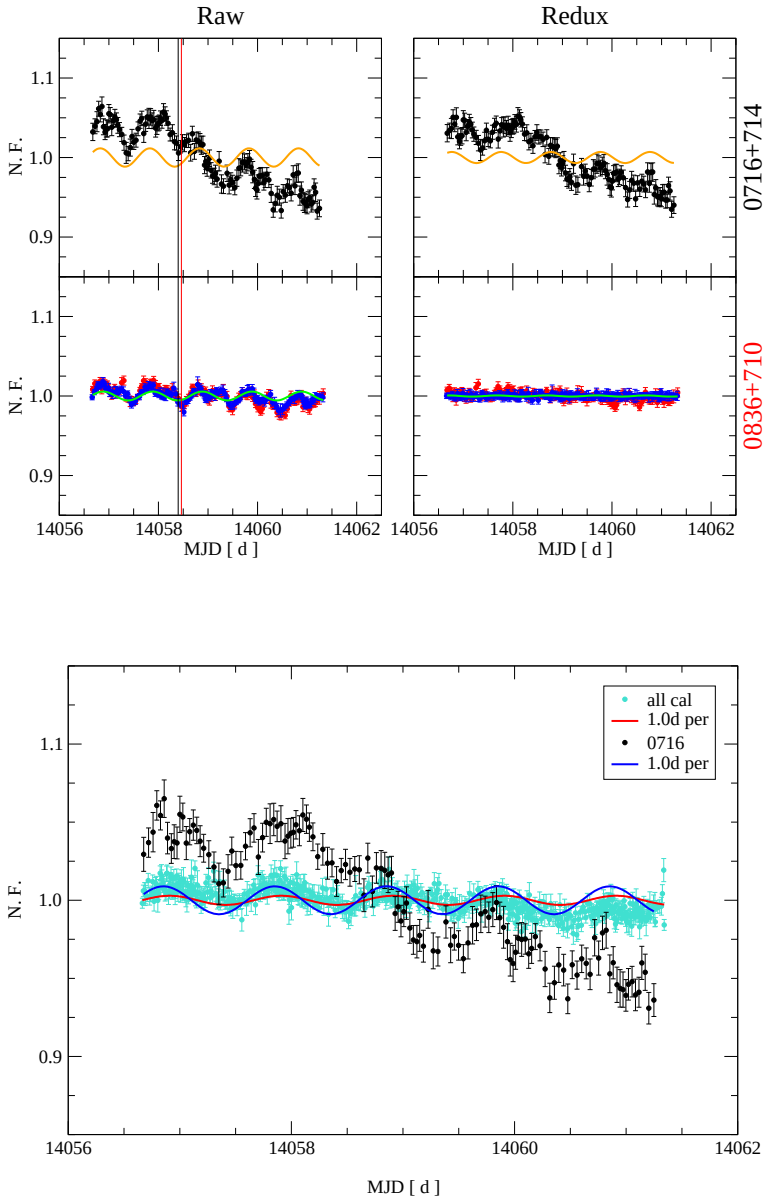

Figure A.10: 2006-11

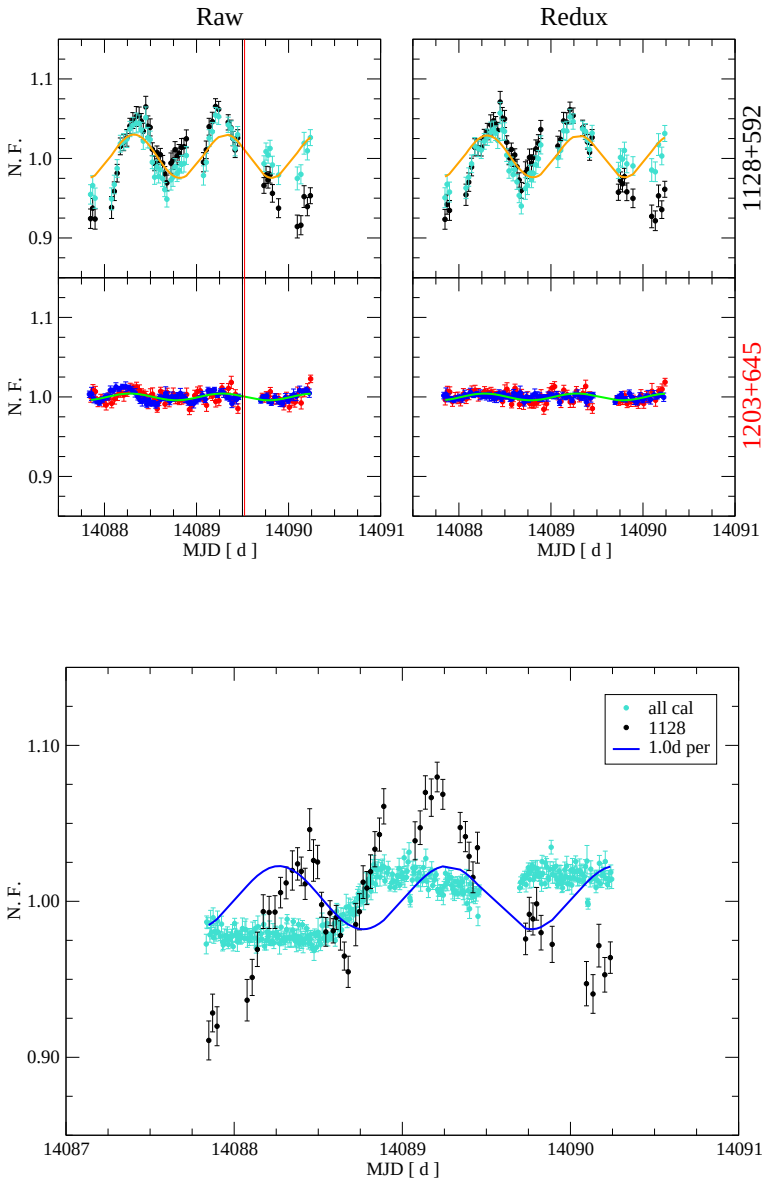

Figure A.11: 2006-12

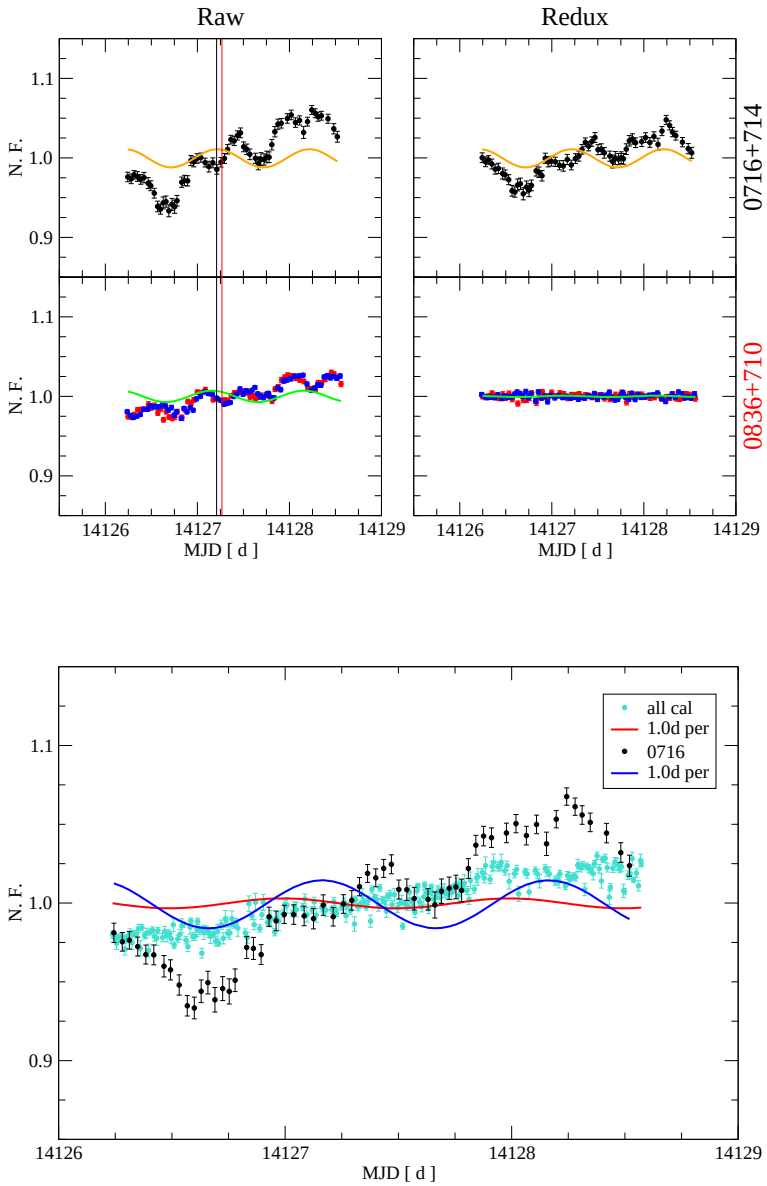

Figure A.12: 2007-01

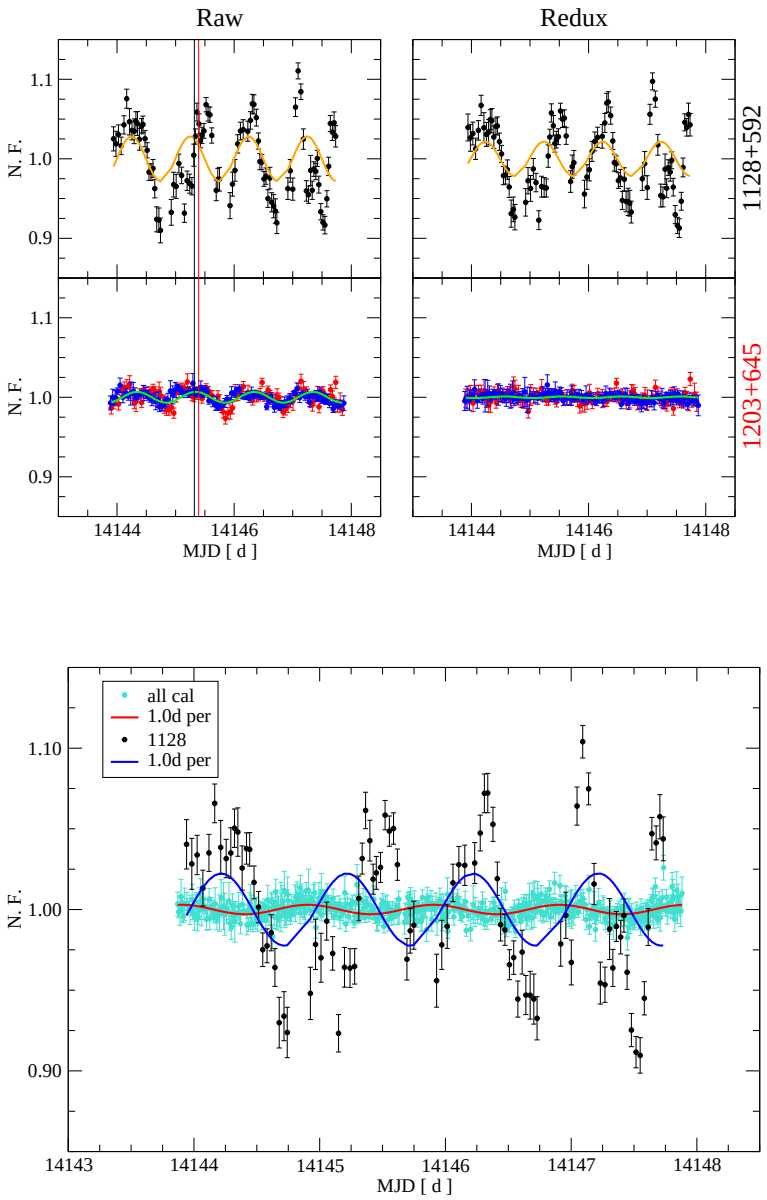

Figure A.13: 2007-02

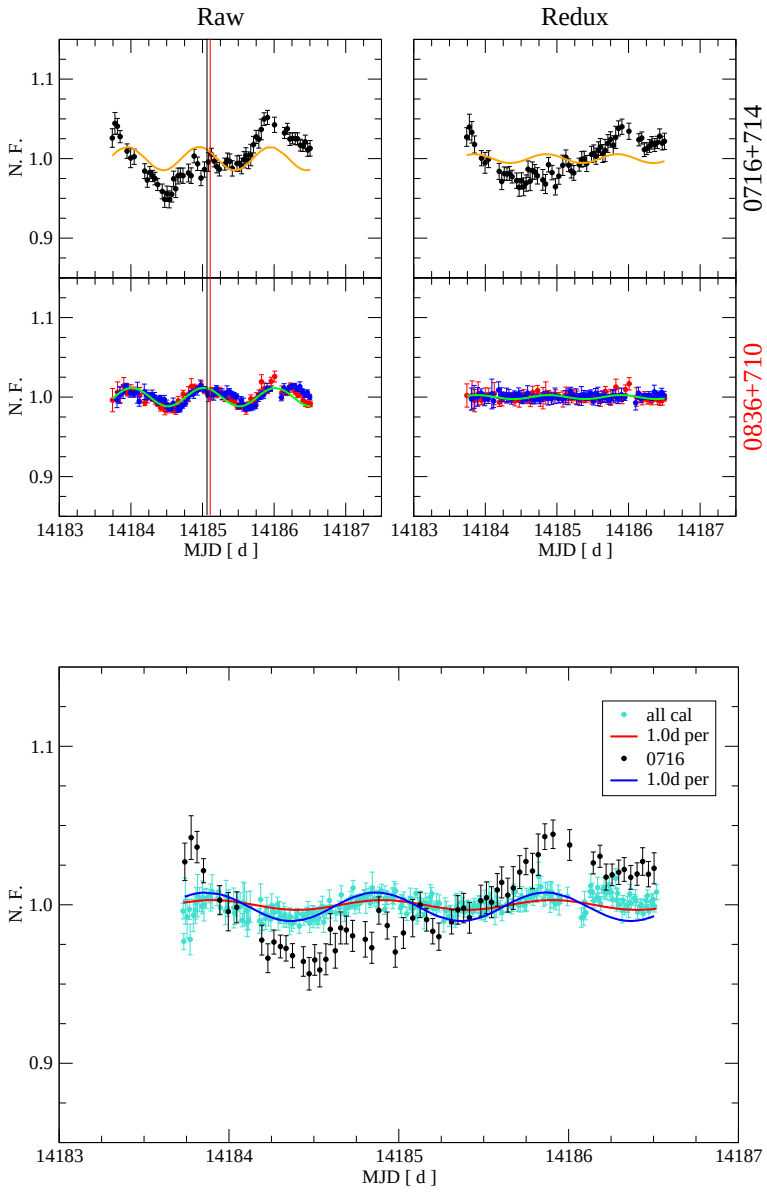

Figure A.14: 2007-03

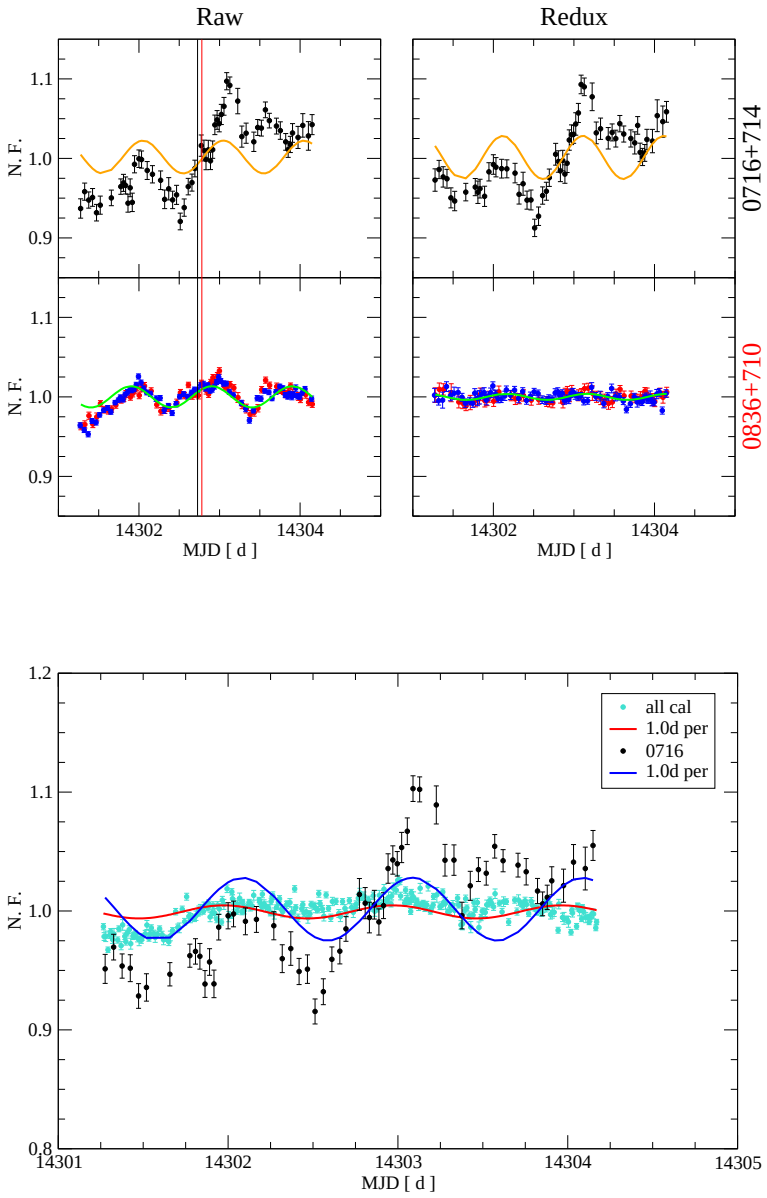

Figure A.15: 2007-07

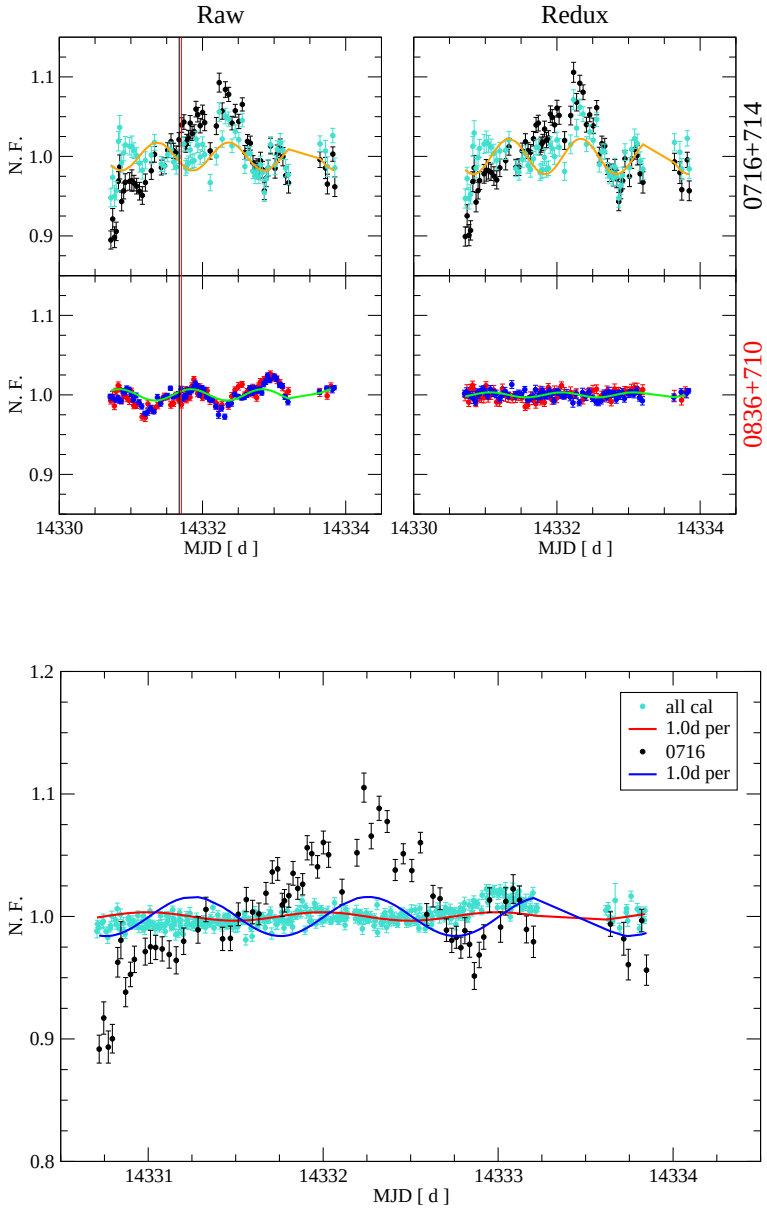

Figure A.16: 2007-08

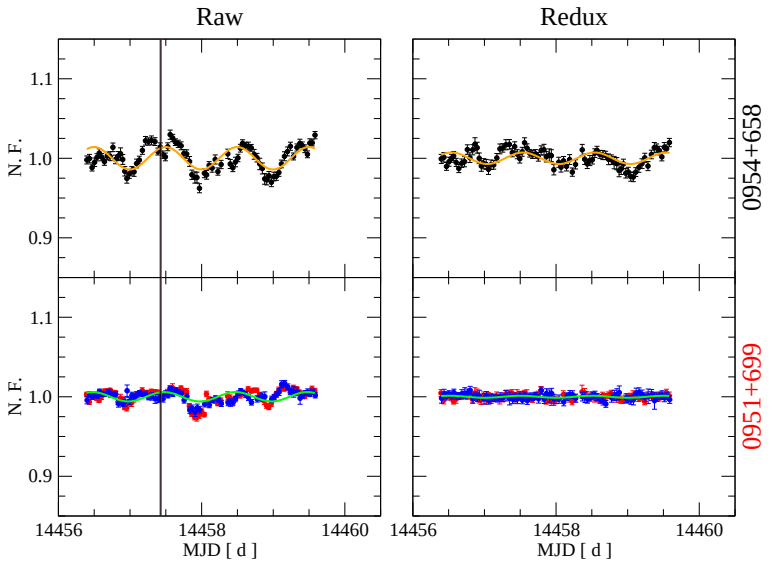

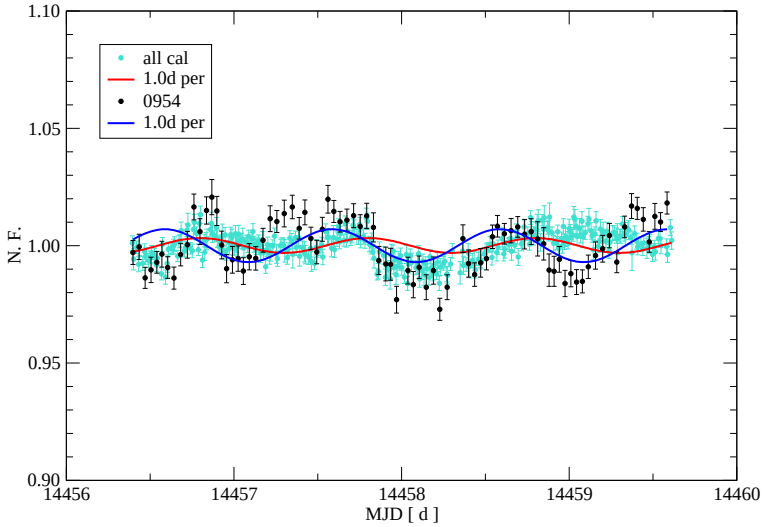

Figure A.17: 2007-12

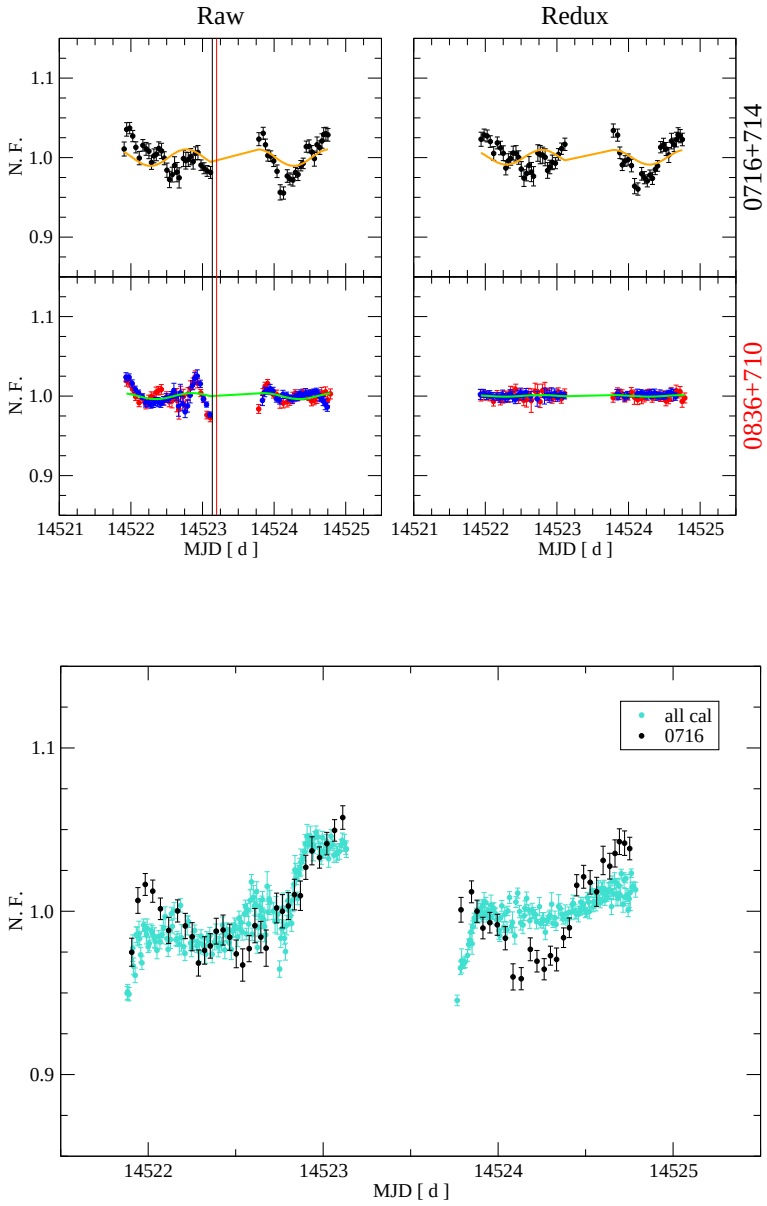

Figure A.18: 2008-02

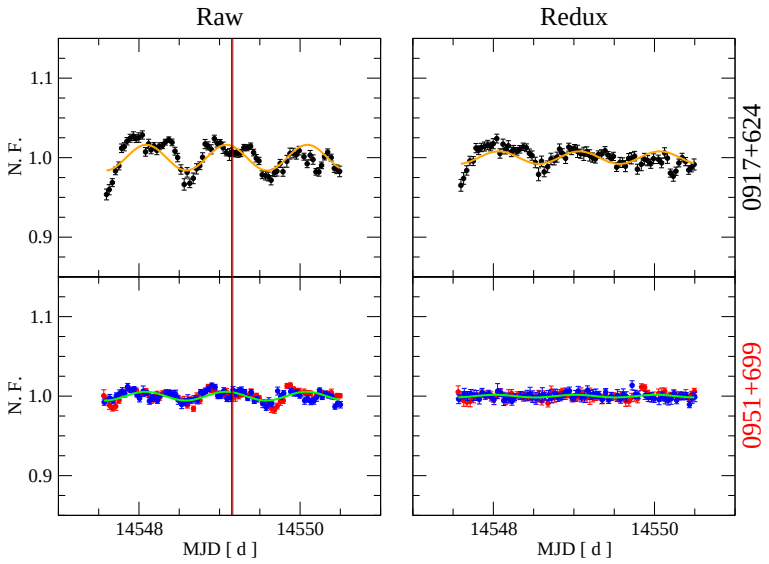

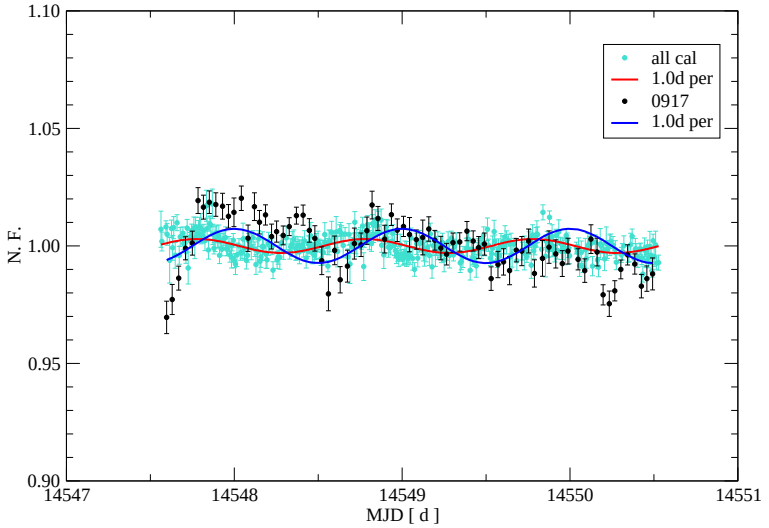

Figure A.19: 2008-03

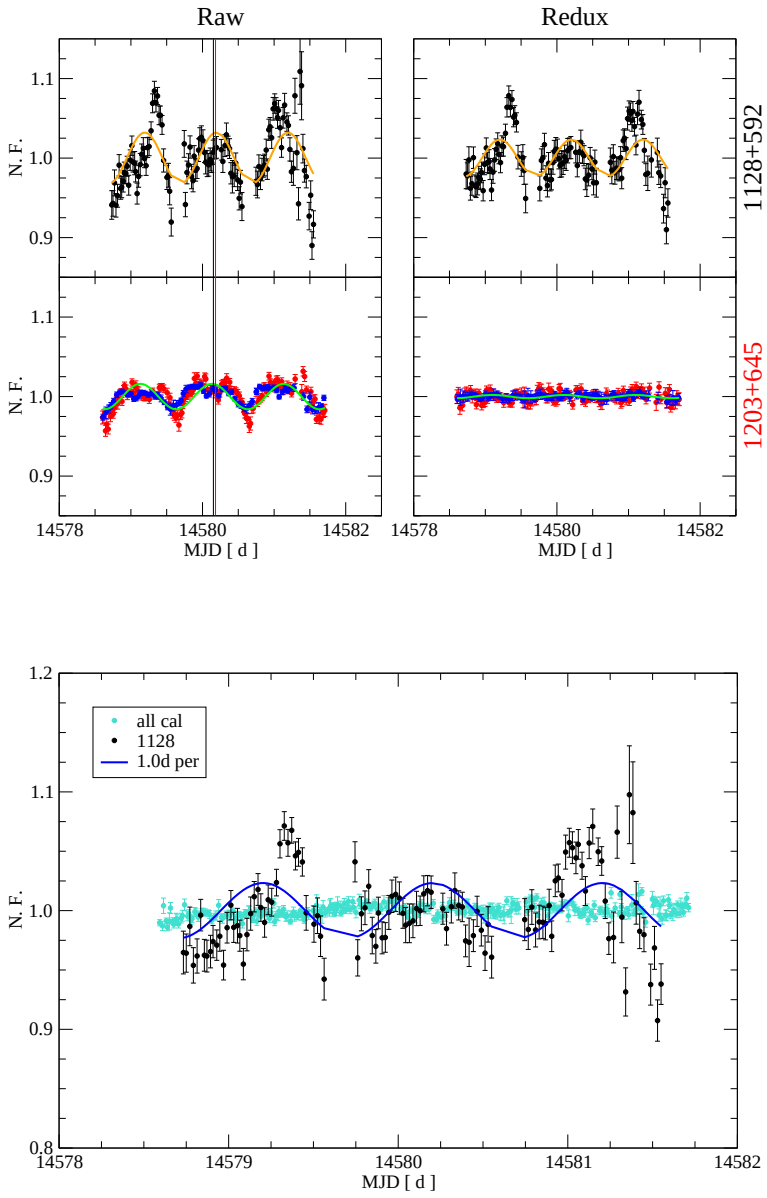

Figure A.20: 2008-04

Appendix B

In this Appendix, we show all the variability curves of the IDV sources discussed in Chapter 6. In the upper panels, along with the variability curves, we plot the dominant SR components – if any. A label indicates the curves for which one or more periodicities, related to the 1-d effect, have been subtracted from the data.

In the lower panels, we plot the SF results. When the latter ones seem to be affected by sampling effects, a red curve indicates the sampling curve. This is proportional to the number of data pairs which are used for the computation of the function at a given time bin. If a time scale is clearly detected, it is indicated by a red arrow, whose length illustrates the uncertainty. A purple arrow, instead, indicates secondary or uncertain time scales.

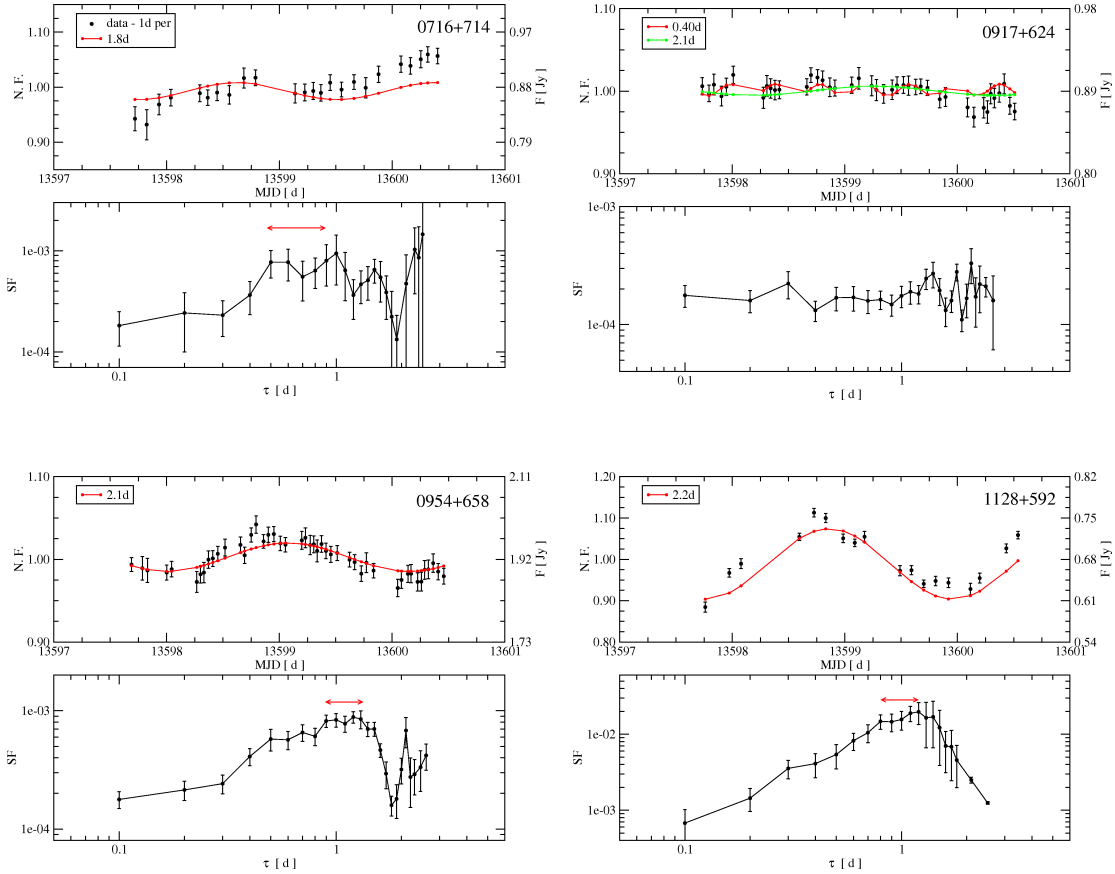

Figure B.1: Urumqi, August 2005

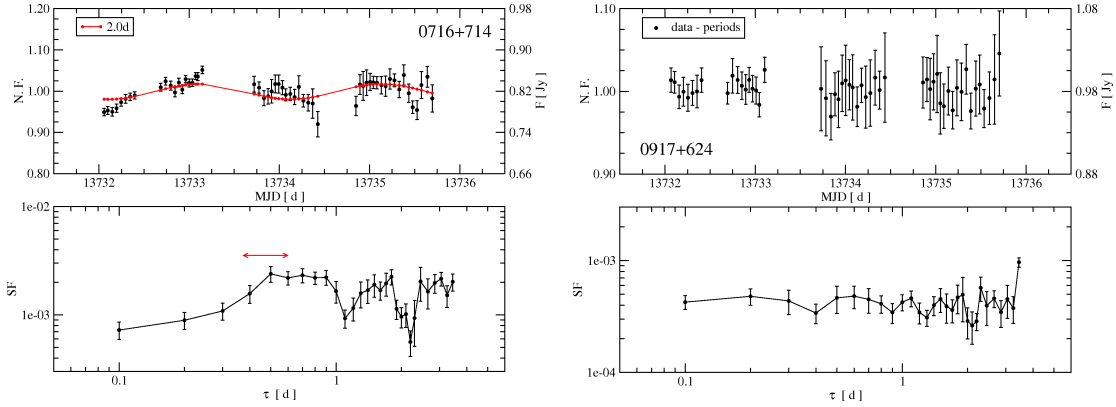

Figure B.2: Urumqi, December 2005

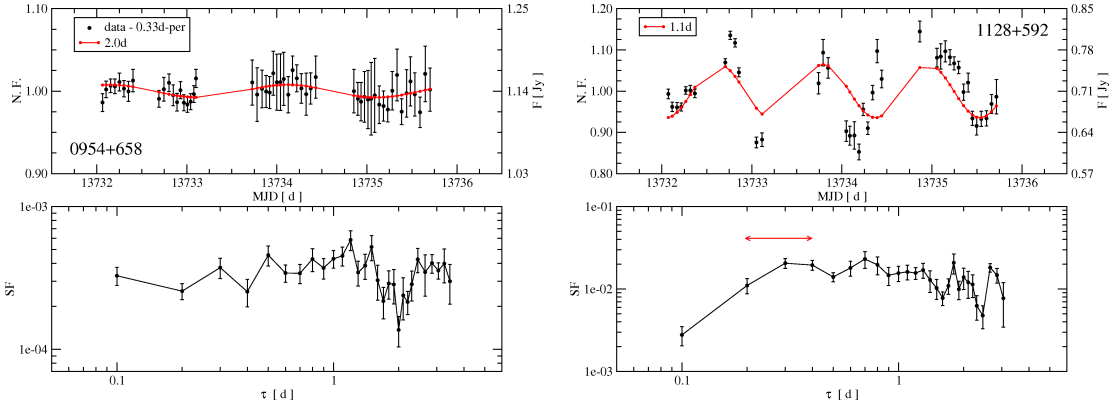

Figure B.3: Urumqi, December 2005

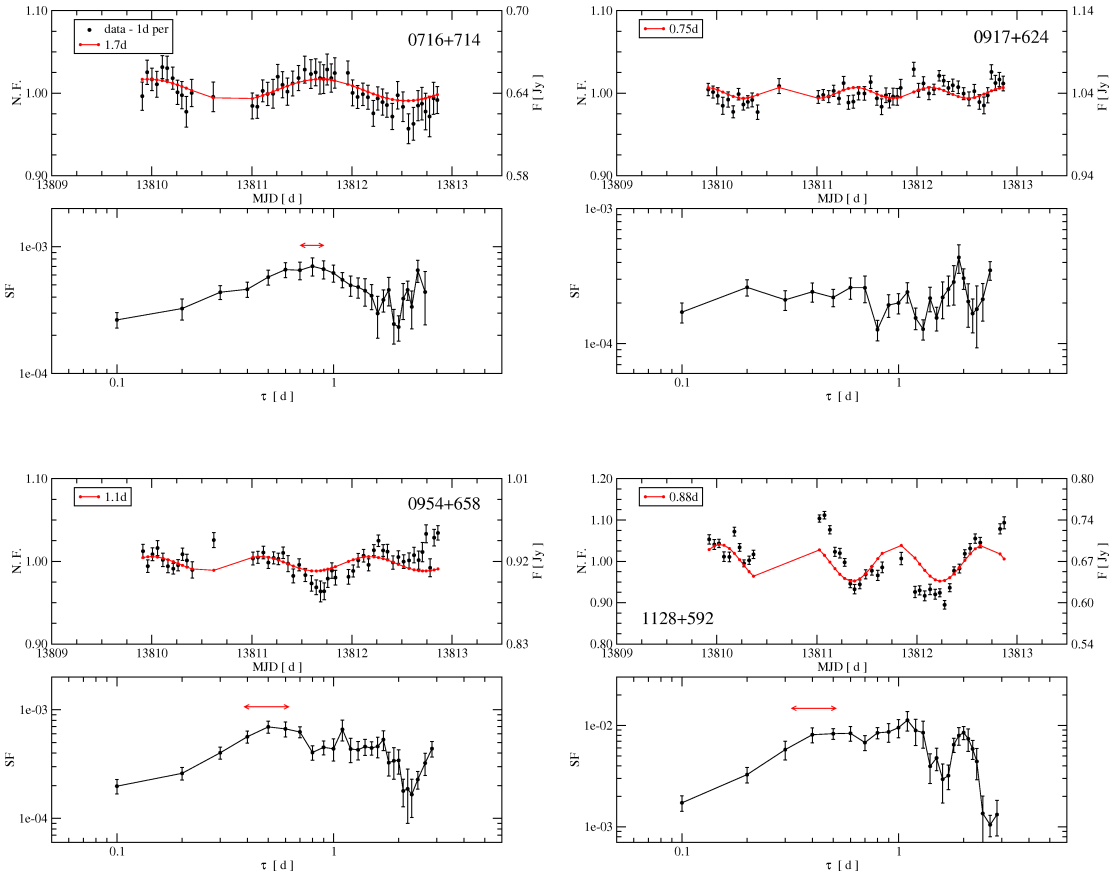

Figure B.4: Urumqi, March 2006

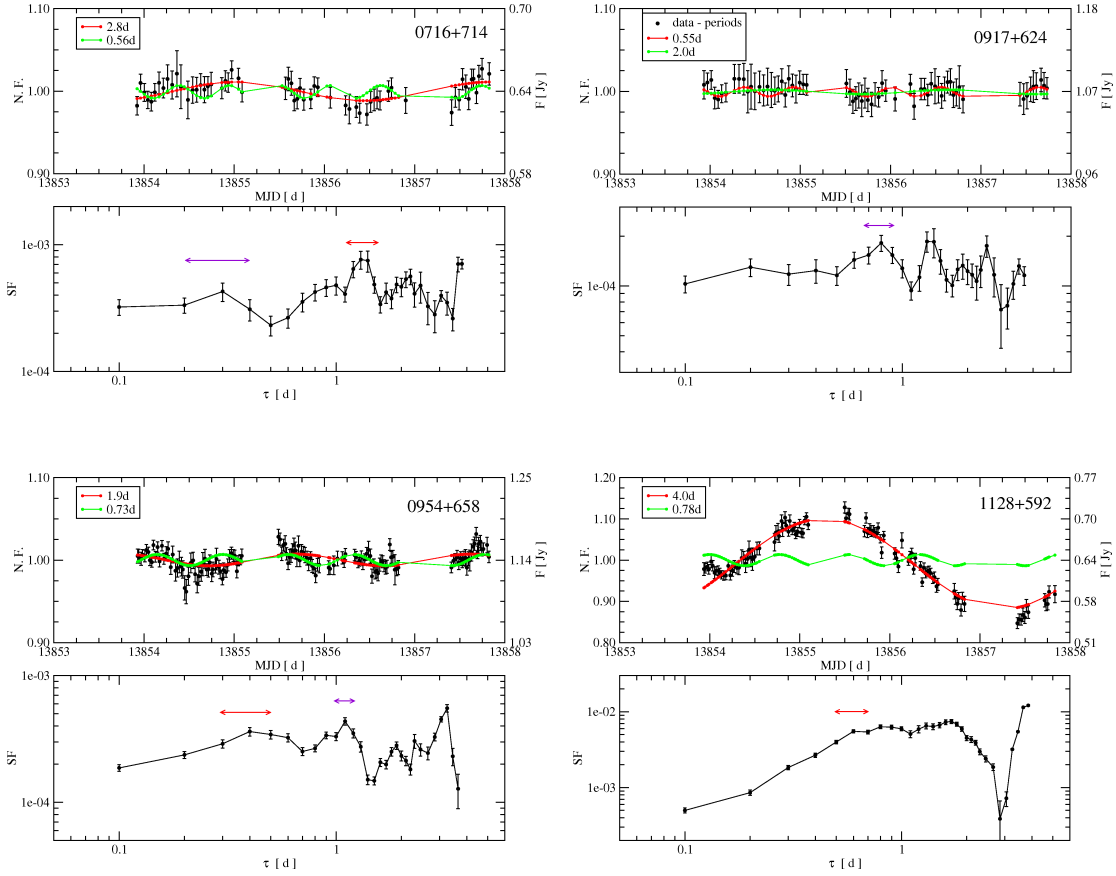

Figure B.5: Urumqi, April 2006

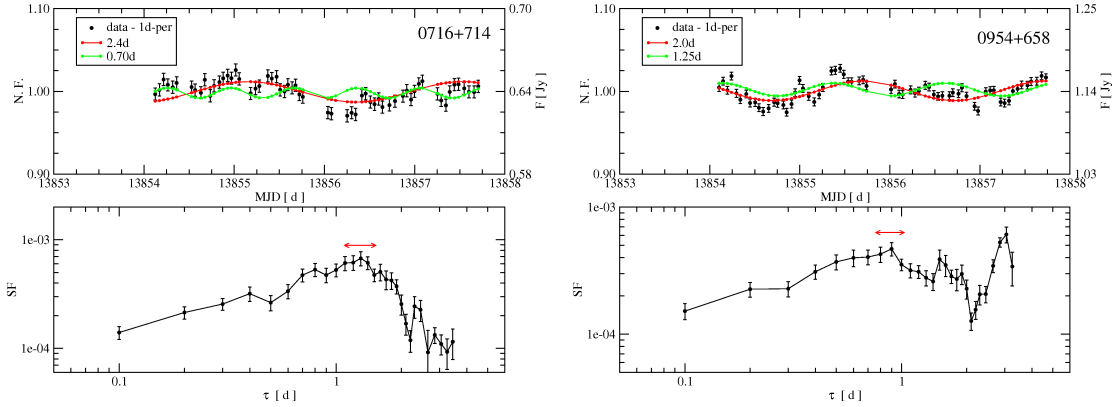

Figure B.6: Urumqi, April 2006 Effelsberg

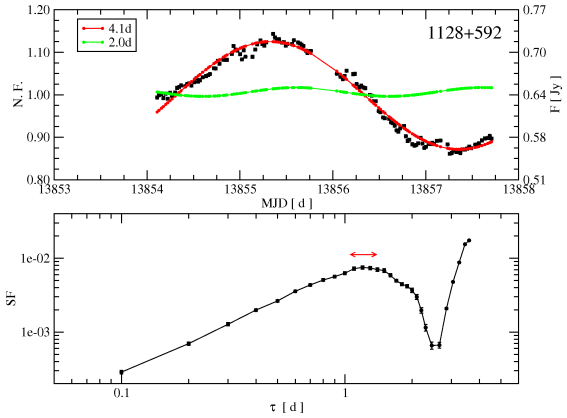

Figure B.7: Urumqi, April 2006 Effelsberg

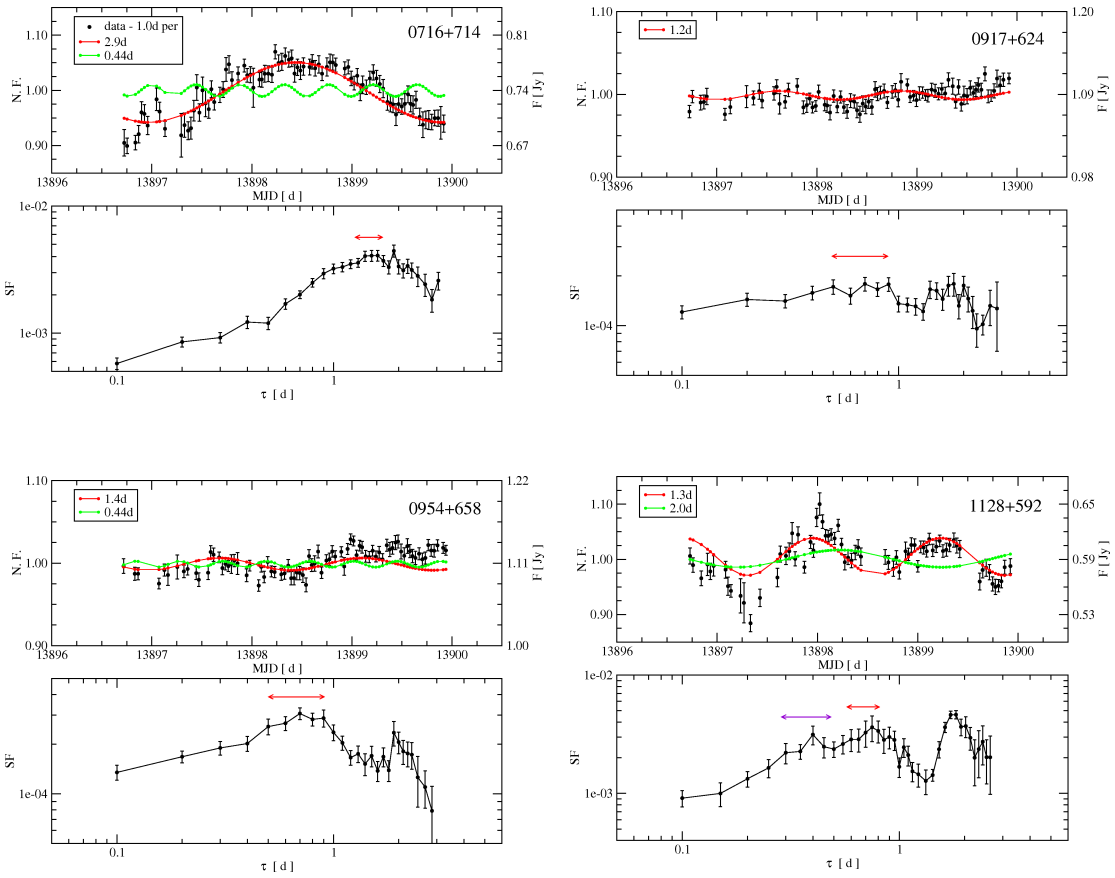

Figure B.8: Urumqi, June 2006

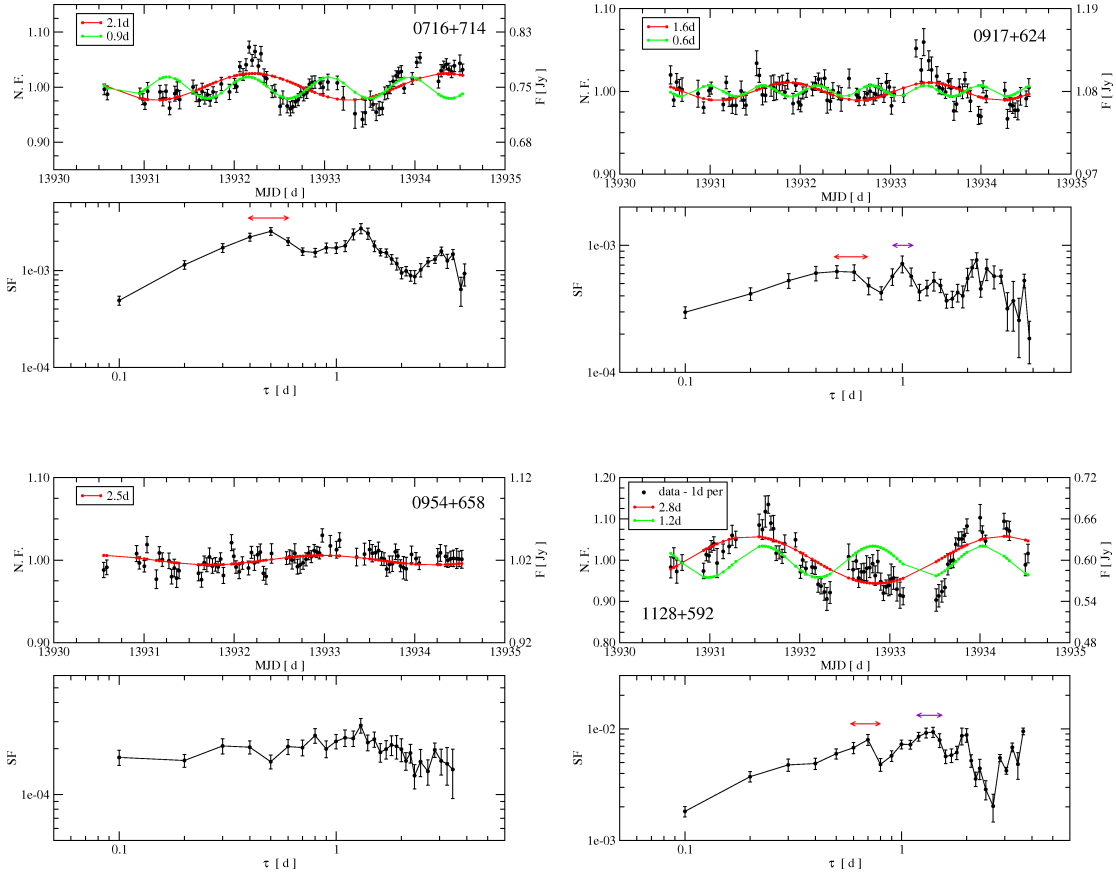

Figure B.9: Urumqi, July 2006

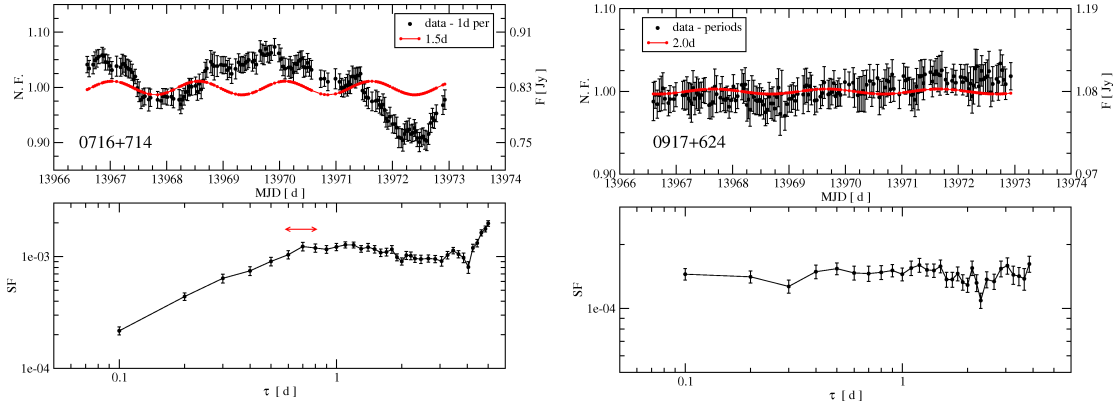

Figure B.10: Urumqi, August 2006

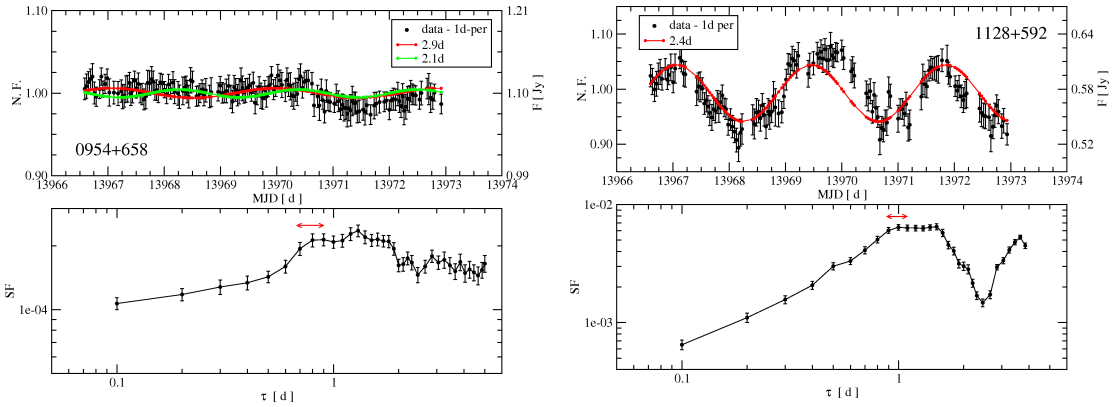

Figure B.11: Urumqi, August 2006

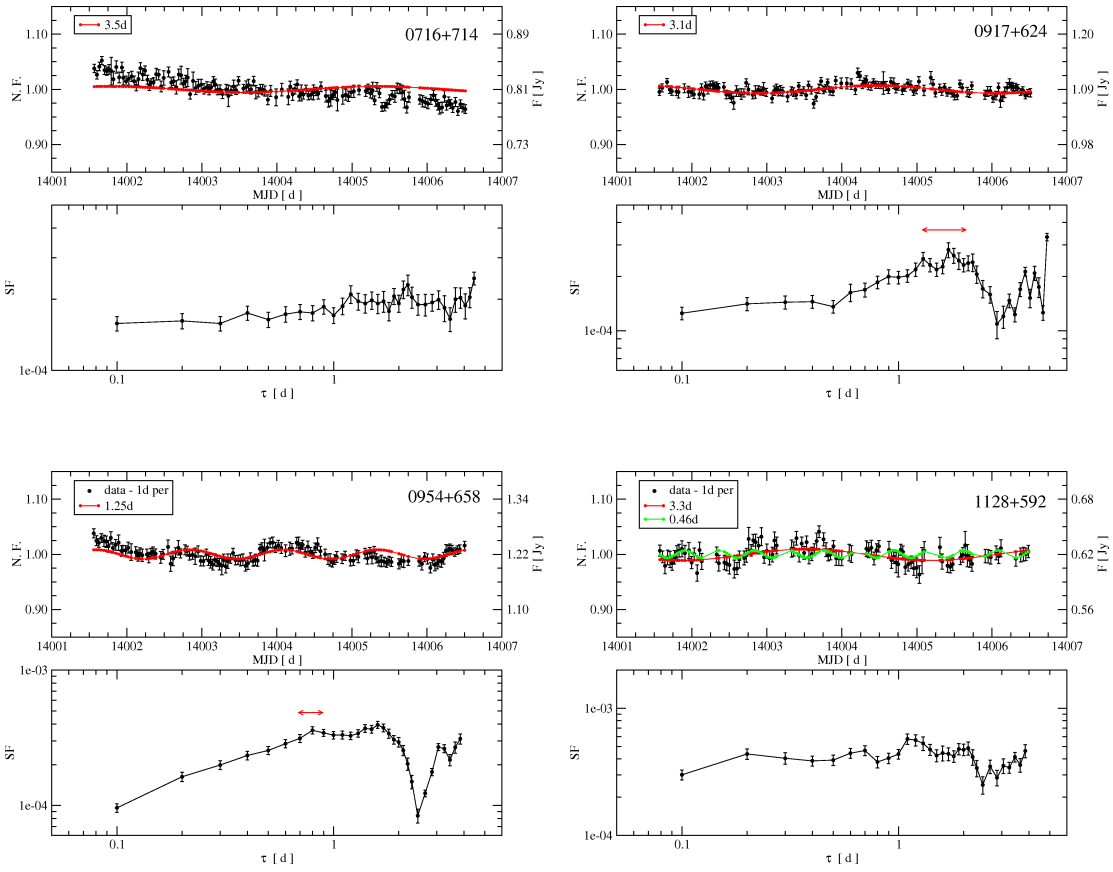

Figure B.12: Urumqi, September 2006

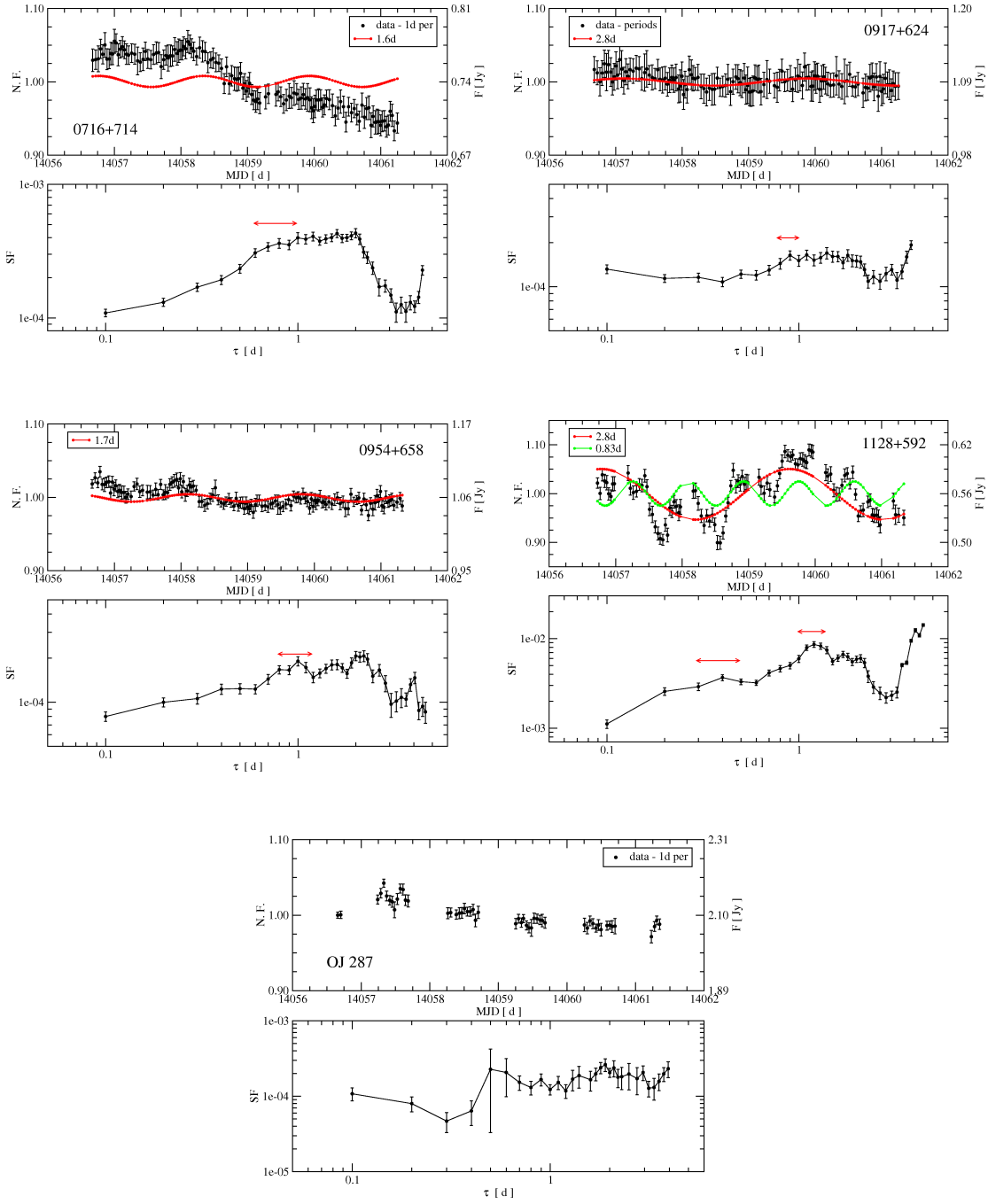

Figure B.13: Urumqi, November 2006

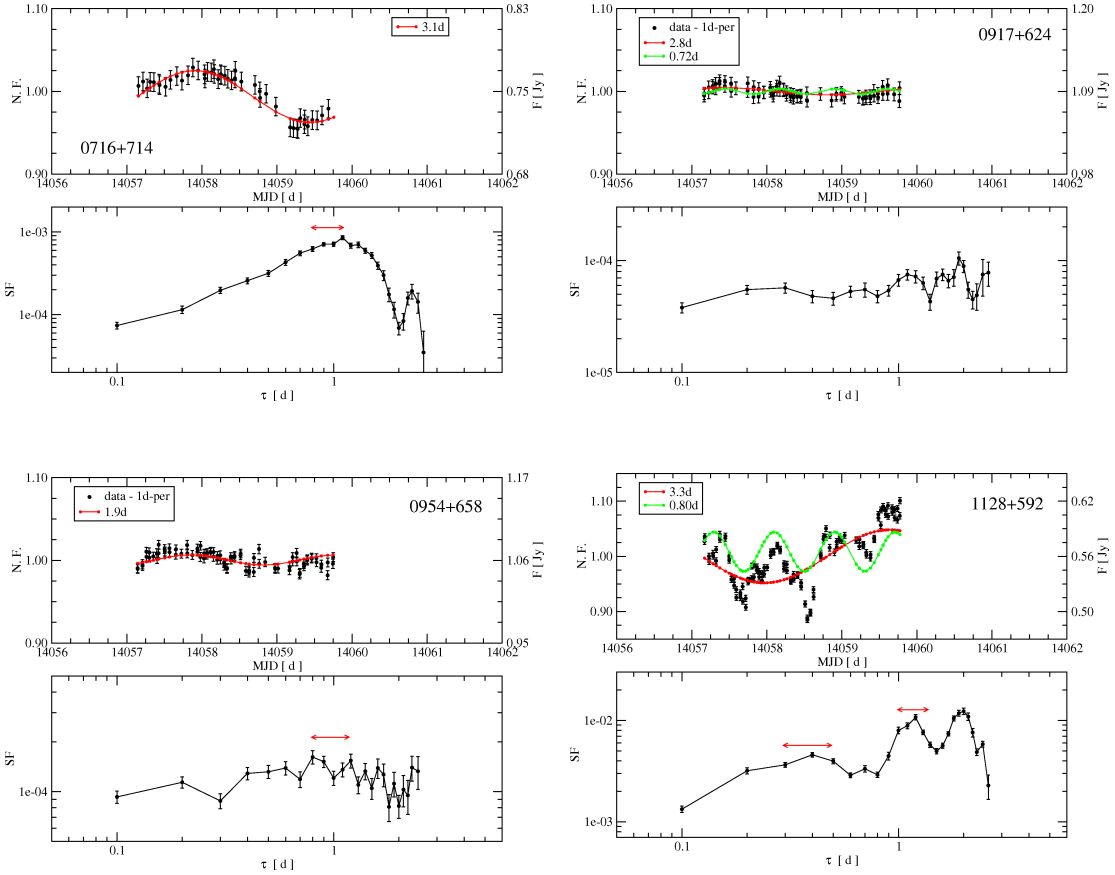

Figure B.14: Urumqi, Novemebr 2006 Effelsberg

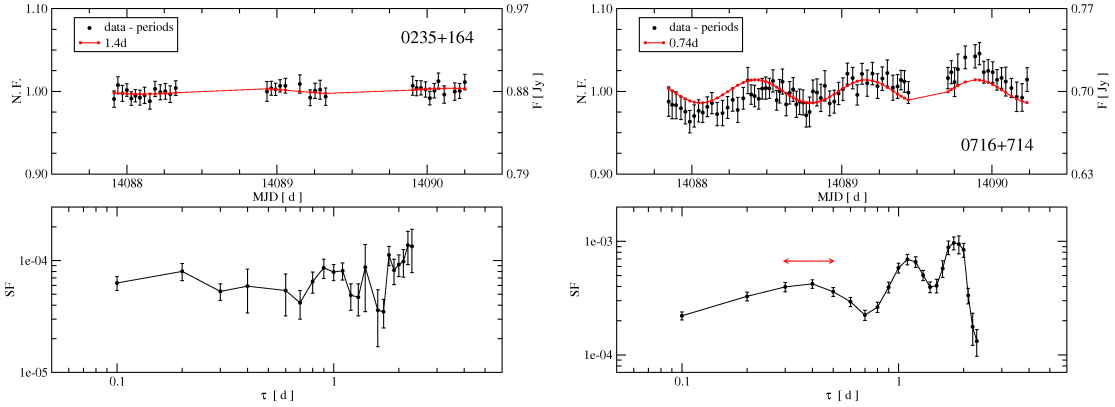

Figure B.15: Urumqi, December 2006

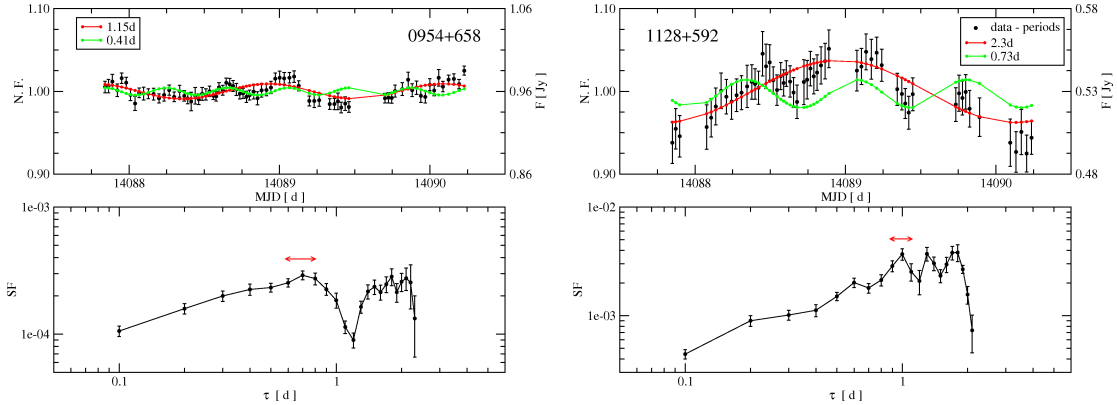

Figure B.16: Urumqi, December 2006

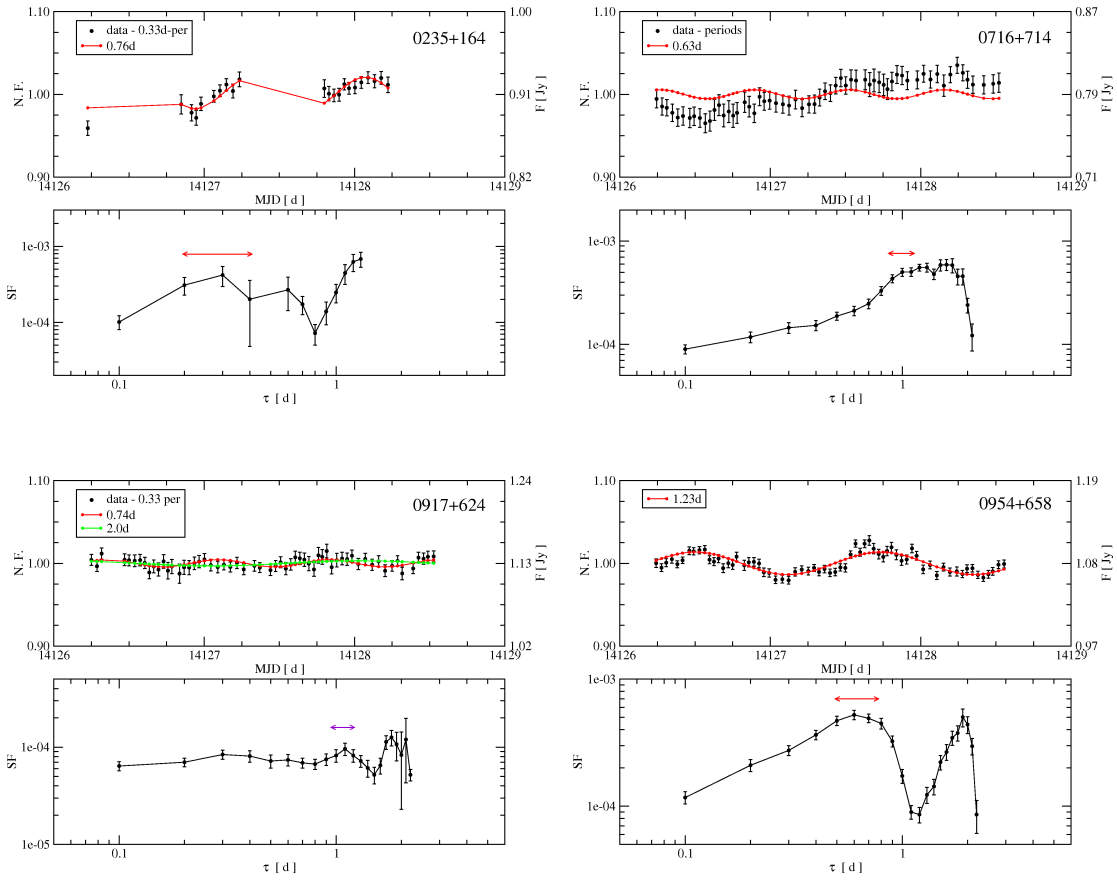

Figure B.17: Urumqi, January 2007

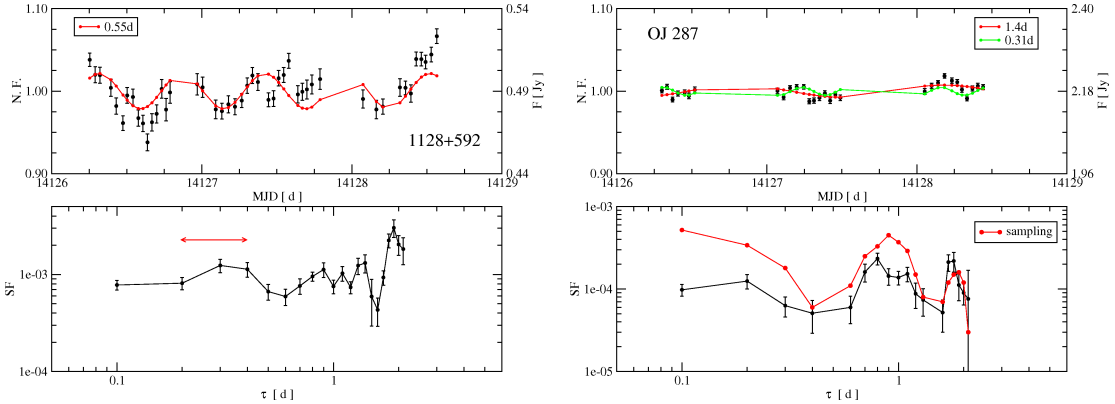

Figure B.18: Urumqi, August 2006

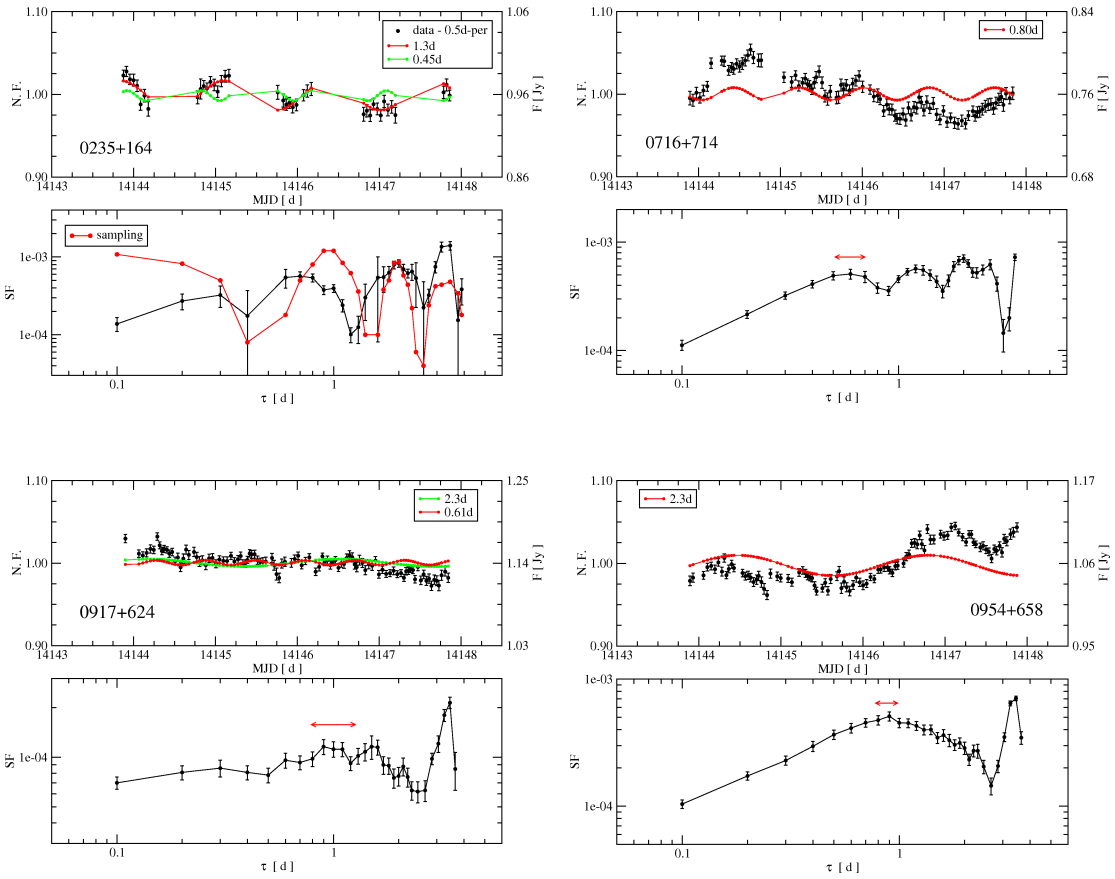

Figure B.19: Urumqi, February 2007

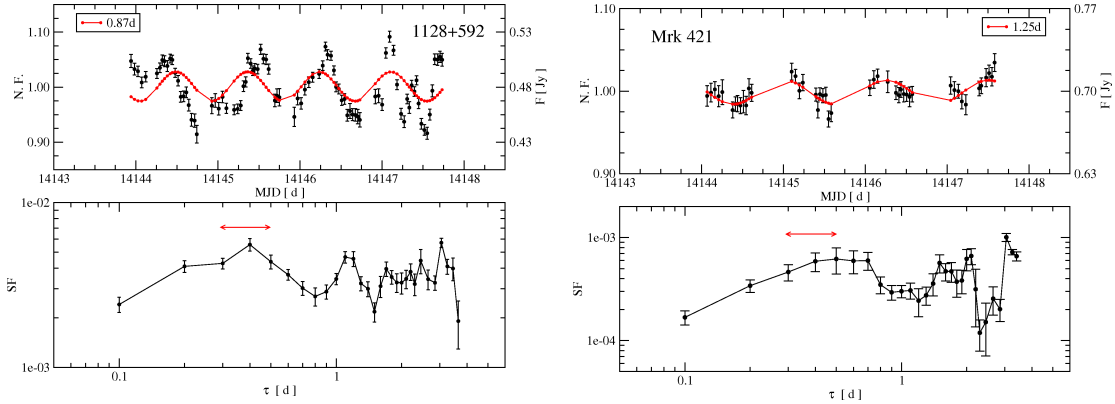

Figure B.20: Urumqi, February 2007

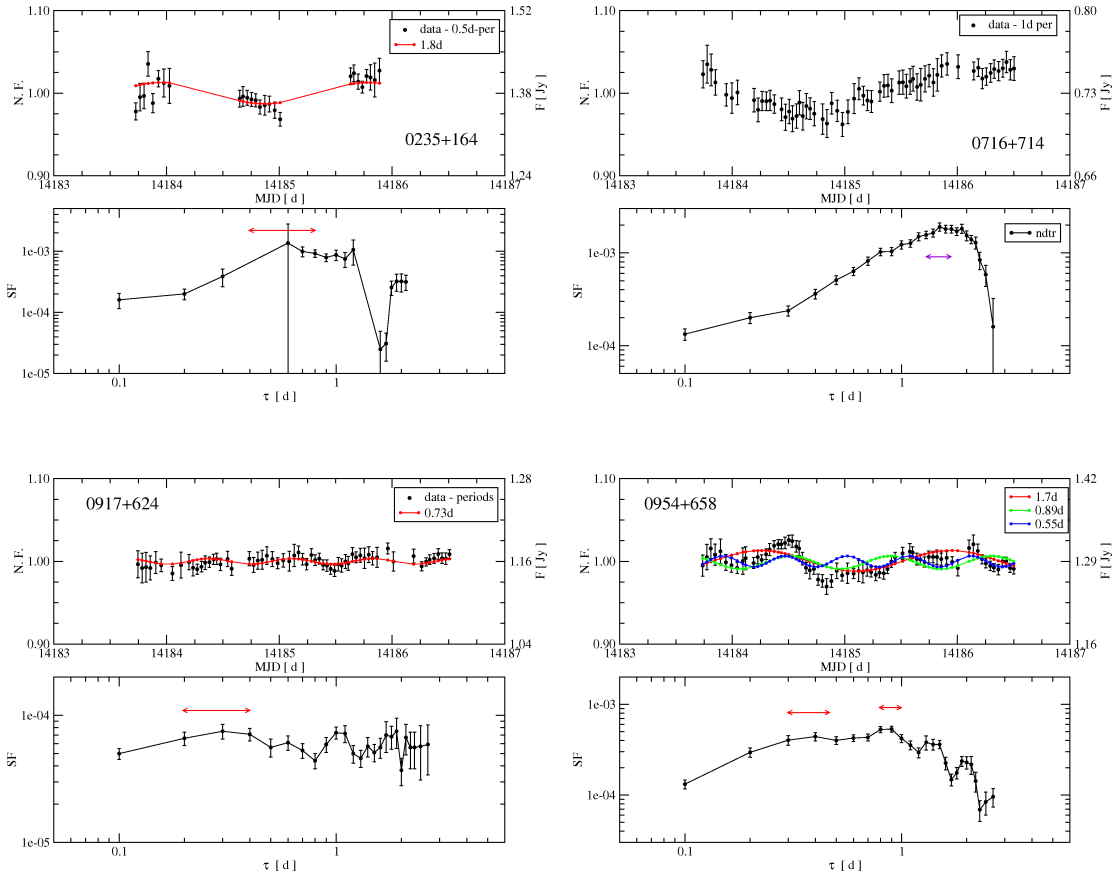

Figure B.21: Urumqi, March 2007

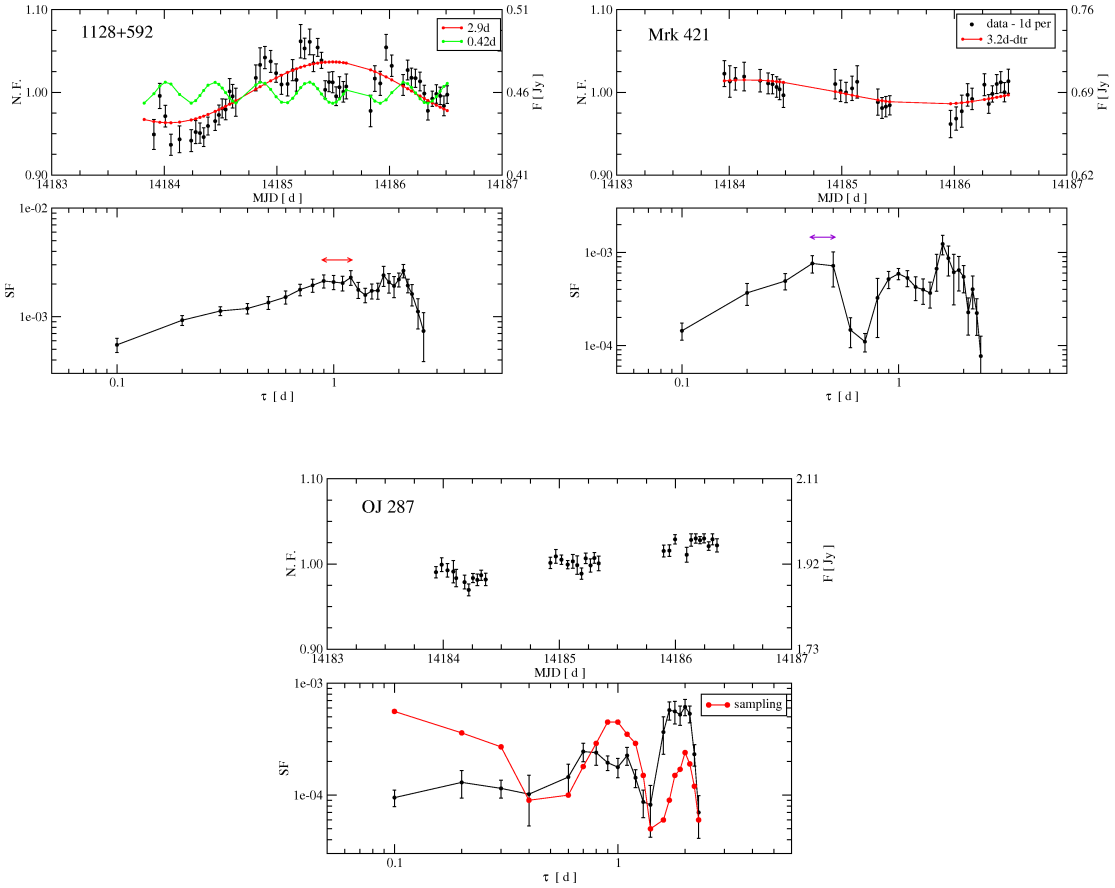

Figure B.22: Urumqi, March 2007

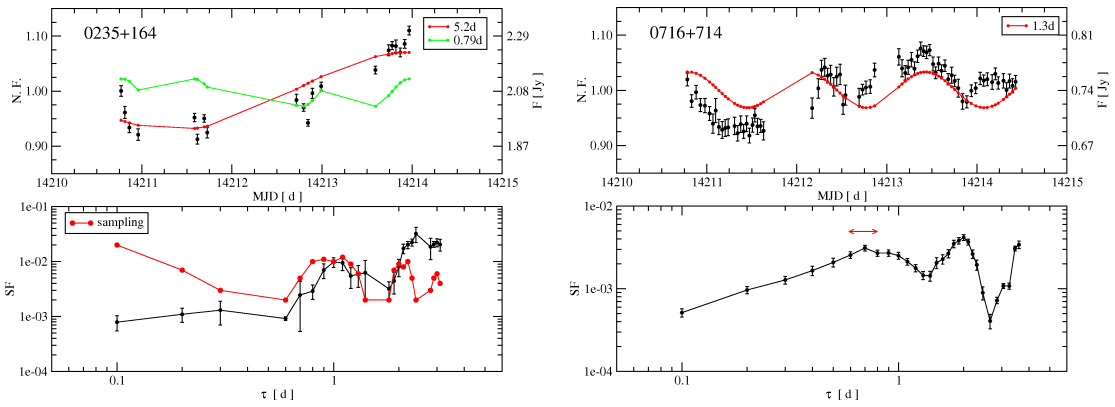

Figure B.23: Urumqi, April 2007

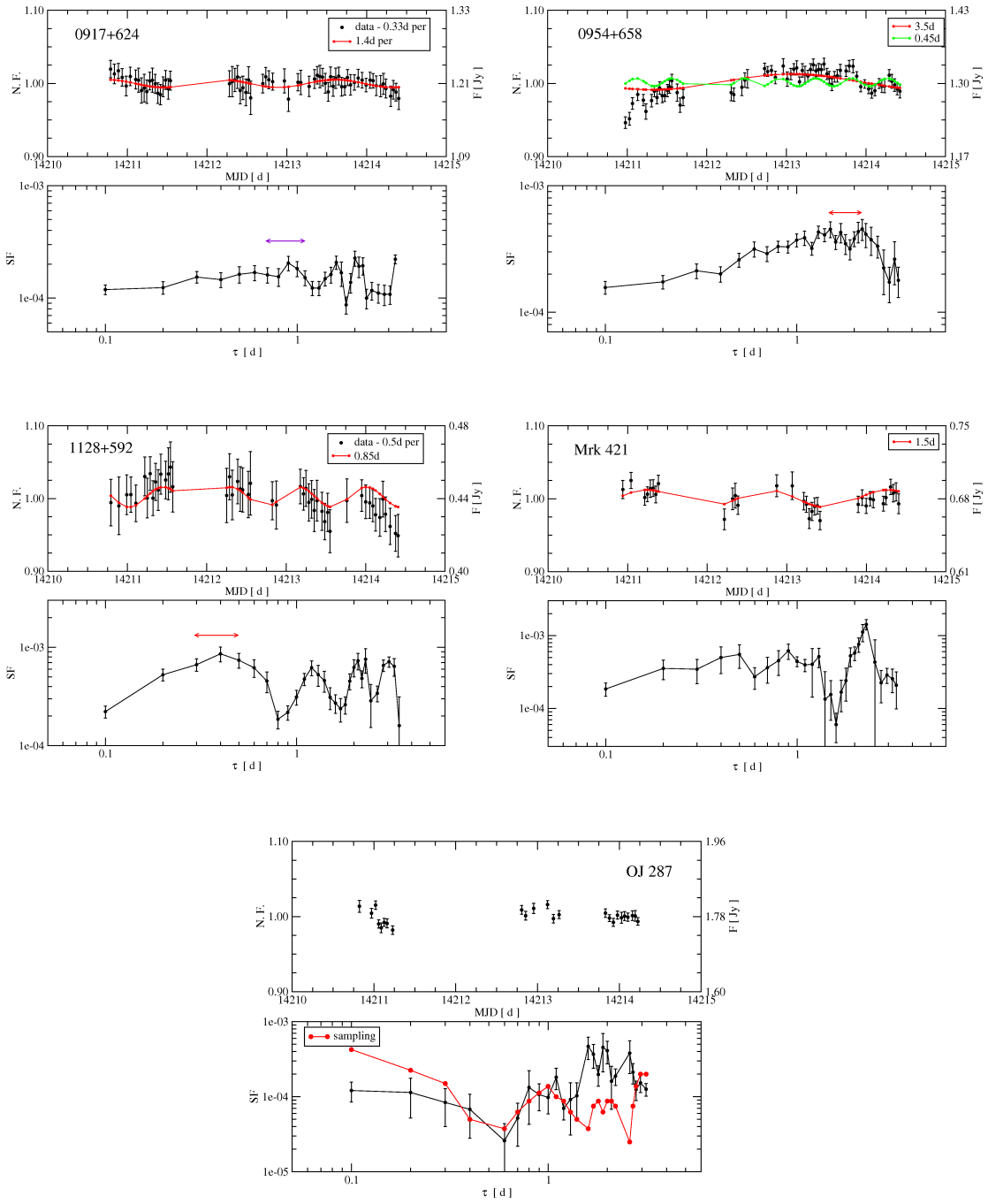

Figure B.24: Urumqi, April 2007

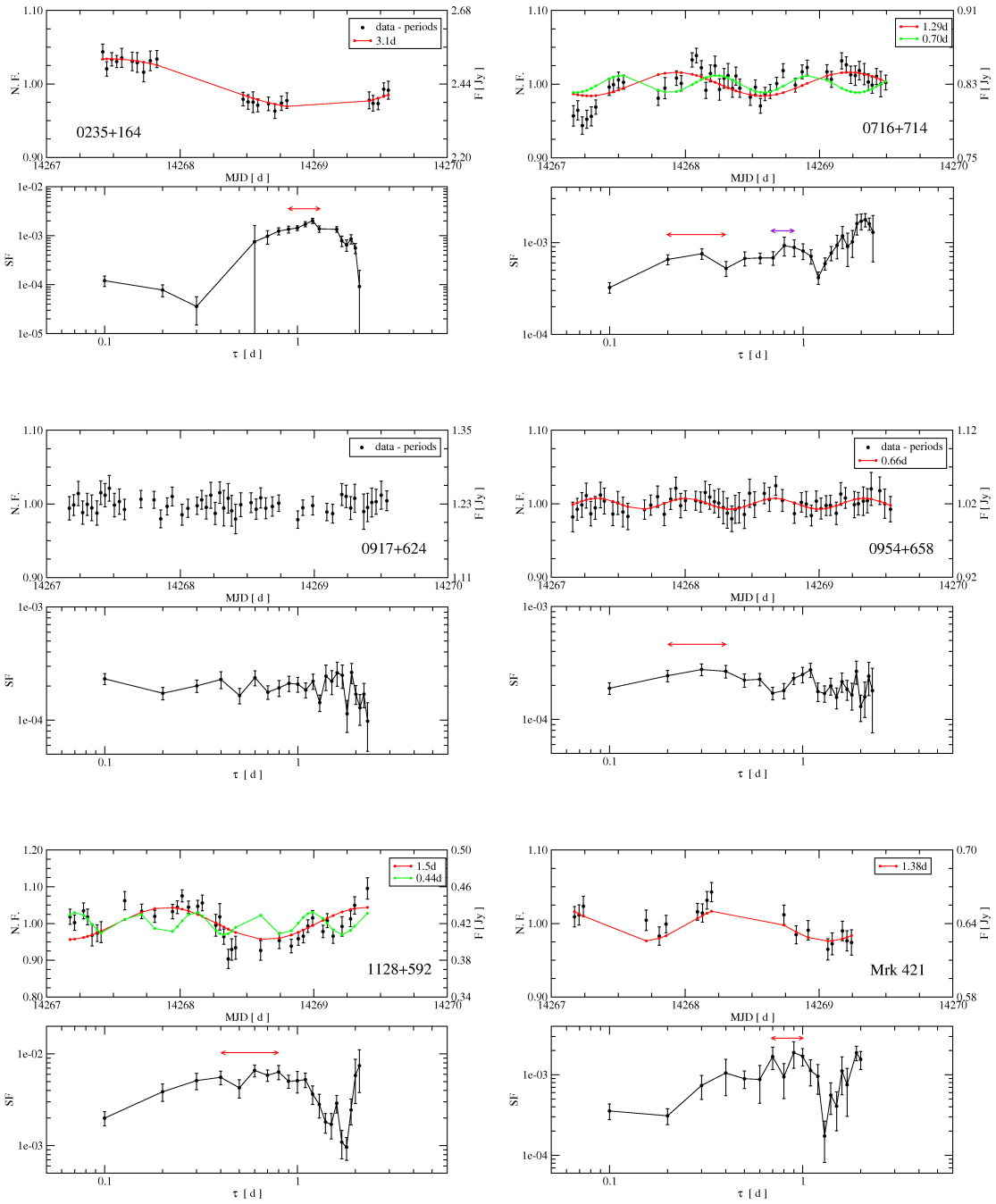

Figure B.25: Urumqi, June 2007

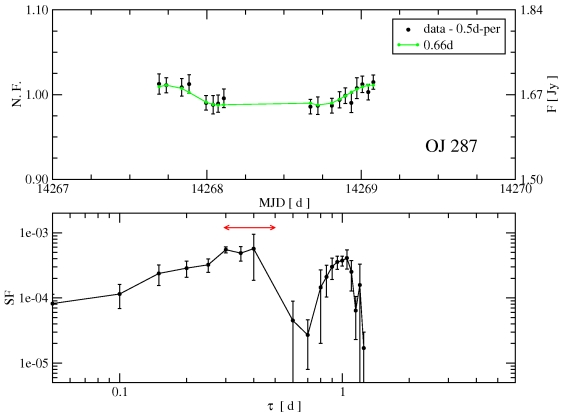

Figure B.26: Urumqi, June 2007

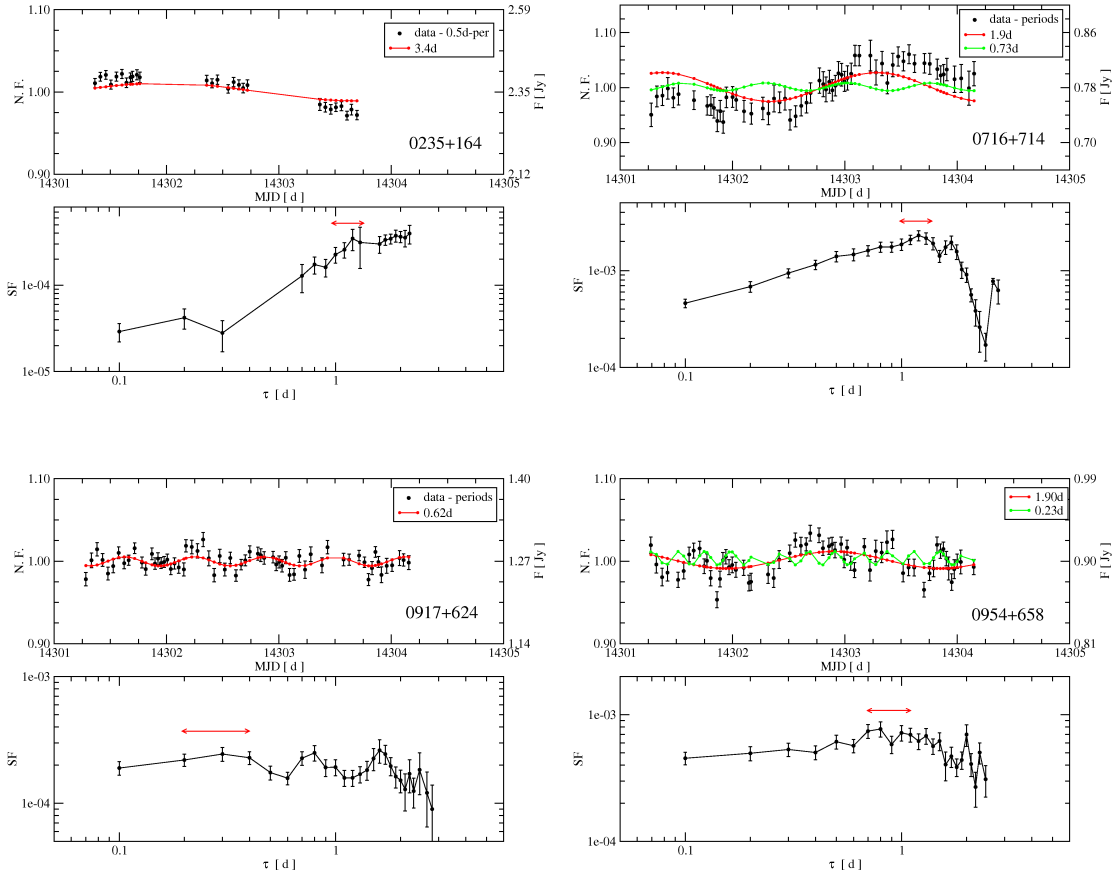

Figure B.27: Urumqi, July 2007

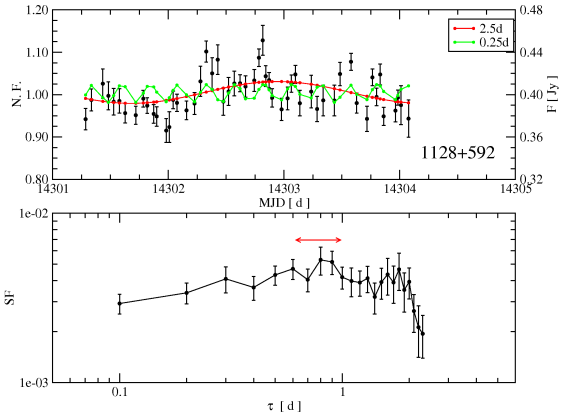

Figure B.28: Urumqi, July 2007

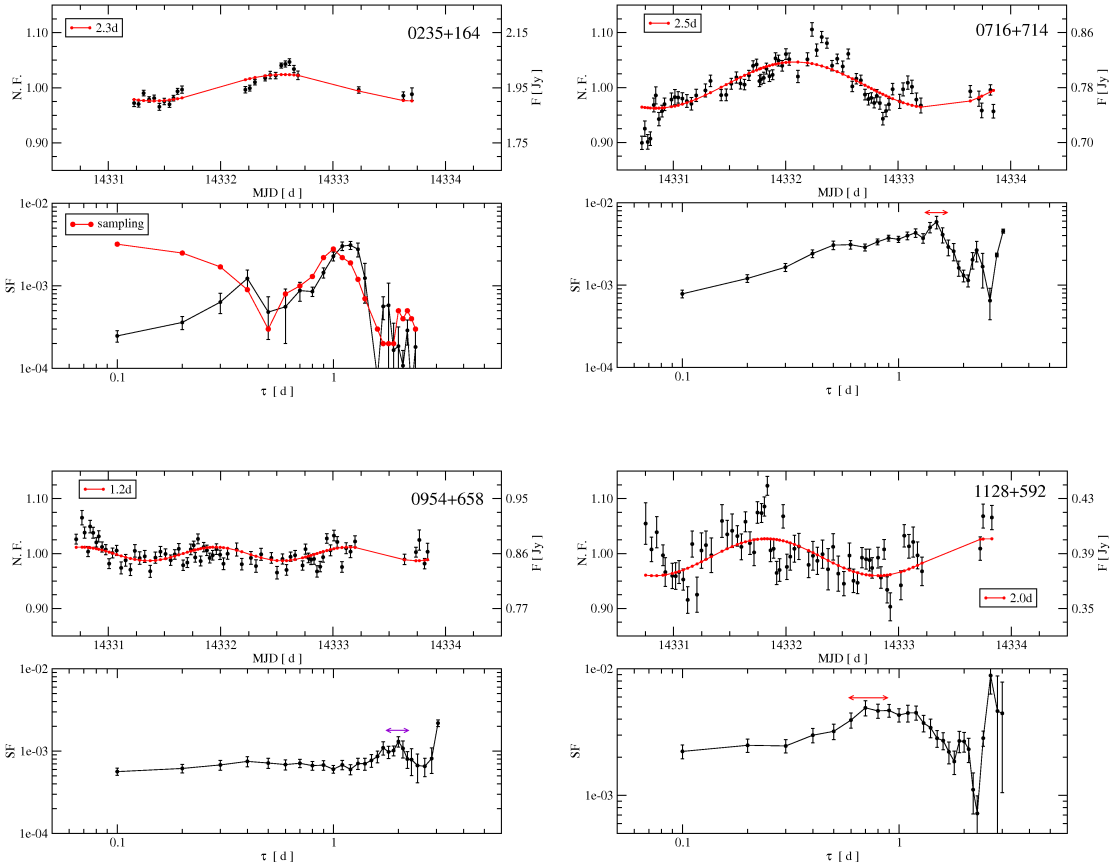

Figure B.29: Urumqi, August 2007

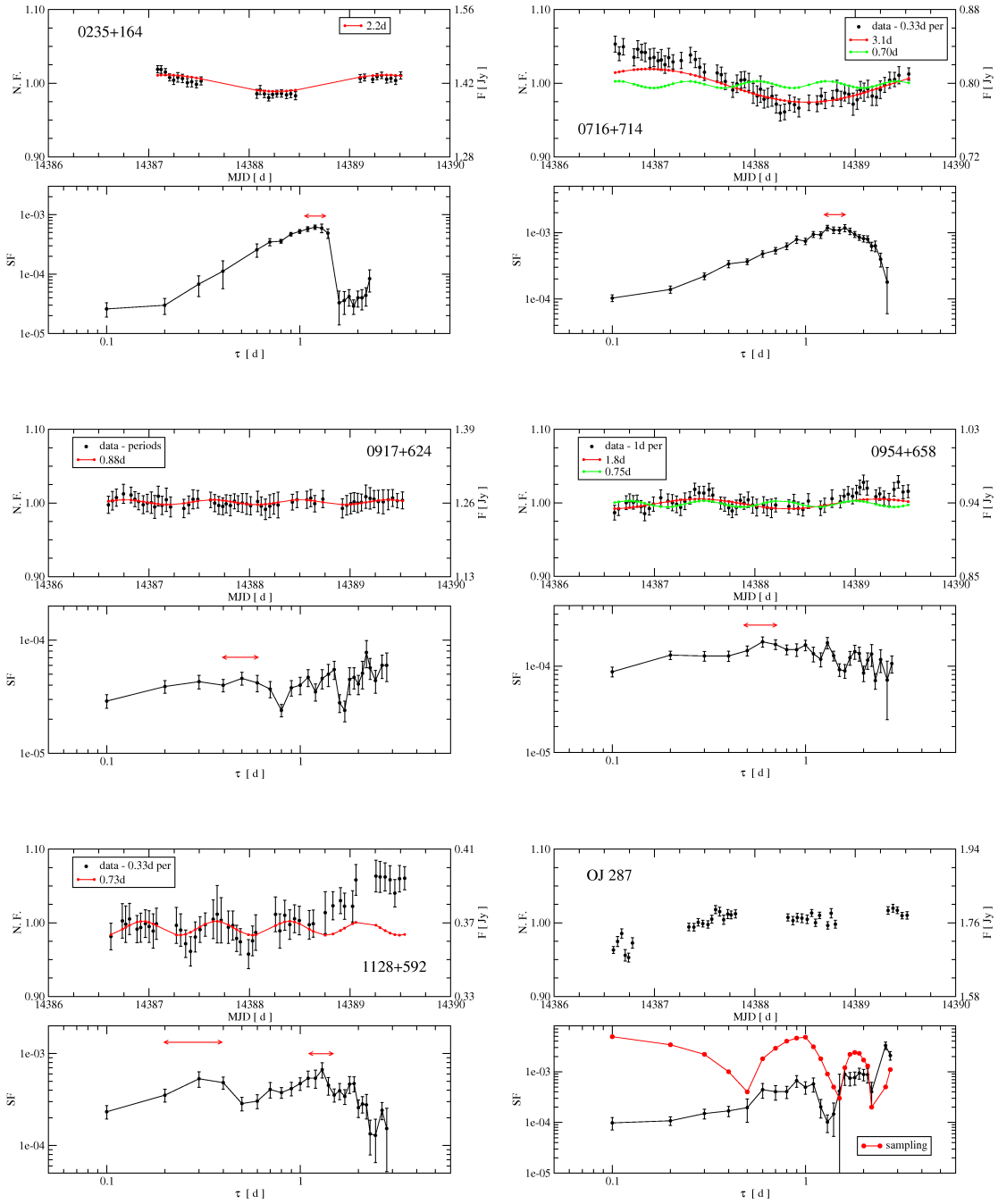

Figure B.30: Urumqi, October 2007

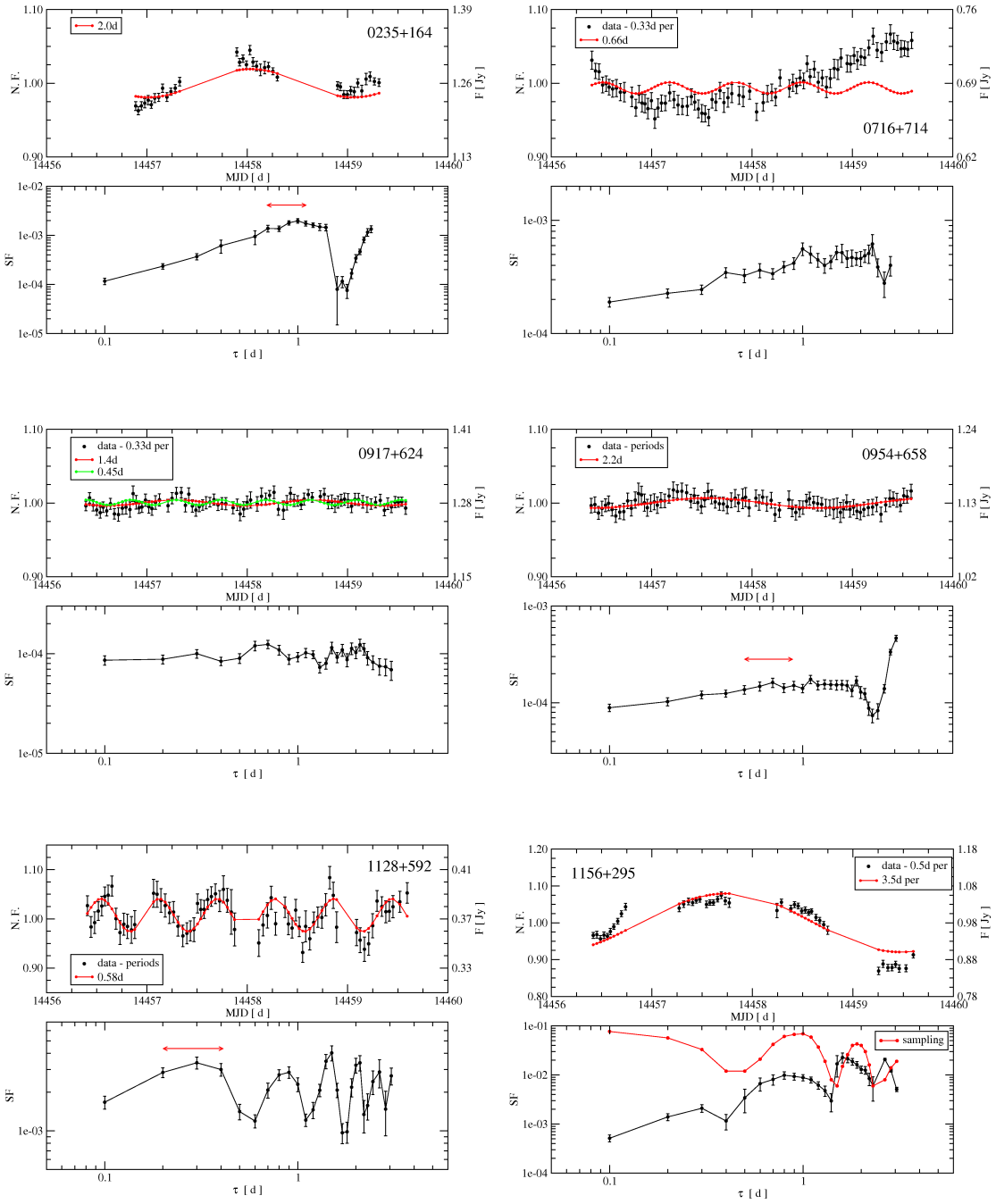

Figure B.31: Urumqi, December 2007

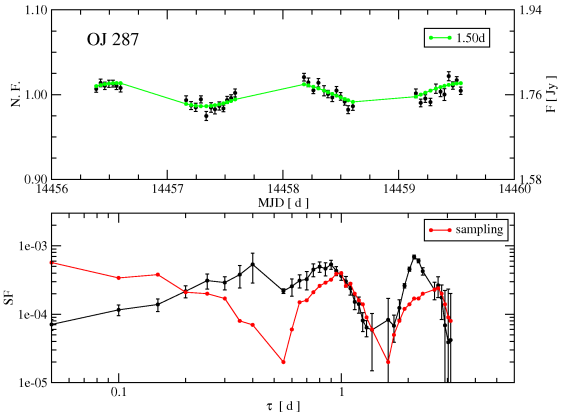

Figure B.32: Urumqi, December 2007

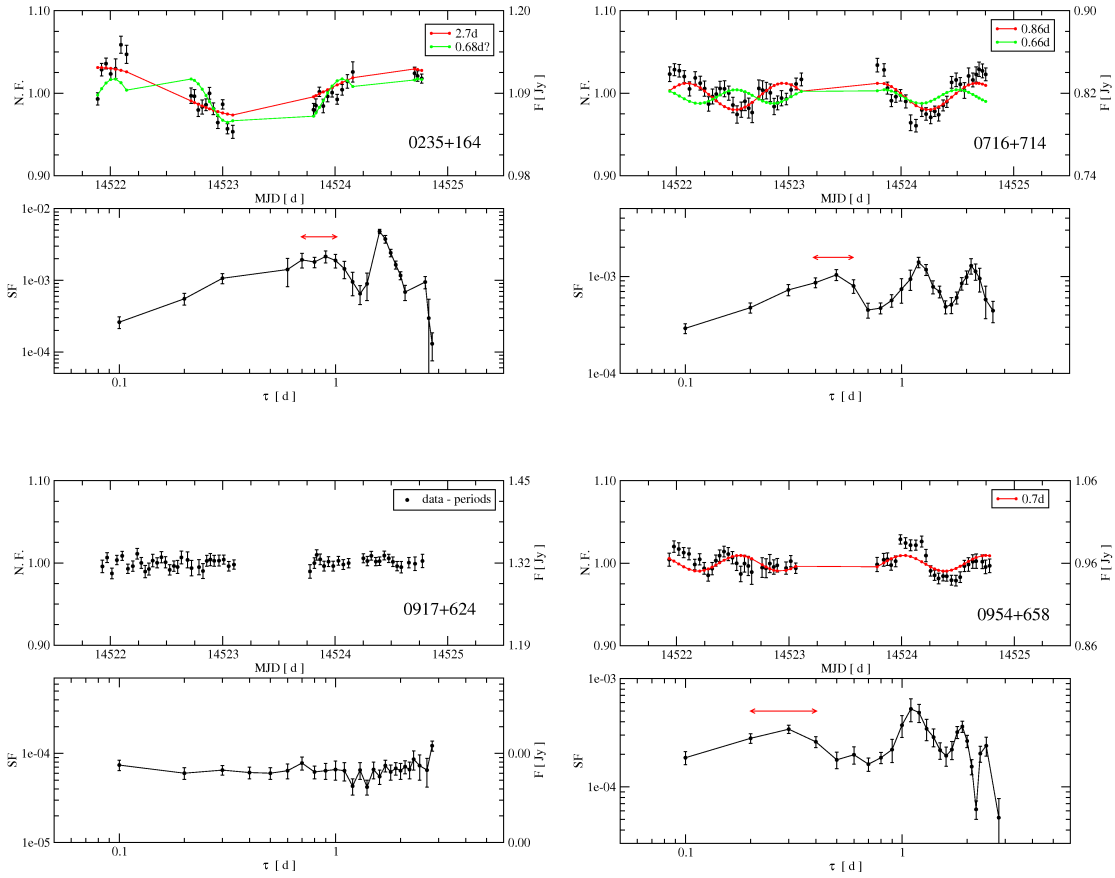

Figure B.33: Urumqi, February 2008

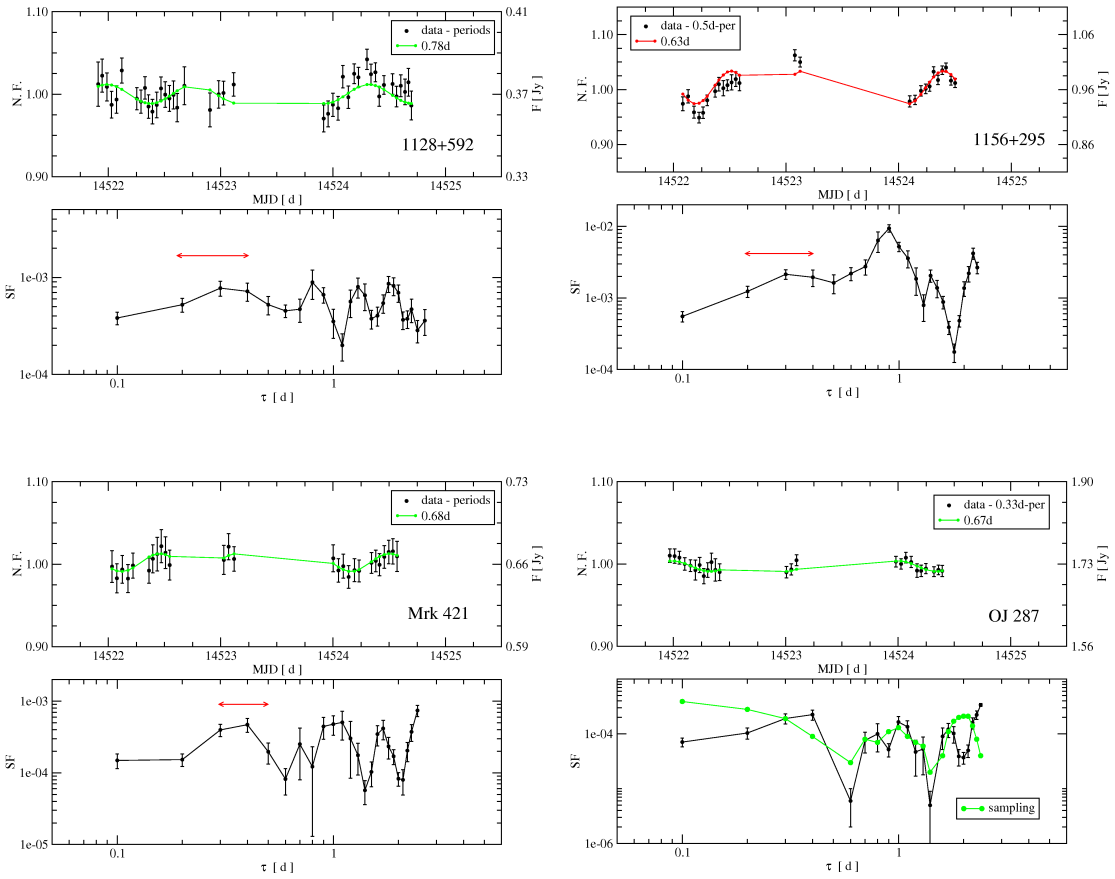

Figure B.34: Urumqi, February 2008

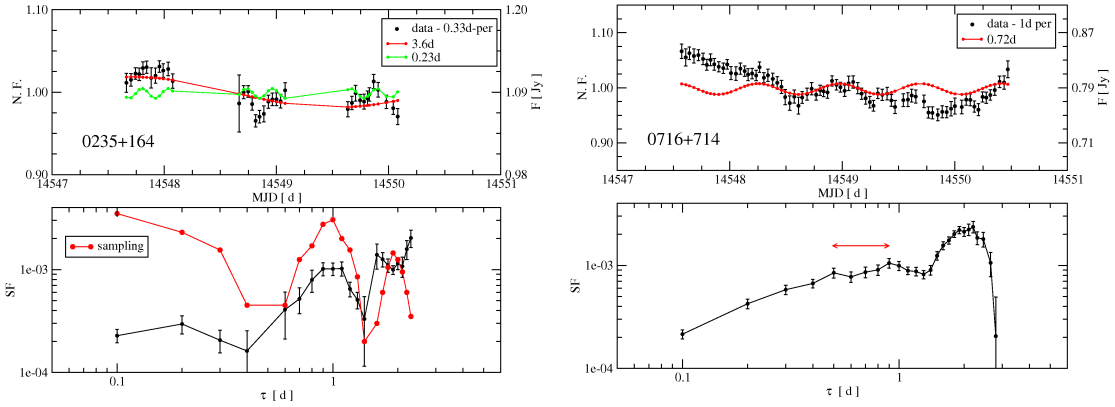

Figure B.35: Urumqi, March 2008

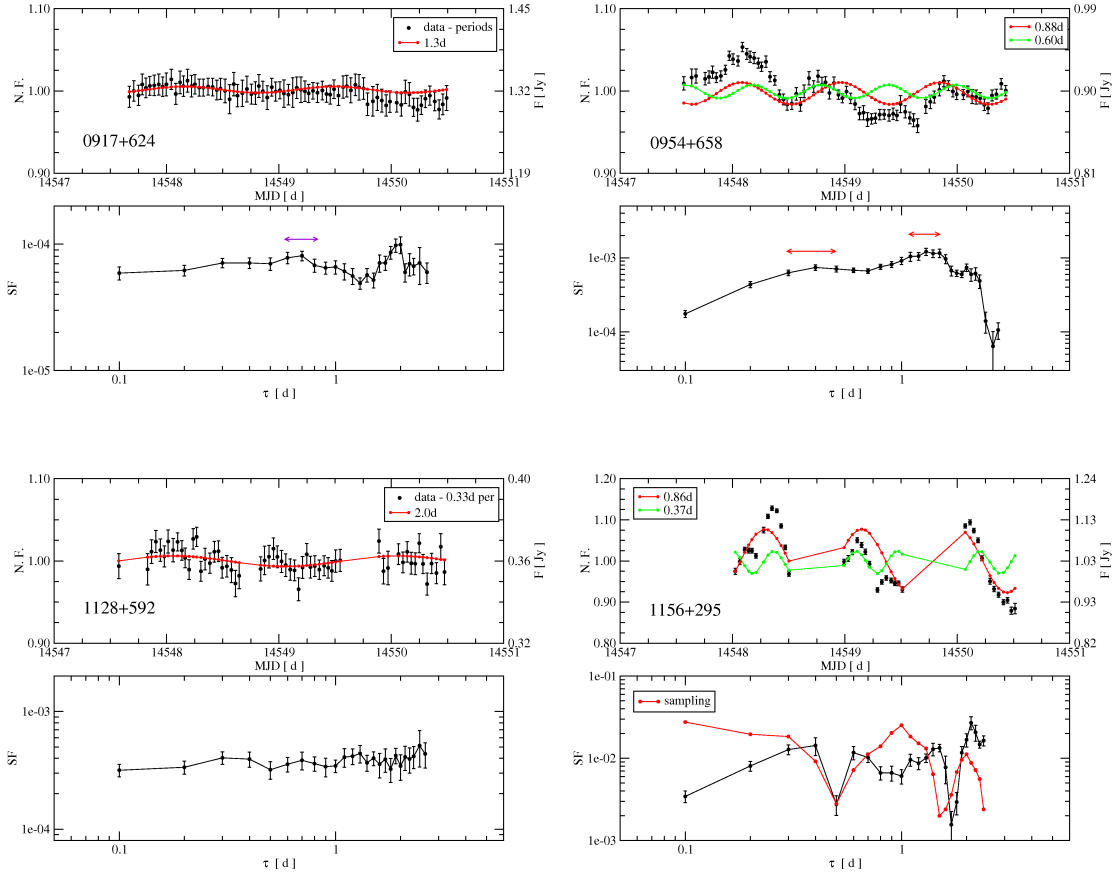

Figure B.36: Urumqi, March 2008

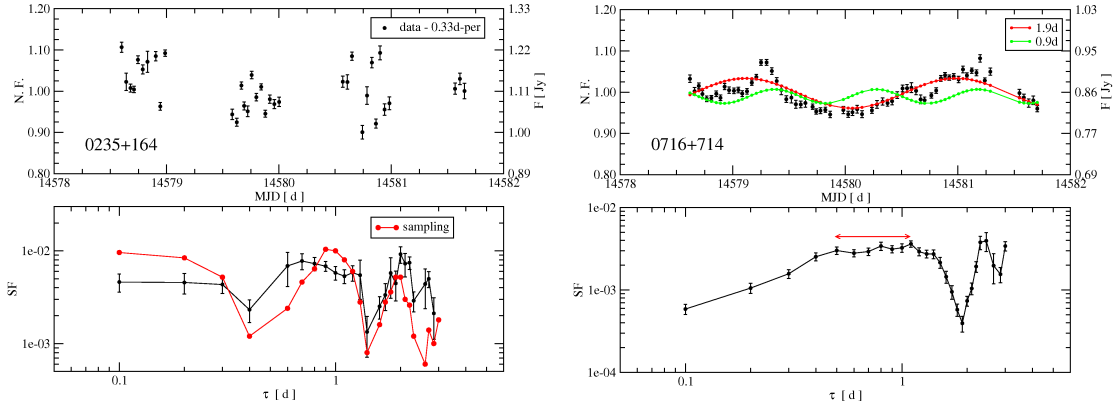

Figure B.37: Urumqi, April 2008

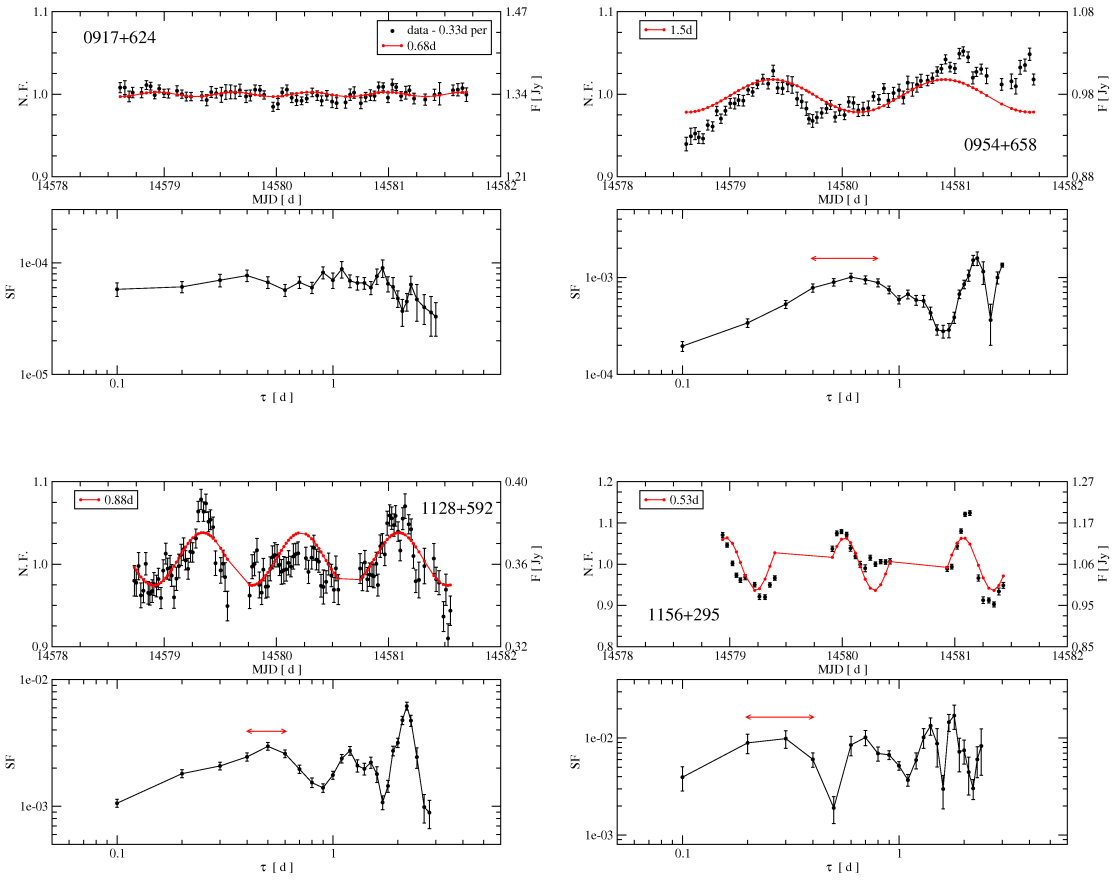

Figure B.38: Urumqi, April 2008

Appendix C

In this appendix we show the MINDEX tables for all the observing sessions performed between December 2004 and April 2008. In the first raw, the residual variability of the calibrators, m_0. Below, in the first column, the name of the source; in column 2, the number of data-points; in column 3 and 4, respectively, the average flux-density and its standard deviation; in column 5 and 6, the modulation index and the variability amplitude (see section 3.4); in column 7 and 8, the χ^2 and the reduced χ^2. Note that the datasets from December 2004 have been excluded from the time-series analysis, given the small number of data-points for each source.

2004-12

```
#  Vergleichsmodulationsindex   m0 =  0.70 %
#-------------------------------------------------------------------
# SRC         ANZ   <S>[Jy]  sigma    m[%]    Y[%]   Chi^2  red.Chi^2
#-------------------------------------------------------------------
0454+844       14    0.323   0.004    1.26    3.14    46.496   3.577
0602+672       14    1.102   0.019    1.74    4.78   119.185   9.168
0716+710       14    1.159   0.023    2.00    5.62   238.296  18.330
0723+679       11    0.986   0.005    0.54    0.00    16.784   1.678
0804+499        7    0.817   0.009    1.10    2.54    26.158   4.360
0809+483        7    4.380   0.019    0.43    0.00    12.436   2.073
0835+580        8    0.609   0.005    0.76    0.85     9.859   1.408
0836+710       13    2.618   0.014    0.53    0.00    24.413   2.034
0917+624       10    0.794   0.007    0.83    1.32    12.405   1.378
0954+658       12    0.898   0.011    1.21    2.98    61.403   5.582
1311+678       12    0.902   0.005    0.56    0.00    15.650   1.423
1634+628       11    1.550   0.008    0.52    0.00    13.106   1.311
1739+522        9    1.759   0.011    0.62    0.00    11.078   1.385
1749+701       14    0.941   0.028    2.94    8.58   551.745  42.442
1803+784       15    1.941   0.011    0.58    0.00    45.300   3.236
1807+698       12    1.856   0.012    0.66    0.00    24.002   2.182
1928+738       16    3.912   0.068    1.75    4.80   337.867  22.524
3C286           4    7.548   0.009    0.12    0.00     0.333   0.111
3C295           9    6.673   0.020    0.30    0.00     8.454   1.057
NGC7027         6    5.461   0.023    0.42    0.00     9.776   1.955
```

2005-08

```
#  Vergleichsmodulationsindex   m0 =  0.80 %
#-------------------------------------------------------------------
# SRC         ANZ   <S>[Jy]  sigma    m[%]    Y[%]   Chi^2  red.Chi^2
#-------------------------------------------------------------------
0346+800       20    0.370   0.009    2.53    7.21    39.546   2.081
0403+768       26    2.887   0.012    0.43    0.00    12.689   0.508
0602+672       26    0.997   0.011    1.12    2.35    38.013   1.521
0633+593       16    0.596   0.009    1.57    4.06    20.899   1.393
0639+732       24    0.987   0.009    0.88    1.11    22.404   0.974
0716+710       24    0.878   0.028    3.23    9.39   178.351   7.754
0723+679       23    0.990   0.007    0.70    0.00    11.034   0.502
0804+499       11    1.052   0.017    1.61    4.21    29.970   2.997
0809+483       15    4.349   0.021    0.48    0.00    11.691   0.835
0835+580       13    0.601   0.007    1.20    2.66     9.767   0.814
0836+710       51    2.242   0.010    0.44    0.00    22.067   0.441
0917+624       41    0.893   0.011    1.19    2.64    48.182   1.205
0951+699       53    3.484   0.010    0.29    0.00    13.406   0.258
0954+556       14    1.916   0.018    0.92    1.35    30.512   2.347
0954+658       46    0.918   0.017    1.87    5.08   156.044   3.468
1017+611       21    0.654   0.008    1.27    2.97    18.509   0.925
1127+565       11    0.431   0.005    1.06    2.09     6.618   0.662
1128+592       18    0.678   0.042    6.22   18.50   583.267  34.310
1148+592       18    0.455   0.004    0.92    1.34     6.996   0.412
1311+678       25    0.886   0.008    0.93    1.42    18.018   0.751
3C286           3    7.449   0.063    0.84    0.81     8.840   4.420
3C295           7    6.613   0.029    0.44    0.00     4.677   0.779
3C48            4    5.526   0.027    0.48    0.00     4.387   1.462
NGC7027         3    5.344   0.013    0.24    0.00     0.591   0.296
```

2005-12

```
#  Vergleichsmodulationsindex   m0 =  1.20 %
0346+800       54    0.421   0.017    4.07   11.66   115.806   2.185
0403+768       57    2.911   0.037    1.28    1.37    46.903   0.838
0716+710       55    0.823   0.043    5.28   15.43  1253.306  23.209
0836+710       57    2.195   0.026    1.20    0.27    45.633   0.815
0917+624       53    0.981   0.020    2.09    5.12   114.590   2.204
0951+699       56    3.501   0.027    0.76    0.00    31.681   0.576
0954+658       54    1.143   0.023    2.03    4.90   231.502   4.368
1017+611       47    0.659   0.014    2.06    5.02    51.636   1.123
1127+565       31    0.436   0.016    3.59   10.16    38.273   1.276
1128+592       40    0.713   0.056    7.88   23.35  1009.000  25.872
1131+437       22    0.528   0.013    2.39    6.19    27.404   1.305
1148+592       40    0.450   0.012    2.73    7.37    31.499   0.808
1203+645       53    1.158   0.017    1.47    2.55    42.702   0.821
1311+678       51    0.894   0.011    1.21    0.35    21.922   0.438
```

# SRC	ANZ	<S>[Jy]	sigma	m[%]	Y[%]	Chi^2	red.Chi^2
3C286	16	7.464	0.098	1.31	1.55	33.835	2.256
3C295	28	6.613	0.092	1.39	2.10	82.586	3.059
3C48	31	5.622	0.081	1.45	2.44	120.637	4.021
NGC7027	26	5.421	0.056	1.04	0.00	27.238	1.090

2006-03

# Vergleichsmodulationsindex m0 = 0.50 %							
0346+800	46	0.423	0.009	2.20	6.41	58.047	1.290
0403+768	48	2.930	0.013	0.43	0.00	38.130	0.811
0716+710	50	0.638	0.012	1.94	5.64	133.477	2.724
0836+710	49	2.192	0.011	0.48	0.00	43.274	0.902
0917+624	50	1.046	0.012	1.13	3.06	97.765	1.995
0951+699	49	3.514	0.008	0.22	0.00	13.994	0.292
0954+658	50	0.919	0.015	1.60	4.54	153.171	3.126
1017+611	46	0.665	0.008	1.24	3.39	48.912	1.087
1128+592	40	0.668	0.038	5.66	16.91	1124.575	28.835
1131+437	26	0.526	0.010	1.86	5.36	56.687	2.267
1148+592	40	0.453	0.006	1.26	3.47	26.947	0.691
1203+645	47	1.164	0.011	0.96	2.47	90.574	1.969
1311+678	46	0.899	0.004	0.48	0.00	14.349	0.319
3C286	25	7.496	0.025	0.33	0.00	32.560	1.357
3C295	30	6.650	0.023	0.34	0.00	18.365	0.633
3C48	23	5.577	0.027	0.49	0.00	44.222	2.010
NGC7027	18	5.431	0.043	0.80	1.88	77.601	4.565

2006-04

# Vergleichsmodulationsindex m0 = 0.50 %							
0716+710	68	0.643	0.009	1.46	4.12	79.886	1.192
0836+710	67	2.180	0.008	0.38	0.00	17.915	0.271
0917+624	71	1.071	0.012	1.12	2.99	104.787	1.497
0951+699	139	3.506	0.012	0.33	0.00	38.562	0.279
0954+658	145	1.144	0.014	1.25	3.44	237.445	1.649
1128+592	104	0.639	0.047	7.30	21.86	2858.890	27.756
1311+678	124	0.898	0.007	0.75	1.69	57.182	0.465
3C286	23	7.462	0.036	0.48	0.00	20.347	0.925
3C48	40	5.559	0.034	0.61	1.07	57.314	1.470

2006-06

```
#  Vergleichsmodulationsindex   m0 =  0.50 %
#-------------------------------------------------------------------
# SRC         ANZ   <S>[Jy]  sigma    m[%]    Y[%]   Chi^2  red.Chi^2
#-------------------------------------------------------------------
0716+710       90    0.736   0.036    4.93   14.71  1879.623  21.119
0836+710       94    2.153   0.008    0.35    0.00    40.714   0.438
0917+624       81    1.090   0.012    1.08    2.88   141.893   1.774
0951+699       97    3.522   0.014    0.39    0.00    72.293   0.753
0954+658       91    1.110   0.022    1.99    5.78   575.414   6.393
1128+592       72    0.595   0.024    4.08   12.16   562.665   7.925
1203+645       84    1.169   0.010    0.87    2.12   112.262   1.353
1311+678       87    0.903   0.004    0.41    0.00    15.797   0.184
3C286          47    7.501   0.099    1.32    3.66   445.514   9.685
3C48           49    5.597   0.048    0.86    2.09   327.021   6.813
NGC7027        40    5.417   0.044    0.81    1.91   157.668   4.043
```

2006-07

```
#  Vergleichsmodulationsindex   m0 =  0.70 %
0716+710       84    0.749   0.021    2.85    8.28   497.476   5.994
0836+710       93    2.158   0.012    0.58    0.00    87.821   0.955
0917+624       91    1.082   0.017    1.58    4.25   199.178   2.213
0951+699       99    3.510   0.019    0.54    0.00   115.285   1.176
0954+658       80    1.016   0.009    0.90    1.71    78.174   0.990
1128+592       75    0.601   0.035    5.77   17.19  1089.207  14.719
1203+645       92    1.162   0.014    1.18    2.84   163.497   1.797
1311+678       83    0.902   0.007    0.79    1.09    60.723   0.741
3C286          46    7.508   0.055    0.74    0.71   164.784   3.662
3C48           53    5.582   0.041    0.73    0.63   202.670   3.897
NGC7027        39    5.423   0.045    0.83    1.33   161.438   4.248
```

2006-08

```
#  Vergleichsmodulationsindex   m0 =  0.70 %
0716+710      158    0.834   0.039    4.66   13.83  2753.675  17.539
0836+710      173    2.190   0.011    0.52    0.00    75.367   0.438
0917+624      164    1.084   0.015    1.40    3.64   295.562   1.813
0951+699      193    3.511   0.024    0.69    0.00   208.891   1.088
0954+658      169    1.090   0.012    1.12    2.63   249.582   1.486
1128+455       87    0.654   0.007    1.13    2.66    57.162   0.665
1128+592      140    0.583   0.027    4.57   13.56  1254.872   9.028
1203+645      179    1.161   0.009    0.77    0.95    87.767   0.493
1311+678      157    0.898   0.007    0.81    1.20    63.601   0.408
3C286          86    7.509   0.040    0.53    0.00    72.377   0.851
```

```
#-------------------------------------------------------------------
# SRC         ANZ   <S>[Jy]  sigma    m[%]    Y[%]   Chi^2  red.Chi^2
#-------------------------------------------------------------------
3C48           87    5.588   0.025    0.45    0.00    46.619   0.542
NGC7027        74    5.421   0.036    0.66    0.00    80.785   1.107
```

2006-09

```
#  Vergleichsmodulationsindex   m0 =  0.80 %
0716+710      139    0.816   0.015    1.83    4.94   573.078   4.153
0836+710      144    2.187   0.012    0.55    0.00   215.851   1.509
0917+624      130    1.092   0.010    0.92    1.35   170.311   1.320
0951+699      143    3.515   0.010    0.29    0.00   106.204   0.748
0954+658      134    1.213   0.015    1.26    2.92   476.747   3.585
1128+455       60    0.656   0.007    1.03    1.96    44.173   0.749
1128+592      104    0.613   0.014    2.28    6.40   309.903   3.009
1203+645      137    1.164   0.009    0.77    0.00   164.275   1.208
1311+678      130    0.898   0.007    0.78    0.00    98.974   0.767
3C286          63    7.521   0.043    0.57    0.00   293.279   4.730
3C48           69    5.589   0.035    0.63    0.00   384.940   5.661
NGC7027        67    5.419   0.032    0.59    0.00   296.227   4.488
```

2006-11

```
#  Vergleichsmodulationsindex   m0 =  0.60 %
0716+710      130    0.742   0.027    3.63   10.74   870.743   6.750
0827+243       51    0.693   0.007    1.04    2.55    50.071   1.001
0827+378       53    0.940   0.007    0.72    1.17    34.346   0.661
0835+580       96    0.609   0.007    1.10    2.78    75.618   0.796
0836+710      133    2.210   0.012    0.53    0.00   147.463   1.117
0851+202       50    2.095   0.031    1.50    4.12   234.840   4.793
0917+624      131    1.093   0.011    1.00    2.41   194.495   1.496
0951+699      135    3.504   0.007    0.21    0.00    31.520   0.235
0954+658      134    1.065   0.012    1.16    2.99   307.795   2.314
1128+592      102    0.551   0.026    4.73   14.07  1394.822  13.810
1203+645      133    1.162   0.007    0.64    0.64   101.811   0.771
3C286          59    7.506   0.030    0.40    0.00    96.987   1.672
3C48           67    5.594   0.027    0.48    0.00    88.194   1.336
NGC7027        74    5.428   0.026    0.48    0.00   123.119   1.687
```

2006-12

```
#  Vergleichsmodulationsindex   m0 =  0.60 %
#-------------------------------------------------------------------
# SRC         ANZ   <S>[Jy]  sigma    m[%]    Y[%]   Chi^2  red.Chi^2
#-------------------------------------------------------------------
0202+149       42    2.350   0.014    0.60    0.00    77.423   1.888
0235+164       35    0.877   0.006    0.67    0.88    38.188   1.123
0716+710       75    0.701   0.013    1.81    5.12   372.170   5.029
0836+710       77    2.215   0.007    0.34    0.00    47.116   0.620
0951+699       78    3.492   0.010    0.29    0.00    39.153   0.508
0954+658       75    0.959   0.009    0.95    2.20   144.052   1.947
1128+592       56    0.529   0.021    3.89   11.54   673.094  12.238
1203+645       76    1.157   0.008    0.70    1.07   108.470   1.446
3C286          33    7.492   0.042    0.56    0.00   117.214   3.663
3C48           44    5.559   0.033    0.59    0.00    83.035   1.931
CTA21          38    2.891   0.013    0.45    0.00    49.440   1.336
NGC7027         4    5.389   0.008    0.15    0.00     0.677   0.226
```

2007-01

```
#  Vergleichsmodulationsindex   m0 =  0.70 %
0235+164       22    0.910   0.015    1.61    4.36   160.669   7.651
0716+710       61    0.786   0.017    2.18    6.20   706.368  11.773
0827+378       29    0.940   0.006    0.59    0.00    34.211   1.222
0836+710       65    2.250   0.007    0.30    0.00    53.144   0.830
0917+624       59    1.130   0.010    0.84    1.41   116.115   2.002
0951+699       66    3.516   0.010    0.29    0.00    71.780   1.104
0954+658       66    1.083   0.012    1.12    2.62   345.376   5.313
1128+592       47    0.488   0.012    2.54    7.31   333.636   7.253
1203+645       63    1.163   0.008    0.66    0.00   132.256   2.133
3C286          36    7.503   0.042    0.56    0.00   221.874   6.339
3C48           25    5.593   0.037    0.66    0.00   198.860   8.286
CTA21          24    2.910   0.014    0.49    0.00    73.337   3.189
NGC7027        27    5.441   0.037    0.68    0.00   204.218   7.855
OJ287          30    2.181   0.017    0.76    0.87   187.037   6.450
```

2007-02

```
#  Vergleichsmodulationsindex   m0 =  0.60 %
0235+164       45    0.951   0.015    1.58    4.39   180.447   4.101
0340+362       45    0.335   0.009    2.75    8.07   122.230   2.778
0459+135       36    0.519   0.006    1.08    2.71    29.749   0.850
0716+710      109    0.753   0.017    2.29    6.63   633.310   5.864
0836+710      102    2.251   0.009    0.42    0.00    35.904   0.355
0917+624      109    1.141   0.016    1.38    3.74   305.353   2.827
0951+699      109    3.503   0.015    0.42    0.00    35.610   0.330
```

# SRC	ANZ	<S>[Jy]	sigma	m[%]	Y[%]	Chi^2	red.Chi^2
0954+658	109	1.061	0.024	2.27	6.56	829.694	7.682
1128+592	92	0.480	0.021	4.31	12.79	1131.674	12.436
1203+645	104	1.161	0.007	0.63	0.60	63.215	0.614
3C286	50	7.522	0.024	0.32	0.00	10.684	0.218
3C48	52	5.586	0.027	0.48	0.00	33.073	0.648
CTA21	41	2.905	0.013	0.43	0.00	16.227	0.406
MRK421	49	0.700	0.010	1.49	4.11	102.076	2.127
NGC7027	51	5.421	0.029	0.54	0.00	37.759	0.755

2007-03

# Vergleichsmodulationsindex m0 = 0.70 %							
0202+149	28	2.400	0.018	0.75	0.77	37.513	1.389
0235+164	26	1.380	0.027	1.95	5.47	212.774	8.511
0716+710	63	0.733	0.016	2.16	6.13	289.271	4.666
0836+710	70	2.260	0.009	0.41	0.00	24.562	0.356
0839+187	30	0.833	0.004	0.44	0.00	8.004	0.276
0917+624	61	1.162	0.010	0.87	1.56	58.479	0.975
0951+699	70	3.508	0.018	0.51	0.00	43.251	0.627
0954+658	70	1.290	0.016	1.27	3.17	210.573	3.052
1128+592	57	0.461	0.016	3.43	10.06	361.892	6.462
1203+645	67	1.159	0.012	1.02	2.23	76.664	1.162
3C286	34	7.521	0.031	0.41	0.00	16.130	0.489
3C48	32	5.582	0.047	0.84	1.40	50.620	1.633
CTA21	29	2.908	0.010	0.35	0.00	8.973	0.320
MRK421	31	0.695	0.011	1.59	4.27	76.624	2.554
NGC7027	36	5.432	0.020	0.37	0.00	10.225	0.292
OJ287	35	1.918	0.043	2.26	6.45	370.562	10.899

2007-04

# Vergleichsmodulationsindex m0 = 0.90 %							
0202+149	6	2.470	0.545	22.05	66.11	723.793	144.759
0235+164	20	2.077	0.131	6.32	18.77	1112.879	58.573
0716+710	74	0.740	0.032	4.35	12.76	950.182	13.016
0836+710	78	2.265	0.012	0.52	0.00	67.291	0.874
0839+187	29	0.836	0.009	1.11	1.93	28.339	1.012
0917+624	66	1.211	0.011	0.89	0.00	73.967	1.138
0951+699	71	3.513	0.015	0.43	0.00	58.848	0.841
0954+658	65	1.301	0.025	1.95	5.19	437.550	6.837
1128+592	49	0.437	0.010	2.21	6.04	64.665	1.347
1203+645	58	1.155	0.013	1.09	1.85	78.462	1.377
3C286	42	7.511	0.102	1.35	3.03	430.243	10.494
3C48	30	5.602	0.028	0.49	0.00	52.647	1.815

# SRC	ANZ	<S>[Jy]	sigma	m[%]	Y[%]	Chi^2	red.Chi^2
CTA21	24	2.925	0.020	0.69	0.00	44.874	1.951
MRK421	32	0.676	0.009	1.38	3.15	39.496	1.274
NGC7027	31	5.422	0.021	0.39	0.00	38.100	1.270
OJ287	24	1.784	0.016	0.87	0.00	52.984	2.304

2007-06

# Vergleichsmodulationsindex m0 = 0.80 %							
0202+149	27	2.347	0.018	0.77	0.00	59.224	2.278
0235+164	23	2.436	0.074	3.03	8.76	740.827	33.674
0716+710	49	0.834	0.018	2.12	5.88	176.926	3.686
0836+710	55	2.257	0.017	0.76	0.00	92.359	1.710
0839+187	18	0.840	0.011	1.28	3.00	22.404	1.318
0917+624	52	1.228	0.016	1.34	3.22	114.626	2.248
0951+699	62	3.520	0.015	0.43	0.00	66.818	1.095
0954+658	57	1.017	0.015	1.47	3.69	144.000	2.571
1128+592	36	0.416	0.019	4.52	13.36	150.730	4.307
1203+645	56	1.167	0.010	0.87	1.06	61.469	1.118
3C286	30	7.533	0.026	0.35	0.00	26.168	0.902
3C48	28	5.581	0.022	0.39	0.00	33.150	1.228
CTA21	24	2.912	0.026	0.88	1.12	89.138	3.876
MRK421	18	0.645	0.014	2.13	5.92	44.383	2.611
NGC7027	31	5.423	0.028	0.51	0.00	64.104	2.137
OJ287	18	1.666	0.019	1.12	2.37	51.376	3.022

2007-07

# Vergleichsmodulationsindex m0 = 0.70 %							
0202+149	29	2.383	0.018	0.77	0.93	92.411	3.300
0235+164	27	2.351	0.044	1.87	5.19	608.854	23.417
0716+710	60	0.776	0.032	4.07	12.01	764.395	12.956
0836+710	65	2.229	0.014	0.65	0.00	138.864	2.170
0917+624	64	1.268	0.016	1.23	3.03	157.438	2.499
0951+699	73	3.520	0.018	0.52	0.00	177.531	2.466
0954+658	62	0.899	0.016	1.73	4.74	204.875	3.359
1128+592	54	0.402	0.018	4.53	13.44	157.461	2.971
1203+645	65	1.170	0.016	1.35	3.47	209.474	3.273
1830-211	15	11.739	0.061	0.52	0.00	69.125	4.937
1908-201	12	2.755	0.038	1.39	3.59	112.957	10.269
1921-293	7	8.904	0.060	0.68	0.00	49.640	8.273
3C286	37	7.521	0.037	0.49	0.00	131.132	3.643
3C454.3	24	9.352	0.037	0.40	0.00	70.183	3.051
3C48	34	5.571	0.031	0.55	0.00	129.869	3.935
CTA102	22	4.318	0.023	0.53	0.00	71.790	3.419
CTA21	29	2.900	0.016	0.54	0.00	55.341	1.976

# SRC	ANZ	<S>[Jy]	sigma	m[%]	Y[%]	Chi^2	red.Chi^2
NGC7027	30	5.433	0.024	0.43	0.00	70.697	2.438

2007-08

# Vergleichsmodulationsindex m0 = 0.80 %							
0202+149	25	2.421	0.031	1.27	2.96	148.024	6.168
0235+164	25	1.954	0.048	2.44	6.91	438.319	18.263
0716+710	72	0.781	0.032	4.16	12.25	1015.345	14.301
0836+710	72	2.241	0.014	0.62	0.00	98.084	1.381
0951+699	75	3.521	0.016	0.45	0.00	78.744	1.064
0954+658	73	0.857	0.017	1.97	5.41	260.799	3.622
1035+562	58	1.223	0.016	1.35	3.26	175.776	3.084
1128+592	65	0.394	0.017	4.32	12.75	254.534	3.977
1203+645	72	1.166	0.015	1.28	2.99	192.994	2.718
3C286	46	7.527	0.036	0.47	0.00	48.034	1.067
3C454.3	24	9.289	0.032	0.34	0.00	20.717	0.901
3C48	27	5.586	0.016	0.29	0.00	12.012	0.462
CTA102	24	4.306	0.026	0.61	0.00	55.707	2.422
CTA21	24	2.905	0.014	0.49	0.00	17.717	0.770
NGC7027	34	5.431	0.023	0.42	0.00	34.705	1.052

2007-10

# Vergleichsmodulationsindex m0 = 0.50 %							
0235+164	30	1.425	0.016	1.14	3.08	155.762	5.371
0716+710	61	0.802	0.021	2.58	7.59	626.420	10.440
0836+710	63	2.178	0.006	0.28	0.00	15.852	0.256
0917+624	57	1.256	0.008	0.60	0.99	53.778	0.960
0951+699	64	3.500	0.007	0.19	0.00	9.380	0.149
0954+658	60	0.940	0.010	1.10	2.93	165.896	2.812
1101+624	53	0.329	0.004	1.29	3.57	29.835	0.574
1128+592	48	0.367	0.011	2.91	8.60	208.156	4.429
1156+295	35	1.019	0.026	2.52	7.40	597.289	17.567
1203+645	51	1.157	0.006	0.50	0.00	34.673	0.693
3C286	35	7.508	0.016	0.21	0.00	11.227	0.330
3C454.3	36	9.103	0.036	0.39	0.00	42.337	1.210
3C48	33	5.584	0.010	0.18	0.00	6.576	0.206
CTA21	31	2.888	0.007	0.26	0.00	9.338	0.311
NGC7027	34	5.435	0.011	0.20	0.00	7.237	0.219
OJ287	34	1.764	0.030	1.72	4.93	315.108	9.549

2007-12

```
#  Vergleichsmodulationsindex   m0 =  0.50 %
#-------------------------------------------------------------------
# SRC         ANZ   <S>[Jy]  sigma    m[%]    Y[%]   Chi^2  red.Chi^2
#-------------------------------------------------------------------
0235+164       37    1.262   0.027    2.15    6.27   520.719  14.464
0716+710       80    0.689   0.021    3.04    9.00  1122.120  14.204
0836+710       80    2.148   0.007    0.33    0.00    33.286   0.421
0917+624       83    1.282   0.010    0.77    1.74   158.540   1.933
0951+699       84    3.511   0.011    0.31    0.00    36.874   0.444
0954+658       85    1.129   0.012    1.03    2.71   259.316   3.087
1128+592       68    0.374   0.014    3.71   11.01   532.357   7.946
1156+295       44    0.979   0.063    6.48   19.38  5467.661 127.155
1203+645       80    1.164   0.007    0.57    0.79    75.807   0.960
3C286          41    7.509   0.014    0.19    0.00     9.748   0.244
3C48           36    5.592   0.014    0.26    0.00    15.078   0.431
CTA21          34    2.902   0.005    0.18    0.00     4.158   0.126
NGC7027        42    5.433   0.015    0.27    0.00    19.257   0.470
NRAO530        21    4.134   0.045    1.10    2.93   109.793   5.490
OJ287          42    1.755   0.020    1.16    3.13   255.353   6.228
```

2008-02

```
#  Vergleichsmodulationsindex   m0 =  0.60 %
0235+164       31    1.078   0.032    3.00    8.81   426.806  14.227
0716+710       57    0.818   0.017    2.09    6.01   415.649   7.422
0836+710       58    2.105   0.010    0.48    0.00    31.967   0.561
0917+624       53    1.317   0.013    0.97    2.29   111.253   2.139
0951+699       46    3.518   0.007    0.20    0.00     6.314   0.140
0954+658       54    0.950   0.014    1.43    3.91   260.276   4.911
1128+592       41    0.369   0.009    2.48    7.22   133.719   3.343
1156+295       26    0.965   0.032    3.34    9.86   580.906  23.236
1203+645       53    1.164   0.006    0.52    0.00    34.662   0.667
3C286          25    7.509   0.031    0.41    0.00    20.312   0.846
3C48           31    5.585   0.034    0.60    0.22    46.059   1.535
CTA21          24    2.894   0.021    0.71    1.14    49.185   2.138
MRK421         27    0.649   0.008    1.25    3.28    50.779   1.953
NGC7027        26    5.441   0.024    0.44    0.00    19.730   0.789
OJ287          25    1.740   0.016    0.92    2.09    68.261   2.844
```

2008-03

```
#  Vergleichsmodulationsindex   m0 =  0.50 %
0235+164       36    1.088   0.021    1.95    5.66   421.503  12.043
0716+710       76    0.786   0.023    2.99    8.84  1111.253  14.817
0836+710       74    2.080   0.008    0.37    0.00    38.383   0.526
0917+624       78    1.319   0.015    1.12    3.01   271.793   3.530
```

# SRC	ANZ	<S>[Jy]	sigma	m[%]	Y[%]	Chi^2	red.Chi^2
0951+699	79	3.529	0.013	0.36	0.00	47.866	0.614
0954+658	74	0.901	0.020	2.26	6.60	836.021	11.452
1128+592	59	0.357	0.007	1.85	5.33	116.498	2.009
1156+295	39	1.028	0.068	6.67	19.94	4660.418	122.643
1203+645	72	1.158	0.006	0.55	0.66	55.657	0.784
1633+382	36	2.550	0.013	0.53	0.49	47.145	1.347
3C286	32	7.503	0.014	0.19	0.00	8.127	0.262
3C48	37	5.580	0.027	0.49	0.00	51.500	1.431
CTA21	29	2.907	0.007	0.24	0.00	8.260	0.295
MRK501	33	1.457	0.010	0.70	1.49	46.175	1.443
NGC7027	36	5.438	0.016	0.29	0.00	16.314	0.466

2008-04

# Vergleichsmodulationsindex m0 = 0.50 %							
0235+164	35	1.114	0.072	6.48	19.38	1035.511	30.456
0716+710	67	0.853	0.029	3.40	10.09	1364.347	20.672
0836+710	69	2.057	0.006	0.29	0.00	19.043	0.280
0917+624	66	1.342	0.009	0.65	1.24	79.377	1.221
0951+699	71	3.601	0.009	0.25	0.00	16.428	0.235
0954+658	73	0.978	0.026	2.63	7.73	1184.493	16.451
1128+592	110	0.361	0.011	3.10	9.17	546.668	5.015
1156+295	36	1.053	0.061	5.80	17.35	3347.483	95.642
1203+645	133	1.159	0.007	0.61	1.04	131.768	0.998
1633+382	26	2.613	0.011	0.41	0.00	21.626	0.865
3C286	28	7.496	0.018	0.23	0.00	10.985	0.407
3C48	36	5.587	0.019	0.33	0.00	19.900	0.569
MRK501	30	1.450	0.006	0.40	0.00	16.785	0.579
NGC7027	34	5.431	0.019	0.34	0.00	16.329	0.495

Bibliography

Agudo, I., T. P. Krichbaum, H. Ungerechts, A. Kraus, A. Witzel, E. Angelakis, L. Fuhrmann, U. Bach, S. Britzen, J. A. Zensus, S. J. Wagner, L. Ostorero, E. Ferrero, J. Gracia, and M. Grewing. 2006. Testing the inverse-Compton catastrophe scenario in the intra-day variable blazar S5 0716+71. II. A search for intra-day variability at millimetre wavelengths with the IRAM 30 m telescope. A&A 456:117–129.

Altadill, D., J. G. Solé, and E. M. Apostolov. 1998. First observation of quasi-2-day oscillations in ionospheric plasma frequency at fixed heights. *Annales Geophysicae* 16:609–617.

Andrew, B. H., G. A. Harvey, and W. J. Medd. 1971. OJ 287: An Exceptionally Active Variable Source. Astrophys. Lett. 9:151–+.

Baars, J. W. M., R. Genzel, I. I. K. Pauliny-Toth, and A. Witzel. 1977. The absolute spectrum of CAS A - an accurate flux density scale and a set of secondary calibrators. A&A 61:99–106.

Beall, J. H., W. A. Snyder, and K. S. Wood. 1989. Short Time Scale Variability of Active Galactic Nuclei: Einstein IPC Observations of PKS 2155-304 - a Report of Rapid Variations of Instrumental Origin. In *Active Galactic Nuclei*, ed. D. E. Osterbrock and J. S. Miller, volume 134 of *IAU Symposium*, 106–+.

Beard, A. G., N. J. Mitchell, P. J. S. Williams, W. Jones, and H. G. Muller. 1997. Mesopause-region tidal variability observed by meteor radar. *Advances in Space Research* 20:1237–1240.

Beckert, T., L. Fuhrmann, G. Cimò, P. Krichbaum, T. A. Witzel, and A. Zensus, J.ȧ2002. Understanding scintillation of Intraday Variables. In *Proceedings of the 6th European VLBI Network Symposium*, 79–+.

Begelman, M. C., R. D. Blandford, and M. J. Rees. 1984. Theory of extragalactic radio sources. *Reviews of Modern Physics* 56:255–351.

Berkhuijsen, E. M. 1971. A Survey of the Continuum Radiation at 820 MHz between Declinations ˜7o and 850.11o. A Study of the Galactic Radiation and the Degree of Polarization with Special Reference to the Loops and Spurs. A&A 14:359–+.

Berkhuijsen, E. M., C. G. T. Haslam, and C. J. Salter. 1971. Are the galactic loops supernova remnants? A&A 14:252–262.

Bernhart, S., T. P. Krichbaum, L. Fuhrmann, and A. Kraus. 2006. Kinematic Studies of the IDV Quasar 0917+624. *ArXiv Astrophysics e-prints* .

Bignall, H. E., D. L. Jauncey, J. E. J. Lovell, A. K. Tzioumis, L. Kedziora-Chudczer, J.-P. Macquart, S. J. Tingay, D. P. Rayner, and R. W. Clay. 2003. Rapid Variability and Annual Cycles in the Characteristic Timescale of the Scintillating Source PKS 1257-326. ApJ 585:653–664.

Bignall, H. E., J.-P. Macquart, D. L. Jauncey, J. E. J. Lovell, A. K. Tzioumis, and L. Kedziora-Chudczer. 2006. Rapid Interstellar Scintillation of PKS 1257-326: Two-Station Pattern Time Delays and Constraints on Scattering and Microarcsecond Source Structure. ApJ 652:1050–1058.

Chapman, S., and R. Lindzen. 1970. *Atmospheric tides. Thermal and gravitational*. Dordrecht: Reidel, 1970.

Chshyolkova, T., A. H. Manson, and C. E. Meek. 2005. Climatology of the quasi two-day wave over Saskatoon (52°N, 107°W): 14 Years of MF radar observations. *Advances in Space Research* 35:2011–2016.

Cimò, G., T. Beckert, T. P. Krichbaum, L. Fuhrmann, A. Kraus, A. Witzel, and J. A. Zensus. 2002. A Very Rapid Extreme Scattering Event in the IDV Source 0954+658. *Publications of the Astronomical Society of Australia* 19:10–13.

Dennett-Thorpe, J., and A. G. de Bruyn. 2000. The Discovery of a Microarcsecond Quasar: J1819+3845. ApJ 529:L65–L68.

Fuhrmann, L., T. P. Krichbaum, G. Cimò, T. Beckert, A. Kraus, A. Witzel, J. A. Zensus, S. J. QIAN, and B. J. Rickett. 2002. Annual Modulation in the Variability Properties of the IDV Source 0917+624? *Publications of the Astronomical Society of Australia* 19:64–68.

Fuhrmann, Lars. 2004. Investigation of intraday variable blazar cores and the connected interstellar medium. Doctoral Dissertation, University of Bonn.

Gabányi, K. É., N. Marchili, T. P. Krichbaum, S. Britzen, L. Fuhrmann, A. Witzel, J. A. Zensus, P. Müller, X. Liu, H. G. Song, J. L. Han, and X. H. Sun. 2007. The IDV source J 1128+5925, a new candidate for annual modulation? A&A 470:83–95.

Gavrilov, M. B., and A. D. Prodanov. 2008. The characteristics of Rossby waves frequencies on planets of the Solar system. Planet. Space Sci. 56:1480–1484.

Goodman, J. 1997. Radio scintillation of gamma-ray-burst afterglows. *New Astronomy* 2:449–460.

Gupta, A. C., J. H. Fan, J. M. Bai, and S. J. Wagner. 2008. Optical Intra-Day Variability in Blazars. AJ 135:1384–1394.

Hagan, M. E., and J. M. Forbes. 2002. Migrating and nonmigrating diurnal tides in the middle and upper atmosphere excited by tropospheric latent heat release. *Journal of Geophysical Research (Atmospheres)* 107:4754–+.

Hagan, M. E., and R. G. Roble. 2001. Modeling diurnal tidal variability with the National Center for Atmospheric Research thermosphere-ionosphere-mesosphere-electrodynamics general circulation model. J. Geophys. Res. 106:24869–24882.

Heeschen, D. S. 1984. Flickering of extragalactic radio sources. AJ 89:1111–1123.

Heeschen, D. S., T. Krichbaum, C. J. Schalinski, and A. Witzel. 1987. Rapid variability of extragalactic radio sources. AJ 94:1493–1507.

Hughes, P. A., H. D. Aller, and M. F. Aller. 1989a. Synchrotron emission from shocked relativistic jets. I - The theory of radio-wavelength variability and its relation to superluminal motion. ApJ 341:54–79.

Hughes, P. A., H. D. Aller, and M. F. Aller. 1989b. Synchrotron Emission from Shocked Relativistic Jets. II. A Model for the Centimeter Wave Band Quiescent and Burst Emission from BL Lacertae. ApJ 341:68–+.

Jacobi, C., Y. I. Portnyagin, E. G. Merzlyakov, B. L. Kashcheyev, A. N. Oleynikov, D. Kürschner, N. J. Mitchell, H. R. Middleton, H. G. Muller, and V. E. Comley. 2001. Mesosphere//lower thermosphere wind measurements over Europe in summer 1998. *Journal of Atmospheric and Solar-Terrestrial Physics* 63:1017–1031.

Kedziora-Chudczer, L., D. L. Jauncey, M. H. Wieringa, M. A. Walker, G. D. Nicolson, J. E. Reynolds, and A. K. Tzioumis. 1997. PKS 0405-385: The Smallest Radio Quasar? ApJ 490:L9+.

Kellermann, K. I. 2002. Brightness Temperature Constraints to Compact Synchrotron Source Radiation Obtained from IDV and VLBI Observations. *Publications of the Astronomical Society of Australia* 19:77–82.

Kellermann, K. I., and I. I. K. Pauliny-Toth. 1969. The Spectra of Opaque Radio Sources. ApJ 155:L71+.

Kinman, T. D., and E. K. Conklin. 1971. Observations of OJ 287 at Optical and Millimeter Wavelengths. Astrophys. Lett. 9:147–+.

Kraus, A. 1997. Doctoral Dissertation, , University of Bonn, Germany, (1997).

Kraus, A., A. Quirrenbach, A. P. Lobanov, T. P. Krichbaum, M. Risse, P. Schneider, S. J. Qian, S. J. Wagner, A. Witzel, J. A. Zensus, J. Heidt, H. Bock, M. Aller, and H. Aller. 1999a. Unusual radio variability in the BL Lacertae object 0235+164. A&A 344:807–816.

Kraus, A., A. Witzel, T. P. Krichbaum, A. P. Lobanov, B. Peng, and E. Ros. 1999b. A change in the variability properties of the intraday variable quasar 0917+624. A&A 352:L107–L110.

Lehar, J., J. N. Hewitt, B. F. Burke, and D. H. Roberts. 1992. The radio time delay in the double quasar 0957 + 561. ApJ 384:453–466.

Lindzen, R. S. 1979. Atmospheric tides. *Annual Review of Earth and Planetary Sciences* 7:199–225.

Lomb, N. R. 1976. Least-squares frequency analysis of unequally spaced data. Ap&SS 39:447–462.

Lovell, J. E. J., D. L. Jauncey, H. E. Bignall, L. Kedziora-Chudczer, J.-P. Macquart, B. J. Rickett, and A. K. Tzioumis. 2003a. First Results from MASIV: The Microarcsecond Scintillation-induced Variability Survey. AJ 126:1699–1706.

Lovell, J. E. J., D. L. Jauncey, A. K. Tzioumis, H. E. Bignall, L. Kedziora-Chudczer, J.-P. Macquart, and B. J. Rickett. 2003b. The Micro-Arcsecond Scintillation-Induced Variability (MASIV) VLA Survey. In *Active Galactic Nuclei: From Central Engine to Host Galaxy*, ed. S. Collin, F. Combes, and I. Shlosman, volume 290 of *Astronomical Society of the Pacific Conference Series*, 347–+.

Lovell, J. E. J., B. J. Rickett, J. Macquart, D. L. Jauncey, H. E. Bignall, L. Kedziora-Chudczer, R. Ojha, T. Pursimo, M. Dutka, C. Senkbeil, and S. Shabala. 2008. The Micro-Arcsecond Scintillation-Induced Variability (MASIV) Survey II: The First Four Epochs. *ArXiv e-prints* .

Macquart, J.-P., and A. G. de Bruyn. 2006. Diffractive interstellar scintillation of the quasar J1819+3845 at λ21 cm. A&A 446:185–200.

Marscher, A. P., and W. K. Gear. 1985. Models for high-frequency radio outbursts in extragalactic sources, with application to the early 1983 millimeter-to-infrared flare of 3C 273. ApJ 298:114–127.

Marscher, A. P., and J. S. Scott. 1980. Superluminal motion in compact radio sources. PASP 92:127–133.

Matheson, D. N., and L. T. Little. 1971. Interplanetary scintillation-Angular distribution of radio waves scattered by the interplanetary medium. Nature 234:29–+.

Muller, H. G. 1972. Long-period meteor wind oscillations. *Royal Society of London Philosophical Transactions. Series A* 271:585–598.

Narayan, R. 1992. The Physics of Pulsar Scintillation. *Royal Society of London Philosophical Transactions Series A* 341:151–165.

Nilsson, K., T. Pursimo, A. Sillanpää, L. O. Takalo, and E. Lindfors. 2008. Detection of the host galaxy of S5 0716+714. A&A 487:L29–L32.

Oberheide, J., Q. Wu, D. A. Ortland, T. L. Killeen, M. E. Hagan, R. G. Roble, R. J. Niciejewski, and W. R. Skinner. 2005. Non-migrating diurnal tides as measured by the TIMED Doppler interferometer: Preliminary results. *Advances in Space Research* 35:1911–1917.

Ott, M., A. Witzel, A. Quirrenbach, T. P. Krichbaum, K. J. Standke, C. J. Schalinski, and C. A. Hummel. 1994. An updated list of radio flux density calibrators. A&A 284:331–339.

Pen, U.-L. 1999. Heating of the Intergalactic Medium. ApJ 510:L1–L5.

Press, W. H., and G. B. Rybicki. 1989. Fast algorithm for spectral analysis of unevenly sampled data. ApJ 338:277–280.

Qian, S. J., A. Kraus, T. P. Krichbaum, A. Witzel, and J. A. Zensus. 2001. Multifrequency polarization variations in 0917+624. Ap&SS 278:119–122.

Qian, S.-J., T. P. Krichbaum, A. Witzel, J. A. Zensus, and X.-Z. Zhang. 2006. High Brightness Temperatures in IDV Sources. *Chinese Journal of Astronomy and Astrophysics* 6:530–542.

Qian, S. J., A. Quirrenbach, A. Witzel, T. P. Krichbaum, C. A. Hummel, and J. A. Zensus. 1991. A model for the rapid radio variability in the quasar 0917 + 624. A&A 241:15–21.

Qian, S.-J., and X.-Z. Zhang. 2001. Annual Modulation in Intraday Variability Timescales of Extragalactic Radio Sources. *Chinese Journal of Astronomy and Astrophysics* 1:133–143.

Quirrenbach, A., A. Witzel, T. P. Kirchbaum, C. A. Hummel, R. Wegner, C. J. Schalinski, M. Ott, A. Alberdi, and M. Rioja. 1992. Statistics of intraday variability in extragalactic radio sources. A&A 258:279–284.

Quirrenbach, A., A. Witzel, S. Wagner, F. Sanchez-Pons, T. P. Krichbaum, R. Wegner, K. Anton, U. Erkens, M. Haehnelt, J. A. Zensus, and K. J. Johnston. 1991. Correlated radio and optical variability in the BL Lacertae object 0716 + 714. ApJ 372:L71–L74.

Raiteri, C. M., M. Villata, V. M. Larionov, M. F. Aller, U. Bach, M. Gurwell, O. M. Kurtanidze, A. Lähteenmäki, K. Nilsson, A. Volvach, H. D. Aller, A. A. Arkharov, R. Bachev, A. Berdyugin, M. Böttcher, C. S. Buemi, P. Calcidese, E. Cozzi, A. di Paola, M. Dolci, J. H. Fan, E. Forné, L. Foschini, A. C. Gupta, V. A. Hagen-Thorn, L. Hooks, T. Hovatta, M. Joshi, M. Kadler, G. N. Kimeridze, T. S. Konstantinova, A. Kostov, T. P. Krichbaum, L. Lanteri, L. V. Larionova, C.-U. Lee, P. Leto, E. Lindfors, F. Montagni, R. Nesci, E. Nieppola, M. G. Nikolashvili, J. Ohlert, A. Oksanen, E. Ovcharov, P. Pääkkönen, M. Pasanen, T. Pursimo, J. A. Ros, E. Semkov, L. A. Sigua, R. L. Smart, A. Strigachev, L. O. Takalo, K. Torii, I. Torniainen, M. Tornikoski, C. Trigilio, H. Tsunemi, G. Umana, and A. Valcheva. 2008. Radio-to-UV monitoring of AO 0235+164 by the WEBT and Swift during the 2006-2007 outburst. A&A 480:339–347.

Rees, M. J. 1978. The M87 jet - Internal shocks in a plasma beam. MNRAS 184:61P–65P.

Rickett, B. 1998. Interstellar Scintillation of Extragalactic Radio Sources. In *Bulletin of the American Astronomical Society*, volume 30 of *Bulletin of the American Astronomical Society*, 879–+.

Rickett, B. J., W. A. Coles, and G. Bourgois. 1984. Slow scintillation in the interstellar medium. A&A 134:390–395.

Rickett, B. J., A. Witzel, A. Kraus, T. P. Krichbaum, and S. J. Qian. 2001. Annual Modulation in the Intraday Variability of Quasar 0917+624 due to Interstellar Scintillation. ApJ 550:L11–L14.

Rossby, C. G. 1939. Relation between variations in the intensity of the zonal circulation of the atmosphere and the displacements of the semi-permanent centers of action. *J. Marine Res.* 2:38–55.

Savolainen, T., and Y. Y. Kovalev. 2008. Serendipitous VLBI detection of rapid, large-amplitude, intraday variability in QSO 1156+295. A&A 489:L33–L36.

Scargle, J. D. 1982. Studies in astronomical time series analysis. II - Statistical aspects of spectral analysis of unevenly spaced data. ApJ 263:835–853.

Schalinski, C. J., P. Biermann, A. Eckart, K. J. Krichbaum, T. P. Johnston, and A. Witzel. 1987. Bulk Relativistic Motion in a Complete Sample of Radio Selected AGN. In *Observational Evidence of Activity in Galaxies*, ed. E. E. Khachikian, K. J. Fricke, and J. Melnick, volume 121 of *IAU Symposium*, 287–+.

Scheuer, P. A. G. 1968. Amplitude Variations in Pulsed Radio Sources. Nature 218:920–+.

Shapirovskaya, N. Y. 1978. Variability of extragalactic decimeter radio sources. *Soviet Astronomy* 22:544–+.

Sillanpaa, A., S. Haarala, M. J. Valtonen, B. Sundelius, and G. G. Byrd. 1988. OJ 287 - Binary pair of supermassive black holes. ApJ 325:628–634.

Simonetti, J. H., J. M. Cordes, and D. S. Heeschen. 1985. Flicker of extragalactic radio sources at two frequencies. ApJ 296:46–59.

Sun, X. H., W. Reich, J. L. Han, P. Reich, and R. Wielebinski. 2006. New λ6 cm observations of the Cygnus Loop. A&A 447:937–947.

Thayaparan, T. 1997. The terdiurnal tide in the mesosphere and lower thermosphere over London, Canada (43°N, 81°W). J. Geophys. Res. 102:21695–21708.

Urry, C. M., and P. Padovani. 1995. Unified Schemes for Radio-Loud Active Galactic Nuclei. PASP 107:803–+.

Valtaoja, E., H. Terasranta, S. Urpo, N. S. Nesterov, M. Lainela, and M. Valtonen. 1992. Five Years Monitoring of Extragalactic Radio Sources - Part Three - Generalized Shock Models and the Dependence of Variability on Frequency. A&A 254:71–+.

Villata, M., C. M. Raiteri, O. M. Kurtanidze, M. G. Nikolashvili, M. A. Ibrahimov, I. E. Papadakis, K. Tsinganos, K. Sadakane, N. Okada, L. O. Takalo, A. Sillanpää, G. Tosti, S. Ciprini, A. Frasca, E. Marilli, R. M. Robb, J. C. Noble, S. G. Jorstad, V. A. Hagen-Thorn, V. M. Larionov, R. Nesci, M. Maesano, R. D. Schwartz, J. Basler, P. W. Gorham, H. Iwamatsu, T. Kato, C. Pullen, E. Benítez, J. A. de Diego, M. Moilanen, A. Oksanen, D. Rodriguez, A. C. Sadun, M. Kelly, M. T. Carini, H. R. Miller, S. Catalano, D. Dultzin-Hacyan, J. H. Fan, R. Ishioka, H. Karttunen, P. Keinänen, N. A. Kudryavtseva, M. Lainela, L. Lanteri, E. G. Larionova, K. Matsumoto, J. R. Mattox, F. Montagni, G. Nucciarelli, L. Ostorero, J. Papamastorakis, M. Pasanen, G. Sobrito, and M. Uemura. 2002. The WEBT BL Lacertae Campaign 2000. A&A 390:407–421.

Voiculescu, M., C. Haldoupis, D. Pancheva, M. Ignat, K. Schlegel, and S. Shalimov. 2000. More evidence for a planetary wave link with midlatitude E region coherent backscatter and sporadic E layers. *Annales Geophysicae* 18:1182–1196.

Volland, H. 1997. Atmospheric tides. *Lecture Notes in Earth Sciences, Berlin Springer Verlag* 66:221–246.

Wagner, S., F. Sanchez-Pons, A. Quirrenbach, and A. Witzel. 1990. Simultaneous optical and radio monitoring of rapid variability in quasars and BL Lac objects. A&A 235:L1–L4.

Wagner, S. J., and A. Witzel. 1995. Intraday Variability In Quasars and BL Lac Objects. ARA&A 33:163–198.

Wagner, S. J., A. Witzel, J. Heidt, T. P. Krichbaum, S. J. Qian, A. Quirrenbach, R. Wegner, H. Aller, M. Aller, K. Anton, I. Appenzeller, A. Eckart, A. Kraus, C. Naundorf, R. Kneer, W. Steffen, and J. A. Zensus. 1996. Rapid Variability in S5 0716+714 Across the Electromagnetic Spectrum. AJ 111:2187–+.

Wagner, S. J., A. Witzel, T. P. Krichbaum, R. Wegner, A. Quirrenbach, K. Anton, U. Erkens, R. Khanna, and A. Zensus. 1993. Intraday variability in the BL Lac object 0954 + 658. A&A 271:344–+.

Wills, B. J. 1971. Daily and Hourly Variations in Flux Density of Radio Sources. ApJ 169:221–+.

Witzel, A. 1990. Intraday Variability of Extragalactic Radio Sources. In *Parsec-scale radio jets*, ed. J. A. Zensus and T. J. Pearson, 206–+.

Witzel, A., D. S. Heeschen, C. Schalinski, and T. Krichbaum. 1986. Kurzzeit-Variabilität extragalaktischer Radioquellen. *Mitteilungen der Astronomischen Gesellschaft Hamburg* 65:239–+.

Wu, D. L., and J. H. Jiang. 2005. Interannual and seasonal variations of diurnal tide, gravity wave, ozone, and water vapor as observed by MLS during 1991 1994. *Advances in Space Research* 35:1999–2004.

Zhao, G., L. Liu, B. Ning, W. Wan, and J. Xiong. 2005. The terdiurnal tide in the mesosphere and lower thermosphere over Wuhan (30°N, 114°E). *Earth, Planets, and Space* 57:393–398.

Acknowledgments

I would like to thank the director of the VLBI group at the MPIfR, Prof. Dr. J. Anton Zensus, for giving me the opportunity and the financial support to work here, among excellent scientists and friendly people.

Many thanks to Prof. Ulrich Klein and Priv.-Doz. Dr. Walter K. Huchtmeier for supervising this thesis.

I wish to express my gratitude to Dr. Thomas P. Krichbaum for the invaluable contribution to this thesis project. For the knowledge he shared with me, for the many suggestions, always precious, which lead this work towards its aim. Thanks for the many hours spent discussing scientific topics with me, which greatly improved not only the quality of this thesis, but, first of all, my understanding of science.

Very special thanks to Dr. Arno Witzel. His continuous support and manifestations of trust have been among my strongest motivations. His profound knowledge of science, of music, of all the things which touch the human soul, is the best demonstration of how beautiful it is to 'keep searching'.

It is hard to decide if I should thank Dr. Emmanouil (Manolis) Angelakis first as a scientist or as a friend. I can not say how many times his scientific skills have been essential to resolve the problems I encountered along my way; how fruitful, always, have been our discussions. The efforts he put in improving this thesis are invaluable. Despite this, I want to thank above all the friend, which always kept sustaining and encouraging me, in good and in bad times.

Without the efforts of Xiang Liu, Huagang Song and all the people of the Urumqi telescope, this thesis would not be. Many thanks to them for the incredible amount of time they dedicated to this project.

I would like to thank P. Müller and Dr. Alex Kraus. The tools they developed for the data calibration made my life much easier! Whenever I had questions, they never denied me neither their time nor competence.

Many important suggestions for this work came from Dr. Lars Fuhrmann, dear friend and collaborator. His advises lead me here in Bonn, giving me the chance to continue my scientific career and to discover unexplored sides of reality – such as the pizza Hawaii (yes, Lars, thanks a lot!!!). I want to thank also Dr. Krisztina É. Gabányi for several years of fruitful collaboration, in which we shared a lot of work, ideas, data and chocolate.

My stay in Bonn would have been much more difficult without the help of Dr. Eduardo Ros, director of the IMPRS, and Gabi Breuer. Their kindness and friendliness made me feel at home from my first day in Bonn.

I want to express my gratitude to Dr. Alan Roy – for the illuminating explanations concerning many technical aspects of radio observations –, to Dr. Silke Britzen, which helped me to improve considerably my knowledge about AGNs, and to all the people of the VLBI group and of the Effelsberg telescope.

During these three and more years, I have had the pleasure to share the office with very nice mates. Thanks to Nadia, Veronika, Chin-Shin and Mar for making the time I spent at work always enjoyable. A special mention for Christian – which succeeded in the difficult task of explaining me the mysteries of German Football – and Gunther (which was never my office mate, and I am really sorry about that!): the conversations we had about science and music have always been inspiring to me.

Altri amici, altro linguaggio. Il posto d'onore nella sezione italica dei miei ringraziamenti va a Carlo, dottore anch'egli, oltre le coste di Bretagna, le cui epistole hanno avuto ruolo determinante nella preservazione della mia salute mentale. 'Caro Generale, come segno della mia gratitudine le affido la Normandia, località amena; dicono che fa sempre caldo e non piove mai, si difende con quattro sassi ed una clava. Mi raccomando, eh?'

Grazie a Emanuele, anche se si fa sentir di rado. Lo so – l'unica forma di comunicazione fra quello sperduto villaggio tra gli Appennini ed il mondo esterno è il telegrafo, ma la linea è rimasta seriamente danneggiata durante l'alluvione del '66; riparala – ne sono consapevole – non è mica una quisquilia. Fortuna che Perugia non è poi così lontana!

Un ringraziamento particolare merita Erminia, che avrebbe avuto la possibilità ed il diritto di impedire questa tesi ed invece l'ha sempre incoraggiata. La sua semplicità e bontà avranno sempre un posto nel mio cuore.

Fisici sparsi per il globo (quando si dice la fuga dei cervelli), grazie anche a voi che non avete scordato l'eremita di Bonn: Moreno il Vichingo, Veronica del Piceno (e congratulazioni per il piccolo Davide!), Andrea più Andrea, l'uno Americano, l'altro... Americano pure lui, e Francesca da quel di Viterbo.

Gli ultimi mesi d'un dottorato possono diventare assai stressanti: lo sa bene Kazi, che con me questi mesi ha condiviso a prezzo di sacrifici non indifferenti. Se giungo alla conclusione di questo lavoro *con un sorriso* lo devo a lei; per il suo sostegno, per la sua capacità di riportarmi alle cose nella loro semplicità, per la dolcezza della sua vicinanza, la mia gratitudine: 'I love you, Parasite!' (Worker).

Questo dottorato è l'ultimo passo d'un percorso lungo e piuttosto complicato, che sarebbe stato impossibile percorrere senza il sostegno e l'affetto di mia madre Elsbeth e di mia sorella Sabina. Non per un solo momento, in questi anni a Bonn, mi sono sentito lontano da loro. Grazie pure al piccolo Gabriele, giovinezza che rifiorisce nella nostra famiglia.

L'ultimo dei ringraziamenti, ovvero il primo, va a mio padre. Mi hai indicato la via, mi hai dato i valori che permettono di seguirla, mi hai preso per mano laddove il sentiero si faceva più difficile. I fondamenti a cui mi volgo per riscoprire cosa renda bella la vita vengono da te, ci sono ora comuni – impossibile che tu non sia più qui a seguire quel cammino. E quando mi volgo ad essi, è come tornare a te. Ciao papà, ci ritroveremo.